Investigations into insulin-regulated trafficking of the facilitative glucose transporter GLUT4 in adipocytes; novel insights from *in situ* studies

A thesis submitted to the
COLLEGE OF MEDICAL, VETERINARY AND LIFE SCIENCES

For the degree of
DOCTOR OF PHILOSOPHY

By Dimitrios Kioumourtzoglou

Institute of Molecular, Cell and Systems Biology
College of Medical, Veterinary and Life Sciences
University of Glasgow

July 2012

Abstract

Trafficking of the facilitative glucose transporter GLUT4 is regulated by insulin in fat and muscle cells. Under basal conditions, GLUT4 is retained intracellularly by continually cycling through the endosomal system, but translocates to the plasma membrane in response to insulin stimulation. Intracellular GLUT4-containing vesicles fall into two categories: cellugyrin-positive (sortilin-free) and sortilin-positive (cellugyrin-negative). The former are the source of GLUT4 that cycles through the plasma membrane under basal conditions while the latter are the source of GLUT4 that translocates to the cell surface upon insulin stimulation. Fusion of GLUT4-containing vesicles with the plasma membrane is mediated by formation of SNARE complexes including the plasma membrane localized t-SNAREs Syntaxin 4 and SNAP23, and the v-SNARE VAMP2 present in the GLUT4-containing vesicles. The Sec1/Munc18 (SM) protein Munc18c also plays a key role in insulin-stimulated GLUT4 translocation, although its precise role remains controversial. Munc18c binds directly to both Syntaxin 4 and VAMP2 as well as to the assembled SNARE complex through a series of different binding modes. It has been suggested that SM/Syntaxin interactions facilitate SNARE complex formation by bringing about a conformational switch to release an inhibitory effect of syntaxins' Habc domain.

In this study I have used *in situ* Proximity Ligation Assay (PLA) to visualize the effects of insulin stimulation on interactions between Syntaxin 4, SNAP23, VAMP2 and Munc18c in 3T3-L1 adipocytes and fibroblasts. I find that insulin treatment results in an increase of the formation of assembled Syntaxin 4/SNAP23/VAMP2 SNARE complexes as well as recruitment of Munc18c to these complexes. These studies also reveal the existence of two pools of Syntaxin 4 under basal conditions: one in complex with SNAP23 (lacking VAMP2 and Munc18c); the other in complex with Munc18c and VAMP2 (lacking SNAP23). Additionally I have used *in vitro* binding studies to demonstrate that Syntaxin 4 binds directly to VAMP2 in a SNARE motif related manner and that this interaction is inhibitory to the rate of Syntaxin 4/SNAP23/VAMP2 SNARE complex assembly. Syntaxin 4 also binds directly to SNAP23, an interaction that enhances SNARE complex formation.

Munc18c is phosphorylated on Tyr-521 in response to insulin-stimulation of 3T3-L1 adipocytes. I report here, that wild-type Munc18c inhibits SNARE complex formation, whereas a phosphomimetic version facilitates this process. Finally PLA studies reveal that the Syntaxin 4 pool in complex with VAMP2 and Munc18c associates with sortilin-positive vesicles, and that it is this pool which facilitates fusion of GLUT4 carrying vesicles upon insulin-stimulation. These studies also demonstrate the other Syntaxin 4 pool, that in complex with SNAP23, associates with cellugyrin-positive vesicles, and likely regulates the basal cycling of GLUT4 through the plasma membrane.

I have used the data presented in this thesis to formulate a model whereby the two pools of Syntaxin 4 described are functionally distinct, and differ in their ability to mediate delivery of GLUT4 to the plasma membrane in response to insulin through the function of Munc18c.

Table of contents

List of tables

List of figures

Acknowledgement

First of all I would like to thank my supervisor Dr. Nia Bryant for all her excellent guidance, creative criticism, moral support and understanding throughout the course of this project. I will always be grateful for the opportunity to work in her lab. Thank you for this adventurous trip!

I would also like to thank Prof Gwyn Gould for his advice and help and everyone in Lab 241 past and present for their support. In particular I would like to thank Dr Chris MacDonald for dedicating so much time introducing me to the project in the early days.

Thanks to Sofia for all the helpful discussions during coffee breaks and for being a true friend. Thanks to Georgia and Panagiota for always being next to me giving me strength when I most needed it.

Finally, profound gratitude must go to my parents Panagiotis and Maria and to my sister Katerina for their unconditional love and constant encouragement and support. There are no words to express my thankfulness.

Σας ευχαριστώ μέσα από την καρδιά μου.

Thank you so much.

Author's declaration

I declare that the work presented in this thesis has been carried out by myself, unless otherwise cited or acknowledged. It is entirely of my own composition and has not, in whole or in part, been submitted for any other degree.

Dimitrios Kioumourtzoglou
July 2012

Definitions/abbreviations

(v/v)	Units volume per unit volume
(w/v)	Units weight per unit volume
˚C	Degrees Celsius
~	Approximately
2YT	Bacterial growth medium:Yeast extract, tryptone, NaCl
ADP	Adenosine diphosphate
ALP	Alkaline phosphatase
Amp	Ampicillin
APS	Ammonium persulfate
AS160	Akt substrate of 160 kilodaltons
ATP	Adenosine 5'-triphosphate
bp	DNA base pair(s)
BRET	Bioluminescent resonance energy transfer
BSA	Bovine serum albumin
BSA/GLY	2% (w/v) BSA, 20mM glycine in PBS
BSA/GLY/SAP	0.1% (w/v) saponin in BSA/GLY
C-terminal	Carboxy terminal
C. elegans	Caenorhabditis elegans
CAA	SNARE Complex Assembly Assay
$CaCl_2$	Calcium chloride
CAP	c-Cbl associated protein
cDNA	Complementary DNA
CuSO4	Copper sulphate
D. melanogaster	Drosophila melanogaster
ddH_2O	Double distilled water
DFP	Diisopropyl fluorophosphate
DMEM	Dulbecco's modified Eagle's medium
DMF	Dimethyl formamide
DMSO	Dimethyl sulphoxide
DNA	Deoxyribonucleic acid
DNaseI	Deoxyribonuclease I
dNTP	Deoxynucleoside (5')-triphosphate
E. coli	Escherichia coli
ECL	Enhanced chemiluminescence
EDTA	Ethylenediaminetetraacetic acid
EM	Electron microscopy
ER	Endoplasmic reticulum
EtBr	Ethidium bromide
FCS	Foetal calf serum
FRET	Förster resonance energy transfer
g	Gram
g	Gravitational force
GDP	Guanosine-5'-diphosphate
GFP	Aequorea victoria green fluorescent protein
GLUT	Glucose transporter
GST	Glutathione S transferase
GSV	GLUT4 storage vesicle
GTP	Guanosine-5'-triphosphate
HA	Influenza haemagglutinin epitope tag
HAc	Acetic acid

HCl	Hydrochloric acid
HEPES	2-[4-(2-Hydroxyethyl)-1-piperazine] ethanesulfonic acid
His_6	Six-histidine residue tag
HOPS	Homotypic fusion and vacuole protein sorting
HP H_20	Hight purity water
HRP	Horseradish peroxidase
IF	Immunofluorescence
IgG	Immunoglobulin G
IHC	Immunochemistry
IP	Immunoprecipitation
IPTG	Isopropyl-ß-D-thiogalactopyranoside
IR	Insulin receptor
IRAP	Insulin responsive aminopeptidase
IRS	Insulin receptor substrate
IRV	Insulin responsive vesicle
k	Kilo (prefix)
K_2HPO4	Di-potassium hydrogen orthophosphate
Kan	Kanamycin
kb	Kilobase
KCl	Potassium chloride
kDa	Kilodalton
KH_2PO4	Potassium dihydrogen orthophosphate
KOH	Potassium hydroxide
L	Litre
LSB	Laemmli's sample buffer
m	Milli (prefix)
M	Molar
M. musculus	Mus musculus
M18c	Munc18c
mA	Milliamp
Mg	Magnesium
mg	Milligram
$MgCl_2$	Magnesium chloride
$MgSO_4$	Magnesium sulphate
min	Minute(s)
ml	Millilitre
n	Nano (prefix)
N-terminal	Amino-terminal
Na_2HPO4	Di-sodium hydrogen orthophosphate
NaCl	Sodium chloride
NaF	Sodium floride
NaH_2PO4	Sodiun Di-hydrogen orthophosphate
NaOH	Sodium hydroxide
NCS	Newborn calf serum
NEM	N-ethyl maleimide
NH_4Cl	Ammonium chloride
Ni-NTA	Nickel-nitrilotriacetic acid
NSF	N-ethylmaleimide sensitive factor
OD_{600}	Optical density at 600 nm
p	Pico (prefix)
PAGE	Polyacrylamide gel electrophoresis
PBS	Phosphate buffered saline
PBS-T	0.1 % (V/V) Tween-20 in phosphate buffered saline

PCR	Polymerase chain reaction
PDB	Protein data bank
PFA	Paraformaldehyde
Pfu	Pyrococcus furiosis
PH	Pleckstrin homology domain
PI	Phosphatidylinositol
PI3K	Phosphatidylinositol 3-kinase
PIP2	Phosphatidylinositol 4,5-bisphosphate
PIP3	Phosphatidylinositol 3,4,5-triphosphate
PKB	Protein kinase B/Akt
PKC	Protein kinase C
PLA	Proximity Ligation Assay
PM	Plasma membrane
PMSF	Phenylmethylsulfonyl fluoride
PrA	Protein A
psi	Pounds per square inch
RCA	Rolling circle amplification
RNA	Ribonucleic acid
rpm	Rotations per minute
S. cerevisiae	Saccharomyces cerevisiae
SDS	Sodium dodecyl sulfate
SDS-PAGE	Sodium dodecyl sulfate polyacrylamide gel electrophoresis
SH2	Src-homology 2
siRNA	Short interfering RNA
SM	Sec1/Munc18
SNAP	Soluble NSF attachment protein
SNAP23	23 kDa synaptosome-associated protein
SNAP25	25 kDa synaptosome-associated protein
SNARE	Soluble NSF attachment protein receptor
SOC	Super Optimal Broth
Sx4	Syntaxin 4
t-SNARE	Target SNARE
TAE	Tris acetate EDTA
Taq	Thermus aquaticus
TB	Terific broth
TEMED	N, N, N', N' - tetramethylenediamine
TGN	*Trans*-Golgi network
TIRF	Total internal reflection fluorescent
Tris	2-Amino-2-(hydroxymethyl)-1,3-propanediol
Tween-20	Polyoxyethylene sorbitan monolaurate
v-SNARE	Vesicle SNARE
VAMP	Vesicle associated membrane protein
WB	Western blot
X-Gal	(5-bromo-4-chloro-3-indolyl-b-D-galacto-pyranoside)
YFP	Yellow fluorescent protein
µ	Micro (prefix)

Chapter 1

Introduction

1.1 Membrane trafficking in eukaryotic cells

The intracellular material of all eukaryotic cells is highly ordered and contains membrane bound-organelles that allow the regulation of complex biochemical reactions (Vellai and Vida, 1999). Although each distinct organelle has its own unique complement of macromolecules, it is essential that there is communication between different membrane-bound compartments as well as between the intracellular and extracellular space (Dacks and Field, 2007). Membrane trafficking is crucial for cells to maintain homeostasis of these organelles. Cells require two principal trafficking pathways to sustain cellular integrity: the secretory and endocytic pathways. In the endocytic pathway defined regions of the plasma membrane invaginate to form endocytic vesicles that are later abscised from the plasma membrane allowing the substance that is included to be finally internalized. After internalization, fate of endocytic vesicles varies and depends on several factors. Vesicles can be either translocated back to plasma membrane (recycling of receptors), transferred to the *trans*-Golgi network *via* late endosomes for further modification of their contents, or be delivered to lysosomes where their cargo is destroyed (van Vliet et al., 2003). Pioneering work that took place more than 35 years ago, using the pancreatic exocrine cell as a model, revealed that newly synthesised proteins intended to be secreted, pass through a series of successive organelles, such as the endoplasmic reticulum, the Golgi network, and secretory granules on their way to the cell surface where vesicles finally fuse with the plasma membrane releasing their contents to extracellular environment (Palade, 1975). This process corresponds to the secretory pathway, which is also known as exocytosis. Secretory pathways can be divided into two principal categories; constitutive and regulated exocytosis. The first controls transport of proteins to the plasma membrane in a continuous manner (usually *via* the *trans*-Golgi network) in contrast to regulated exocytosis that is responsible for delivery of cargo either to the plasma membrane or to the extracellular environment in response to a specific signal (Figure 1-1). Regulated exocytosis is found principally in cells specialised for secreting molecules such as hormones, neurotransmitters, digestive enzymes etc. and/or translocating different receptors to the cellular surface in response to specific extracellular signals. In these cells cargo is usually stored in secretory vesicles that commonly

accumulate below the plasma membrane prior to signals that stimulated their regulated secretion (van Vliet et al., 2003). The non-disruptive transportation of these vital molecules between organelles and to plasma membrane *via* the formation of membrane bound vesicles is of extreme physiological importance and is achieved through membrane fusion (Bonifacino and Glick, 2004).

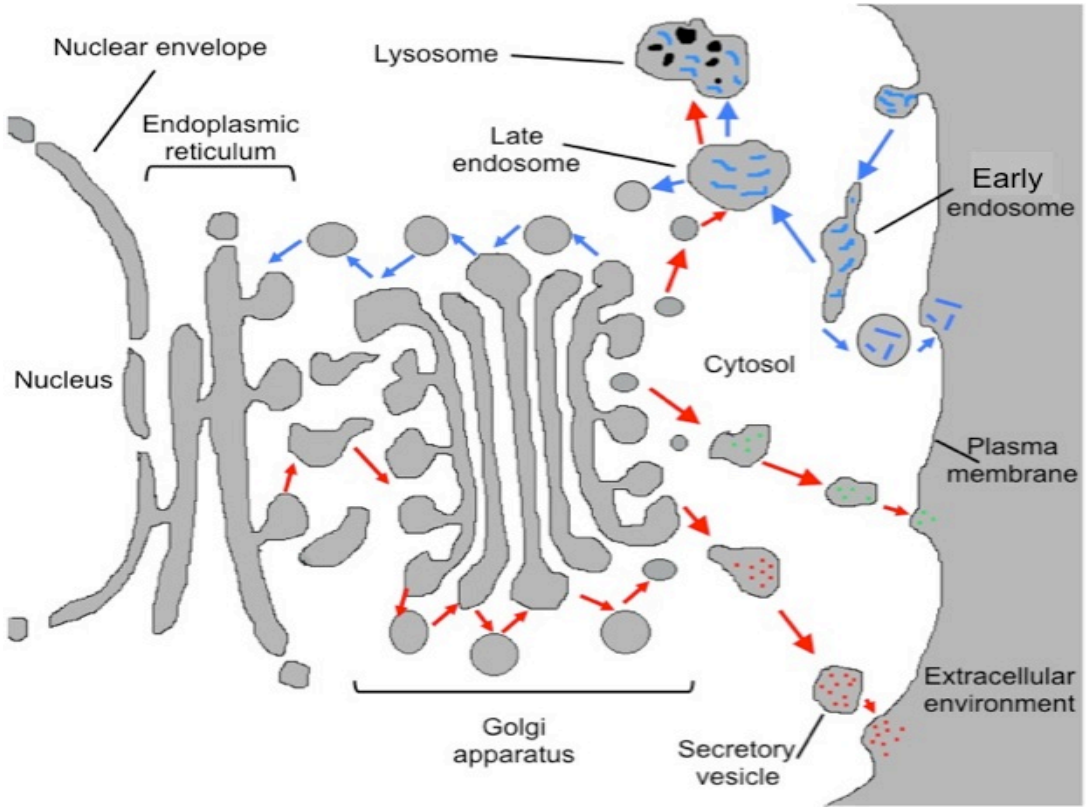

Figure 1-1: Membrane trafficking. Secretory and endocytosis pathways

This figure illustrates the major components of eukaryotic endomembrane system. Red arrows correspond to the secretory (biosynthetic) pathways. Newly synthesised proteins in endoplasmic reticulum are transferred *via* Golgi apparatus either to the plasma membrane for secretion or to lysosomes for further modification or destruction. Blue arrows correspond to endocytic pathway where substances that are about to enter into the cell are packed into a portion of plasma membrane that is invaginated and pinched off forming a membrane bound vesicle (endosome). Cargo from early endosomes can either return to the plasma membrane (endosome recycling) or *via* late endosomes can be delivered to lysosomes. An alternative endocytotic route is through the Golgi apparatus to the endoplasmic reticulum. Figure edited from Molecular biology of the cell, fourth edition, 2002.

1.1.1 Membrane fusion

In all trafficking pathways budding of transport vesicles from donor organelles allows cargo to be transported throughout the cell. These vesicles travel to and

subsequently fuse with the appropriate target compartment that can either be another organelle (Pfeffer, 1999) or the plasma membrane in the case of exocytosis (Palade, 1975). Membrane fusion in eukaryotic cells does not occur spontaneously because at close range (1-3 nm) biological membranes are subject of a strong repulsive hydration force due to hydrophilic lipid head groups (Rand, 1981). The generally accepted model that explains the energy requirements of membrane fusion termed “hemi-fusion” and proposed by Chernomordik and Kozlov in 2005. Based on this model the mechanism of membrane fusion is assumed to occur through the formation of a fusion intermediate in which the contacting outer membrane leaflets merge in contrast to distal monolayers that do not fuse (hemi-fusion). Following hemi-fusion state, a fusion stalk is formed that then progresses into a fusion pore, this develops into complete membrane fusion of the two bilayers (Chernomordik and Kozlov, 2005) (Figure 1-2). There are still many unanswered questions regarding how fusion is triggered and performed. As almost every vital cellular process relies on the orderly execution of membrane fusion, it is of paramount importance that trafficking events are tightly regulated to ensure specificity. Intracellular membrane fusion involves a highly conserved family of proteins called SNAREs (Soluble N-ethylmaleimide sensitive factor Attachment protein Receptors). These proteins constitute the core biochemical membrane fusion machinery, and have been characterised as the minimal components required for fusion since they are sufficient to provide the essential energy to overcome the repulsive forces of the two approaching membranes at least *in vitro* (Weber et al., 1998). SNARE proteins along with a variety of tethering factors contribute to the specificity between target membranes and transport vesicle but are not solely responsible. Members of another gene family the Sec1/Munc18 genes, referred to as SM genes, are also highly conserved among species and their products regulate the function of SNAREs to enhance the control of membrane trafficking (Toonen and Verhage, 2003).

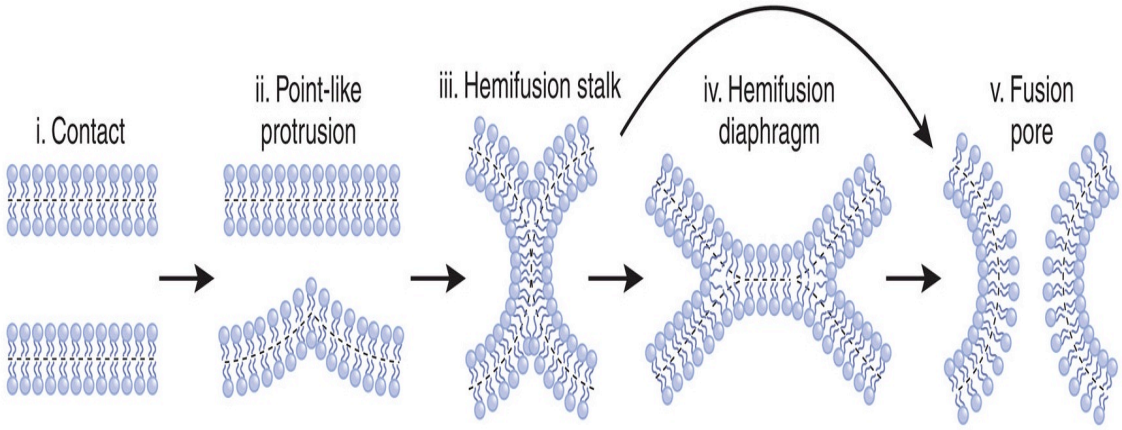

Figure 1-2: Model of membrane fusion *via* hemifusion formation.

(i) Membrane bilayers come into close contact. (ii) A point-like membrane protrusion minimizes the energy of the hydration repulsion between the proximal leaflets of the membranes coming into immediate contact. (iii) The proximal leaflets merge into a fusion stalk (which allows lipid mixing between these leaflets. (iv) The stalk expands into a hemifusion diaphragm that can break to form a fusion pore allowing lipid and content mixing (v). Figure edited from (Chernomordik and Kozlov, 2008)

1.2 SNARE proteins and the SNARE hypothesis

SNAREs comprise a superfamily of proteins that function in all membrane fusion steps of the intracellular vesicle trafficking and secretory pathways with the exception of chloroplast and mitochondria; consistent with the endosymbiotic theory their fusion is regulated by another set of proteins (Malsam et al., 2008). SNARE proteins were first identified as indirect receptors for two proteins involved in membrane fusion: NSF (N-ethylmaleimide Sensitive Factor) and SNAP (Soluble NSF Attachment Protein) (Sollner et al., 1993b). SNAREs are small proteins that vary in structure and size but share a defining evolutionary conserved homologous domain of 60-70 amino acids containing eight heptad repeats, termed the SNARE motif, which is crucial for interaction with other SNARE proteins to form a core complex of 4 SNARE motifs to facilitate membrane fusion (Antonin et al., 2002). The number of SNAREs varies between different organisms ranging from 25 in *Saccharomyces cerevisiae*, 36 in *Homo Sapiens*, to 56 in *Arabidopsis Thaliana* (Malsam et al., 2008). The importance of SNAREs for membrane fusion was confirmed by their necessity for neurotransmission since they are the targets of central nervous system proteases

such as Tetanus and Botilinum B neurotoxins (Schiavo et al., 1992). Different SNARE proteins localise to different membrane compartments within cells and are divided into two functional groups: v-SNAREs are found on donor organelles or transport vesicles, and t-SNAREs reside in target organelle membranes (Figure 1-3). The SNARE hypothesis states that a v-SNARE on the vesicle membrane binds to a particular t-SNARE on the target membrane, allowing specific membrane trafficking to occur in the cell (Sollner et al., 1993a). The compartmental specificity of the cell correlates with the physical chemistry of isolated SNAREs. It was shown that it is necessary for three t-SNAREs motifs to reside on one membrane and the appropriate v-SNARE to be located on the opposite membrane for fusion to occur. No other combination of SNAREs located on the opposing membranes results in fusion (Parlati et al., 2000). Only a dozen or so combinations of SNAREs are fusogenic corresponding to the known transport processes. The intracellular distribution of SNAREs is thought to provide a roadmap for membrane trafficking pathways enhancing their role in fusion specificity. Despite the fact that each trafficking pathway seems to be mediated by a specific set of SNAREs some of the SNARE proteins participate in more than one vesicle transport pathway and are able to interact with different SNARE partners (Parlati et al., 2002). This functional redundancy is highlighted by the finding that some SNARE proteins can be substituted with another of the same family (Sorensen et al., 2003). The specificity of SNARE complex assembly is significantly reduced *in vitro*, which underlines the existence of additional regulatory mechanisms *in vivo*.

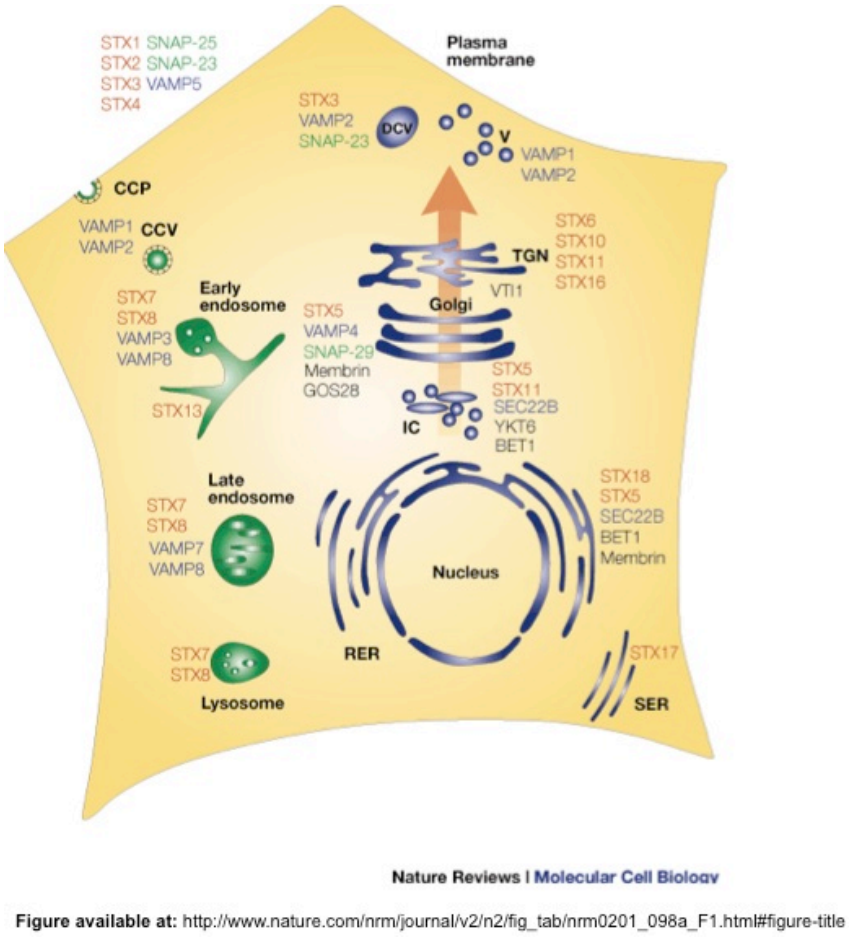

Figure available at: http://www.nature.com/nrm/journal/v2/n2/fig_tab/nrm0201_098a_F1.html#figure-title

Figure 1-3: Intracellular location of mammalian SNARE proteins.

Distinct intracellular locations of mammalian SNAREs enhance the specificity of SNARE mediated membrane fusion. Red: Syntaxin family, green: SNAP25 family, (t-SNAREs) blue: VAMP family (v-SNAREs) and black: other SNAREs. Figure taken from (Chen and Scheller, 2001).

1.2.1 SNARE protein classification

SNAREs were initially classified according to their predominant localization as vesicle-localized (v-SNAREs) or target-membrane-bound (t-SNAREs) (Rothman, 1994). This classification turned out to be somewhat imprecise and ambiguous since the same SNARE proteins can reside on different vesicular or target membranes. A systematic sequence analysis revealed that most v-SNAREs have a well-conserved arginine residue in their SNARE domain (R-SNAREs) and most t-SNAREs (syntaxins and their partners-SNAP25 like proteins-) have an evolutionary conserved glutamine (or aspartate) residue in their SNARE motif (Q-SNAREs) (Fasshauer et al., 1998). Further refinement of this structural, rather than spatial, classification led to sub-classification of Q-SNARES into Qa- (syntaxins), Qb- and Qc-SNAREs (or light chains of t-SNAREs contributed by SNAP25 like

proteins) (Bock et al., 2001). The significance of the classification of SNAREs based on the conserved amino acids in their SNARE motifs is underlined by the fact that all functional SNARE complexes consist of four SNARE domains contributed by one of the four SNARE classes (R, Qa, Qb and Qc) (Sutton et al., 1998). The conserved structure of SNARE complexes shall be described later (section 1.2.3).

1.2.2 Structure of the neuronal-synaptic SNARE proteins

Exocytosis of synaptic vesicles and regulated secretory granules are among the best-studied fusion events. Synaptic vesicles are highly enriched in proteins that mediate vesicle fusion at the active zone (Sudhof, 2004). Neuronal SNARE proteins were first discovered in synaptic vesicle preparations due to their abundance and interaction with one another (Baumert et al., 1989; Bennett et al., 1992; Trimble et al., 1988). The proteins involved in the fusion of the synaptic vesicle and the release of the neurotransmitters are Syntaxin 1A, SNAP25 and VAMP2 (Synaptobrevin 2). In the following sections the description of SNARE proteins and complexes will be limited to the neuronal/synaptic SNARE proteins as it is considered to be paradigmatic for most SNARE complexes studied so far.

1.2.2.1 Syntaxin 1A-(Qa) SNARE family

Syntaxin 1A is a protein composed of 288 amino acids (rat protein). It is found in high concentrations in neurons and neuroendocrine cells but is absent from non-neuronal cells (Lang and Jahn, 2008). Syntaxin 1A is a member of the Qa SNARE class and like most members of this family, is anchored to the membrane by a short C-terminal domain (Masaki et al., 1998). The SNARE domain follows immediately after the transmembrane domain of Syntaxin 1A, carrying the conserved motif essential for interaction with other SNARE proteins. The N-terminal domain is composed of an antiparallel bundle of three alpha helixes (with a small N-terminal extension) called the Habc domain that is linked to the SNARE domain through a long flexible linker (Fernandez et al., 1998). Syntaxin 1A has the ability of intramolecular interaction by folding back its N-terminal domain to contact the SNARE domain forming what is known as the closed conformation (Dulubova et al., 1999). This mechanism of interaction lead to the

suggestion of a regulatory mechanism for SNARE complex formation since the closed conformation of Syntaxin 1A hides its SNARE motif responsible for interaction with other proteins' SNARE motifs (Figure 1-4 A and B).

1.2.2.2 SNAP25-(Qb and Qc) SNARE family

SNAP25 (synaptosomal protein of 25 KDa) is a ubiquitously expressed protein of 208 amino acids (rat protein) that differs from the typical SNARE protein structure in that it contributes two SNARE domains to the SNARE complex (Qb and Qc) (Lang and Jahn, 2008). A flexible linker region joins the two SNARE domains. Since SNAP25 lacks a transmembrane domain the linker contains a cluster of four palmitoylated cysteine residues, which anchor the protein to the membrane (Gonzalo and Linder, 1998). After the discovery of SNAP25 it was revealed that the majority of the non-syntaxin t-SNARE proteins contain only one SNARE domain meaning that two of them participate to the formation of the SNARE complex contributing each one Q helix (either Qb or Qc) (Fukuda et al., 2000). Furthermore the homology between the C- and N- terminus of SNAP25 with Qb and Qc respectively raises the possibility that this protein may have been derived *via* evolutionary fusion of those two t-SNARE light chains. This might explain why SNAP25 represents only a small subgroup of SNAREs with similar structure such as SNAP23, SNAP29 and SNAP47 (Lang and Jahn, 2008) (Figure 1-4 C).

1.2.2.3 VAMP2-(R) SNARE family

VAMP2 (Synaptobrevin 2) is composed of 118 amino acids (rat protein). It is a member of the synaptobrevin protein family. VAMP2 is typically the smallest protein in a core complex contributing an R SNARE domain. It is expressed in neurons and neuroendocrine cells as well as in adipose and muscle cells (Lang and Jahn, 2008). VAMP2 contains a SNARE motif with a short N-terminal domain that lacks any particular structural conformation (Lang and Jahn, 2008) (Sutton et al., 1998). The protein possesses a C-terminal transmembrane domain that localizes VAMP2 on the membranes and it is connected with the SNARE motif *via* a short flexible linker. Several genetic studies using knockout mice lacking VAMP2 underlined its significance in synaptic vesicle fusion (Deak et al., 2004; Schoch et al., 2001) (Figure 1-4 D).

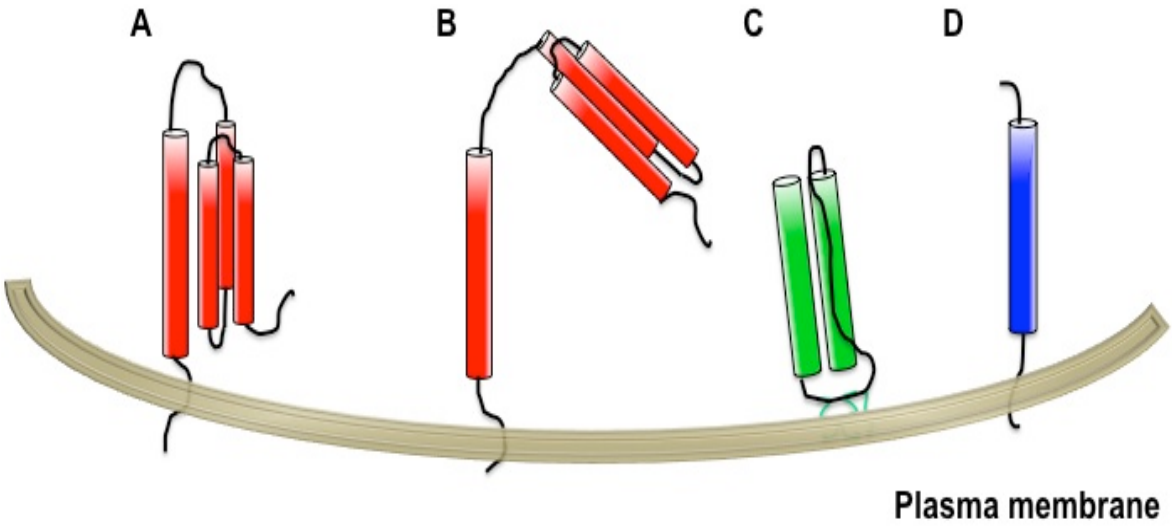

Figure 1-4: SNARE proteins structure.

Schematic diagram of Syntaxin 1A (red), SNAP25 (green) and Synaptobrevin (VAMP2) (blue) attached to plasma membrane. The thick cylinders represent SNARE domains. (A): Syntaxin 1A in its closed conformation where the Habc domain (three thin clustered cylinders) folds and hides the SNARE domain. (B): Syntaxin 1A in its open conformation. Habc domain can move away from SNARE domain to which is attached by a flexible linker. Both representations of Syntaxin 1A are anchored to plasma membrane *via* a transmembrane domain. (C): SNAP25 contains two SNARE domains and is anchored to target membrane through palmitoylated cysteine residues in the linger region between the two SNARE motifs. (D) VAMP2 (synaptobrevin) is attached to vesicle by a C-terminal transmembrane domain (here for simplicity reasons VAMP2 is illustrated attached to plasma membrane).

1.2.3 SNARE complex structure

Individual SNAREs are largely unfolded and relatively unstable (Margittai et al., 2001) in contrast to the fully assembled SNARE complex that is extremely stable and resistant to various denaturing agents such as sodium dodecyl sulphate (SDS) and high temperatures (80^{o}C) (Hayashi et al., 1994). Analysis of the crystal structure at 2.4 Å of the core-region of the neuronal SNARE complex (Sutton et al., 1998) was paradigmatic for all other SNARE complexes studied so far. The SNARE complex, as mentioned previously, consists of four SNARE motifs contributed by the R-SNARE and one each by Qa-, Qb- and Qc-SNAREs. Each of these adopts an alpha helical structure and all 4 are aligned in parallel giving rise to a coiled-coil structure (Sutton et al., 1998). According to the "zipper" hypothesis, assembly of the SNARE complexes is a stepwise procedure that initiates at the N-terminus and proceeds towards the C-terminus, thus pulling the two opposing membranes together and lowering the energy barrier for fusion (Pobbati et al., 2006). Strikingly, new crystallographic data revealed that the

neuronal complex extends into the membrane as continuous helical bundle suggesting a novel additional function of the transmembrane domain of SNARE proteins, along with its primary role as energy transporter for membrane fusion (Stein et al., 2009). This model of SNARE complex assembly proposes that successive layers of interaction between the SNARE domains are formed sequentially one after the other, pulling the two membranes together in a stepwise manner. Indeed the centre of the bundle contains 16 stacked layers of interacting side chains (Sutton et al., 1998). Each layer is formed by four amino acids each contributed by a different SNARE domain. The nature of these interactions is mainly hydrophobic with the exception of the central layer, which is ionic and consists of three glutamine and one arginine residues that are all evolutionary conserved (Fasshauer et al., 1998) (Figure 1-5). Interestingly the positions of the R and Q residues can be swapped among the different SNARE domains without having any affect on the structure of the SNARE complex as a total as long as the 3Q:1R ratio is preserved (Katz and Brennwald, 2000). More crystallographic data from the structure of the endosomal SNARE complex revealed that the helix alignment and the layered structure of interactions are very similar to those of the synaptic complex (Antonin et al., 2002). Taking into consideration that the sequence homology among SNARE proteins is weak (20-30%) (Sudhof and Rothman, 2009), these data indicate that this overall structure is highly conserved.

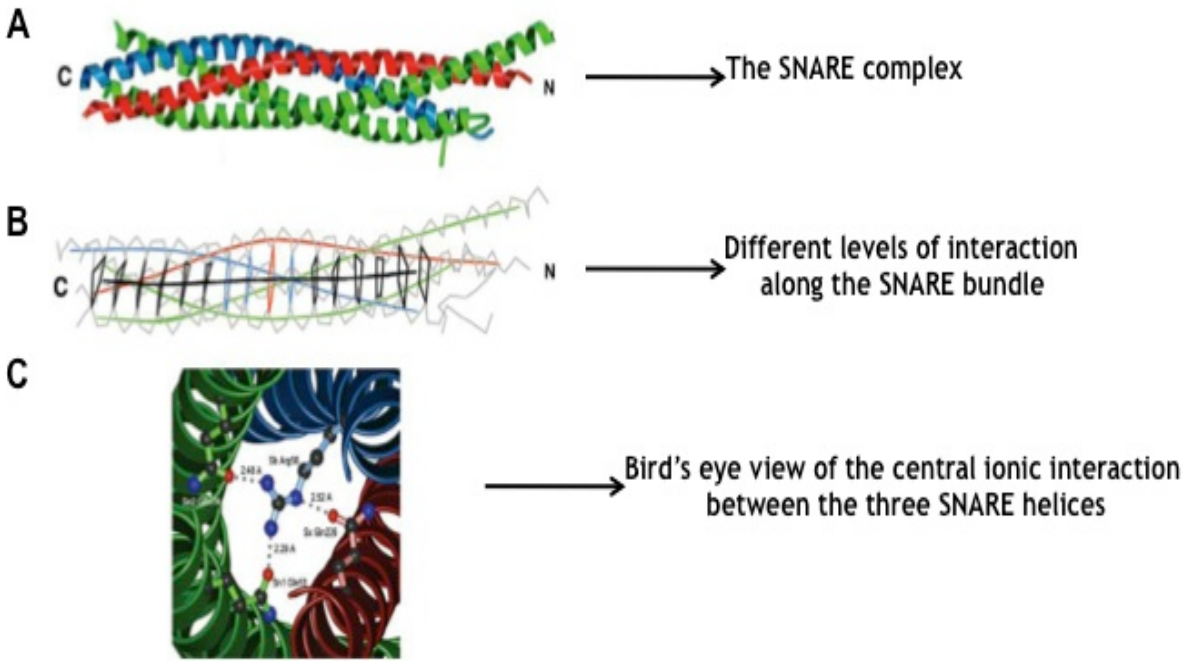

Figure 1-5: SNARE complex structure.

(A): Backbone ribbon diagram of an assembled complex of parallel SNARE domains of Syntaxin 1A (red) VAMP2 (blue) and both domains of SNAP25 (green). (B): Layers of interaction. Each square represents a level of interaction between the four SNARE domains; the central red square illustrates the unique ionic interaction between the four helices. (C): Expanded view of the ionic central layer. An arginine residue from Synaptobrevin interacts with three glutamine residues from Syntaxin 1 and SNAP25. Figure edited from: (Sutton et al., 1998)

1.3 SNARE mediated membrane fusion

The primary function of SNARE proteins is to drive the fusion of the membranes. Initial *in vitro* data indicated that SNARE mediated fusion was significantly slower compared to the speed of fusion observed *in vivo* (Weber et al., 1998). This likely reflects a high level of regulation of membrane fusion machinery in eukaryotic cells. There are many proteins that interact with SNAREs and these may serve to fine-tune and control SNARE-mediated membrane trafficking. Membrane fusion is a multistep procedure that begins with the unbound vesicle containing a v-SNARE on its membrane coming into close proximity to the target membrane where the t-SNARE proteins are localized. During the next steps of docking and tethering the vesicle comes in contact with its cognate membrane *via* a series of molecular interactions. Rab proteins and their effectors function in tethering and docking and this extensive protein family of small GTPases are thought to play a role in the specificity of membrane fusion through interactions

with SNARE proteins (Zerial and McBride, 2001). As the vesicle aligns the syntaxin on the target membrane adopts its "open" conformation by unfolding the Habc domain and revealing its SNARE motif. The following priming step (or nucleation) requires the four SNARE domains to form the core complex, which is known as the trans-complex with participating SNAREs bound to opposing membranes (Parlati et al., 2000). This interaction of proteins facilitates membrane fusion since assembly of SNARE complex is associated with a major release of energy, which is used to compensate the repulsing force of the two merging membranes (Figure 1-6). The resultant SNARE complex is known as *cis*-complex, with the SNARE proteins now located on the same membrane following fusion (Sollner, 2003). Consequently the SNAREs need to be liberated from the SNARE complex to perform further rounds of fusion. This procedure is ATP dependent and is an important stage in the cycle of SNARE complex assembly (Lang and Jahn, 2008). Recycling of SNARE proteins from the highly stable *cis*-complex is carried out by the specialized adenosine triphosphatase (ATPase) NSF (N-ethylmaleimide sensitive factor) and its adaptor SNAP. SNAP binds directly to the *cis*-SNARE complex and recruits the ATPase (Brunger, 2005). NSF functions as a hexamer that uses three to six ATP molecules per SNARE complex (Rizo and Sudhof, 2002). The hydrolysis of ATP induces major conformational changes in, and leads to the disassembly of, the *cis*-SNARE complex to its free constituents (Sudhof and Rothman, 2009) (Figure 1-7).

The minimum number of SNARE complexes required for membrane fusion it is controversially debated. Exocytosis of synaptic vesicles during fast synaptic transmission was used as a model to estimate the number of necessary SNARE complexes. Various studies have proposed that several of these SNARE complexes might assemble in cyrcle-shaped multivalent supercomplexes, forming a ring, around the fusion pore; nonetheless, there is no direct evidence to support this model (Montecucco et al., 2005; Tokumaru et al., 2001). Based on this model the number of required SNARE complexes varies from 3 to 15 (Weber et al., 1998). Quite recently performance of controlled *in vitro* Förster resonance energy transfer (FRET) experiments revealed that liposomes bearing only a single SNARE molecule are still capable of fusion with other liposomes or with purified synaptic vesicles (van den Bogaart et al., 2010). One year later Jahn and his colleagues proposed that 2 synaptobrevins (VAMP2) and

subsequently 2 SNARE complexes are necessary for fusion of synaptic vesicle to plasma membrane based on fluorescence responses from single fusing vesicles expressing synaptopHluorin experiments (Sinha et al., 2011). All these contradictory data and models make the identification of the minimum required number of SNARE complexes sufficient to drive membrane fusion very challenging.

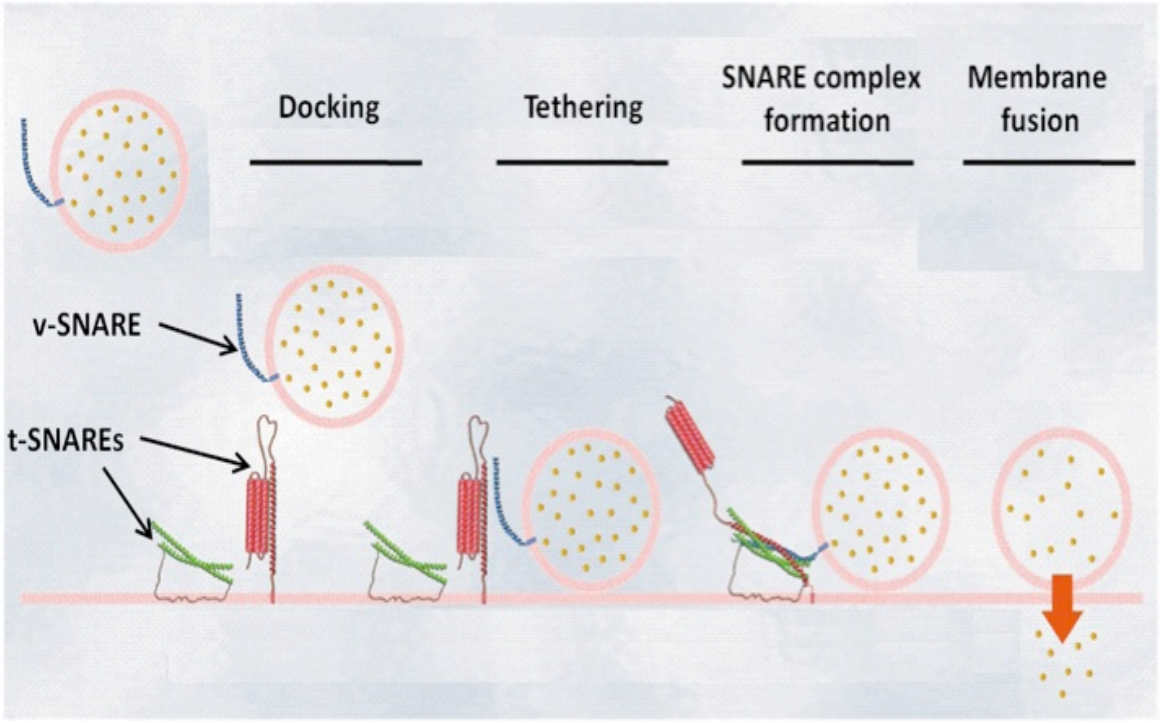

Figure 1-6: SNARE mediated membrane fusion.

Diagram outlining the final fusion step of a vesicle approaching the target membrane a syntaxin like SNARE protein (red), Synaptobrevin (VAMP2) like SNARE protein (blue) and SNAP25 like SNARE protein (green) facilitate the fusion. The Habc domain of syntaxin folds back to reveal its SNARE domain, which can now interact with the other SNARE domains of the cognate t- and v-SNAREs to form the core SNARE complex which triggers the membrane fusion. Figure edited from (Toonen and Verhage, 2003).

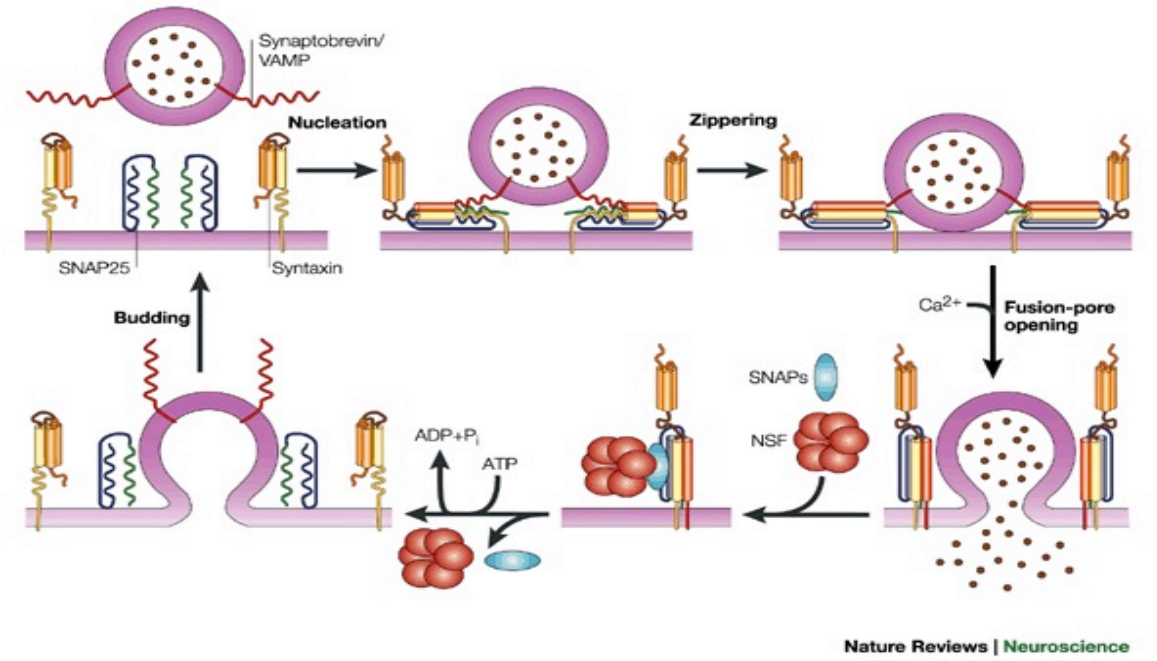

Figure available at: http://www.nature.com/nrn/journal/v3/n8/fig_tab/nrn898_F1.html

Figure 1-7: SNARE complex cycle.

Cycle of assembly a disassembly of the SNARE complexes in synaptic vesicle exocytosis. From top left clockwise: The syntaxin adopts its open conformation and the zippering of the SNARE domains starts, leading to formation of a *trans*-SNARE complex. After membrane fusion the *cis*-complex is disassembled into monomeric SNARE proteins, by NSF and SNAP proteins. Consumption of energy is required in order for a new cycle to begin. Picture taken from (Rizo and Sudhof, 2002).

1.3.1 Regulation of SNARE mediated membrane fusion

Although SNARE proteins comprise the molecular machinery that performs membrane fusion by providing the necessary energy *via* SNARE complex formation, they are not the sole mediators of membrane fusion. Membrane fusion is a rapid process that needs to be well orchestrated both spatially and temporally. Several different protein families appear to work in concert to regulate both the membrane fusion function and specificity of SNAREs (Lang and Jahn, 2008).

1.3.2 Sec1/Munc18 (SM) proteins

SM proteins were initially discovered in genetic screens for membrane traffic defects which led to either secretion deficiency in *Saccharomyces cerevisiae* (Novick et al., 1980) or uncoordinated movement in *Caenoharbditis elegans*

(Brenner, 1974). Family members have subsequently been identified in other eukaryotes. The genomes of *Saccharomyces cerevisiae*, *Caenoharbditis elegans*, *Drosophila melanogaster*, *Mus musculus* and *Homo sapiens* each contains four to seven SM genes. Due to small number of SM proteins it is apparent that some of them participate in more than one membrane trafficking pathway (Toonen and Verhage, 2003). These cytosolic proteins of 60-70 KDa size are composed of three domains that form an arch shaped molecule with a central cleft (Bracher and Weissenhorn, 2002; Misura et al., 2000). Loss of function mutations in various species leads to a block of the corresponding fusion reaction, severe impairment of vesicle trafficking and even in some cases, which the transport step is essential for cell survival, to organism death (Toonen and Verhage, 2003; Verhage et al., 2000). SM proteins have a higher sequence homology than SNARE across their entire length which indicates a conserved overall structure and function (Sudhof and Rothman, 2009). In contrast to SNAREs, SM proteins do not appear to have functional redundancy although SM proteins from different and distant species can replace each other in the case of participating at the same vesicular trafficking pathway (Gengyo-Ando et al., 1996; Khan et al., 2001).

Consistent with a key role in regulating membrane traffic, most SM proteins have strong binding affinity (dissociation constants are in the nanomolar range) for their cognate syntaxins (Pevsner et al., 1994; Smyth et al., 2010). Originally it was believed that SM proteins were limited only to ensuring specificity of fusion and their function could be determined by this specific interaction. Further investigations revealed that SM proteins interact not only with syntaxins but with other members of the SNARE family through a variety of biding modes (Toonen and Verhage, 2003). While this confusing variety of binding modes between SM proteins and SNAREs has attracted intense research into SM proteins as critical regulators of SNARE mediated fusion, with various proposed functional roles being hypothesised, this heterogeneity of ideas regarding their function makes the proposal of a unifying model, which can describe their role, a very challenging issue.

1.3.2.1 Mode-1 binding

As it was mentioned previously Syntaxin 1A (section 1.2.2.1) can adopt a so-called closed conformation *via* intramolecular interaction of its Habc domain

with its SNARE motif. This structural conformation prohibits the SNARE domain from interacting with the other cognate SNARE motifs and thus prevents the assembly of the core SNARE complex. This closed conformation of Syntaxin 1A is required for Munc18-1 binding (Dulubova et al., 1999). *In vitro* binding studies, nuclear magnetic resonance (NMR) and crystallographic data helped to characterise this binding mode (Misura et al., 2000; Yang et al., 2000). According to these data Munc18-1 has three domains forming an arch shaped structure with a central cavity formed by domains I and III. Almost the entire cytosolic domain of Syntaxin 1A is required, in a closed conformation, to bind to that central cleft of the SM protein (Misura et al., 2000). Characterisation of this binding mode led to the proposal of an inhibitory role of SM proteins by stabilization of the closed structure of syntaxin preventing the assembly of the core SNARE complex and thus the membrane fusion (Figure 1-8). However, genetic studies showed that deletion of Munc18-1 results in a block of in vesicular transport (Verhage et al., 2000). Additionally, more studies involving SM/syntaxin binding revealed that SM protein binding is not inhibitory to fusion (Carr et al., 1999; Scott et al., 2004). These results led to the assumption that binding of Munc18-1 to closed Syntaxin 1A is an atypical feature restricted to neuronal exocytosis that might have evolved to meet its specific requirements (Lang and Jahn, 2008).

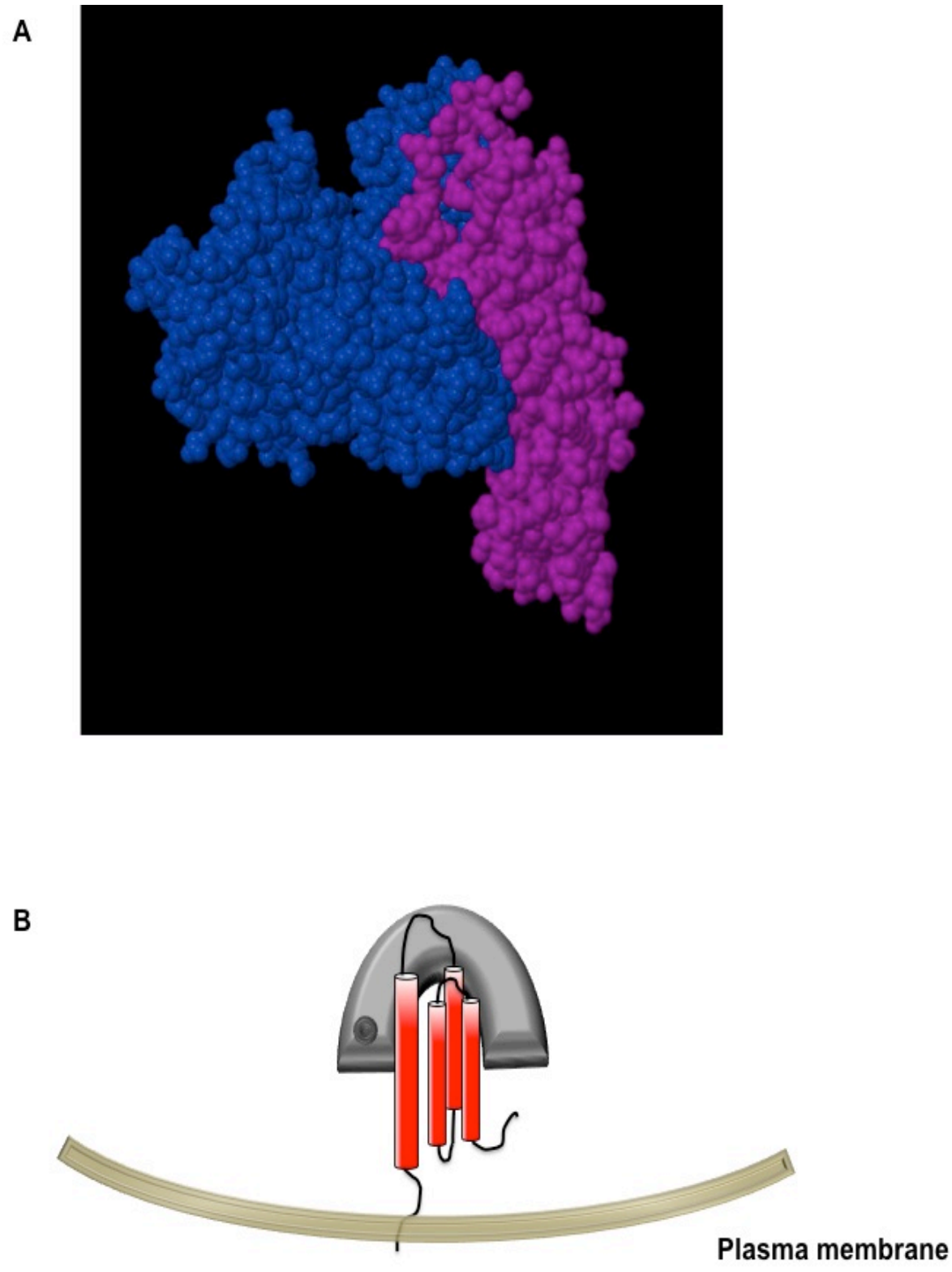

Figure 1-8: Mode 1 binding of SM proteins.

(A): Space filling diagram of Munc18-1 (blue) in complex with Syntaxin 1A (purple). Picture was edited using Rasmol software. PDB accession code: 3C98. (B): schematic diagram of mode 1 binding between SM protein (grey) and syntaxin (red) anchored to plasma membrane. Habc domain of syntaxin interacts with the SNARE domain in a closed conformation. SM protein binds to syntaxin by clasping the closed conformation in its central cavity.

1.3.2.2 Mode-2 binding

In stark contrast to the interaction between the neuronal pairing of Munc18-1 and Syntaxin 1A, the yeast syntaxin Sed5 in the Golgi apparatus binds to its cognate SM protein Sly1 in a totally different way. This mode of binding does not require the syntaxin to form a closed conformation. Indeed, only the N-terminal 44 residues of Sed5 are sufficient to bind Sly1 (Yamaguchi et al., 2002). The crystal structure of Sly1 was shown to be an arch shape very similar to that of Munc18-1, but the central cavity is not involved in binding Sed5. Instead the N-terminal peptide of the syntaxin inserts into a hydrophobic pocket on the outer face of the SM protein (Bracher and Weissenhorn, 2002) (Figure 1-9). Similar results have been found for the yeast Tlg2 (syntaxin like protein)/Vps45 (SM protein) and their mammalian orthologues Syntaxin 16/mVps45 which are involved in *trans*-Golgi network/ early and late endosome vesicle trafficking (Dulubova et al., 2002). Quite strikingly Munc18c has been shown to bind Syntaxin 1A not only its closed conformation but via its N-terminus as well (Khvotchev et al., 2007; Shen et al., 2007). Mode-2 binding is consistent with the SM protein binding either to an open or closed conformation of the cognate syntaxin. Additionally this binding mode could allow simultaneous binding of SM proteins to SNARE complexes which has been proposed to facilitate assembly (see section 1.3.2.3). This mode of binding does not support a negative/inhibitory role for the SM proteins regarding the membrane fusion (Bryant and James, 2001; Peng and Gallwitz, 2002).

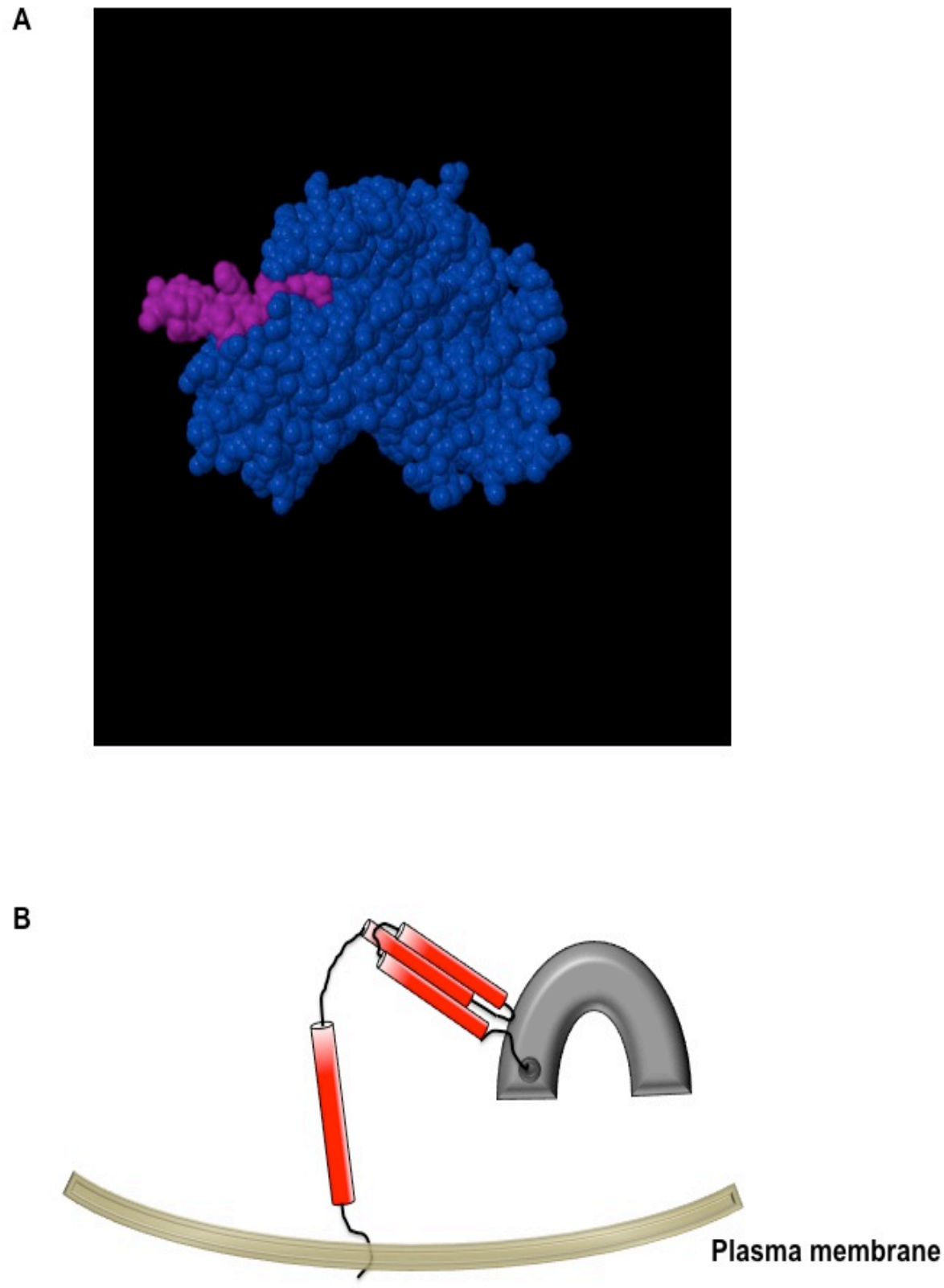

Figure 1-9: Mode 2 binding of SM proteins.

(A): Space fill diagram of Munc18c (blue) in complex with N-terminal segment of Syntaxin 4 (purple). Picture was edited using Rasmol software. PDB accession code: 2PJX. (B): schematic diagram of mode 2 binding between SM protein (grey) and syntaxin (red) anchored to plasma membrane. N- terminus of syntaxin interacts with a hydrophobic pocket on the surface domain I of SM protein. This binding mode does not argue against syntaxin's open conformation in which Habc domain folds back and reveals SNARE motif.

1.3.2.3 Mode-3 binding

SM proteins have also been found to bind assembled SNARE complexes. This appears to be a common feature of almost all SM proteins. It was first reported for the yeast SM protein Sec1, which regulates the fusion of vesicles with the plasma membrane (Carr et al., 1999). It is interesting that despite the fact that Sso1 protein (the Sec1 cognate syntaxin) can adopt a closed conformation akin to that first (Munson et al., 2000) Sec1 binds very weakly to it (Scott et al., 2004). SM proteins bind to either *cis* or *trans*-SNARE complexes preferentially. One interesting example is the yeast SM protein Vps45 that dissociates from its cognate syntaxin Tlg2 before fusion, does not bind to *trans*-SNARE complex, but associates again after fusion through binding to the *cis*-SNARE complex (Bryant and James, 2003). Munc18-1, which binds syntaxin 1A in its closed conformation with high affinity, has also been shown to bind fully assembled SNARE complexes (Dulubova et al., 2007; Latham et al., 2007). This binding mode (Figure 1-10) is is the least well-characterised of the 3 but has been hypothesised to facilitate contribute to the specificity of membrane fusion by 'proof reading' assembled SNARE complexes and only stimulating fusion of cognate SNARE complex members.

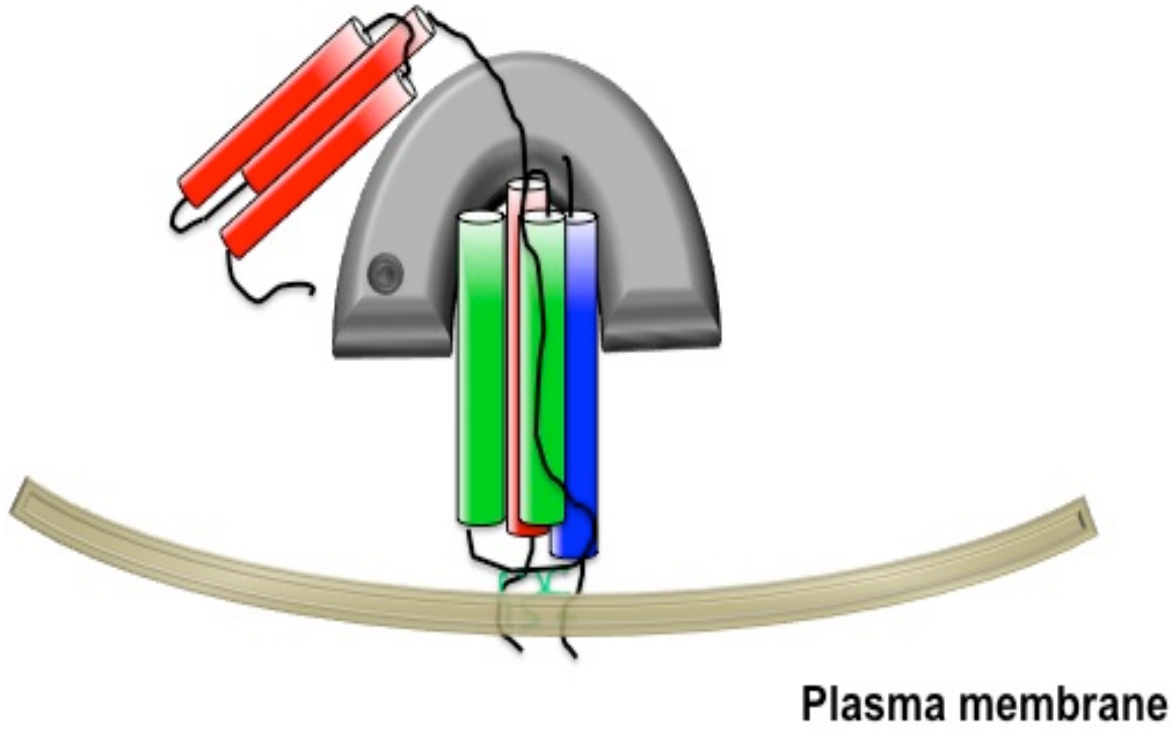

Figure 1-10: Mode-3 binding of SM proteins.

Schematic diagram of mode-3 binding between SM protein (grey) and ternary *cis*-SNARE complex that consists of SNARE domains of syntaxin-like protein (red), VAMP2-like protein (blue), both t-SNARE proteins are anchored to plasma membrane *via* their C-terminal transmembrane domains and SNAP25-like protein (green), which is anchored to plasma membrane by plamitoylated cysteine residues in its linker region. SM protein clasps the ternary SNARE complex in its central cavity. Since there is no crystal structure of SM protein interacting with ternary SNARE complex, the schematic representation of mode-3 is based on biochemical analysis of the proteins involved, and so the orientation and the relative positions of proteins are presumed.

1.3.2.4 Other SM protein interactions

SM proteins have also been shown to bind syntaxins indirectly. The yeast SM protein Vps33 is a part of a larger complex (C-Vps or HOPS complex) that functions in membrane traffic from the Golgi to the vacuole and binds the syntaxin homolog Vam3 (Sato et al., 2000). As discussed above Sly1 binds strongly to the syntaxin Sed5 on Golgi membranes. A significant fraction of Sly1 localises to the Golgi apparatus in a Sed5-independent manner through interaction with other Golgi non-syntaxin, SNARE proteins (Peng and Gallwitz, 2004). Other SM proteins have subsequently been found to bind to non-syntaxin SNAREs. These include Vps45 binding directly to its cognate v-SNARE Snc2 as well as to its syntaxin Tlg2 (Carpp et al., 2006) and the mammalian SM protein

Munc18c, which binds to the v-SNARE VAMP2 as well as to Syntaxin 4 (Brandie et al., 2008).

Many SM proteins interact with tethering factors and Rab proteins that play an important role in directing transport vesicles to the appropriate target membrane (see sections 1.3.4.1 and 1.3.4.2). Quite recently, a direct interaction between the Golgi SM protein Sly1 and the N terminal portion of Cog4 has been identified (Laufman et al., 2009). Gog4 is one of the components of a multisubunit-tethering factor called conserved oligomeric Golgi (COG) complex. Additionally, SM protein Vps45 has been shown to indirectly associate with Rab5 through an interaction with one of Rab5 effectors, Rabenosyn-5 (Nielsen et al., 2000). Furthermore genetic studies using Rab3a mutants locked in the GTP- or GDP-bound form in wild-type and Munc18-1 null mutant mammalian chromaffin cells revealed association of Rab3a with Munc18-1 (van Weering et al., 2007). These findings point towards an involvement of SM proteins in the tethering and docking steps of vesicle trafficking and illustrate how the many regulatory proteins act in concert to achieve the exquisite control required.

1.3.3 The role of SM proteins-forming a universal model

The role of SM proteins does not appear to be restricted to regulation of SNARE complex assembly. SM proteins also seem to act as chaperone like molecules for their corresponding syntaxins. Munc18-1 null mice have low levels of Syntaxin 1A (Verhage et al., 2000). Similarly, yeast cells that lack the SM protein Vps45 and showed decreased levels of Tlg2 (syntaxin like protein) (Bryant and James, 2001). The rate of Tlg2 synthesis in these cells is not affected and thus it seems that syntaxins protect their cognate SM proteins from degradation. In mice heterozygous for a Syntaxin 4 null allele, Munc18c protein levels are reduced by 40% (Yang et al., 2001). It has been suggested that SM proteins might protect syntaxins from premature membrane reactions while they are transferred to their specific membrane (Medine et al., 2007; Rowe et al., 2001).

Another essential role for SM proteins is that they confer specificity to SNARE-dependent trafficking. As it was mentioned previously there is no preference *in vitro* between SNARE motifs for the complex assembly (as long as R, Qab and c

SNARE domains are present) (Fasshauer et al., 1999; Yang et al., 1999). In contrast, *in vivo* experiments have illustrated that there is no functional redundancy between the SM proteins. This may indicate that specificity of intracellular trafficking is more a function of the SM proteins than the SNARE proteins. Furthermore the implication of SM proteins in tethering and docking procedures during vesicle trafficking (Nielsen et al., 2000; van Weering et al., 2007), stresses the importance of SM proteins for the specificity of vesicular trafficking. The ultimate role of SM proteins is perhaps based on their ability to interact with SNARE complexes. They are fundamentally designed to clasp four-helix bundles (a feature of SM proteins that explains the binding of Munc18-1 to closed Syntaxin 1A) (Sudhof and Rothman, 2009). Their established ability to bind SNARE complexes could not only contribute to the specificity of fusion by proofreading essential sequences of assembled SNARE complexes, but also to the stimulation of fusion of cognate complexes as well (Shen et al., 2007). A kinetic role in which SM proteins assist in the assembly of a productive complex is very appealing (Rizo et al., 2006). In other words SM proteins can be considered as regulators of SNARE function, while SNAREs provide the mechanistic force for membrane fusion (Sudhof and Rothman, 2009). Finally the binding of SM proteins to *cis*-SNARE complexes might suggest a regulatory role downstream of membrane fusion for example in SNARE complex disassembly and SNARE protein recycling (Bryant and James, 2003). Until recently, quite diverging working models existed for the central role of SM proteins. The confusing variety of different binding modes between SM proteins and their cognate syntaxins and SNARE complexes makes the proposal of a unifying and universal model of SM protein action in membrane fusion very difficult and challenging. The first established binding mode (Munc 18-1/ closed Syntaxin 1) led to the assumption that SM proteins have a negative role in membrane fusion, by preventing assembly of the core SNARE complex (Pevsner et al., 1994). However, SM proteins are required in all fusion reactions. Genetic screens of proteins involved in fusion reactions have identified all the SM genes. These findings clearly underlined the importance of SM proteins for SNARE-mediated membrane traffic (Brenner, 1974; Novick et al., 1980). Furthermore numerous loss of function mutations, in various SM genes, and different species, all lead to an impairment in vesicle trafficking (Toonen and Verhage, 2003). These findings all point towards to a positive role for SM protein function in membrane fusion.

However, the method by which SM proteins facilitate fusion remains unclear. The identification of the N-terminus binding mode of syntaxin to a hydrophobic pocket on the surface of SM proteins shed some light in understanding how SM proteins facilitate SNARE complex formation. This mode of binding allows syntaxins to interact both with SM protein and the other SNAREs as the SNARE domain is free to form the core SNARE complex. There are data that underline the importance of the N-terminus binding mode in triggering membrane fusion. Indirect perturbation of this binding mode in mammalian cells leads to trafficking defects (Munson and Bryant, 2009). Moreover, two different mutants in *C. elegans*, each one selectively disrupting mode 1 or 2 binding, revealed the significance of the N-terminus binding mode for vesicle trafficking, in contrast to the first binding mode that seems not to be essential (Johnson et al., 2009). The identification of mode 2 additionally to mode 1, binding between Munc18-1/Syntaxin 1A, (Burkhardt et al., 2008) further supports the importance of N-terminus binding for membrane fusion. Although these findings emphasise mode 2 binding importance for fusion, there is also evidence that argues against the central role of N-terminus binding for regulation of SNARE mediated membrane fusion. As it is in the case of its direct abolition in two different yeast SM proteins, Sly1 (Peng and Gallwitz, 2004) and Vps45 (Carpp et al., 2006) that did not result in any obvious defective phenotype. However, if we take into consideration that SNARE complex assembly/disassembly is a multistep process and each trafficking pathway is likely to have a different rate-limiting step, the absence of any obvious defective phenotype might illustrate that the step regulated by the function of SM protein that has been perturbed is not rate limiting for the pathway being examined (Munson and Bryant, 2009). The idea that the SM protein can transition between binding modes during the various steps of SNARE assembly/disassembly cycle becomes more and more appealing (Figure 1-11). This view incorporates all modes of SM and SNARE protein interaction that have been identified. It also may go some way to explain the contradictory data regarding the positive or the negative roles of SM proteins for membrane fusion.

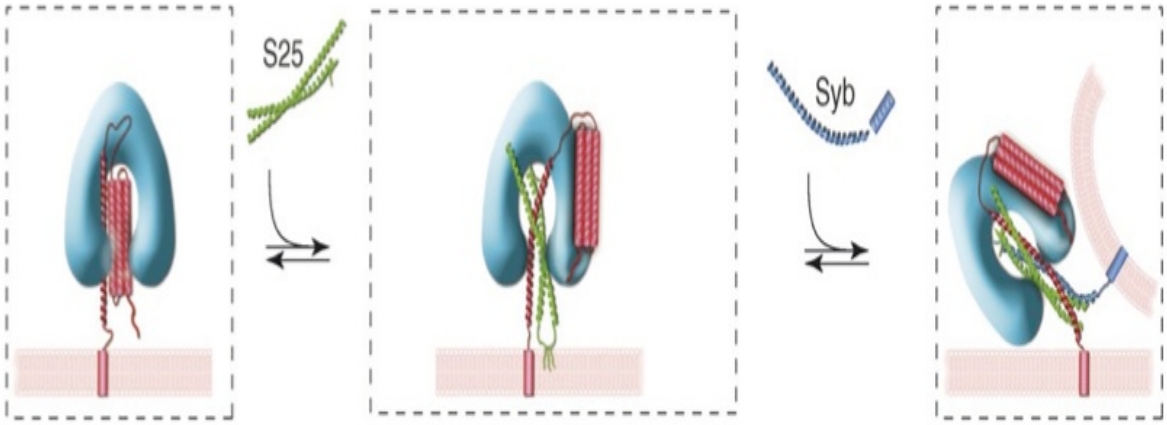

Figure 1-11: Schematic diagram illustrating the current model of SM proteins function.

SM protein (blue arch shaped molecule), syntaxin-like protein (red), SNAP25-like protein (green) and VAMP2-like protein (blue). From left to right: SM protein binds to closed syntaxin. N-terminus of syntaxin interacts with a hydrophobic pocket on the surface of SM protein which results in a conformational change of the former in order to be able interact first the SNAP25-like and later the VAMP2-like SNARE domains and form the ternary SNARE complex. Finally SM protein binds with *trans*-SNARE complex *via* its central cavity. Figure edited from (Toonen and Verhage, 2007)

1.3.4 Other regulatory factors of SNARE-mediated membrane fusion

Membrane trafficking is accomplished through the fusion of vesicles with different cellular organelles and/or the plasma membrane. Vesicle fusion is achieved by the assembly of SNARE complexes at the site of fusion. Before, during and after fusion various factors participate in this process acting to coordinate it. Some of these factors are discussed bellow.

1.3.4.1 Tethering factors

Tethering factors comprise a group of proteins that are responsible for enhancing membrane trafficking specificity. Their primary role is the mediation of the first physical contact between the target membrane and the approaching vesicle (Pfeffer, 1999). A crude distinction between types of tethering factors can be made as to whether they comprise of large multi-subunit complexes or are long coiled-coil proteins (monomers or homo-dimers) (Whyte and Munro, 2002). The yeast tethering factor Uso1 is a long parallel homo-dimer with two globular heads at the N-terminus coiled-coil tethering factor (Yamakawa et al., 1996). It functions to mediate bending of endoplasmic reticulum derived

vesicles (Barlowe, 1997), and it has been suggested that it also facilitates their fusion to the Golgi apparatus by assisting the formation of functional SNARE complexes (Sapperstein et al., 1996). Multi-subunit tethering factors vary from one another as far the number and the structure of the single protein units are concerned. Despite this, numerous of them have been found to be conserved across different species (Whyte and Munro, 2002). The best-characterized conserved tethering complex factor is the exocyst, it was first identified at the sites of vesicle fusion with the plasma membrane of *S. cerevisiae* (TerBush et al., 1996). The exocyst is an octameric protein complex involved in vesicle trafficking, specifically spatial targeting and tethering of post-Golgi vesicles with the plasma membrane prior to vesicle fusion (Whyte and Munro, 2002). The exocyst is composed of eight subunits that aggregate in a polar fashion. In *S. cerevisiae*, there are eight subunits: Sec3, Sec5, Sec6, Sec8, Sec10, Sec15, Exo70, and Exo84 (TerBush and Novick, 1995). Mammalian homologues have also been identified, indicating its importance for membrane fusion in all eukaryotes (Kee et al., 1997). Sec3 and Exo70 subunits are localized to the plasma membrane and are physically attached to the membrane by Rho GTPases such as CDC42. In contrast Sec15 and Sec4 are located to vesicle membranes (He and Guo, 2009). Exocyst proteins on the plasma membrane bind to vesicular exocyst proteins through recruitment of the rest units of the complex and finally bring the vesicle into close proximity to the plasma membrane. This allows SNARE proteins to form a coiled coil and to execute membrane fusion (He and Guo, 2009). The exocyst belongs in a subgroup of tethering complexes, named quatrefoil, which are made up of multiples of four (Whyte and Munro, 2002). Other members include the COG complex and the Golgi associated retrograde protein (GARP) complex, associated with intra-Golgi (Wuestehube et al., 1996) and Golgi-endosomal (Conboy and Cyert, 2000) trafficking respectively. There are other tethering complexes that do not belong to quatrefoil family. These are the transport protein particle (TRAPP I) complex associated with ER-Golgi traffic, and TRAPP II that has a less well characterised connection to later Golgi traffic (Sacher et al., 2008), the Dsl1p complex that is related to reversing traffic from the Golgi to the ER (Andag et al., 2001) and has yet to be characterised. Finally the HOPS complex is associated with vacuolar trafficking (Ostrowicz et al., 2008) contains the SM protein Vps33p (mentioned in section 1.3.2.4). Components of tethering complexes do not share great sequence

homology but they do have similar rod-like structures composed of two or more successively packed helical bundles, with each bundle containing of three to five a-helices linked by unstructured linkers (He and Guo, 2009). These findings suggest that all these different components of multi-subunit tethering factors may have evolved and diverged from a common ancestor (Cavanaugh et al., 2007; Tripathi et al., 2009).

1.3.4.2 Rab proteins

Preservation of undisrupted membrane trafficking between organelles is fundamental to the existence of eukaryotic cells. Ras-associated binding proteins (Rab) play central role in coordinating membrane traffic and fusion events. Rab proteins belong to the largest family of small GTPases (20-29 kDa). There are abundant isoforms which are present across different species (11 in budding yeasts, 29 in *C. elegans* and *D. melanogaster* and ~70 in human and rodents (Fukuda, 2008)). Rab proteins function as molecular switches that alternate between two conformational states: the GDP bound (inactive) and the GTP bound (active) (Stenmark, 2009). Interchanging between these two states is tightly regulated by two distinct groups of enzymes: guanine nucleotide exchange factor (GEF) that stimulates binding of GTP and switches Rab proteins to their active state (Delprato et al., 2004) and GTPase-activating proteins (GAP) that enhance the hydrolytic properties of Rab proteins, which eventually hydrolyse bound GTP to GDP (Pan et al., 2006). Rab proteins are maintained to their inactive state (GDP bound) by a factor termed Rab GDP dissociation inhibitor (GDI), which prevents release of GDP from Rab (Matsui et al., 1990). This factor along with Rab escort proteins (REP) (Alexandrov et al., 1994) mediate the delivery of Rabs to their cognate membranes (vesicles, organelles and plasma membrane) and back to the cytosol (Ullrich et al., 1993). Active Rab proteins (GTP bound) can interact with several types of effector molecules that vary from sorting adaptors, tethering factors and rotors to phosphatases and kinases (Stenmark, 2009). This considerable variety of effector molecules dictates the wide range of Rab functionality, regarding vesicle trafficking. Rab proteins are involved in every single membrane trafficking event; including vesicle budding (Carroll et al., 2001), uncoating (Semerdjieva et al., 2008), motility (Seabra and Coudrier, 2004) and fusion (Ohya et al., 2009). A representative example of a mammalian Rab protein involved in membrane

trafficking is Rab10. This protein is implicated in the regulation of facilitative glucose transporter 4 (GLUT4) vesicle trafficking in adipocyte and muscle cells. During insulin signal transduction, insulin-dependent kinase Akt substrate AS160 serves as Rab-GAP for Rab10 (Sano et al., 2008). Abolition of Rab10 by siRNA results in inhibition of GLUT4 translocation in adipocytes (Sano et al., 2008). These findings illustrate the important role Rab proteins play in coordinated membrane trafficking.

1.4 Glucose transport

1.4.1 Glucose homeostasis and type 2 diabetes

Glucose is a fundamental source of energy for all eukaryotic cells. In mammals, under normal physiologic conditions, plasma glucose remains within a narrow range between 4 and 7 mM. Glucose homeostasis is regulated by the opposing function of two hormones, glucagon which increases plasma glucose levels and insulin, which decreases plasma glucose levels. Insulin is produced by the beta-cells of the pancreatic islets of Langerhans and secreted into the bloodstream in response to glucose uptake by these cells (Bell and Polonsky, 2001). Insulin receptors (members of the tyrosine kinase family of receptors) on the cell surface of peripheral insulin-sensitive tissues receive the insulin signal and initiate a cascade of intracellular signalling events resulting in an increase in the uptake of glucose into these cells and modification of their metabolic profile (Saltiel and Kahn, 2001). Defects within beta-cells and/or peripheral tissues (adipose, muscle) can result in hyperglycaemia. Hyperglycemia is a major symptom of a heterogeneous group of disorders called Diabetes Mellitus. At a clinical level there are two major forms of diabetes: type 1 diabetes, previously known as juvenile or insulin-dependent diabetes, and type 2 diabetes previously known as adult or non-insulin-dependent diabetes. Type 1 diabetes is caused by a deficiency in the production and/or secretion of insulin by the beta cells usually due to beta cell destruction. Type 2 diabetes has different aetiology that is characterized by variable degrees of insulin-resistance in peripheral tissues, and beta-cell dysfunction. The global prevalence of type 2 diabetes is predicted to reach 300 million cases by 2025 (Zimmet et al., 2001).

1.4.2 Glucose transporters and GLUT4

Insulin maintains glucose homeostasis largely by increasing glucose uptake into muscles (80% of the total blood circulating glucose), adipose (15%) and other insulin responsive tissues (Jewell et al., 2010). This is a process mediated by the facilitative glucose transporter 4 (GLUT4). Glucose transporters (GLUTs) are a family of integral membranes proteins that shuttle sugars across the cell membrane. GLUTs are predicted to span the membrane 12 times with both amino- and carboxyl-termini exposed to the cytosol (Bryant et al., 2002) (Figure 1-12). The GLUT protein family consists of 13 members that are divided in 3 different subgroups according to sequence homology, structural similarity and kind of the sugar that transport: Class 1, which includes GLUTs 1 to 4 (glucose transporters), class 2, which includes GLUTs 5,7,9 and 11 (fructose transporters) and class 3, which includes GLUTs 6,8,10,12 and HMIT1 (structurally atypical and functionally undefined at present) (Bryant et al., 2002). More than 30 years ago two independent investigations of insulin action in adipocyte cells revealed that insulin triggers the translocation of glucose transporters from an intracellular pool to the plasma membrane (Cushman and Wardzala, 1980; Suzuki and Kono, 1980). Almost 10 years later it was clarified that insulin stimulates the translocation of only one GLUT protein, GLUT4 (James et al., 1988), which was later cloned (James et al., 1989). The effect of insulin on GLUT4 was shown subsequently to occur in other insulin responsive tissues such as heart (Watanabe et al., 1984) and skeletal muscle (Hirshman et al., 1990). All these findings put GLUT4 and its trafficking at centre of research into insulin-regulated glucose uptake.

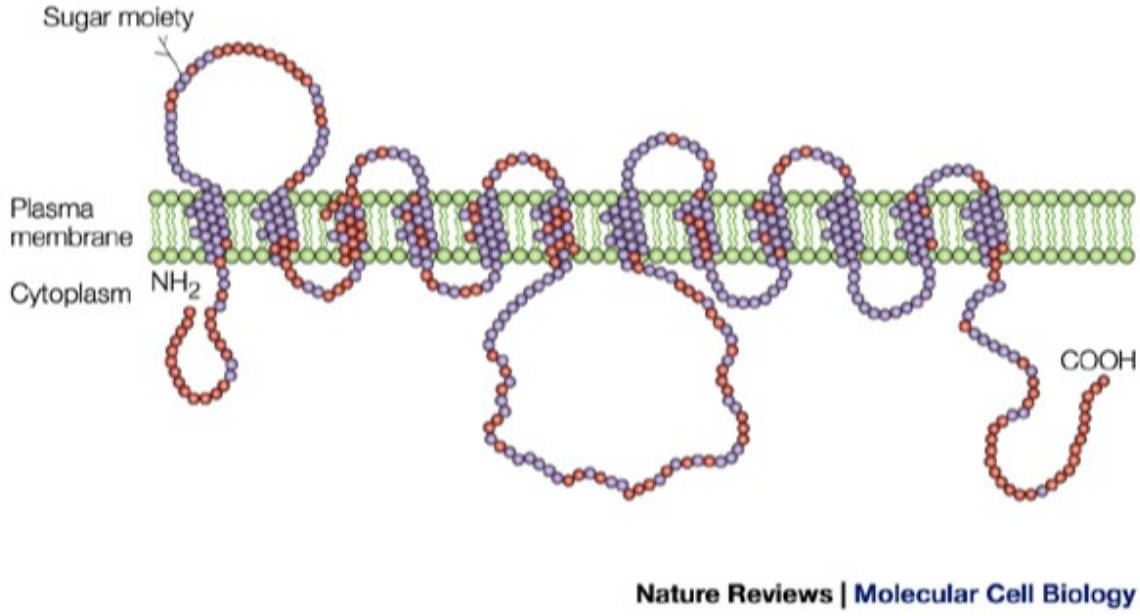

Figure available at: http://www.nature.com/nrm/journal/v3/n4/fig_tab/nrm782_F1.html

Figure 1-12 Schematic representation of a typical glucose transporter.

Glucose transporters are predicted to have 12 helical transmembrane spanning domains with N- and C-termini of the transporter cytosolically disposed. Glucose transporters have two large loops one extracellular that connects transmembrane helices one and two and one intracellular connecting transmembrane helices six and seven. Figure taken from (Bryant et al., 2002).

1.4.3 Insulin signalling

Activation of the insulin receptor by insulin elicits a wide range of cellular responses that together coordinate translocation of GLUT4 from perinuclear depots to the plasma membrane (Rowland et al., 2011). Although, many signalling molecules required for GLUT4 translocation to the plasma membrane have been identified, our understanding of how activation of the insulin receptor leads to the fusion of GLUT4 carrying vesicles with the plasma membrane is far from complete. Briefly, the starting point of insulin signal transduction is the insulin receptor (IR), which contains 2 disulphide linked heterodimers, corresponding to 2 α extracelullar subunits and 2 ß intracellular subunits that span the membrane and contain intrinsic tyrosine kinase activity (Gual et al., 2005). Upon insulin binding to the α subunits of the receptor, the ß subunits phosphorylate each other, resulting in activation of their tyrosine kinase activity (Gammeltoft and Van Obberghen, 1986). Autophosphorylation of the IR also leads to the recruitment and phosphorylation of the canonical insulin receptor substrates (IRS) through a phosphotyrosine binding domain (Jewell et al., 2010).

Phosphorylated IRS is recognized by phosphatidylinositol 3 kinase (PI3K) *via* its src Homology 2 domain (Leney and Tavare, 2009). This interaction activates PI3K which subsequently phosphorylates phosphatidylinositol from 4,5 bi- to 3,4,5 tri-phosphate (PIP2 to PIP3) (Rowland et al., 2011). PIP3 recruits 3-phosphoinositide dependent kinase (PDK1) and protein kinase B (PKB a.k.a Akt) to the plasma membrane through their pleckstrin homology domains (PH). PDK1 interaction with PIP3 activates the former, which phosphorylates Akt (Alessi et al., 1997) along with atypical protein kinase C (PKC) isoforms PKCζ and PKCλ (Jewell et al., 2010). Subsequently Akt phosphorylates AS160, which is a Rab-GTPase activating protein (Rab-GAP) (Sano et al., 2003). AS160 signals downstream to multiple Rab targets (Rabs 2A, 8A, 10 and 14) (Miinea et al., 2005). Rab proteins as described earlier (section 1.3.4.2) are presumed to facilitate GLUT4 containing vesicles trafficking to and docking at the plasma membrane (Figure 1-13). Evidence for Akt involvement comes from studies showing that a constitutively active form of Akt enhances both glucose transport and GLUT4 translocation to plasma membrane in adipocytes (Kohn et al., 1996).

While the PI3K depended pathway of GLUT4 translocation, outlined above is the most thoroughly characterised insulin signal transduction pathway, other studies have indicated an additional signaling pathway that operates independently of PI3K, which might be also of significant importance (Baumann et al., 2000). This pathway involves a dimeric complex that comprises c-Cbl 9 (a homologue of the transforming v-Cbl oncogene) and the c-Cbl associated protein (CAP) (Baumann et al., 2000). This association promotes tyrosine phosphorylation of c-Cbl, which triggers translocation of this complex to specialized membrane domains in the plasma membrane, *via* a lipid raft protein called flotillin (Kimura et al., 2001). Phosphorylated c-Cbl recruits a small adaptor protein Crk II that in turns recruits C3G, a guanine-nucleotide exchange factor (Chiang et al., 2001). C3G activates TC10 (a member of the Rho family of GTPases) by promoting exchange of GDP for GTP. Activated TC10 seems to trigger GLUT4 transloction to the plasma membrane through a yet uncharacterized mechanism (Chiang et al., 2001) (Figure 1-13). The potential importance of this pathway for GLUT4 externalization was underlined by studies that showed the vital role of lipid raft localization of TC10 (Watson et al., 2001). However, neither abolishment of key components using siRNA in adipocytes (Mitra et al., 2004), nor adipocytes from

c-Cbl knocked-out mice (Molero et al., 2004) show any evidence of reduced insulin stimulated glucose uptake, challenging the physiological significance of the PI3K independent pathway in GLUT4 translocation. These contradictory findings underline the need for further investigation in order to elucidate the role, if any, of this additional pathway in insulin-stimulated GLUT4 translocation.

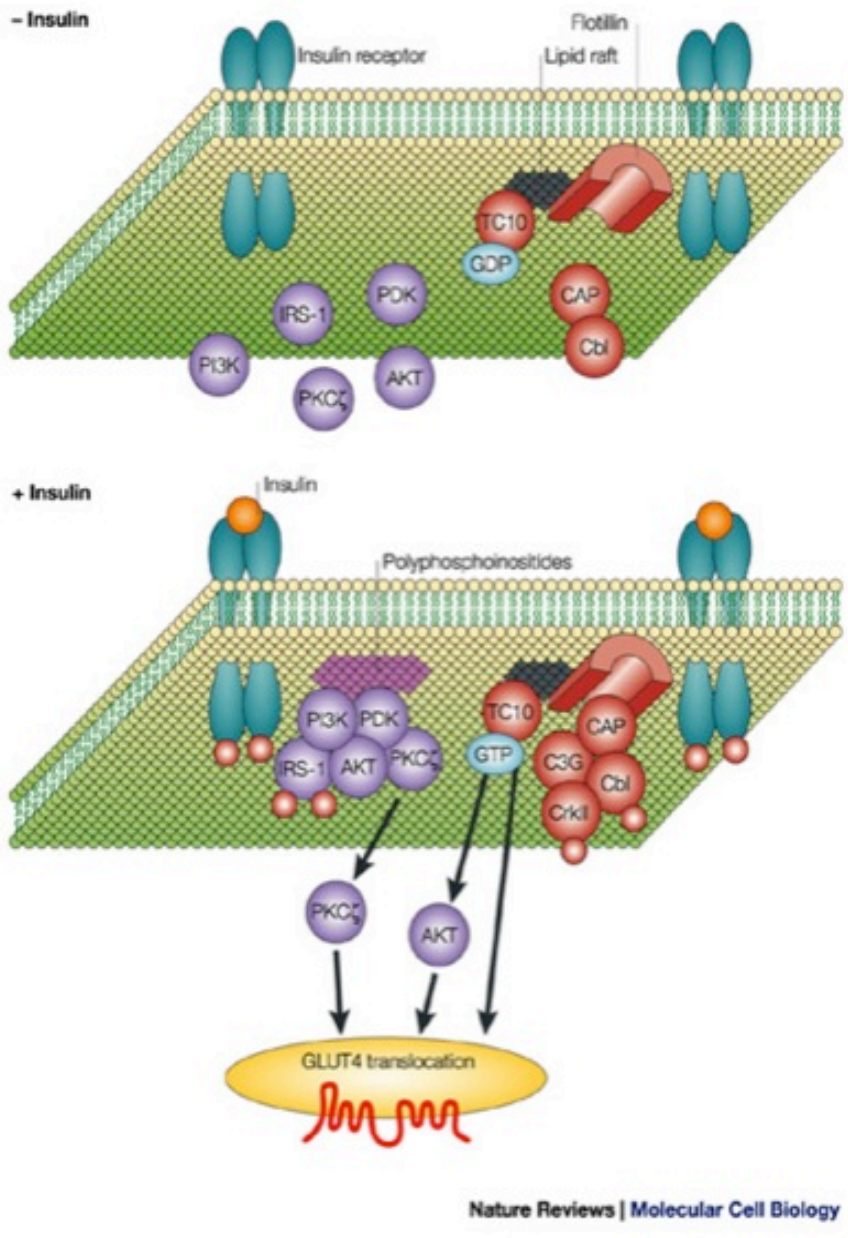

Figure available at: http://www.nature.com/nrm/journal/v3/n4/box/nrm782_BX2.html

Figure 1-13: Insulin signalling.

Schematic represention of insulin signalling in muscle and adipose tissues. In the PI3K dependent pathway (left hand side) extracellular insulin binds to the α-subunit of the insulin receptor (IR), triggering autophosphorylation and activation the ß-subunit kinase activity. This induces recruitment of IRS-1 which reqruits PI3K. PI3K phosphorylates PIP2 to yeald PIP3 that reqcruits PDK1 to plasma membrane where it phosphorylates and activates atypical PKC (isoform ζ) and AKT. Activation of these two kinases are thought to trigger GLUT4 translocation to the plasma membrane *via* AS160 phosphorylation, which targets various Rab proteins (not shown in the figure). The PKI3 independent pathway of insulin signalling (right hand side) functions *via* tyrosine phosphorylation of the Cbl-CAP complex by the insulin receptor in response to insulin. Activated Cbl recruits CrkII/C3G complex to the lipid raft where TC10 protein is located. In lipid rafts CrkII/C3G complex, which are an adapter protein and a nucleotide exchange factor respectively, can stimulate GTPase activity of TC10 which subsequently promotes GLUT4 translocation to the plasma membrane. Figure taken from (Bryant et al., 2002).

1.4.4 GLUT4 trafficking

Insulin-dependent translocation of GLUT4 from intracellular storage compartments to the plasma membrane is central to whole body glucose homeostasis in mammals (Bryant and Gould, 2011). Immunoelectron microscopy studies estimate that in the basal state more than 95% of the total GLUT4 is held intracellularly (Smith et al., 1991) localised to numerous compartments including endosomes and the *trans*-Golgi network (TGN) (Slot et al., 1991b). Although intracellular GLUT4 populates a variety of membrane bound compartments the majority of the total pool of GLUT4 (80%) in fully differentiated adipocytes and skeletal muscle cells is found in vesicles and tubes of small diameter (~50nm), that cluster around the TGN but are distinct from it, as shown by immunoelectron microscopy (Slot et al., 1991b), sucrose gradient centrifugation and other biochemical methods (Kandror et al., 1995). Studies in adipocytes have shown that these small vesicles are the source of the GLUT4 which translocates to the plasma membrane in response to insulin (Slot et al., 1991b). A similar shift in GLUT4 localisation, from intracellular tubule-vesicular compartments to the plasma membrane upon insulin stimulation was also observed in other insulin responsive tissues such as cardiomyocytes (Slot et al., 1991a) and muscle (Ploug et al., 1998). Various experimental approaches based on either endosomal ablation (Livingstone et al., 1996), or subcellular fractionation (Hashiramoto and James, 2000) have led to the proposal that two separate pools of intracellular GLUT4 exist in adipocytes, the one associated with endosomes and the other, which is insulin responsive, distinct from the endosomal recycling system. Studies in skeletal muscle supported the notion of an intracellular GLUT4 pool, distinct from endosomes, that consists of small GLUT4 containing vesicles that responsd to insulin (Aledo et al., 1997). These specialized vesicles are known as GLUT4 storage vesicles (GSVs) and contain 60% of the total cellular GLUT4 (Livingstone et al., 1996), which equates to approximately 75% of the small intracellular tubule-vesicular GLUT4 compartments. As mentioned above, a major effect of insulin is the translocation of these small GLUT4 containing vesicles to the plasma membrane. The size of the intracellular small vesicular GLUT4 compartment is reduced two-fold by insulin, concomitant with an increase in GLUT4 at cell surface (Kandror and Pilch, 2011), supporting the model described above in which there are two intracellular stores of GLUT4 one of which is insulin responsive. However the

associated increase of plasma membrane GLUT4 upon insulin stimulation is rather higher (10 to 20 fold) (reviewed by (Bryant et al., 2002)). This observation raises the possibility that insulin triggers formation of new GSVs from a larger GLUT4 store alongside triggering GLUT4 translocation to plasma membrane from GSVs (Lampson et al., 2001). According to popular current working models of GLUT4 trafficking, under basal conditions GLUT4 circulates *via* two interrelated cycles. The first is a prototypical endosomal system that traffics GLUT4 quickly between the plasma membrane and recycling endosomes while the second one recycles GLUT4 more slowly through recycling endosomes, the *trans*-Golgi network and GSVs (Bryant et al., 2002) (Figure 1-14). It is most likely that the second cycle is the source of GSVs which provide the pool of GLUT4 vesicles that fuse with the plasma membrane in a SNARE dependent manner upon insulin stimulation (Kandror and Pilch, 2011). Small GLUT4 vesicles are not structurally or functionally homogeneous. Preparation of these vesicles by sucrose gradient centrifugation produces an overlapping mixture of at least two vesicle populations. One contains cellugyrin, a transmembrane protein with unknown physiological function (cellugyrin positive vesicles), while the other does not (cellugyrin negative vesicles) (Kupriyanova and Kandror, 2000). Cellugyrin-negative vesicles contain five to six times more GLUT4 than cellugyrin-positive vesicles, and are the source of GLUT4 translocated to cell surface after insulin stimulation. Conversely cellugyrin-positive vesicles maintain their intracellular localization in the presence of insulin (Kupriyanova et al., 2002). Sequential immunoadsorption experiments of GLUT4 enriched sucrose gradient fractions, using antibodes against cellugyrin and then against GLUT4, under both basal conditions and upon insulin stimulation revealed that more than 90% of GLUT4, IRAP (insulin responsive aminopeptidase), which is a constituent of the vesicles that contain the insulin-regulated glucose transporter GLUT4, and sortilin containing vesicles that redistribute in response to insulin, come from cellugyrin negative vesicles (Jedrychowski et al., 2010). Furthermore, approaches based on reversible crosslinking and immunoprecipitation revealed a direct interaction of GSV proteins LRP1 (low density lipoprotein receptor-related protein), IRAP, GLUT4 and sortilin but not cellugyrin (Jedrychowski et al., 2010). These findings suggest that sortilin is a potential marker of insulin responsive vesicles. It has been reported that some cellugyrin positive vesicles, especially under basal conditions, contain the same

proteins as the insulin responsive vesicles but at a lower frequency (Jedrychowski et al., 2010). These vesicles are large and rapidly sedimenting and are likely to represent recycling endosomes or/and vesicles within the TGN (Kandror and Pilch, 2011). Studies based on fractionating 3T3-L1 adipocyte lysates under basal conditions into plasma membrane and vesicular fraction showed that majority of endogenous cellugyrin was recovered in the vesicular fraction. However it is noteworthy that a small amount of cellugyrin was recovered in the plasma membrane fraction as well (Li et al., 2009). This might indicate that some cellugyrin positive GLUT4 vesicles translocate to the plasma membrane under basal conditions. However, comparison of this plasma membrane fraction with that obtained from insulin treated adipocytes showed no increase of in the amount of cellugyrin, which suggests that GLUT4 translocation in response to insulin is cellugyrin independent. Collectively these data support the existence of two independent pools of small GLUT4 containing vesicles: cellugyrin-positive which retain their intracellular localization after insulin stimulation and might be involved to GLUT4 translocation under basal conditions, and cellugyrin-negative/sortilin positive vesicles which respond to insulin and translocate to the plasma membrane (Figure 1-14).

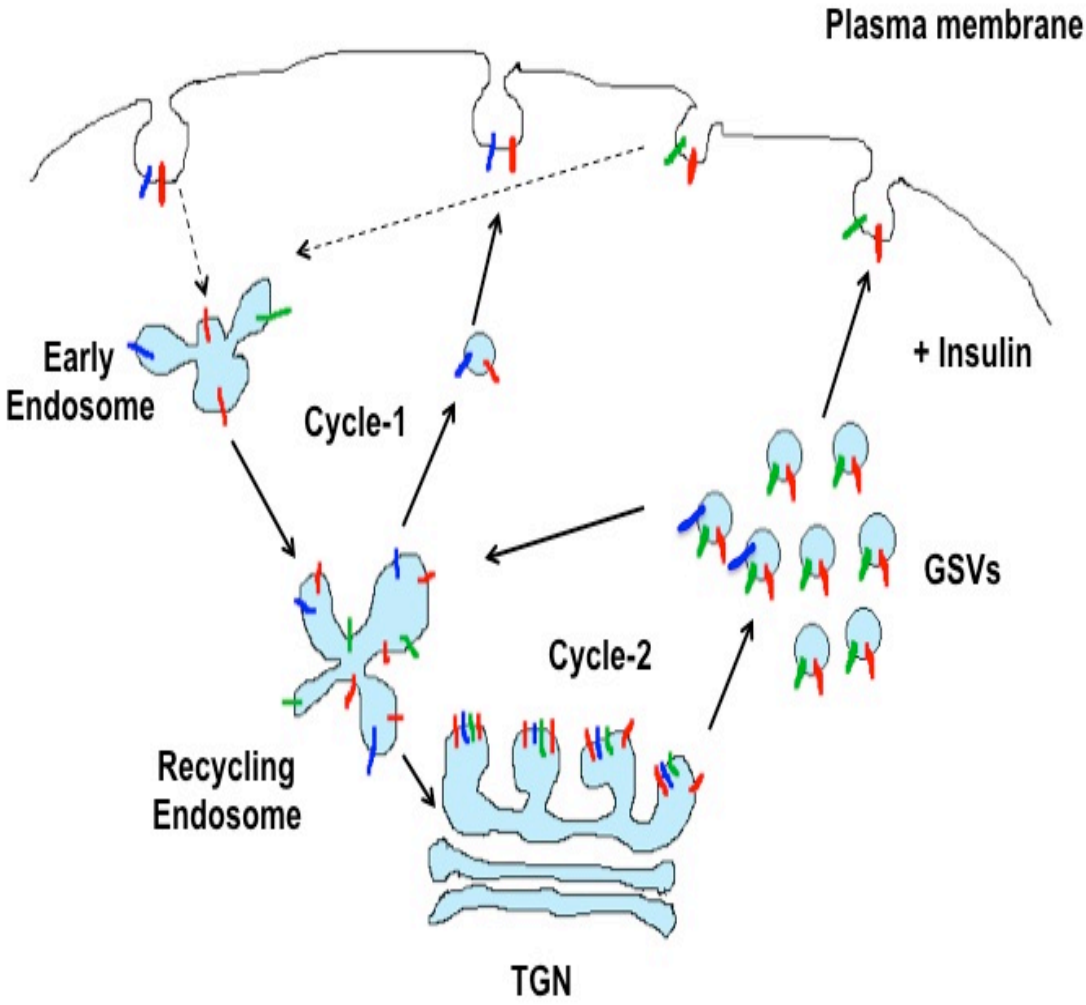

Figure 1-14: A model for GLUT4 trafficking in insulin responsive tissues.

GLUT4 (red) has been proposed to cycle in two separate intracellular cycles. Under basal conditions GLUT4 seems to recycle between the plasma membrane early endosome, recycling endosome and back to plasma membrane. This cycle is the prototypical endosomal system (cycle-1), which cycles rapidly. Having entered this pathway GLUT4 is further sorted to into a slowly recycling pathway (cycle-2) that operates between recycling endosomes the *trans*-Golgi network (TGN) and a population of vesicles termed GSVs (GLUT4 storage vesicles). There are two membrane bound proteins that dictate the trafficking fate of the GLUT4 containing vesicles: cellugyin (blue) and sortilin (green). Under basal conditions GLUT4 is translocated to the plasma membrane *via* vesicles that come from cycle one and contain cellugyrin but not sortilin (cellugyrin positive vesicles). According to this model insulin mobilizes GLUT4 to cell membrane from an intracellular store (GSVs) that moves slowly between TGN and recycling endosome under basal conditions. Strikingly upon insulin stimulation sortilin carrying but not cellugyrin carrying vesicles (sortilin positive vesicles) from GSVs translocate to plasma membrane. Figure modified from (Bryant et al., 2002).

1.4.5 SNARE-mediated GLUT4 translocation to plasma membrane

Fusion of GLUT4 vesicles with the plasma membrane is a key terminal step in insulin-regulated glucose transport. This fusion event is mediated by the SNARE proteins, Syntaxin 4, SNAP23 (t-SNAREs located to plasma membrane) and VAMP2 (Bryant and Gould, 2011) (v-SNARE anchored to the GLUT4 carrying vesicles), through formation of a very stable, SDS-resistant (Hayashi et al., 1994) ternary complex. This complex is made up of the SNARE domains from Syntaxin 4, SNAP23 and VAMP2 and provides mechanical force for fusion (Pobbati et al., 2006). The whole process is regulated by a series of accessory proteins including Munc18c (a member of Sec1p/Munc18 family) which has a predominant role in this process (Jewell et al., 2010).

1.4.5.1 Syntaxin 4

Syntaxin 4 is a t-SNARE (Qa) protein localized to the plasma membrane of pancreatic ß-cells, adipocytes and muscle cells, that regulates insulin secretion (pancreatic ß-cells) and GLUT4 translocation (adipocytes and muscle cells) (Spurlin et al., 2004; Spurlin et al., 2003; Volchuk et al., 1996). The importance of Synaxin 4 for insulin regulated GLUT4-translocation was demonstrated by studies that used Syntaxin 4 heterozygous knock out mice. These mice exhibited diminished GLUT4 translocation to plasma membrane along with reduced glucose uptake into skeletal muscle (Yang et al., 2001). Consistent with this, transgenic mice overexpressing Syntaxin 4 in skeletal muscle cells appear to have a twofold higher GLUT4 translocation and enhanced glucose uptake upon insulin stimulation (Spurlin et al., 2004). Co-immunoprecipitation experiments from solubilized rat adipocyte plasma membranes suggested that Syntaxin 4 interacts with SNAP23 (St-Denis et al., 1999), forming an intermediate complex (Araki et al., 1997) that mediates ternary SNARE complex formation with their corresponding v-SNARE protein (Kawanishi et al., 2000; St-Denis et al., 1999). It has also been shown that Syntaxin 4 interacts directly with its cognate v-SNARE VAMP2 *in vitro* (Calakos et al., 1994), although whether this is interaction is of any physiological significance has not been determined. As previously mentioned syntaxins interact strongly with their cognate SM proteins (section 1.3.2). Consistent with this Munc18c binds to Syntaxin 4 with high affinity

(Tellam et al., 1997). The role of this interaction still remains controversial and it will be discussed later (section 1.4.5.4).

1.4.5.2 SNAP23

A yeast two-hybrid screen using Syntaxin 4 as bait identified SNAP23, a novel SNAP25 isoform (the two proteins share 59% identity) with an approximate molecular weight of 23 kDa (Ravichandran et al., 1996). Subsequent studies revealed that SNAP23 is highly expressed in adipocytes and like Syntaxin 4 is localized mostly at the plasma membrane (Wang et al., 1997). Interactions between SNAP23 and Syntaxin 4 were confirmed by co-immunoprecipitation studies, which also indicated that the SNAP23/Syntaxin 4 interaction and localization are unaffected by insulin (St-Denis et al., 1999). The importance of SNAP23 in GLUT4 translocation to the plasma membrane was established directly by microinjection of antibodies directed the protein into adipocytes; significantly reducing insulin-triggered GLUT4 translocation (Rea et al., 1998). Finally, surface plasmon resonance studies demonstrated that Syntaxin 4, SNAP23 and VAMP2 form an extremely stable SNARE complex *via* their conserved SNARE domains (Rea et al., 1998). Consistent with this, overexpression (*via* the use of adenovirus) of a mutant of SNAP23 able to bind Syntaxin 4 but not VAMP2 resulted into reduction of GLUT4 translocation upon insulin stimulation (Kawanishi et al., 2000).

1.4.5.3 VAMP2

The identity of the v-SNARE protein that regulates the fusion of GLUT4 vesicles with the plasma membrane upon insulin stimulation is an area of some controversy. Immunoblotting studies from rat adipocytes identified two members of the synaptobrevin family, VAMP2 and VAMP3 (cellubrevin) (Cain et al., 1992). Both of these colocalise with GLUT4 in adipocytes and are enriched on GLUT4 containing vesicles (Volchuk et al., 1995). Immunoprecipitation of VAMP3 carrying vesicles revealed that these vesicles contain GLUT4 but not VAMP2. This finding is in line with the existence of two separate pools of GLUT4 containing vesicles (Volchuk et al., 1995). Additionally there is evidence of specific involvement of VAMP2 in insulin stimulated GLUT4 translocation to plasma membrane, since it has been found localised with GLUT4 in the GSVs in

contrast to the majority of VAMP3, which localizes to endosomes (Martin et al., 1996). Introduction of tetanus resistant forms of either VAMP2 or VAMP3 along with tetanus toxin into myoblasts demonstrated that only VAMP2 was able to rescue insulin depended GLUT4 translocation by toxin inhibition (Randhawa et al., 2000). Furthermore introduction of recombinantly produced soluble domains of either VAMP2 or VAMP3 into adipocytes revealed that only VAMP2 inhibited GLUT4 translocation upon insulin stimulation (Martin et al., 1998) (Millar et al., 1999). Although this work supports the involvement of VAMP2 in insulin-stimulated externalization of GLUT4 to the plasma membrane, recent proteomic characterisation of GLUT4 Storage Vesicles demonstrated the presence not only of VAMP2, and VAMP3 but also of VAMP8 on GSVs (Jedrychowski et al., 2010; Larance et al., 2005). All three of these v-(R-)SNARE proteins are able to form ternary SNARE complexes with SNAP23 and Syntaxin 4 (Polgar et al., 2002). Additionally, studies in which VAMP8 and VAMP3 were simultaneously disrupted in differentiated adipocytes from VAMP2 depleted mouse embryonic fibroblasts revealed that there is some level of plasticity regarding the requirements of v-SNAREs for GLUT4 externalization (Zhao et al., 2009). Collectively these data underline the need of further work to clarify which v-SNARE(s) contributes to GLUT4 translocation in insulin responsive tissues.

1.4.5.4 Munc18c

Munc18c is a mammalian SM protein involved in exocytotic pathways. Munc18c and its cognate t-SNARE Syntaxin 4 are ubiquitously expressed in most mammalian cells (Tellam et al., 1997) and regulate a variety of exocytotic trafficking events including the insulin-stimulated exposure of GLUT4 to the cell surface in muscle and fat cells (Tamori et al., 1998), the highly regulated transport of cytokines in macrophages (Pagan et al., 2003) and regulated exocytosis in pancreatic acinar cells (Gaisano et al., 2004). Munc18c has been shown to bind directly to monomeric Syntaxin 4 in a manner that resembles the yeast proteins Sly1 and Sed5 (*via* syntaxin's N-terminus-mode 2) (Latham et al., 2006). This interaction was confirmed by determination of the crystal structure of the Munc18c/Syntaxin 4 N-peptide complex where the short N-terminal peptide of Syntaxin 4 interacts with a hydrophobic pocket on the outer surface of domain I of Munc18c (Hu et al., 2007). As far as mode 1 (closed syntaxin)

binding between Munc18c and Syntaxin 4 is concerned data are controversial. Although the high sequence homology between Syntaxin 4 and Syntaxin 1A regarding the residues for intra-molecular interactions (D'Andrea-Merrins et al., 2007), and binding studies between Syntaxin 4 and its cognate SM protein Munc18c (Aran et al., 2009) suggest that Syntaxin 4 , like Syntaxin 1A could possibly interact with Munc18c by adopting its closed conformation (mode-1 binding), recent studies using small-angle X-ray scattering and small-angle neutron scattering with contrast variation have been interpreted as showing that Munc18c and Syntaxin 4 interact only in the open binding mode and not the closed one (Christie et al., 2012).

Like the yeast SM proteins Vps45 and Sly1 (Carpp et al., 2006; Peng and Gallwitz, 2004), Munc18c can also bind to its cognate v-SNARE Vamp 2. Both Syntaxin 4 and VAMP2 compete for SM binding with Syntaxin 4 having the higher affinity (Brandie et al., 2008). It has been shown that Munc18c can bind to binary Syntaxin 4/SNAP23 complex as well to cognate ternary SNARE complex (Syntaxin 4/SNAP23/VAMP2) and further more that the interaction between syntaxin 4 and Munc18c accelerates SNARE complex assembly *in-vitro* (Latham et al., 2006). In contrast to this presence of Munc18c seems to have an inhibitory effect on membrane fusion *in vitro* (Brandie et al., 2008). Similarly, contradictory results have been obtained from genetic studies. Homozygous knockout of Munc18c in mice resulted in an increased sensitivity of GLUT4 exocytosis in response to insulin suggesting that Munc18c has a negative effect on GLUT4 exocytosis (Kanda et al., 2005). Consistent with this, overproduction of Munc18c in 3T3-L1 adipocytes inhibits insulin–stimulated GLUT4 exposure at the cell membrane (Thurmond et al., 1998). However, Munc18c heterozygous knockout mice appear to have severe glucose intolerance (Oh et al., 2005), which suggests a positive role of the SM protein for GLUT4 exocytosis.

Munc18c is known to become tyrosine phosphorylated upon insulin treatment at two discrete motifs Tyr219 and Tyr521 (Jewell et al., 2011; Oh and Thurmond, 2006; Schmelzle et al., 2006). Tyr521 phosphorylation upon insulin stimulation seems to be more important since the insulin receptor (IR) tyrosine kinase was found to target Munc18c at this residue *in vitro*. This phosphorylation has functional significance regarding GLUT4 externalization as demonstrated by studies in MIN6 beta cells showing that phosphorylation facilitates vesicle

exocytosis (Oh and Thurmond, 2006). Further, in contrast to wild-type and phosphomimetic constructs, phospho-resistant mutants fail to rescue defective insulin-stimulated GLUT4 translocation of Munc18c knockdown in adipocytes) (Jewell et al., 2011). Finally, from a mechanistic point of view a variety of studies in both adipocytes and MIN6 beta cells have established that phosphorylation of Munc18c upon insulin stimulation results in its dissociation from Syntaxin 4 (Jewell et al., 2008; Umahara et al., 2008). These findings have been substantiated by *in vitro* binding studies (Aran et al., 2011). It is likely that tyrosine phosphorylation of Munc18c upon insulin stimulation not only plays an important role in SNARE-mediated membrane fusion but also emerges as a crucial regulatory step in GLUT4 trafficking. However, the precise role of Munc18c in insulin-regulated GLUT4 traffic to the plasma membrane remains to be clarified.

1.4.5.5 Other regulators of SNARE-mediated GLUT4 externalization

As discussed in section 1.3.4 SM proteins are not the only regulators of SNARE complex assembly, the process being subject to multiple levels of regulation. This seems to be particularly relevant to regulated-trafficking pathways such as insulin-regulated GLUT4 trafficking. Tomosyn and synip are two binding partners of GLUT4 cognate SNARE proteins and regulate its translocation to plasma membrane upon insulin stimulation.

Tomosyn is a 130 kDa protein that was first identified as binding partner of Syntaxin 1A in neuronal cells (Fujita et al., 1998). Tomosyn has 7 different isoforms which are expressed from two genes, tomosyn 1 and 2 (Groffen et al., 2005). Tomosyn 1 has three splice variants referred as m (original or medium), b (big), and s (small) (Yokoyama et al., 1999). It has a coiled-coil VAMP2-like domain in its C-terminal whereas its N-terminal consists of 40 WD repeats (Fujita et al., 1998). Tomosyn was also identified in adipocytes where the isoform that is predominantly expressed is b-tomosyn (Yokoyama et al., 1999). Full-length b-tomosyn binds Syntaxin 4, SNAP23, as well as SNAP23/Syuyntaxin 4 binary complex *via* its VAMP2-like C-terminally domain (Widberg et al., 2003). In the same study it was shown that Munc18c and tomosyn are able to bind Syntaxin 4 simultaneously and that overexpression of tomosyn in adipocytes notably reduces GLUT4 translocation to the cell surface, which assigns to tomosyn an

inhibitory role for insulin dependent GLUT4 externalization (Widberg et al., 2003).

Synip (syntaxin-interacting protein) is a 62 kDa protein that was initially discovered in a two-yeast hybrid screen of a 3T3-L1 adipocyte cDNA library as a novel Syntaxin 4 binding protein and has been implicated in the control of GLUT4 vesicle translocation to the plasma membrane in insulin sensitive tissues (Min et al., 1999). Synip seems to interact with Syntaxin 4 and although this interaction does not inhibit SNAP23 interacting with Syntaxin 4 it is not permissive to VAMP2 interaction with the t-SNARE binary complex (SNAP23/Syntaxin 4) and thus it inhibits SNARE complex formation (Min et al., 1999). Synip binds to Syntaxin 4 in an insulin depended manner. This mechanism appears to function through synip phosphorylation at residue serine 99 in response to insulin activation of Akt. Synip phosphorylation dissociates it from Syntaxin 4 and subsequently promotes SNARE complex formation and GLUT4 vesicle fusion to plasma membrane (Yamada et al., 2005). The role of synip phosporylation in insulin stimulated GLUT4 translocation is a disputed finding since overexpression of a synip phospho-resistant mutant (S99A) in adipocytes resulted in inhibition of GLUT4 translocation in one case (Okada et al., 2007) but had no effect when a different group tried to contest this observation (Sano et al., 2005).

1.5 Aims of this study

The initial overall aim of this project was to test the hypothesis that insulin regulates GLUT4 delivery to the plasma membrane by altering interactions between the SNARE (Syntaxin 4, SNAP23, VAMP2) and SM (Munc18c) proteins. The results obtained are presented in four chapters with the objectives of my investigations presented in this thesis are detailed below.

1.5.1 Aims of chapter 3

Trafficking of the facilitative glucose transporter GLUT4 is regulated by insulin in fat and muscle cells and GLUT4 translocation is regulated by Syntaxin 4-containing SNARE complex formation (Bryant et al., 2002). Based on these observations it is tempting to hypothesise that insulin regulates Syntaxin 4-containing SNARE complex formation. In this chapter, in order to directly test

this hypothesis I have used an *in situ* Proximity Ligation Assay (PLA) to visualize protein-protein associations and study the effects of insulin on associations between Syntaxin 4, SNAP23, VAMP2 and Munc18c protein in 3T3-L1 adipocytes and fibroblasts.

1.5.2 Aims of chapter 4

In chapter 4 I present *in vitro* binding assays to further investigate the interactions of Syntaxin 4 with its cognate SNARE proteins. Additionally a Complex Assembly Assay was used to examine the effect of the interactions between the SNARE proteins on the rate of the formation of the SNARE complex

1.5.3 Aims of chapter 5

In chapter 5 I used *in vitro* approaches to investigate the effects of tyrosine phosphorylation of Munc18c on residue 521 on its interaction with Syntaxin 4 SNAP23 and VAMP2 and whether Munc18c phosphorylation facilitates Syntaxin 4/SNAP23/VAMP2 SNARE complex formation.

1.5.4 Aims of chapter 6

As discussed above there are two different internal GLUT4 containing vesicles; cellugyrin-positive and cellugyrin-negitive (sortilin-positive) that are potentially involved in two functionally distinct pathways of GLUT4 delivery to the cell surface: Cellugyrin-positive vesicles being involved in GLUT4 cycling through the cell surface under basal conditions and cellugyrin-negative vesicles responsible for its insulin-stimulated plasma membrane delivery. In the last result chapter I investigate how the fusion of these two separate pools of GLUT4 carrying vesicles to plasma membrane are mediated under basal and insulin-stimulated conditions.

Chapter 2

Materials and methods

2.1 Materials

2.1.1 Reagents

General chemicals, molecular biology enzymes and other reagents used in this study were of high quality and obtained from the following suppliers:

- Ambion, Austin, USA
- Anachem Ltd, Luton, UK
- BD Biosciences, Oxford, UK
- BDH Laboratory Supplies, Poole, UK
- BioRad Laboratories Ltd, Hertfordshire, UK
- Clontech Laboratories Inc, California, USA
- Fisher Scientific Ltd, Loughborough, Leicestershire, UK
- Formedium™, Norfolk, UK
- GE Healthcare Bio-Sciences Ltd, Buckinghamshire, UK
- Invitrogen Ltd, Paisley, UK
- Kodak Ltd, Hertfordshire, UK
- New England Biolads UK Ltd, Hertfordshire, UK
- Novo-Nordisc, Bagsveard, Denmark
- Melford Laboratories Ltd, Ipswich, Suffolk, UK
- Merck Chemicals Ltd, Nottingham, UK

- Millipore Ltd, Livingston, UK
- New England Biolabs, Ipswich, USA
- Novus Biologicals Ltd, Cambridge, UK
- Pierce, Perbio Science UK Ltd, Cheshire, UK
- Premier Brands UK, Staffordshire, UK
- Promega Ltd, Southampton, UK
- Roche Diagnostics Ltd, Burgess Hill, UK
- Severn Biotech Ltd, Worcestershire, UK
- Sigma Aldrich Company Ltd, Dorset, UK
- Spectrum Laboratories Inc, Netherlands
- Sterilin Limited, Caerphily, UK
- Stratagene Technologies, California, USA
- Synaptic Systems, Göttingen, Germany
- VWR UK Ltd, Leicestershire, UK
- Whatman Plc, Kent, UK

2.1.2 Kits

Four different kits were used in this study and obtained from the following suppliers:

- Qiagen, West Sussex, UK

- QIAfilter Mini-plasmid Purification kit
- QIAquick Gel Extraction kit

- Invitrogen Ltd, Paisley UK
- pCRII_TOPO© kit

- Olink AB, Uppsala, Sweden
- Duolink *in situ* PLA technologies (PLA probes and Amplification/Detection Kit)

2.1.3 Solutions and media

In all the solutions used in this study high purity sterile water was used as dissolving agent unless otherwise stated.

- 2xSDS-PAGE Loading Buffer: 10% (v/v) ß-mercaptoethanol 1M in Laemlli buffer
- 6xDNA Loading Dye: 2.5% (w/v) Bromophenol Blue or Xylene Cyanole.FF, 67% (v/v) Ficoll Type 400
- Adipocytes lysis/pull-down buffer: 50mM HEPES, 150mM NaCl, 1mM NEM, 1% (v/v) TRITON-X, 5mM EDTA, 100mM NaF, 1 tablet of EDTA- free protease inhibitor mix per 50ml (Roche).
- BSA/GLY: 2% (w/v) BSA, 20mM glycine in PBS
- BSA/GLY/SAP: 0.1% (w/v) saponin in BSA/GLY
- Buffer C: 25mM HEPES, 0.4M KCl, 10% (w/v) glycerol pH7.4, 1 tablet of EDTA- free protease inhibitor mix per 50ml (Roche)
- Coomassie destain: 15% (v/v) methanol, 15% (v/v) acetic acid

- Coomassie stain: 0.05% (w/v) Coomassie brilliant blue R250, 50% (v/v) methanol, 10% (v/v) acetic acid

- Dialysis buffer: 10% (w/v) glycerol in PBS

- ECL reagent solution 1: 100mM Tris-HCl pH 8.5, 2.25mM Luminol in 2% (v/v) DMSO, 0.4 mM ρ-coumaric acid in 1 % (v/v) DMSO

- ECL reagent solution 2: 100mM Tris-Hcl pH 8.5, 0.018% (v/v) H_2O_2

- GST-Elution Buffer: 50mM Tris base pH 8.0, 25mM reduced glutathione, 10% (w/v) glycerol

- GST-Preparation Buffer: 100 mM HEPES, 500mM NaCl, 5mM $MgCl_2$, 5mM ß-mercaptoethanol 10% (w/v) glycerol into which 1 tablet of complete protease inhibitor mix per 50ml (Roche) was dissolved.

- Laemmli Sample Buffer (LSB): 100mM Tris-HCl pH 6.8, 4% (w/v) SDS, 20% (v/v) glycerol, 0.2% (w/v) Bromophenol Blue

- PBS: 85mM NaCl, 1.7mM KCl, 5mM Na_2HPO_4, 0.9mM KH_2PO_4, pH 7.4

- Ponceau Stain: 0.2% (w/v) Ponceau Stain, 1% (v/v) glacial acetic acid

- SDS-PAGE resolving buffer: 75mM Tris-HCl, pH 8.8, 0.2% (w/v) SDS

- SDS-PAGE running Buffer: 20mM glycine, 62mM Tris-Base, 0.1% (w/v) SDS

- SDS-PAGE stacking buffer: 25mM Tris-HCl, pH 6.8, 0.2% (w/v) SDS

- Semi-dry transfer Buffer: 24mM Tris base, 20mM glycine, 0.1% (w/v) SDS 20% (v/v) ethanol

- TAE: 40mM Tris-Acetate pH 8, 1mM EDTA

- TBST: 20mM Tris-HCl pH 7.5, 137mM NaCl, 0.1% (v/v) Tween-20

- TST: 50mM Tris-HCl pH 7.6, 150mM NaCl, 0.05% (v/v) Tween-20

All bacterial growth media were sterilised through autoclaving immediately after preparation, before use

- TB: 1.2% (w/v) tryptone, 2.4% (w/v) yeast extract, 0.4% (v/v) glycerol, 17mM KH_2PO_4, 72mM K_2HPO_4 (obtained from Melford Labs Ltd)

- 2YT: 1.6% (w/v) tryptone, 1% (w/v) yeast extract, 0.5% (w/v) NaCl

Antibiotics were routinely added as required for selection following sterilization when the medium had cooled to 60^{o}C or below. Antibiotics were added from a 1000x stock solution. The concentrations of these were: 100mg/ml Ampicillin sodium salt in high purity sterile water, 50mg/ml Kanamycin sulphate in high purity sterile water and 34mg/ml of Chloramphenicol in 100% filtered sterile ethanol. For solid media, 2% (w/v) micro agar was added prior to autoclave sterilisation.

All cell culture media were sterilized through a 0.2 µm pore size filter.

- 3T3-L1 fibroblast growth media: 10% (v/v) NCS in DMEM

- 3T3-L1 adipocyte growth media: 10% (v/v) FCS in DMEM

- 3T3-L1 differentiation media 1: 0.5mM IBMX, 0.25mM dexamethasone, 1µM insulin in 3T3-L1 adipocyte growth media

- 3T3-L1 differentiation media 2: 1µM insulin in 3T3-L1 adipocyte growth media

2.1.4 Primary antibodies

α-Cellugyrin: IgG1 monoclonal antibody raised in mouse immunised with rat cellugyrin aa 95-204. Purchased from BD Transduction Laboratories™ (catalogue# 611128). Used at a1/1000 (WB) or 1/200 (PLA) dilution.

α-GAPDH: IgG1 monoclonal antibody (clone 6C5) raised in mouse immunised with purified rabbit muscle GAPDH. Purchased from Ambion (catalogue#AM4300). Used at a 1/20000 dilution (WB).

α-His_6: IgG2a monoclonal antibody raised in mouse immunised with a recombinant His-tagged fusion protein. Purchased from SIGMA (catalogue# H1029). Used at a 1/1000 dilution (WB).

α-HA: IgG monoclonal rat antibody (clone 3F10). Purchased form Roche (catalogue# 11867423001). Used at a 1/50 dilution (IF).

α-HSP-70: IgG monoclonal that recognizes amino acid residues 436-503 of HSP70 - raised in mouse (clone C92F3A-5) immunised with the same amino acid sequence peptide. Purchased from Novus Biologicals (catalogue# NB110-61582). Used at a 1/1000 dilution (WB).

α-Munc18c:

Polyclonal antiserum raised in rabbit. Purchased from Abcam (catalogue# ab26331). Used at a 1/100 (WB) or 1/200 (PLA) dilution.

Polyclonal antiserum raised in mouse against full length human Munc18c. Purchased from Novus Biologicals (catalogue# H00006814-B01). Used at a1/1000 (WB) or 1/200 (PLA) dilution

α-SNAP23:

Mouse monoclonal IgG1 antibody raised against full length SNAP23 of human origin. Purchased from SantaCruz Biotechnology Inc (catalogue#sc-101303). Used at a 1/200 dilution (PLA).

Rabbit polyclonal affinity purified antibody raised against whole murine SNAP23 protein. Purchased from Synaptic Systems (catalogue# 111203). Used at a 1/1000 (WB) or 1/200 (PLA) dilution.

α-Snc2: polyclonal affinity purified antibodies raised in rabbit immunised with peptides corresponding to residues 11-25. Used at a 1/1000 dilution (WB) (a kind gift from Dr Marion Struthers).

α-sortilin: IgG polyclonal antibody raised in rabbit immunised with synthetic peptide corresponding the C-terminus of human sortilin (from residue 800-end). Purchased from Abcam (catalogue# ab16640). Used at a 1/1000 (WB) or 1/200 (PLA) dilution.

α-Syntaxin 4:

IgG1 monoclonal mouse antibody (clone 49) generated against human Syntaxin 4. Purchased from BD Transduction Laboratories (catalogue# 610439). Used at a 1/1000 (WB) or 1/200 (PLA) dilution.

Mouse monoclonal IgG1 antibody generated against a protein fragment corresponding to amino acids 19-120 of human Syntaxin 4. Purchased from Abcam (catalogue# ab77037). Used at a 1/1000 (WB) or 1/200 (PLA) dilution.

Polyclonal rabbit antibody (antiserum) raised against a recombinant protein corresponding to the cytosolic domain of rat Syntaxin 4 (amino acids 1 - 273). Purchased from Synaptic Systems (catalogue# 110042). Used at a 1/1000 (WB) or 1/200 (PLA) dilution.

α-Tlg2: rabbit polyclonal affinity purified using PrA Agarose antibodies that specifically recognise peptide residues 272-287 and 381-396 of Tlg2. Used at a 1/1000 dilution (WB) (a kind gift from Dr Marion Struthers).

α-VAMP2:

Rabbit polyclonal IgG antibody generated from a synthetic peptide corresponding to amino acids 36-56 of rat VAMP2. Purchased from Abcam (catalogue# ab18014). Used at a 1/1000 (WB) or 1/200 (PLA) dilution.

IgG1 mouse monoclonal antibody (clone 69.1) generated against a synthetic peptide corresponding to amino acids 2-17 of rat VAMP2. Purchased from

Synaptic Systems (catalogue# 104211) used at a 1/1000 (WB) or 1/200 (PLA) dilution.

2.1.5 Secondary antibodies

All secondary antibodies were obtained from GE healthcare Bio-Sciences Ltd unless otherwise stated below.

Anti-mouse IgG Horseradish peroxidise-linked, species-specific, whole antibody produced in sheep (catalogue# NA931). Used at 1/1000 dilution (WB).

Anti-rabbit IgG Horseradish peroxidise-linked, species-specific, whole antibody produced in donkey (catalogue# NA934). Used at 1/2000 dilution (WB).

Anti-rat IgG Alexa Fluorescent 488-linked antibody produced in donkey. Purchased from Invitrogen (catalogue# A21207). Used at a 1/50 dilution (IF).

Anti-mouse IgG antibody produced in donkey conjugated to duolink II oligonucleotide PLUS. Purchased from Olink AB (catalogue# 92001-0100). Used at a 1/5 dilution using the solution provided (PLA).

Anti-rabbit IgG antibody produced in donkey conjugated to Duolink II oligonucleotide MINUS. Purchased from Olink AB (catalogue# 92005-0100). Used at a 1/5 dilution using the solution provided (PLA).

2.1.6 *E. Coli* strains and cell lines

Table 2.1: *E.Coli* strains used in this study

E. coli strains used in this study		
Strain	**Genotype**	**Source**
BL21(DE3)	F- *ompT hsdSB*(rB-mB-) *gal dcm* (DE3)	Invitrogen Ltd
Top10	*F- mcrA _(mrr-hsdRMS-mcrBC) φ80lacZ_M15 _lacX74 nupG recA1 araD139 _(ara-leu)7697 galE15 galK16 rpsL(StrR) endA1 λ-*	Invitrogen Ltd
XL-1 Blue	*recA1 endA1 gyrA96 thi-1 hsdR17 supE44 relA1 lac* [F´*proAB lacIqZ_M15* Tn10 (Tetr)]	Stratagene Technologies

Table 2.2: Cell lines used in this study

Cell lines used in this study		
Strain	**Genotype**	**Source**
3T3-L1	American Type Culture Collection (ATCC)/LGC Promochem	CL-173

2.1.7 Primers

Table 2.3: Table of oligonucleotides used in this study

Primer	Key	Sequence (5'-3')
Syntaxin 4 SNARE domain sense	*Bam*HI start SX4 SNARE domain	GGATCCATGCTGAATGAGATCTCTGCGCG
Syntaxin 4 SNARE domain antisense	*Eco*RI stop SX4 SNARE domain	GAATTCTTAGGCTATCTTGACGTGCTCTTGCC
VAMP2 sense	*Bam*HI start VAMP2	AAGGATCCATGTCGGCTACCG CTGC
VAMP2 antisense	*Eco*RI stop VAMP2	AAGAATTCTTACTTGAGGTTTTTCCACCAGTAT

Oligonucleotides were purchased from Yorkshire Biosciences Ltd, Yorkshire, UK. Primers were routinely diluted to a concentration of 50pM in high purity, nuclease free, sterile water and stored at -20^{o}C upon arrival.

2.1.8 Plasmids

Table 2.4: Parental vectors used for cloning of plasmids used in this study

Parent vectors	Description	Source
pCR®2.1-TOPO®	pUC *ori*, f1 ori, Ap^R, Kn^R,*E. coli* cloning vector.	Invitrogen Ltd
pET28(a-c)	F1 *ori*, *lacI*, Kn^R; *E. coli* expression vector.	Merck Chemicals Ltd
pETDuet-1	ColE1 *ori*, *lacI*, Ap^R; *E. coli* expression vector.	Merck Chemicals Ltd
pETDuet-1:GST	*E. coli* expression vector encoding glutathione S transferase (GST) at the c-terminus.	*Xho*I and *Pac*I were used to remove C-terminal S-tag ORF from pETDuet-1, GST ORF sequence preceded by a thrombin cleavage site then inserted with the same sites. Created by Dr. Fiona Brandie.
pETDuet-1:PrA	*E. coli* expression vector encoding two repeats of the IgG binding domains of *S.aureus* protein A at the C-terminus.	*Xho*I and *Pac*I were used to remove C-terminal S-tag ORF from pETDuet-1, Sequence encoding two synthetic repeats of the IgG binding domains of *S.aureus* protein preceded by a thrombin cleavage site then inserted with the same sites. Created by Dr. Lindsay Carpp.
pGEX-4T-1	pBR322 *ori*, *lacI*, Ap^R; *E. coli* expression vector.	GE Healthcare Bio-Sciences Ltd
pQE-30	pUC *ori*, *lacO*, Ap^R. *E. coli* expression vector.	Qiagen Ltd
pET41a	pBR322 *ori*, *lacI* Kn^R; *E. coli* expression vector	Merck Chemical Ltd

Table 2.5: Plasmids used/constructed in this study

Plasmid name	Description	Source
pETDUET-1:GST	*E. coli* expression vector encoding glutathione S transferase (GST).	Constructed by Dr Fiona Brandie
pETDUET:PrA	*E. coli* expression vector encoding two repeats of the IgG binding domains of S.aureus protein.	Constructed by Dr Lindsay Carpp
pETDUET-1:Snc2-PrA	*E. coli* expression vector encoding a C-terminally PrA -tagged version of the cytosolic domain of Snc2 , residues 1 - 88.	Constructed by Dr Lindsay Carpp
pETDUET:Sx4-GST	*E. coli* expression vector encoding a C-terminally GST-tagged version of the cytosolic domain of Sx4.	Constructed by Dr Fiona Brandie
pETDUET:SX4-GST(open)	*E. coli* expression vector encoding a C-terminally GST-tagged version of the cytosolic domain of Sx4 harbouring two mutations in the hinge region (L173A/ E174A).	Constructed by Dr Veronica Aran-Ponte
pETDUET:SX4-GST(ΔN36)	*E. coli* expression vector encoding a C-terminally GST-tagged version of the cytosolic domain of Sx4 lacking the first 36 amino acids.	Constructed by Dr Veronica Aran-Ponte
pETDUET:SX4-GST(Double)	*E. coli* expression vector encoding a C-terminally GST-tagged version of the cytosolic domain of Sx4 harbouring the L173A/ E174A mutations in the hinge region and also lacking the first 36 amino acids.	Constructed by Dr Veronica Aran-Ponte

pETDUET:Tlg2-GST	*E. coli* expression vector encoding a C-terminally GST-tagged version of the cytosolic domain of Tlg2, residues 221 - 309.	Constructed by Dr Chris MacDonald
pETDUET:VAMP2-PrA	*E. coli* expression vector encoding a C-terminally PrA-tagged version of the cytosolic domain of VAMP2.	Constructed by Dr Fiona Brandie
pET28a:His-MUNC18c	*E. coli* expression vector encoding a N-terminally His-tagged version of MUNC18c.	Constructed by Dr Fiona Brandie
pET28b:MUNC18c-His	*E. coli* expression vector encoding a C-terminally His-tagged version of MUNC18c	Constructed by Dr Fiona Brandie
pET41a:GST-SNAP23	*E. coli* expression vector encoding a N-terminally GST-tagged version of SNAP23 (Thrombin cleavable).	Constructed by Dr Fiona Brandie
pGEX-4T-1:GST-Sx4	*E. coli* expression vector encoding a N-terminally GST-tagged version of the cytosolic domain of Sx4 (Thrombin cleavable).	Constructed by Dr Fiona Brandie
pGEX-4T-1:GST-Sx4(ΔHabc)	*E. coli* expression vector encoding a N-terminally GST-tagged version of the cytosolic domain of Sx4 lacking the Habc domain. (Thrombin cleavable).	SNARE domain of Sx4 from pETDUET:Sx4-GST was amplified with the addition of *Bam*HI/*Eco*RI restriction sites and subcloned into pGEX-4T-1 using the same restriction sites
pGEX-4T-1:GST-VAMP2	*E. coli* expression vector encoding a N-terminally GST-tagged version of the cytosolic domain of VAMP2 (Thrombin cleavable).	Cytosolic domain of VAMP2 from pETDUET:VAMP2-PrA was amplified with the addition of BamHI/EcoRI restriction sites and subcloned into pGEX-4T-1 using the same restriction sites

pGEX-4T-1:GST-VAMP(ΔN30)	*E. coli* expression vector encoding a C-terminally GST-tagged version of the cytosolic domain of VAMP2 lacking the first 30 amino acids	Constructed by Dr Veronica Aran-Ponte
pQE30:His-P-MUNC18c	*E. coli* expression vector encoding a N-terminally His-tagged, phosphomimetic (Y521E) version of MUNC18c	Constructed by Dr Veronica Aran-Ponte
pQE30:His-SNAP23	*E. coli* expression vector encoding a N-terminally His-tagged version of SNAP23	Constructed by Dr Fiona Brandie
pQE30:His-VAMP2	*E. coli* expression vector encoding a N-terminally His-tagged version of the cytosolic domain of VAMP2	Constructed by Dr Fiona Brandie

2.1.9 Computer Software

- Blobfinder, Swedish University of Agricultural Science, Uppsala, Sweden
- Image J V1.41, National Institutes of Health, Bethesda MD, USA
- LSM Viewer Carl Zeiss AxioVision LE Rel 4.5, Hertfordshire, UK
- Photoshop CS5, Adobe Systems Europe Ltd, Uxbridge, UK
- RasMol 2.7.3, Mods by Herbert J. Bernstein, Bellport NY, USA
- SPSS PASW® statistics 18, IBM, Portsmouth, UK
- Vector NTI V10.3, Invitrogen, Carlsbad, CA, USA

2.2 General molecular biology methods

2.2.1 Small scale DNA preparations

A single colony of freshly transformed bacteria (section 2.3.1) was used to inoculate 10ml sterile 2YT supplemented with the appropriate antibiotic for selection (section 2.1.3) and grown overnight at 37^{o}C in a shaking incubator. Bacteria were pelleted and plasmid DNA was extracted using the QIAfilter Mini-plasmid Purification kit following the manufacturer's instructions. 100µl of high purity sterile, nuclease free, water was routinely used in the final elution. Purified DNA was routinely stored at -20^{o}C.

2.2.2 Determination of DNA concentration

DNA concentration was routinely assessed by ultraviolet absorbance measurements at 260nm on a spectrophotometer (WPA S2000, Cambridge, UK). DNA concentration in mg/ml was calculated by multiplying the optical density reading by the dilution factor of sample (usually 100) and then by the extinction coefficient for double stranded DNA (50).

2.2.3 Agarose gel electrophoresis

DNA samples were routinely analyzed by agarose gel electrophoresis. Gels were prepared by dissolving agarose powder in TAE buffer by boiling in a microwave. Agarose gel concentration varied from 0.8-2% (w/v) depending on the size of DNA fragments to be visualised. Agarose solution was allowed to cool to approximately 60°C prior to the addition of Ethidium Bromide to a final concentration of 0.5µg/ml. The molten gel solution was poured in a cassette with the appropriate comb and left to set at room temperature before being immersed into a tank containing TAE buffer. DNA samples were prepared by addition of 6x DNA loading buffer and loaded on the gel alongside a DNA ladders (100bp and/or 1kbp; New England Biolabs Ltd) to provide reference for the size of the resolved DNA fragments. Gels were routinely run at 150 volts and DNA fragments were visualised using an ultraviolet transilluminator.

2.2.4 DNA gel extraction and purification

DNA fragments that had been resolved by agarose gel electrophoresis were visualized using an ultraviolet transilluminator. The fragment of interest was identified by size and excised using a clean scalpel. The agarose gel piece containing the DNA fragment was placed into a sterile eppendorf tube and DNA was extracted using the QIAquick Gel Extraction kit following the manufacturer's instructions. Extracted and purified DNA was eluted from the column using either 30 or 50µl high purity sterile nuclease free water depended on the following application.

2.2.5 DNA amplification by polymerase chain reaction (PCR)

PCR was performed routinely to amplify DNA sequences of interested often to facilitate subcloning through incorporation of restriction endonuclease recognition sites in oligonucleotide primers. Appropriate forward and reverse DNA primers containing the desired restriction sites were designed and obtained from York Bioscience Ltd. Primers were routinely diluted in high purity sterile nuclease free water to a concentration of 50pM and stored at -20^{o}C upon arrival. A mixture of equal concentration (10mM each) of dNTPs (dATP, dGTP, dCTP, dTTP) was used along with high fidelity proof-reading polymerase *Pfu* and its buffer (all purchased from Promega Ltd). The following protocol was followed to set up PCR reactions (50µl total volume)

Template DNA (1-10 µg/ml)	1µl
10 x Pfu polymerase buffer	5µl
Forward primer (5pM)	1.5µl
Reverse primer (5pM)	1.5µl
dNTPs (10mM)	1µl
Nuclease free water	39µl
Pfu DNA polymerase	1µl (5 units)

Reactions were performed in thin wall PCR tubes and using a thermocycler. The following standard conditions were used routinely:

Initial denaturation	95°C	5min	
Denaturation	94°C	1min	30 cycles
Annealing of primers	(~55°C)*	1min	
Elongation	72°C	2min/kbp	
Final Elongation	72°C	10min	
End	4°C	∞ min (hold)	

* The melting point of the primers was estimated to set the annealing temperature for individual reactions. Molecular weight, amount and relative purity of PCR products was checked by agarose gel electrophoresis (section 2.2.3) and if necessary the desired protein was cleaned up and purified following gel extraction (section 2.2.4).

2.2.6 Restriction endonucleases digestion

Digestions were carried out in eppendorf tubes incubated in a heat block at the optimal temperature for the enzymes used. Simultaneous digestion by 2 different restriction endonucleases was performed if required, but if this was not possible (e.g. due to incompatible buffer requirements) sequential digestions were performed.

A typical reaction mixture (total volume) was set up as follows.

Plasmid/DNA (1-10mg/ml)	5µl
10x buffer	1µl
Restriction enzyme A	1µl (20 units)
Restriction enzyme B	1µl (20 units or 0 in the case of single digest)
Sterile water	2µl (or 3µl in the case of single digest)

Restriction reactions were performed at 37°C for 4 hours or at 4-22°C overnight depending on the enzymes used. All restriction enzymes and their buffers were obtained from Roche or New England Laboratories. The digestion products were analysed by agarose gel electrophoresis and if appropriate the desired fragment was extracted and purified (section 2.2.4).

2.2.7 DNA ligation reactions

Linearised vector by restriction digestion and DNA fragment with compatible cohesive overhangs (or blunt ends) generated by restriction endonuclease digestion were used for ligation. In cases where the vector had been linearised using only one restriction enzyme it incubated with shrimp alkaline phosphatase for 15min at 37°C (followed by 15min at 65°C to inactivate the phosphatase) prior to use to prevent self-ligation. Ligation reactions were performed in thin wall PCR tubes in a total volume of 10µl using T4 DNA ligase and its appropriate buffer (obtained from New England Biolabs Inc). A typical reaction was as follows:

Linearised vector DNA (1mg/ml)	2µl
Fragment DNA (1mg/ml)	6µl
10 x T4 DNA ligase buffer	1µl
T4 DNA ligase	1µl (10 units)

Ligation reactions were incubated at 16°C overnight along with a series of controls lacking vector, fragment or both. Reactions were then used to transform Top 10 cells (section 2.3.1) with transforments being selected on appropriate antibiotic agar plates.

2.2.8 Topo© cloning

High fidelity proof reading PCR was used to amplify desired DNA fragments (section 2.2.5) which were subsequently gel purified (section 2.2.4). Taq polymerase was then used to generate polyadenosine overhangs on each of the 5'ends of the double stranded DNA fragment by setting up the following reaction:

DNA fragment (1mg/ml)	16µl
10 x Mg free buffer	2µl
$MgCl_2$ (25mM)	1.2µl
Taq polymerase	0.4µl (10 units)
dATP (10mM)	0.4µl

In a total volume of 20 µl in a thin-walled PCR tube which was incubated 72°C for 20 min. 2µl of the reaction product was cloned into the pCR©2.1-TOPO© vector using the pCRII-TOPO© kit following the manufacturer's directions. The ligation reaction was subsequently used to transform Top10 cells (section 2.3.1) and selected using 2YT plates containing both the appropriate antibiotic and X-gal (0.04µg/ml). Plasmid DNA was isolated from white colonies and analysed (by PCR, restriction digest and/or sequencing).

2.2.9 DNA sequencing

Sequencing of DNA was performed by the University of Dundee sequencing service. Results obtained were compared to archived sequences from DNA databases using the Vector NTI computer software. Sequencing was performed after any procedure that involved the generation of new DNA (e.g. PCR).

2.3 General protein methods

2.3.1 Bacterial transformation

Chemically competent bacterial cells (either purchased from Invitrogen Ltd) were thawed on ice for 30 min. 1µl of DNA plasmid (1mg/ml) was added carefully into 10µl of competent cells and incubated on ice for 45 min. Cells then were heat shocked at 42^{o}C for 45 seconds before being placed immediately on ice for 2 min. 250µl of SOC medium was added to cells which were then incubated at 37^{o}C with shaking for an hour to allow recovery from heat shock and establishment of antibiotic resistance. The transformation mix was spread onto agar plates containing appropriate antibiotic and incubated at 37^{o}C overnight.

2.3.2 Expression of recombinant proteins

A single colony of freshly transformed BL21 cells harbouring the plasmid of interest was used to inoculate 10ml 2YT containing the appropriate antibiotic. Following overnight incubation at 37^{o}C in a shaking incubator, bacteria were collected by centrifugation at 1000g for 10 min and resuspended in 10ml TB. Resuspended cells were used to inoculate 3-12 conical flasks (depended on the protein expression efficiency of the plasmid) each containing 1L TB with the appropriate antibiotic. The resultant cultures were incubated at 37°C with shaking until an OD_{600} of 0.5-0.8 was reached at which point protein production then induced by the addition of IPTG (to a final concentration of 0.5-1mM). Cultures were left shaking overnight at 22^{o}C.

2.3.3 General purification protocol of tagged recombinant proteins

Cells from induced cultures (section 2.3.2) were collected by centrifugation at 3000*g* for 40 min and resuspended in 100 ml per 3 lit of liquid culture using the appropriate buffer (depending on the protein tag). Cells were lysed using a Microfluidizer M-110P cell disrupter at 10000 psi. The resultant lysate was treated with DNAseI (10 units/ml) at 4^{o}C under rotation for 40 min after which time it was clarified by centrifugation in a Beckman JA-20 rotor at 20000rpm for 60 min at 4^{o}C. Affinity matrix (this varied based on the tag present on the

protein of interest) that had been washed and preequilibrated with the appropriate buffer was added to the clarified lysate and incubated at 4^{o}C for 4 hours under rotation to allowed tagged proteins to bind. Beads were then collected by centrifugation at 1000*g* for 2min and washed 3-5 times using the appropriate buffer (at least 20 bed bead volumes of buffer were used in total) to remove any unbound and/or nonspecifically bound protein. Bound protein of was eluted from the beads using appropriate elution buffer. Three successive elutions, each using 1 volume of bead bed volume were combined and dialysed against 5lit dialysis buffer overnight at 4^{o}C using float-a-lyzers (purchased from Spectrum Laboratories Inc) of the appropriate molecular weight cut off. Dialysed material was aliquoted and stored at -80^{o}C. Samples from all steps during protein purifications were collected and analysed routinely by SDS-PAGE (section 2.3.8).

2.3.4 Purification of His_6 tagged proteins

Purification of bacterially expressed recombinant proteins carrying a His_6 tag was based on the general protein purification protocol described in section 2.3.3. In this case the affinity matrix used was Ni^{2+}-NTA beads (with 2ml of a 50% slurry being used per litre of induced culture) and lysis buffer was Buffer C containing 2.5mM imidazole and 5mM ß-mercaptanoethanol. Washing was performed in the same containing 25mM imidazole, and protein elution achieved by further increasing the same buffer imididazole concentration to 250mM.

2.3.5 Purification of GST tagged proteins

Purification of bacterially expressed recombinant proteins tagged with GST was achieved by following the general protein purification protocol (section2.3.3). In this case glutathione-Sepharose 4B beads (purchased from GE Healthcare Bio-Sciences Ltd) were used as the affinity matrix (with 1.3 ml of a 80% slurry being used per litre of induced culture) along with GST preparation buffer. PBS containing 0.5M NaCl was used as washing buffer and GST elution buffer for final elution.

2.3.6 Purification of PrA tagged proteins

Purification of bacterially expressed proteins carrying a PrA tag was based on the general protein purification protocol described in section 2.3.3. IgG-Sepharose TM 6 Fast Flow beads (purchased from GE Healthcare Bio-Sciences Ltd) was used as the affinity matrix (with 1.3 ml of a 80% slurry being used per litre of induced culture) according to the manufacturer's instructions. Protein elution was achieved using 0.5 M acetic acid, pH 3.4.

2.3.7 GST tag cleavage using thrombin

Thrombin cleavage was performed by incubating dialysed, GST-tagged proteins with thrombin (1 unit of thrombin per 1ml of dialysed protein sample) at room temperature for 3 hours with constant mixing. Protease activity was inhibited by the addition of DFP (to a final concentration of 10mM). Cleaved GST tags and uncleaved fusion protein was removed from the solution by incubation with washed glutathione-Sepharose (usually 1ml bed volume per 3ml solution volume) for 2 hours at 4^{o}C with rotation. Beads were removed by centrifugation at 1000*g* for 5 min prior to the supernatant being aliquoted and stored at -80^{o}C (following analysis by SDS-PAGE).

2.3.8 SDS PAGE

Discontinuous sodium dodecyl sulphate polyacrylamide gel electrophoresis (SDS-PAGE) was used to resolve proteins. The resolving gel used in these studies varied in density from 10-15% acylamide depending on the molecular wieghts of the proteins being resolved. A 30% acrylamide / bisacrylamide mixture (Anachem Ltd, Luton, Bedfordshire, UK) was used to form a stacking mixture of 5% in stacking buffer (25 mM Tris.HCl pH 6.8, 0.2% (w/v) SDS) and a resolving mixture of the desired percentage (v/v) in separating buffer (75 mM Tris.HCl pH 8.8, 0.2% (w/v) SDS). Gels were polymerised by addition of ammonium persulfate (APS) and N, N, N', N' - tetramethylenediamine (TEMED). Gels were set up in Bio-Rad mini-PROTEAN III apparatus and immersed in running buffer (25 mM Tris base, 190 mM glycine, 0.1% (w/v) SDS). Protein sample were prepared for electrophoresis by incubating at 95^{o}C for 5 minutes in an equal volume of 2x LSB (100 mM Tris.HCl pH 6.8, 4% (w/v) SDS, 20% (v/v) glycerol, 0.2% (w/v) bromophenol blue, 10% (v/v) ß-mercaptoethanol). Samples were loaded on to

the gel with a BioRad Broadrange Protein Marker, and a constant electric potential of 120 volts was applied.

2.3.9 Coomassie staining/de-staining

After the proteins were resolved by SDS-PAGE (section 2.3.8) the gel was carefully immersed in coomassie staining solution for at least 45 min with gentle shaking. Gels were destained using Coomassie de-staining buffer for as long as necessary.

2.3.10 Semi-dry protein transfer

Proteins resolved by SDS-PAGE (section 2.3.8) to be analysed by immunodetection were transferred to a nitrocellulose membrane using the following protocol. Gels were removed from the tank and immersed into semi-dry transfer buffer. Then they were placed on the semi-dry transfer apparatus along with filter paper and the nitrocellulose membrane in the following order. First three pieces of moist (in semi-dry transfer buffer) filter papers were layered on the surface of the apparatus, followed by the nitrocellulose membrane (also equilibrated with transfer buffer) then the gel, followed by 3 more moist filter papers. All air bubbles were removed prior to placing the lid on the apparatus and applying a constant current of 180mA for 30-60 min. Time of transfer was determined by the number, the percentage, and the thickness of gels used and also on the size of the protein(s) of interest. Efficiency of transfer was checked by staining the membrane with Ponceau stain.

2.3.11 Western blotting (protein immunodetection)

Following transfer (section 2.3.10) membranes were washed with TBST for 5 min before being incubated with a blocking solution of 5% (w/v) non-fat dry milk in TBST for at least 1 hour. Membranes were then incubated with primary antibody diluted as appropriate (section 2.1.4) in blocking solution. Incubation with primary antibody was routinely performed overnight at 4^{o}C with constant mixing. Membranes were subsequently washed with TBST for 30 min (6 x 5 min) prior to incubation with the appropriate secondary antibody diluted in blocking solution for at least 2 hours at room temperature with gentle shaking. Following another round of washes (with TBST, 6 x 5 min) the membranes were treated with a

mixed solution made from equal volumes of ECL solutions 1 and 2 for 1-2 min and placed in a light proof cassette under clear plastic. X-ray films were exposed to membranes for 5 sec-20 min (depending on the amount of the protein on the membrane, and the affinity of the antibody for its antigen) before being developed through a Kodak x-omat 2000 device.

2.3.12 Estimation of the protein concentration

Total protein concentration in a sample was estimated based on the Bradford assay (Bradford, 1976). All measurements were made using a spectrophotometer at 595nm. A concentration gradient of BSA was used to produce a concentration standard curve that was used to estimate the concentration of protein in assayed samples.

2.4 Pull down and Complex Assembly Assay (CAA)

1-10μg of recombinant tagged protein were immobilised on the appropriate beads (sections 2.3.4-2.3.6). 10-20μl (bed volume) of the beads (with the indicated amount of bound protein) were incubated with the described purified proteins in 1ml of PBS containing 100 μg/ml BSA for various time points at 4^{o}C on a rotating wheel. The recombinant proteins added to the immobilised 'bait' were in at least 10 times molar excess compared to the protein bound to the beads. After incubation beads were collected by centrifugation (1000*g* for 1 min at 4^{o}C) and washed at least 5 times with 1ml of the appropriate buffer (based on the fusion protein bound to the beads - sections 2.3.4-2.3.6). After the final wash, beads were resuspended in 50μl of 2x SDS-PAGE loading buffer and boiled for 5 min at 95^{o}C. Protein samples were analysed by SDS-PAGE followed by Coomassie staining and immunodetection (sections 2.3.9-2.3.11)

2.5 Dot Blot assay

Membranes were prepared by dotting 2 μl of a series of successive dilutions of purified, dialysed protein (in PBS). Once the proteins had been left to dry onto the membranes, they were incubated in a blocking solution of 5% (w/v) non-fat dried milk in PBS. Following a brief wash with PBS the membrane was then incubated in a solution of the indicated protein (4 ^{o}C for 2 hours with gentle

mixing). Membranes were washed 6 x 5 min with PBS after which immunodetection analysis using the proper antibody (section2.3.11) was performed.

2.6 General cell culture methods

2.6.1 Culture of 3T3-L1 cells

Murine fibroblasts 3T3-L1 cells are an L1 substrain of 3T3 (Swiss albino) that can be differentiate into adipocytes upon contact inhibition and treatment with phosphodiesterase and hormones (section 2.6.4). 3T3-L1 fibroblasts were cultured in T75 flasks containing 15 ml fibroblast growth media and were maintained as sub-confluent cultures (70-80% confluence) at 37^{o}C in a 10% CO_2 humidified incubator. Post-differentiation adipocytes were cultured in 15 ml adipocyte growth media at 37^{o}C in a 10% CO_2 humidified incubator for 8-12 days after differentiation. In both cases medium was replaced every other day.

2.6.2 Resurrection of 3T3-L1 fibroblasts

Aliquots of fibroblasts were stored in liquid nitrogen. Cryogenic vials were removed as required and thawed in a 37°C in water bath until culture was liquefied and then was added into a T75 flask containing pre-heated fibroblast growing medium under sterile conditions.

2.6.3 Trypsinisation of 3T3-L1 fibroblasts

When fibroblast cultures reached 70-80% confluence, media was removed from the flask and cells were washed with serum-free DMEM medium. 2 ml 0.5 g/L Trypsin- 0.2 g/L EDTA·4Na (Initrogen Ltd) was added to the cells which were incubated at 37°C for 5 min. Cells were then pelleted by centrifugation at 800*g* for 5 min. The cell pellet was then resuspended in 10ml fibroblast growth medium and 0.1-1ml (depended on dilution required) added to plates or flasks containing the same medium as required.

2.6.4 Differentiation of 3T3-L1 cells

Fibroblasts were grown to confluency and subsequently starved for 3 days (no medium replacement). On the day of differentiation cells were washed with serum free DMEM medium and differentiation medium 1 was added to the flask (15ml). After three days the medium was carefully replaced by differentiation medium 2 (15ml/flask) and after two days cells started being fed normally with adipocyte growth media (replacing the media every other day until the adipocytes were used for experiments (typically on the 8^{th}-12^{th} day after differentiation).

2.6.5 Insulin stimulation of 3T3-L1 cells

Cells that were to be stimulated with insulin (or not, in the case of basal controls) were 'serum starved' for at least two hours by replacing their medium with serum free DMEM medium. Cells were then stimulated by addition of 100nM insulin into the flasks and incubated at 37°C for various time periods (based on the experiment). Basal control cells were left untreated.

2.6.6 Preparation of whole cell lysates

Two 10cm plates per condition (e.g. insulin-stimulated/basal) were placed into a tray on top of a bed of ice. Medium was removed and cells were washed three times with cold sterile PBS (15ml per wash). Cells then were scraped in adipocyte lysis buffer (250µl per plate) and homogenized by pulling 10 times through a 24 x G, and subsequently two times through a 26 x G needle. A lipid layer was separated out by centrifugation for 15 min at 500*g* at 4°C and carefully discarded. The remaining homogenate was agitated for an hour at 4°C after which time insoluble material were pelleted by centrifugation for 20 min at 15000*g* at 4°C. Cleared lysates were stored in Eppendorf tubes at -80°C (for up to 7 days). If necessary the volume of different lysate samples was adjusted to equalize total protein concentration (estimated as in section 2.3.12). Lysates were prepared for SDS-PAGE analysis by the addition of an equal volume of SDS-PAGE loading buffer and heating to 65°C for 10min.

2.7 Pull down assay from adipocyte lysate

0.5-5µg of purified 'bait' protein was immobilized on the appropriate affinity matrix (section 1.4). 10-20µl bed volume of beads (with the indicated amount of bound protein) were added to Eppendorf tubes containing 400µl adipocytes lysate obtaneid from 2 plates. Following incubation for at least 2 hours at 4^{o}C under rotation, beads were collected by centrifugation at 1000*g* for 1 min at 4^{o}C and washed at least 5 times using adipocyte lysis buffer (1ml per wash). After removal of the final wash, beads and associated proteins were resuspended in 50µl of 2x SDS-PAGE loading buffer and heated to 65^{o}C for 10min.

2.8 Surface staining of HA-tagged GLUT4 in fibroblasts

Virally transformed fibroblasts expressing HA-GLUT4-GFP were grown on ethanol washed coverslips in 24 well-plates. Following insulin-stimulation (section 1.6.5) cells were washed three times with PBS and fixed for 30min by the addition of 3% PFA (200µl per well). Two washes with GLY solution followed (200µl per well to quench PFA) and cells were subsequently blocked with BSA/GLY solution for 30min (200µl per well). Cells were exposed to α-HA antibody for 45min at room temperature by placing coverslips cell-side down onto a 40µl drop of primary antibody containing solution (diluted at a 1/500 dilution in BSA/GLY) on parafilm. Coverslips were then washed four times in BSA/GLY solution in the same way (from drop to drop, 40µl per drop). Secondary antibody was diluted (1/200) in BSA/GLY solution and applied to coverslips the same way as the primary for 30 min. After the second incubation coverslips were washed four times in BSA/GLY as before and left to dry before being mounted onto slides using Immumount (Thermo) and visualised using a 63x oil immersion objective lens fitted to a Zeiss LSM Pascal Exciter confocal fluorescence microscope (images were analysed using LSM software; Zeiss).

2.9 Proximity Ligation Assay (PLA)

Cells (fibroblasts or adipocytes) were grown on Labtech 8-chamber slides. After insulin-stimulation (section 2.6.6) cells were washed three times with PBS and fixed for 30min by the addition of 3% PFA (200µl per well). Two washes with

GLY solution followed (200μl per well to quench PFA) before cells were blocked and permeabilized in BSA/GLY/SAP solution for 30min (200μl per well). Primary antibodies were diluted 1/200 in BSA/GLY/SAP and added (100μl per well) and incubated overnight at 37°C in a humidity incubator. The following day wells were removed from the slides and the PLA protocol was performed following the manufacturers' instructions. Based on these cells were washed using the permeabilization buffer and the proximity probes (secondary antibodies attached to single stranded DNA oligonucleotides) were added in a 1/5 dilution using the same buffer as the primary antibodies. Cells were incubated at 37°C in a humidity chamber for 90 min. After incubation cells were washed carefully with 0.05% (v/v) tween-20 in TBST and the hybridisation/ligation solution, which is included to the kit, added and cells were incubated for 30 min at 37°C in a humidity chamber. Keeping the cells always wet was of great importance in order to avoid the intense fluorescent background due to staining artefacts. Use of humidity chamber is necessary since the working volumes of the assay are ~ 40-50 μl per 1 cm^2 of slide area. After hybridisation and successful ligation of the additional oligonucleotides cells were washed again using the same washing buffer and then treated with the amplification and detection solution (provided by the kit) and were incubated for at least two hours in a humidity chamber at 37°C. During that step the RCA took place and complementary single stranded oligonucleotides carrying the fluorescent moiety were hybridised to the elongated DNA single stranded molecule attached to one of the proximity probes (secondary antibody). After this step cells on the slides were washed thoroughly using a series of dilutions of a washing buffer (0.2M Tris base and 0.1M NaCl). Slides left dry at room temperature and were mounted using kit's mounting medium, which contains the nuclear stain (DAPI). Finally the mounted slides were examined using a 63x oil immersion objective lens fitted to a Zeiss LSM Pascal Exciter confocal fluorescence microscope, and images were analyzed using LSM software (Zeiss). Pictures were further studied using Blobfinder software (signal estimation). The following parameters were adjusted as described and kept constant throughout all the figure analysis: Blob Threshold: 120 (arbitrary units). Minimum nucleus size: 100 pixels. Cytoplasm size: 200 pixels. Blob size: 3x3 pixels. The data were statistically analyzed using SPSS (statistical analysis software).

Chapter 3

Use of Proximity Ligation Assay to Investigate Associations Between SNARE and SM proteins involved in GLUT4 vesicle exocytosis

3.1 Introduction

3.1.1 Insulin function and SNARE-mediated delivery of GLUT4 to the plasma membrane

Insulin stimulates glucose uptake by adipose tissue, skeletal muscle and the heart by regulating the trafficking of facilitative glucose transporter 4 (GLUT4) (James et al., 1988; James et al., 1989) from an intracellular store to the plasma membrane (reviewed in (Bryant et al., 2002)). Under basal conditions around 95% of cellular GLUT4 localises to various intracellular compartments (Slot et al., 1991b) and is retained intracellularly by continually cycling through the endosomal system. Upon insulin stimulation a signalling cascade is initiated which results in redistribution of GLUT4 from perinuclear depots termed GSVs, for GLUT4-storage vesicles, to the plasma membrane (Bryant and Gould, 2011). This 10 to 20 fold increase of GLUT4 at the cell surface in response to insulin is attained by a significant increase in the exocytic rate of GLUT4 (Bryant et al., 2002) and a concomitant decline of GLUT4-endocytosis (Yang et al., 1992).

Membrane traffic is regulated by the formation of specific SNARE complexes in all eukaryotic cells (Cai et al., 2007; St-Denis et al., 1999). The insulin dependent translocation of GLUT4 from GSVs to the plasma membrane is a specialised example of regulated membrane trafficking. Various studies in both adipocytes and muscle cells have revealed that GLUT4-vesicle fusion is mediated by the formation of a functional SNARE complex between the plasma membrane localized t-SNAREs Syntaxin 4 and SNAP23, and the v-SNARE VAMP2 present in the GLUT4-containing vesicles (Bryant and Gould, 2011). It is of great importance that all trafficking steps mediated by the function of SNARE proteins are both spatially and temporally coordinated. One family of proteins that orchestrate SNARE function is the Sec1/Munc18 (SM) protein family (Toonen and Verhage, 2003) (section 1.3.2). Various studies have established that the SM protein, which mediates GLUT4 vesicle fusion with the plasma membrane, is Munc18c, and that this is achieved *via* a series of interactions of the SM protein with Syntaxin 4, VAMP2 as well as with the assembled SNARE complex (Aran et al., 2009; Brandie et al., 2008; Latham et al., 2006). Understanding the interactions that occur between SNARE proteins themselves and also with Munc18c in insulin-responsive cells, and how these might change upon insulin-

stimulation is likely to give insight into both insulin-action SNARE protein function and was an overall aim of the research presented in this thesis.

3.1.2 Techniques to Assay Protein-Protein interactions

Important insight into cell function can be gained by studying the 'interactome' of molecules known to function in the process of interest. Various techniques have been developed and are widely used to investigate protein-protein interactions. The majority of these rely on probe-based targeting or direct labelling of proteins. In probe-based targeting assays the target molecule is usually labelled by using a high specific affinity reagent (routinely an antibody), which can be labelled (e.g. with a flurofore or an enzyme). Co-immunoprecipitation (co-IP), a procedure that uses an antibody to pull down the protein of interest along with interacting partners from cell lysates has been used widely for SNARE protein interaction studies. The major disadvantage of this technique is that it is extremely invasive in that it requires cell destruction, and can give misleading results since protein localisation in the cell, which often enhances specificity of protein interaction, is disrupted. It can be hard to ascertain whether an interaction observed by co-IP occurs in the cell before lysis or occurs post-lysis. Similarly, weak or transient interactions can be missed, or underestimated by co-IP as they may be disrupted during the procedure. Immunochemistry (IHC) and immunofluorescence (IF), methods that use a reporter molecule on the antibody specific to target molecule, can overcome these problems and allow detection of proteins *in situ*. IF has been used to study SNARE protein interactions in insulin sensitive cells by co-localizing two different fluorophores attached to antibodies against two different proteins. However, the microscopic resolution in these studies is poor, and at best they indicate whether the two proteins of interest are within 200 nm of each other (maximum resolution of light microscopy). In addition, the qualitative nature of this technique makes comparison of a specific protein-protein interaction under different conditions difficult. Some of these limitations can be overcome by using direct targeting methods such as Förster resonance energy transfer (FRET) or bioluminescent resonance energy transfer (BRET) that use fusion constructs linked to reporter molecules. These are more quantitative and the proximity of the two proteins can be delineated more precisely since the energy transfer from donor reporter to acceptor reporter is only possible in a range of 5-10nm

(Vogel et al., 2006). However, the accuracy of those assays is shadowed by their requirement for tagged proteins. Addition of a protein tag can alter protein's native structure and function, and is of particular concern when studying SNARE protein function. The same drawback applies to split yellow/green fluorescent protein assays (split-YFP/GFP) methods that signal when the two domains of YFP or GFP fused to different proteins are close enough together to form the fluorescent protein, as in the case of protein-protein interaction.

3.1.3 Proximity ligation assay (PLA)

PLA is a relatively new technique that allows detection of protein-protein interactions, or more precisely, protein-protein associations (Soderberg et al., 2006). PLA combines advantages associated with probe-targeted methods (i.e. it can be used to study endogenous, untagged proteins) with those of a split-reporter assay, providing a sensitive and selective approach for protein-protein interaction studies. This method (outlined in Figure 3-1) uses a pair of proximity probes - two secondary antibodies, specific for primary antibodies against the two proteins whose interactions are being investigated raised in different species- with a single stranded oligonucleotide attached to each one. In the case of interacting proteins the binding of the oligo-tagged secondary antibodies to adjacent primary antibodies allows hybridisation of two additionally added connector oligonucleotides. Following hybridisation, enzymatic ligation of the hybridised oligonuceotides forms a circular single stranded DNA molecule that can serve as a template for rolling circle amplification (RCA). The polymerase used is φ29 DNA polymerase that is highly possessive (Soderberg et al., 2008). The amplification is primed from one of the oligonucleotides attached to the secondary antibodies. The other is chemically modified at its 5' and not available for extension (Soderberg et al., 2006). As amplification continues, the polymerase displaces the newly synthesised strand resulting in production of an elongated single stranded DNA polynucleotide whose sequence consists of complementary repeats of the circularised template. The RCA product can be visualised by hybridisation of fluorescently labelled oligonucleotides complementary to a sequence contained within the circular DNA template. The amplified single stranded DNA consists of numerous repeats, a property that allows hybridisation of a large number of detection oligonucleotides to provide signal amplification. The resulting signal can be visualised using a fluorescent

microscope, with each protein-protein interaction, or more accurately, association, given that a positive signal is dictated by the length of the oligonucleotides coupled to the secondary antibodies, typically 10-15 nm, being represented as a fluorescent dot. Use of the blobfinder software it was of great importance in order to obtain reliable results. The fact that the same parameters were used regarding the estimation of cell size as well as the size and intensity of PLA spots (signal), as described in section 2.9 warrants that any biased evaluation of the PLA signal was avoided (distinction problem between background and actual signal). The main advantages of PLA as a technique to monitor protein-protein interactions can be summarised as follows.

- Non invasive (*in situ* studies).
- Detects endogenous native proteins.
- Provides data that can be easily enumerated and statistically analysed

Like FRET, BRET and split YFP/GFP systems, PLA enables changes in protein-protein interactions under different conditions to be monitored but offers the advantage that endogenous proteins can be followed.

The main caveat of this method is that it is almost impossible to clarify whether the assay detects single molecule pairs or cohorts of molecules. The fact that spots of uniform size were always obtained in every single cell whenever PLA was performed (chapters 3 and 5) argues in favor of the first possibility. Nevertheless PLA was used not to estimate the actual extent of the interactions but rather how this change upon different conditions. So the nature of PLA signal whatever it is should not affect the results. As an immunofluorescent based method, PLA faces the same common problems with other immunodetection approaches such as incomplete immobilization, re-organisation, cytoskeletal changes, epitope accessibility and antibody ‘pathching’. These difficulties were overcome by the use of appropriate technical controls (omission of one of the primary antibodies) and the fact that PLA was used to compare the difference, if any, of interactions in two different conditions.

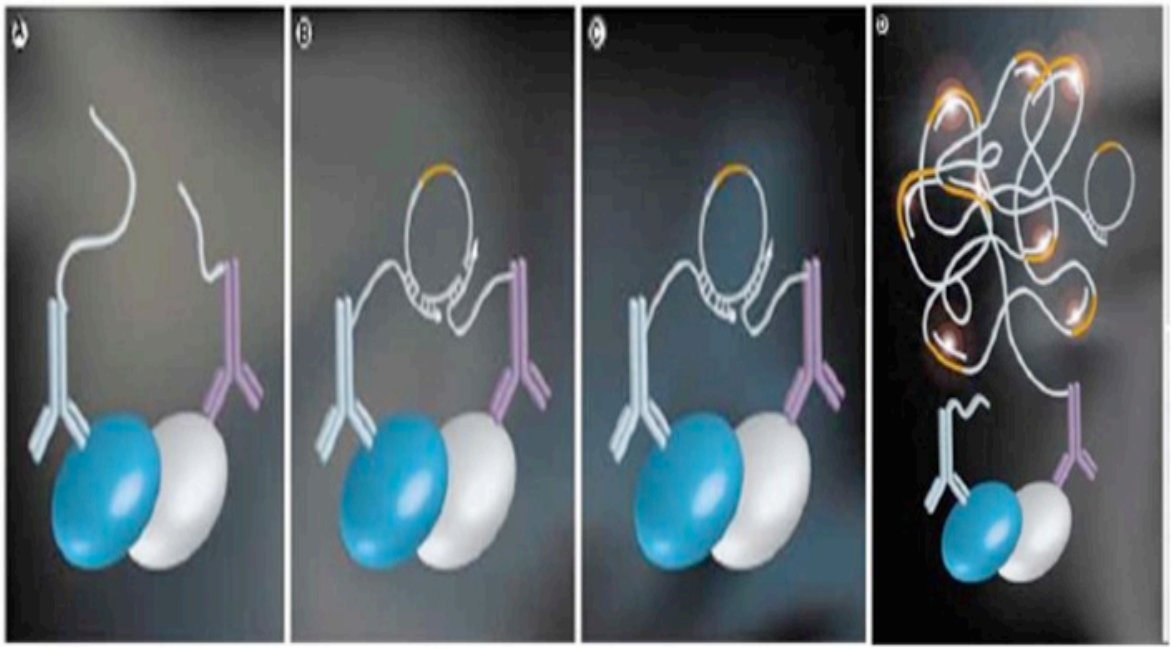

Figure 3-1. *In situ* detection of protein-protein interactions.

(A) If two proximity probes bind close to each other, such as binding two proteins present in the same complex, (B) then subsequently added linear connector oligonucleotides are guided to form a circular structure covalently joined by enzymatic DNA ligation. (C) After ligation, rolling circle amplification is initiated using one of the proximity probes as a primer. (D) The amplification product is detected through hybridization of fluorescence-labelled oligonucleotides complementary to a tag sequence in the amplification product. Picture modified from (Weibrecht et al., 2010)

3.2 Aims of this chapter

Trafficking of the facilitative glucose transporter GLUT4 is regulated by insulin in fat and muscle cells; under basal conditions, GLUT4 is retained intracellularly by continually cycling through the endosomal system, but translocates to the plasma membrane in response to insulin-stimulation (Bryant et al., 2002). Fusion of GLUT4-containing vesicles with the plasma membrane is mediated by formation of SNARE complexes containing the plasma membrane localized t-SNAREs Syntaxin 4 and SNAP23 and the v-SNARE VAMP2 present in the GSVs (Bryant et al., 2002). Putting these two observations together, i.e. that insulin regulated GLUT4 translocation and that GLUT4 translocation is regulated by Syntaxin 4-containing SNARE complex formation, it is tempting to hypothesize that insulin regulate Syntaxin 4- containing SNARE complex formation. Here, in order to directly test this hypothesis I have used *in situ* Proximity Ligation Assay (PLA) to visualize protein-protein interactions and study the effects of insulin

stimulation on associations between Syntaxin 4, SNAP23, VAMP2 and Munc18c protein in 3T3-L1 adipocytes and fibroblasts.

3.3 Results

3.3.1 GLUT4 is translocated to the plasma membrane upon insulin stimulation of 3T3-L1 fibroblasts expressing HA-GLUT4-GFP.

Due to their large size, high lipid content and lengthy differentiation procedure, adipocytes, which are cells most commonly used to study insulin regulated GLUT4 traffic were not used to optimise the PLA technique. The combination of their large, spherical morphology makes focusing problematic, and the lipid droplets are present in abundance in their cytosol give a strong fluorescent background due to their hydrophobicity. While confocal microscopy along with the use of appropriate filters can circumvent such problems, I chose instead to optimise the use of PLA in an easier to handle cell line, namely fibroblasts. To investigate the validity of using fibroblasts as a model to study the effects of insulin on SNARE complex assembly it was crucial to establish whether fibroblasts regulate trafficking of GLUT4 in response to insulin. For that reason GLUT4 surface immunostaining was performed on 3T3-L1 fibroblasts virally infected to stably express GLUT4 tagged with HA in the first exofacial loop and green fluorescent protein (GFP) at the C terminus (kind gift from Prof Gould). Construction of exofacially HA-tagged GLUT4 expression vector and production of a stably expressing cell line is thoroughly described in (Shewan et al., 2000). This construct allows total GLUT4 to be visualised by virtue of the GFP tag, and the presence of GLUT4 at the cell surface to be assayed by staining for the HA-epitope in the absence of cell permeabilisation. Figure 3-2 demonstrates that fibroblasts translocate ectopically expressed HA-GLUT4-GFP to the cell surface in response to insulin. It is believed that paraformaldehyde fixation might permeabilise the cells and gives false positive results (cytoplasmic detection). Nevertheless ‘nuclear sparing’ that insulin treated cells appear to have is rather a result of confocal microscopy, which excludes the relatively bulky nucleus from the visualised layer, and not due to any failure of cell fixation. These data establish fibroblasts as good model in which to study changes in SNARE protein interactions upon insulin stimulation.

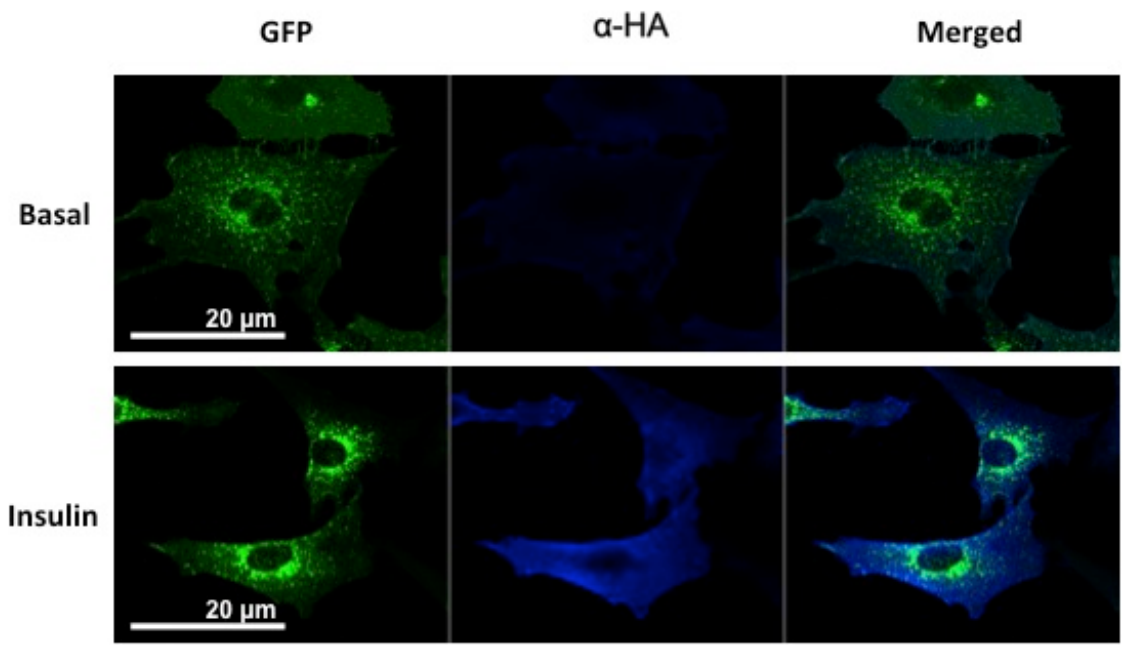

Figure 3-2. GLUT4 translocation in fibroblasts

Sub confluent 3T3-L1 virally infected fibroblasts stably expressing HA-GLUT4-GFP were grown on sterile coverslips to 70-80% confluency. The cells were serum starved for 2 hours and either treated with 100 nM insulin for 30 minutes (Insulin) or not (Basal) (section 2.6.5), prior to being fixed using 3 % (v/v) paraformaldehyde and stained for surface (blue) HA epitope (located in the first extracellular loop of GLUT4). The total amount of GLUT4 was visualized by the GFP tag (green). Images are representative of three independent experiments.

3.3.2 Selection of Primary Antibodies for PLA between Syntaxin 4, SNAP23, VAMP2 and Munc18c

The choice of primary antibodies is a crucial factor for both the reliability and success of PLA. The primary antibodies should be of IgG class, and specific for the target to be detected and ideally affinity purified according to kit's requirements. It is essential that the two different antibodies, that recognise the two proteins whose interaction/association are being assayed, are raised in different species (in this study, I used mouse and rabbit) and must bind to their target under the same conditions (e.g. following the same fixation protocol, in the presence of the same dilution/permeabilising buffer).

Sufficient different antibodies against the three SNARE proteins (Syntaxin 4, SNAP23 and VAMP2) and the SM protein (Munc18c) involved in regulating GLUT4 exocytosis were purchased in order that all possible pairwise associations between these 4 proteins could be examined using PLA with the required 'two-

different-species-raised antibodies' criterion fulfilled (section 2.9). As an initial characterisation, each of these antibodies were used in immunoblot analysis against cell lysate, to check that, as stated by the manufacturers, they recognise a single band of the appropriate molecular weight. Figure 3-3 demonstrates that this is the case and these antibodies were subsequently used as the primary antibodies for PLA in this study.

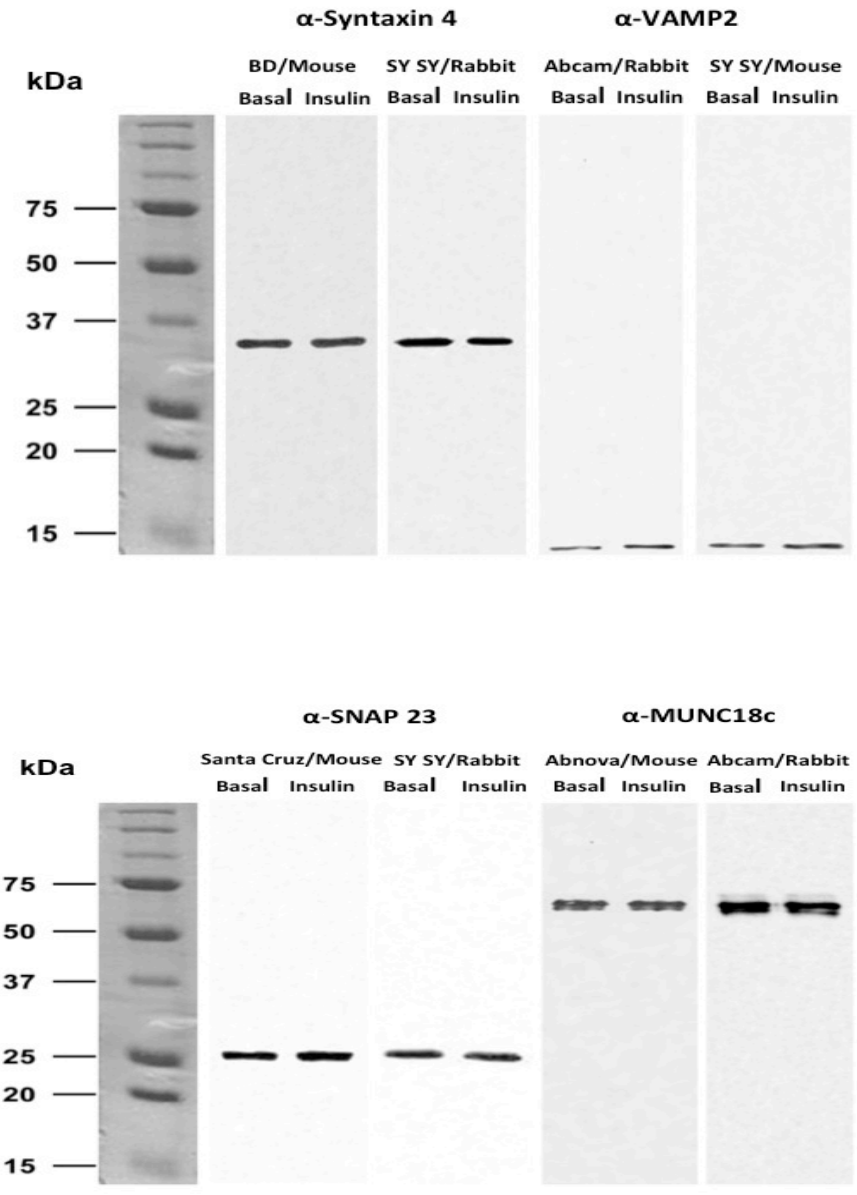

Figure 3-3. Immunoblot Analysis Characterisation of Primary antibodies used for PLA

Cell lysates (~10 mg/ml) prepared from 3T3-L1 adipocytes treated with insulin (100 nM for 30 min) (insulin) or not (basal) as described in section 2.6.5 were subject to immunoblot analysis using the commercially available antibodies against Syntaxin 4,SNAP23 (upper panel) and VAMP2, Munc18c (lower panel) listed in section 2.1.4.

Having validated fibroblasts as a suitable model in which to study insulin-stimulated GLUT4 translocation, these cells were used initially to optimise conditions for PLA given that they are quicker (and less expensive) to grow and less problematic to image. It was, however, considered essential that these studies were also carried out in differentiated adipocytes and therefore this chapter presents data obtained using both 3T3-L1 fibroblasts, and adipocytes in the presence and absence of insulin-stimulation.

As described in section 2.6.5, cells were serum starved for two hours prior to stimulation with 100 nM insulin for five minutes or not (basal). The short period of five minutes stimulation was chosen since interactions between SNARE proteins themselves and/or with Munc18c are relatively transient in contrast to the time frame of GLUT4 translocation to the plasma membrane upon insulin stimulation (which is an additive phenomenon so longer periods of insulin treatment are required to have significant impact) (Bryant and Gould, 2011). After insulin stimulation cells were rapidly fixed (to provide a snapshot of protein-protein interactions) prior to permeabilisation and incubation with the appropriate primary antibodies (or just one antibody in the case of control experiments)

3.3.3 PLA for Syntaxin 4/Munc18c in 3T3-L1 cells

Like most SM proteins, Munc18c has been demonstrated to bind its cognate syntaxin *via* several different modes (Aran et al., 2009; Latham et al., 2006). PLA using antibodies specific for Syntaxin 4 and Munc18c performed in both fibroblasts and adipocytes demonstrate that this technique can be used to visualise protein-protein interactions in these cells. It is important to note that in control experiments, where either one of the primary antibodies was omitted, no signal was observed in either cell type. Similarly, no signal was observed if either of the secondary antibodies was omitted. These were the criteria used to optimise conditions for each pairwise interaction (only one control is shown in each of the following data sets, but for each experiment presented all these controls were negative).

Figure 3-4 demonstrates that Syntaxin 4 and Munc18c are found in close proximity (i.e. within 10-15 nm of each other) in both fibroblasts and adipocytes

under both basal and insulin-stimulated conditions. These data are consistent with previous studies showing that Munc18c interacts with Syntaxin 4 under basal conditions (D'Andrea-Merrins et al., 2007; Latham et al., 2006).

Statistical analysis of the PLA results was made using the blobfinder and the SPPS software (Mann-Whitney U test) as described in section 2.9 was used to ascertain whether there was any change is the number of associations detected between Syntaxin 4 and Munc18c following insulin-stimulation. No statistically significant difference was found between basal and insulin stimulation conditions in either cell type (Figure 3-4). It was perhaps surprising that the addition of insulin didn't result in fewer interactions of Munc18c with Syntaxin 4, as it has been proposed that insulin acts to release an inhibitory interaction between the two proteins and subsequently allows Syntaxin 4 to adopt its fusogenic conformation (open conformation) essential for SNARE complex formation and membrane fusion (Tamori et al., 1998). Based on the data presented in Figure 3-4 it appears that Munc18c remains bound to Syntaxin 4 following insulin-stimulation. It has been previously suggested that Syntaxin 4 and Munc18c bind *via* different modes under different physiological conditions (Smithers et al., 2008), and one possibility if that the associations detected under insulin stimulation are *via* a different binding mode from those observed in basal cells. Such a switch in binding modes may form part of a regulatory mechanism (discussed further in section 1.3.3). In addition, Munc18c binds Syntaxin 4, not only in its monomeric state, but also as part of the Syntaxin 4/SNAP23 binary t-SNARE complex, and also the assembled SNARE complex (Latham et al., 2006; Widberg et al., 2003); any one of these associations will result in a positive signal by PLA.

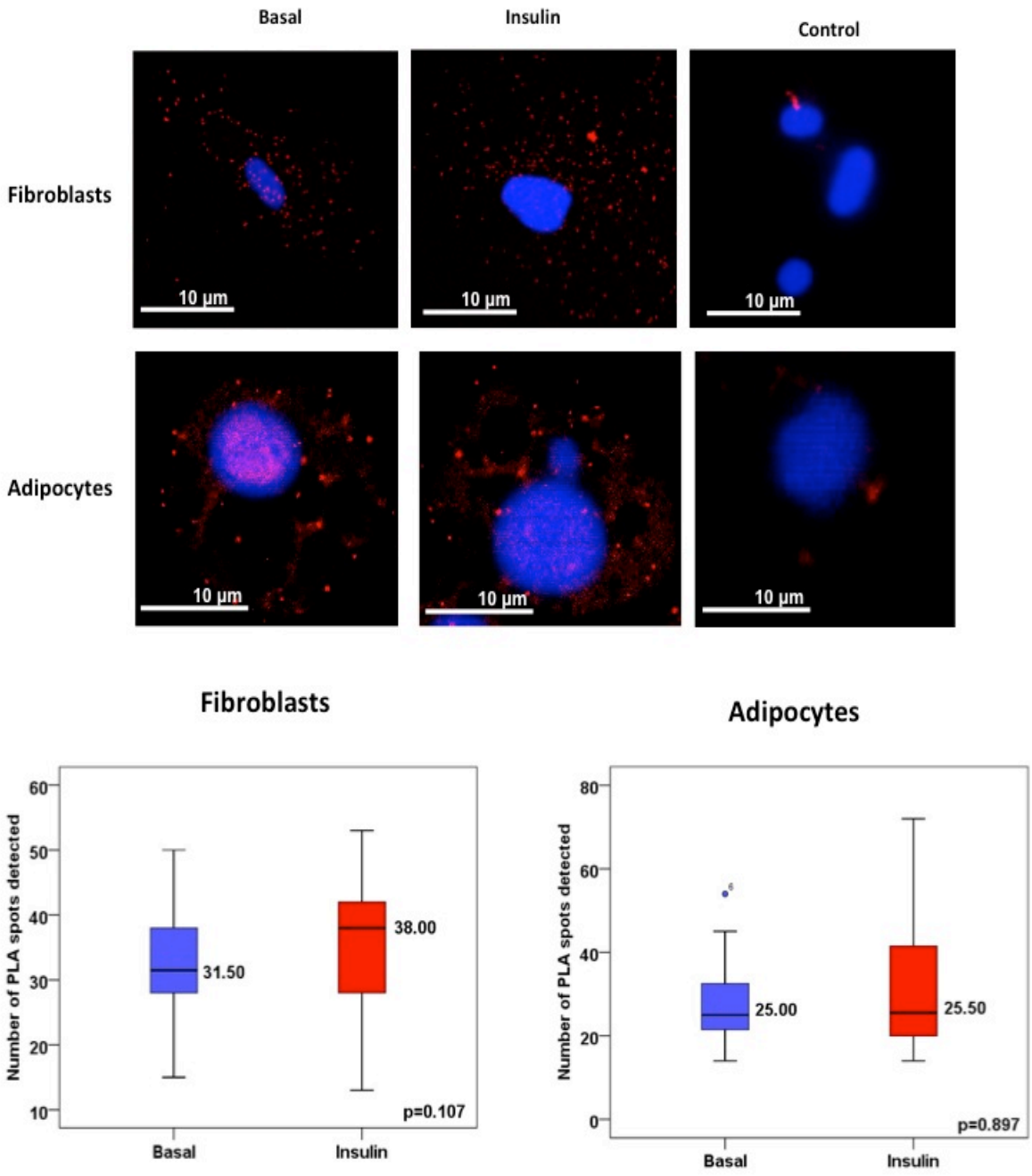

Figure 3-4. Syntaxin 4/Munc18c PLA

PLA using antibodies against Syntaxin 4 (BD mouse) and Munc18c (Abcam rabbit) was performed in 3T3-L1 fibroblasts and adipocytes treated with insulin (100nM for 5 min) or not (basal). Red spots correspond to protein protein interaction couples. Blue: DAPI stained nuclei. The control shown represents the omission of the primary antibody against Syntaxin 4. Statistical analysis of the PLA results was performed using blobfinder and SPSS software (Mann-Whitney U test) (see appendix Figure 8-1 Figure 8-2 Figure 8-3). The numbers in the boxes illustrate the median value (30 to 95 cells per experiment). Images are representative of three independent experiments.

3.3.4 PLA for VAMP2/Munc18c in 3T3-L1 cells

Several SM proteins have been shown to bind directly to their cognate R-SNARE (section 1.3.2.4), including Munc18c which binds directly to the R-SNARE VAMP2 *in vitro* (Brandie et al., 2008). PLA on both 3T3-L1 fibroblast and adipocytes as using primary antibodies against VAMP2 and Munc18c revealed that Munc18c and VAMP2 are in proximity to each other under basal and insulin-stimulated conditions in both fibroblast and adipocytes (Figure 3-5). Of course, while this is consistent with a direct interaction between these two proteins, these data do not exclude other possibilities such as Munc18c binding to the assembled SNARE complex. No statistically significant differences in association were found upon insulin-stimulation compared to basal conditions, which might indicates that Munc18c is not released from the site of fusion. This is consistent with studies reporting that the neuronal SM protein Munc18a is not released from fusion site (Rodkey et al., 2008) and is consistent with its potential role in the formation of SNARE complexes.

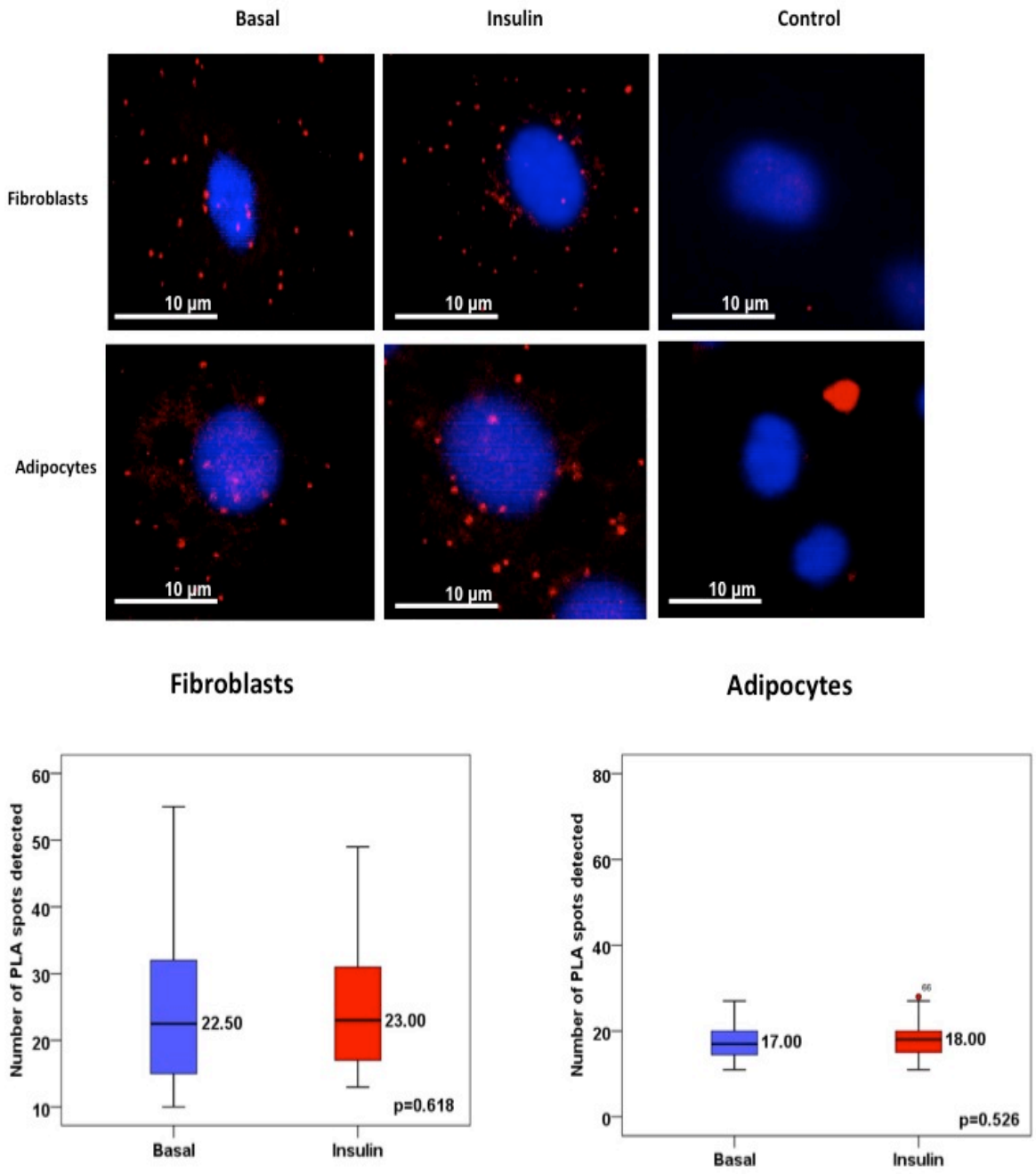

Figure 3-5. VAMP2/Munc18c PLA

PLA using antibodies against VAMP2 (SySy mouse) and Munc18c **(Abcam rabbit) w**as performed in 3T3-L1 fibroblasts and adipocytes treated with insulin (100nM for 5 min) or not (basal). Red spots correspond to protein protein interaction couples. Blue: DAPI stained nuclei. The control shown represents the omission of the primary antibody against VAMP2. Statistical analysis of the PLA results was performed using blobfinder and SPSS software (Mann-Whitney U test) (see appendix Figure 8-4 Figure 8-5 Figure 8-6). The numbers in the boxes illustrate the median value (30 to 95 cells per experiment). Images are representative of three independent experiments.

3.3.5 PLA between SNAP23/Munc18c in 3T3-L1 cells

PLA on both 3T3-L1 fibroblasts and adipocytes using primary antibodies against SNAP23 and Munc18c revealed no proximity between the two under basal conditions (Figure 3-6). This was not surprising, as no direct interaction between these two proteins has been reported (or indeed between homologous proteins such as SNAP25 and Munc18a). Strikingly a significant increase of PLA signal was observed in both cell types after insulin stimulation. Given that no direct interaction appears to exist between these two proteins (see also section 5.3.4), these data suggest that Munc18c is recruited to either a binary complex of SNAP23 with Syntaxin 4 (assembled t-SNARE complex), or the assembled Syntaxin 4/SNAP23/VAMP2 SNARE complex.

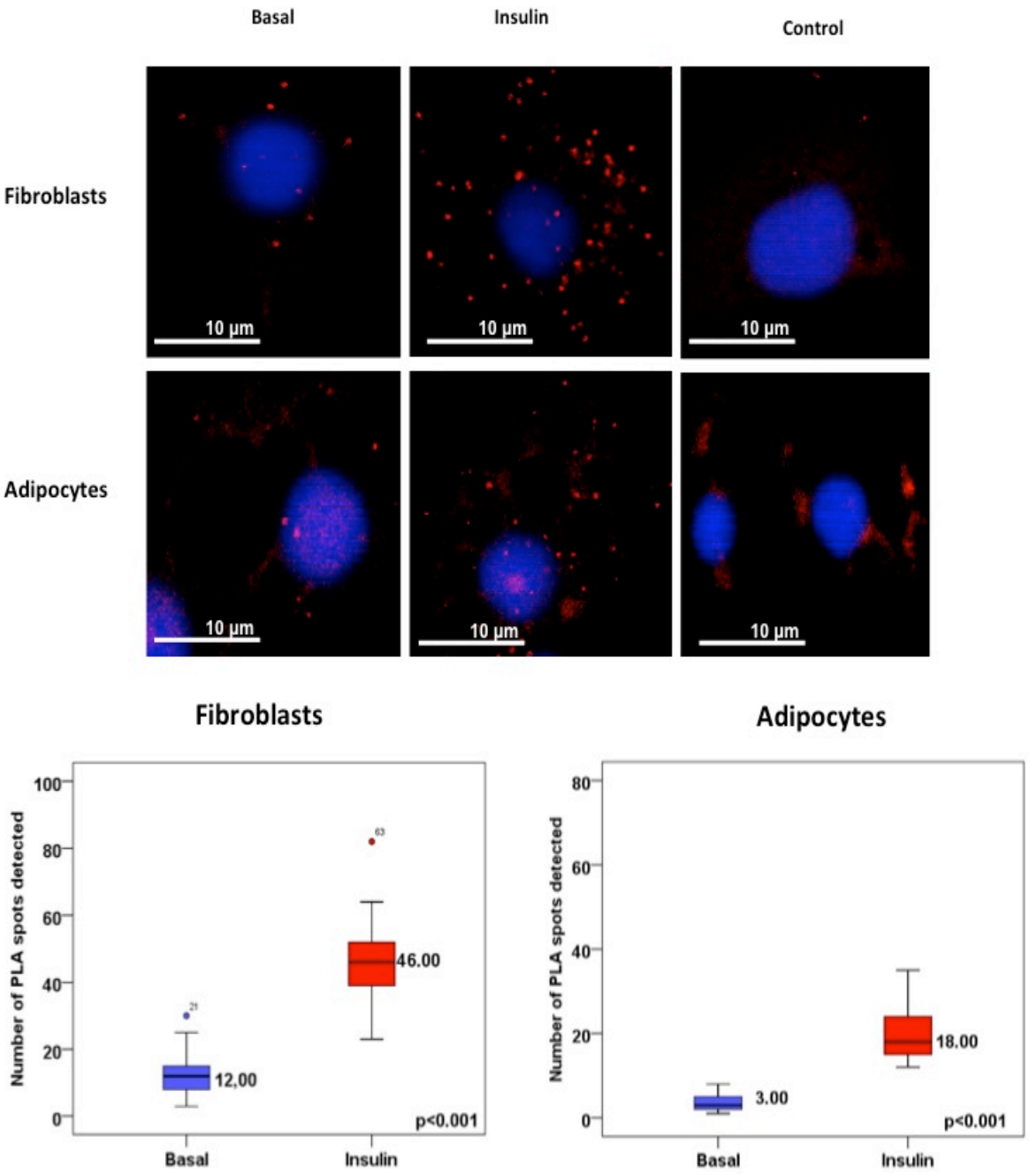

Figure 3-6. SNAP23/Munc18c PLA

PLA using antibodies against SNAP23 (Santa Cruz mouse) and Munc18c (Abcam rabbit) was performed in 3T3-L1 fibroblasts and adipocytes treated with insulin (100nM for 5 min) or not (basal). Red spots correspond to protein protein interaction couples. Blue: DAPI stained nuclei. The control shown represents the omission of the primary antibody against Munc18c. Statistical analysis of the PLA results was performed using blobfinder and SPSS software (Mann-Whitney U test) (see appendix Figure 8-7 Figure 8-8 Figure 8-9). The numbers in the boxes illustrate the median value (30 to 95 cells per experiment). Images are representative of three independent experiments.

3.3.6 PLA between SNAP23 and Syntaxin 4 in 3T3-L1 cells

Current models of SNARE complex formation favour the formation of a t-SNARE complex prior to functional SNARE complex assembly (Halemani et al., 2010; Kawaguchi et al., 2010). Co-immunoprecipitation studies in rat adipocytes have been used to report that SNAP23 and Syntaxin 4 form a stable hetero dimer at the cell surface under basal conditions whose abundance is not affected by insulin-stimulation of these cells (St-Denis et al., 1999). PLA performed on both adipocytes and fibroblasts under basal and insulin stimulation conditions produced results consistent with this conclusion, with positive signals being observed in all cases, the number of which did not alter in response to insulin-stimulation (Figure 3-7).

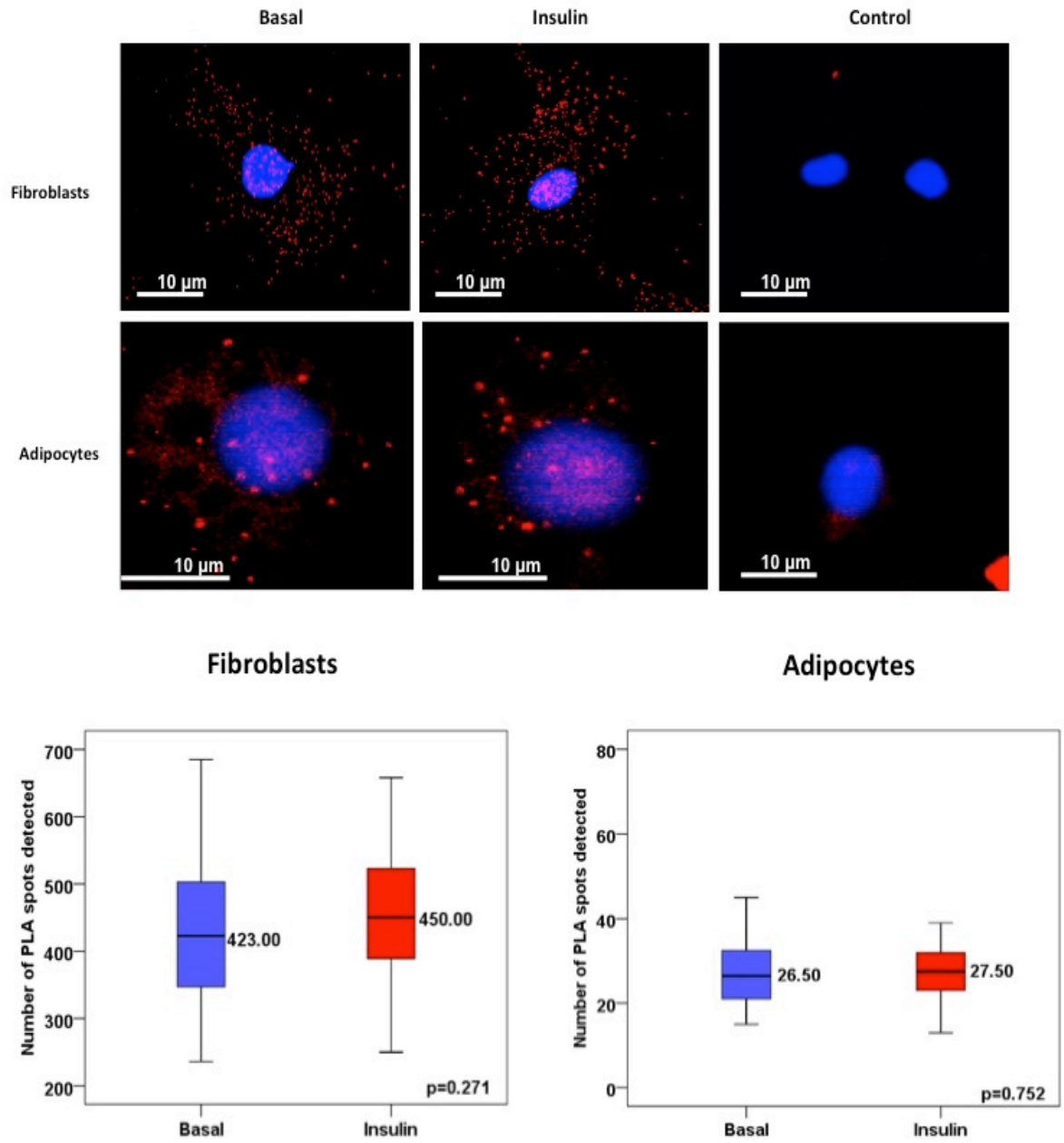

Figure 3-7. SNAP23/Syntaxin 4 PLA

PLA using antibodies against SNAP23 (Santa Cruz mouse) and Syntaxin 4 (SySy rabbit) was performed in 3T3-L1 fibroblasts and adipocytes treated with insulin (100nM for 5 min) or not (basal). Red spots correspond to protein protein interaction couples. Blue: DAPI stained nuclei. The control shown represents the omission of the primary antibody against Syntaxin 4. Statistical analysis of the PLA results was performed using blobfinder and SPSS software (Mann-Whitney U test) (see appendix Figure 8-10 Figure 8-11 Figure 8-12). The numbers in the boxes illustrate the median value (30 to 95 cells per experiment). Images are representative of three independent experiments.

3.3.7 PLA between VAMP2 and Syntaxin 4 in 3T3-L1 cells

PLA on 3T3-L1 fibroblasts and adipocytes using primary antibodies against VAMP2 and Syntaxin 4 revealed that the two proteins are in close proximity to each other in both cell types with no statistical differences in the associations being observed under insulin-stimulated, as compared to basal conditions (Figure 3-8). While, as discussed above for associations between SNAP23 and Munc18c (section 3.3.5) this is not proof of a direct interaction between VAMP2 and Syntaxin 4, it is an intriguing observation as *in vitro* binding studies have reported that the two do bind directly to each other (Calakos et al., 1994) The data presented here indicates a possible interaction between VAMP2 and Syntaxin 4 may exist under basal conditions prior to formation of SNARE complex, a possibility that will be further discussed later in this thesis (chapter 4).

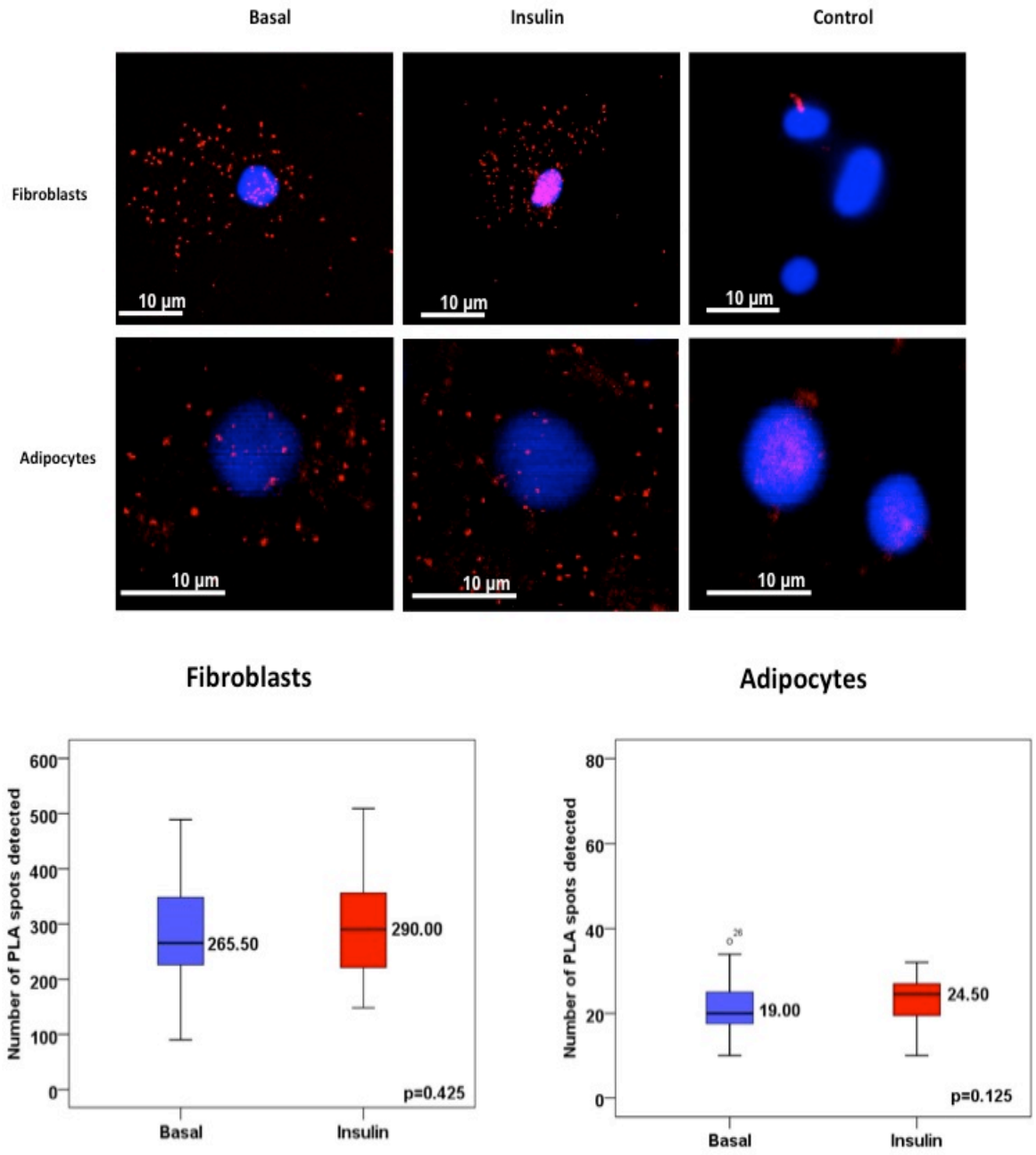

Figure 3-8. VAMP2/Syntaxin 4 PLA

PLA using antibodies against VAMP2 (Abcam rabbit) and Syntaxin 4 (BD mouse) was performed in 3T3-L1 fibroblasts and adipocytes treated with insulin (100nM for 5 min) or not (basal). Red spots correspond to protein protein interaction couples. Blue: DAPI stained nuclei. The control shown represents the omission of the primary antibody against VAMP2. Statistical analysis of the PLA results was performed using blobfinder and SPSS software (Mann-Whitney U test) (see appendix Figure 8-13 Figure 8-14 Figure 8-15). The numbers in the boxes illustrate the median value (30 to 95 cells per experiment). Images are representative of three independent experiments.

3.3.8 PLA for SNAP23/VAMP2 interaction in 3T3-L1 cells

Associations between the last pairwise combination (SNAP23/VAMP2) in this study were also examined using PLA in both adipocytes and fibroblasts, again under basal and insulin-stimulated conditions. Figure 3-9 demonstrates that very little PLA signal was observed under basal conditions in both cell types. This was not surprising as there is no convincing evidence for a direct interaction between those proteins. Yet Roche and his colleagues showed that SNAP23 binds to VAMP2 in vitro (Ravichandran et al., 1996). This observation was rather an artefact than an actual interaction of these two proteins since the buffer was used did not contain any reducing agent. This would favour the formation of disulphide bonds between the multiple cysteine residues of SNAP23 altering its structure or/and forming SNAP23 dimers. A significant increase in PLA signal between SNAP23 and VAMP2 was observed in both cell types upon insulin-stimulation. The simplest explanation for this is that SNAP23 and VAMP2 are brought into close proximity as part of the assembled Syntaxin 4/SNAP23/VAMP2 SNARE complex, the number of which increases in response to insulin.

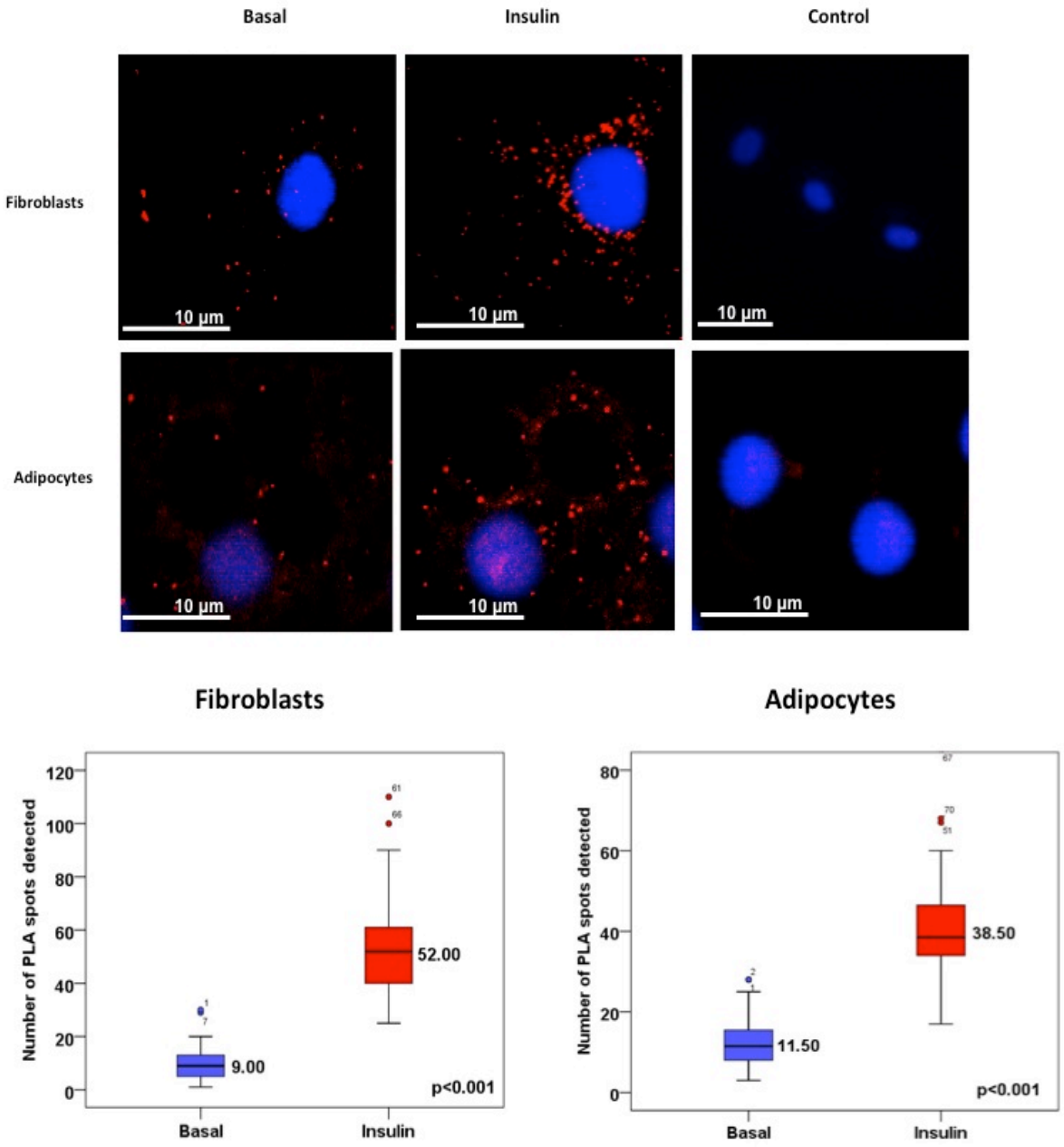

Figure 3-9. SNAP23/VAMP2 PLA

PLA using antibodies against VAMP2 (Abcam rabbit) and SNAP23 (Santa Cruz mouse) as performed in 3T3-L1 fibroblasts and adipocytes treated with insulin (100nM for 5 min) or not (basal). Red spots correspond to protein protein interaction couples. Blue: DAPI stained nuclei. The control shown represents the omission of the primary antibody against SNAP23. Statistical analysis of the PLA results was performed using blobfinder and SPSS software (Mann-Whitney U test) (see appendix Figure 8-16 Figure 8-17 Figure 8-18). The numbers in the boxes illustrate the median value (30 to 95 cells per experiment). Images are representative of three independent experiments.

3.4 Discussion

Fusion of GLUT4-containing vesicles with the plasma membrane in response to insulin is mediated by formation of SNARE complexes containing the plasma membrane localized t-SNAREs Syntaxin 4 and SNAP23 and the v-SNARE VAMP2 present in the GLUT4-containing vesicles (Bryant and Gould, 2011; Bryant et al., 2002). The Sec1/Munc18 (SM) protein Munc18c also plays a key role in insulin-stimulated GLUT4 translocation, likely through regulating Syntaxin 4-containing SNARE complexes (Bryant and Gould, 2011; Bryant et al., 2002). In this chapter I used Proximity ligation Assay (PLA) to visualize associations between Syntaxin 4, SNAP23, VAMP2 and Munc18c in all six possible pairwise combinations and also asked whether these are altered in response to insulin. This series of experiments was performed to investigate whether insulin-stimulation regulates SNARE complex formation.

I successfully established the technique of PLA in both fibroblasts and adipocytes using the established interactions of Syntaxin 4 with Munc18c and SNAP23 that have been characterised both *in vitro* and *in vivo* (D'Andrea-Merrins et al., 2007; Latham et al., 2006; Pevsner et al., 1994; St-Denis et al., 1999). The data presented in figures Figure 3-4 and Figure 3-7 are consistent with these studies and provide the first visualised of these interactions *in situ*. In addition, PLA between the SM protein Munc18c and the R-SNARE protein VAMP2 indicates that the direct interaction of these two proteins shown *in vitro* (Brandie et al., 2008) also occurs in the cell – although the positive PLA signal between these two proteins alone can not exclude the possibility of (a) bridging protein(s) e.g. an assembled SNARE complex.

Perhaps the most powerful aspect of PLA is its use to compare changes in associations between proteins under different conditions. The table in Figure 3-10 A summarises changes in associations between the pairwise combinations of Syntaxin 4, SNAP23, VAMP2 and Munc18c upon treatment of cells with insulin. It is important to note that there was complete agreement regarding such changes of data obtained in both adipocytes and fibroblasts. The only changes observed in associations between the 4 proteins upon insulin-stimulation are increased numbers of associations between SNAP23/Munc18c And SNAP23/VAMP2 (Figure 3-10 A). Given that and there is no evidence for direct interaction of SNAP23

with either Munc18c or VAMP2, but Munc18c does bind the assembled Syntaxin 4/SNAP23/VAMP2 complex (Latham et al., 2006; Widberg et al., 2003), these data support the hypothesis that insulin-stimulation results in an increase in the number of Syntaxin 4, VAMP2 and SNAP23 SNARE complexes between and that these have Munc18c bound to them.

Drawing on numerous other studies performed in a variety of different systems (Jewell et al., 2010) there are 3 possible ways in which insulin might drive the assembly of Syntaxin 4/SNAP23/VAMP2/Munc18c complexes. These are that insulin-stimulation results in either of the following options:

- Syntaxin 4, SNAP23, VAMP2 and Munc18c all coming together from separate monomeric pools.
- Preformed Syntaxin 4/SNAP23 binary complexes binding VAMP2 and Munc18c (either as monomers or as a preformed VAMP2/Munc18c complex).
- A Syntaxin 4/SNAP23/Munc18c complex binding VAMP2.

Each of these options has different predictions that we don't see. Option 1 predicts that we would see an increase in the number of all pairwise combinations (e.g. between Syntaxin 4 and SNAP23, and between Syntaxin 4 and Munc18c), but we don't. Option 2 predicts increased associations between, at least, Syntaxin 4/VAMP2, Syntaxin 4/Munc18c, and VAMP2/Munc18c – none of which are observed. The third option predicts increased associations between VAMP2/Syntaxin 4 and VAMP2/Munc18c, neither of which were observed. It is, of course possible that any one, or indeed all, of these increased associations do occur in response to insulin, but we don't see them perhaps due to the newly formed associations that occur masking one, or both, of the antibody epitopes. Arguing somewhat against this is the fact that several of the antibodies used were polyclonal, raised against a large portion of the antigen. For this reason additional PLA was performed on fibroblast cells using different combination of

antibodies against Syntaxin 4 and Munc18c than the one described above (section 3.3.3) and simililar results were obtained (see appendix figures Figure 8-46Figure 8-47Figure 8-48). Nevertheless this caveat (epitope issue) must be kept in mind.

In order to explain the observed associations in response to insulin without any of the accompanying increases (from options 1-3 above) I postulated that there are two pools of Syntaxin 4 under basal conditions, one in complex with SNAP23 and one in complex with VAMP2 and Munc18c – the latter being the source of the proteins recruited into the Syntaxin 4/SNAP23/VAMP2/Munc18c complex that forms in response to insulin.

The same conclusion is reached upon examination of the changes in associations between the six protein pairs upon insulin stimulation in groups of three (Figure 3-10 B). Taking the first group of three pairs as Syntaxin 4/Munc18c, Syntaxin 4/SNAP23 and Munc18c/SNAP23. The only observed increase is between Munc18c and SNAP23 association. This could result either from Munc18c being recruited to a Syntaxin 4/SNAP23 containing complex or SNAP23 to a Syntaxin 4/Munc18c containing complex. Application of the same logic to the second group of three pairs; Syntaxin 4/VAMP2, Syntaxin 4/SNAP23 and SNAP23/VAMP2, with only significant increase being observed between SNAP23 and VAMP2 associations suggests that either VAMP2 recruited to a Syntaxin 4/SNAP23 containing complex or SNAP23 to a Syntaxin 4/VAMP2 containing complex (Figure 3-10 B). Together, these two analyses we predict that there are three different Syntaxin 4-containing complexes under basal conditions: Syntaxin 4/SNAP23, 4/Munc18c and Syntaxin 4/VAMP2. Bringing the last group of 3 into the analyses, i.e. Syntaxin 4, VAMP2 and Munc18c, between which there are no changes in pairwise associations upon insulin-stimulation indicates that two of the previously mentioned complexes (Syntaxin 4/Munc18c and Syntaxin 4/VAMP2) they are not individual but rather one complex containing Syntaxin 4, VAMP2 and Munc18c.

A

	Syntaxin4	SNAP23	VAMP2	Munc18c
Syntaxin4		no change	no change	no change
SNAP23	no change		increase	increase
VAMP2	no change	increase		no change
Munc18c	no change	increase	no change	

B

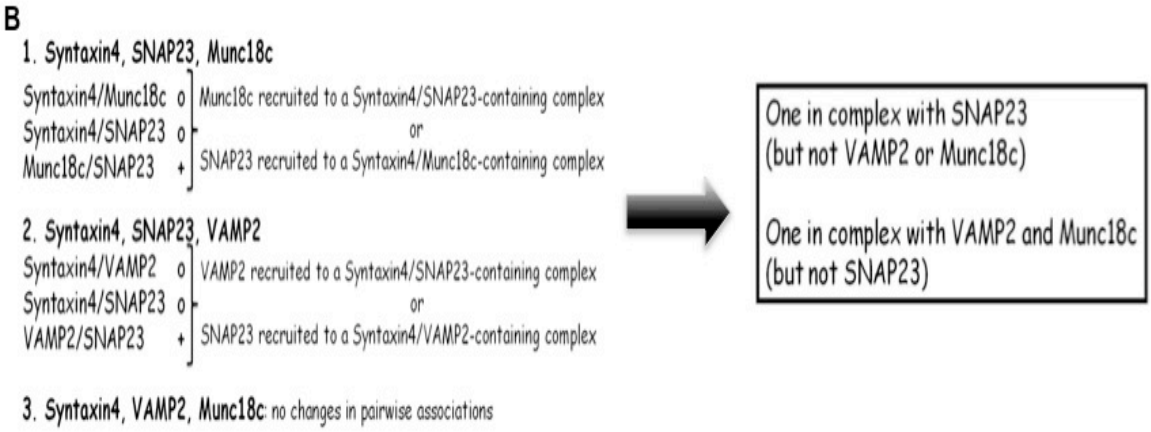

Figure 3-10. PLA results summary table and interpretation

A) This table summarizes results of PLA performed on both fibroblats and adipocytes 3T3-L1 cells between Syntaxin 4 SNAP23 VAMP2 and Munc18c in all possible pairs. The shadowed cells compare the signal obtained under basal conditions and upon insulin stimulation (100 nm for 3 min) of PLA performed for a specific pair of proteins (protein pairs are formed by combining any protein from the first row with any from the first column of the table). Coloured cells indicate a statistical significant difference, regarding PLA results, between the two different conditions (basal and insulin) of the corresponding protein pair. Statistical analysis was performed using the SPSS and applying the Mann-Whitney U test. B) Interpretation scheme based on PLA analysis results. Existence of two individual polls of Syntaxin 4 in 3T3-L1 cells

In summary, PLA of all possible pairwise combinations of Syntaxin 4, SNAP23, VAMP2 and Munc18c in the presence and absence of insulin raises the possibility that there are two separate Syntaxin 4 pools under basal conditions; one in complex with SNAP23 and one in complex with VAMP2 and Munc18c.

As mentioned above, the binary complex formed between Syntaxin 4 and SNAP23 is generally accepted and well characterized, as are analogous t-SNARE complexes in numerous other systems (Kawanishi et al., 2000). However, the

existence of a complex containing Syntaxin 4 and VAMP2, but lacking SNAP23 is more contentious. Given the potential caveat raised above regarding the reliance of my hypothesis on lack of observed PLA signal, the possibility of a Syntaxin 4-VAMP2 interaction in the absence of SNAP23 was further examined in the following chapters.

Chapter 4

In vitro analyses of interactions between SNARE proteins involved in GLUT4 vesicle exocytosis

4.1 Introduction

4.1.1 Regulation of GLUT4 externalization to the plasma membrane by SNARE proteins

Membrane traffic is regulated by the formation of specific SNARE complexes in all eukaryotic cells (Cai et al., 2007). SNARE proteins have been classified into two major families: t-SNAREs that mark specific target organelles and v-SNARE that localise to donor membranes (Hong, 2005) (section 1.2.1). The formation of highly-stable complexes (Hayashi et al., 1994) between specific t-SNARE proteins and their cognate v-SNAREs is sufficient to drive membrane fusion by providing both the necessary energy to overcome the repulsive force emerging from the two opposing bilayers (Pobbati et al., 2006) and a degree of specificity that is essential for coordinated membrane traffic (Hong, 2005). The insulin-dependent fusion of GLUT4-containing vesicles with the surface of adipocytes and muscle cells is a specialised example of regulated membrane trafficking and a crucial terminal step in controlled glucose transport (Bryant et al., 2002). The t-SNARE required for the final delivery of the transporter to the cell surface in insulin-regulated GLUT4 trafficking is comprised of Syntaxin 4 and SNAP23 that form a binary (t-SNARE) complex (Araki et al., 1997) that in turn forms a ternary SNARE complex with the corresponding v-SNARE protein (Kawanishi et al., 2000; St-Denis et al., 1999). In contrast to t-SNARE, the identity of v-SNARE protein(s) that regulate(s) fusion of GLUT4 vesicles with the plasma membrane upon insulin stimulation is an area of some controversy. A substantial body of experimental work has identified VAMP2 as the v-SNARE within GLUT4 containing vesicles that forms, together with the t-SNARE complex (Syntaxin 4/SNAP23), the ternary SNARE complex essential for vesicle fusion (reviewed in (Bryant and Gould, 2011). However detailed proteomic characterisation of GLUT4 Storage Vesicles identified the presence of not only VAMP2, but also VAMP3 and VAMP8 in GSVs (Jedrychowski et al., 2010; Larance et al., 2005). All three of these v-SNAREs are known to be involved in exocytosis in various systems, and form ternary SNARE complexes with SNAP23 and Syntaxin 4 (Polgar et al., 2002). Furthermore studies in which VAMP8 and VAMP3 were disrupted in differentiated adipocytes from VAMP2 depleted mouse embryonic fibroblasts revealed plasticity in the v-SNARE requirements for GLUT4 externalization (Zhao et al., 2009). Although these data raise interesting questions regarding which v-SNARE contributes to

GLUT4 exocytosis and when, I used VAMP2 to investigate SNARE complex formation since its involvement in insulin-regulated exocytosis is the best characterized to date.

4.1.2 Structural conformations of Syntaxin 4

As previously described in section 1.2.2.1 mammalian syntaxins are attached to membranes *via* highly hydrophobic transmembrane domains at their carboxyl terminus, and contain three helices toward their N-terminus (collectively called the Habc domain) connected to the SNARE domain *via* a flexible linker (Fernandez et al., 1998). This linker can fold in such a way to bring the Habc domain closer to the carboxyl-terminal segment of the protein, where it can make several intra-molecular interactions with the membrane-proximal SNARE domain (Calakos et al., 1994; Dulubova et al., 1999; Misura et al., 2000). Thus syntaxins can change between two conformations; open and closed. This ability is considered to provide an important regulatory step regarding the formation of SNARE complex (Dulubova et al., 1999), as the closed conformation is incompatible with SNARE complex formation, in contrast to the open. While crystallographic studies of the neuronal Syntaxin 1A have substantiated biochemical evidence that support the existence of the 2 syntaxin conformations and captured it in the closed conformation (Burkhardt et al., 2008; Misura et al., 2000), no such high-resolution data exist to prove the existence of a closed conformer of Syntaxin 4. Recent studies using small-angle X-ray scattering and small-angle neutron scattering with contrast variation revealed that Munc18c/Syntaxin 4 adopts only the open binding mode and not the closed one (Christie et al., 2012). However the high level of sequence homology between Syntaxin 4 and Syntaxin 1A, particularly of the residues involved in intra-molecular interactions (D'Andrea-Merrins et al., 2007) as well as biochemical/biophysical studies and analyses of bindings between Syntaxin 4 and its cognate SM protein Munc18c (Aran et al., 2009) suggest that Syntaxin 4 , like Syntaxin 1A, does adopt a closed conformation that regulates its ability to form SNARE complexes.

4.2 Aims of this chapter

In chapter 3 I presented PLA results of all possible pairwise combinations of Syntaxin 4, SNAP23, VAMP2 and Munc18c in the presence and absence of insulin which suggest that there are two separate Syntaxin 4 pools under basal conditions; one in complex with SNAP23 and one in complex with VAMP2 and Munc18c. The binary complex formed between Syntaxin 4 and SNAP23 is generally accepted and well characterized, as are analogous t-SNARE complexes in numerous other systems (Kawanishi et al., 2000). Nevertheless, the existence of a complex containing Syntaxin 4 and VAMP2, but lacking SNAP23 is more argumentative. Here I have used *in vitro* approaches to further examine the interactions of Syntaxin 4 with its cognate SNARE proteins SNAP23 and VAMP2. Additionally Complex Assembly Assay was also used to investigate any potential effect of the interactions between the SNARE proteins on SNARE complex formation rate.

4.3 Results

4.3.1 The cytosolic domains of Syntaxin 4, SNAP23 and VAMP2 form an SDS-resistant complex

Studies of platelet granules secretion established that recombinant VAMP2 forms SDS-resistant SNARE complexes with SNAP25 and Syntaxin 4 (Polgar et al., 2002). I set out to use this characteristic to assay the ability of SNARE proteins involved in fusion of GLUT4 carrying vesicles with plasma membranes (Syntaxin 4/SNAP23/VAMP2) to form ternary complexes *in vitro*. For this purpose, I established a GST pull-down assay designed to follow SNARE formation (section 2.4). All proteins for this assay were produced in *E. coli* (sections 2.3.2 and 2.3.3) and the minimal nature of the assay (i.e. that I could control which molecules were present) allowed me to investigate precise contributions that individual events make to regulation of SNARE complex formation. Figure 4-1 shows samples analyzed by SDS-PAGE followed by Coomassie staining of various stages in the purification process of C-terminally Protein A-tagged VAMP2 (VAMP2-PrA) (A), C-terminally GST-tagged Syntaxin 4 (Sx4-GST) (B), N-terminally His-tagged SNAP23 (His-SNAP23) (C) and GST, PrA tags alone (D) and (E) that were used as controls in the complex assembly assay. The *in vitro* SNARE

complex assembly assay was performed as follows. Sx4-GST or GST immobilized on glutathione-Sepharose beads was incubated with His-SNAP23, VAMP2-PrA and PrA in various combinations, as indicated, for the indicated times (Figure 4-2). Figure 4-2 (A) shows that there is a time-dependent increase in the amount of the SNARE complex formed, shown by increasing band intensity in the α-VAMP2, α-Sx4 and α-SNAP23 immunoblots at a molecular weight corresponding to the sum of that of the three recombinant SNARE proteins (total~110 kDa), when, and only when, all three are incubated together. Figure 4-2 (B) demonstrates that the formation of the SDS-resistant ternary complex of Syntaxin 4/VAMP2/SNAP23 recombinant SNARE proteins is not due to nonspecific interactions through the affinity tags present.

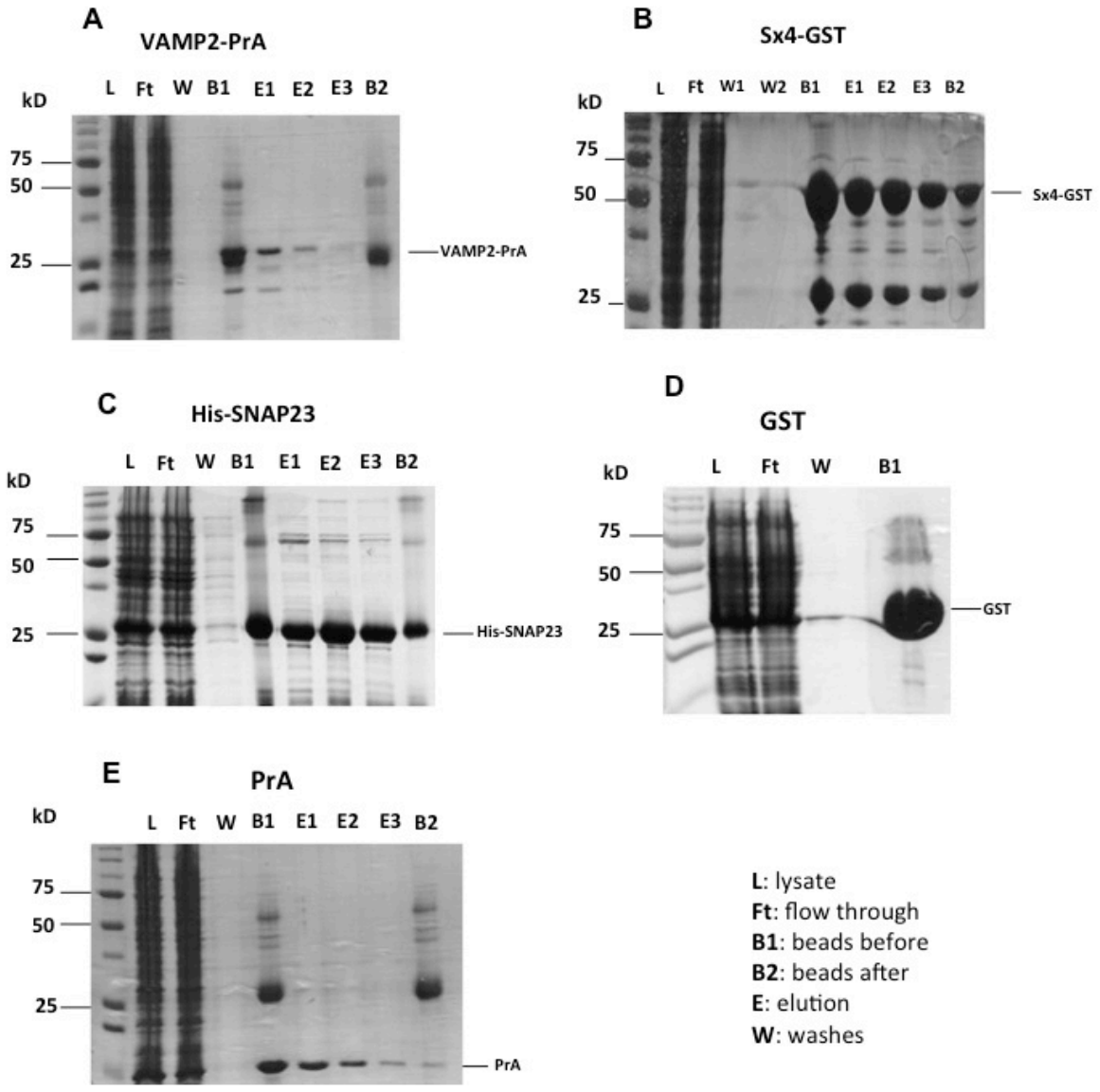

Figure 4-1: Purification of SNARE proteins involved in complex formation and their tags.

Appropriate constructs (Table 2.5) were used to produce C-terminally PrA-tagged cytosolic domain of VAMP2 (A), C-terminally GST-tagged cytosolic domain of Syntaxin 4 (B) N-terminally His-tagged SNAP23 (C), as well as the GST and PrA moieties that were used as tags, alone (D and E respectively. This was achieved by transforming the constructs into BL21 cells and inducing protein production in 3-9 L (depending on the construct) cultures with IPTG prior to purification using their affinities for IgG, glutathione or Ni-affinity as outlined in methods (sections 2.3.4, 2.3.5 and 2.3.6). Purity of the proteins was analyzed at various stages by SDS-PAGE on a 15% agarose gel (10µl loading) followed by Commassie staining. Soluble proteins (Lysate samples) were bound to appropriate beads as described (section 2.3.3). The protein fractions not bound and bound to the column ("Flow through" and "beads before" samples respectively) are shown. After multiple washes ("washes" samples represent the first wash) of the beads proteins were eluted using the appropriate buffer 3 times successively (samples "E1-E3"). The remaining protein on the beads after the elution is shown ("Beads after"). Circled bands represent the corresponding eluted protein from the beads. N.B. The GST protein as illustrated in panel D was not eluted but remained on the beads and used as negative control in binding studies below.

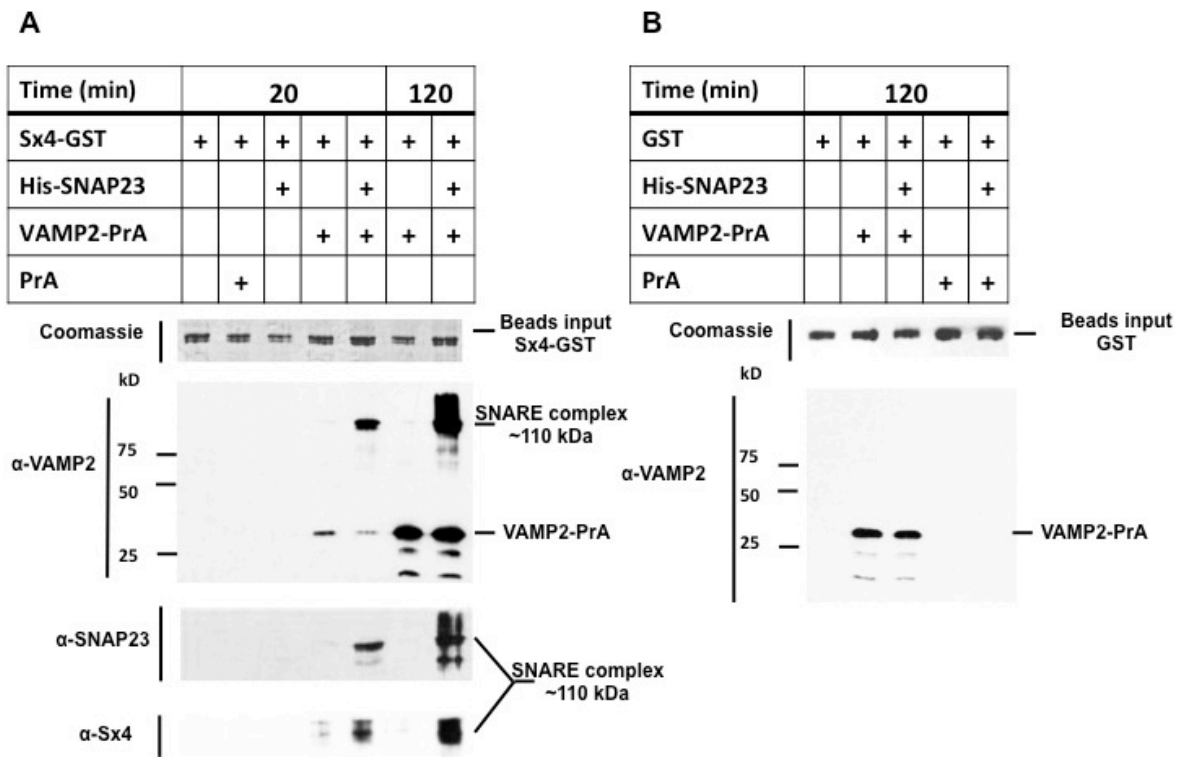

Figure 4-2: Sx4-GST/VAMP2-PrA/His-SNAP23 form an SDS resistance complex *in vitro.*

50 µg Sx4-GST (A) or GST (B), bound to glutathione-Sepharose (10µl bed volume) were incubated in 1ml PBS (as described in section 2.4) containing His-SNAP23, VAMP2-PrA and PrA in ~10x molar excess each in various combinations as indicated. Following incubation for the indicated times on a rotating wheel at 4˚C the beads were washed extensively using PBS prior to final resuspension in 50µl 2xLSB and heating to 95˚C for 5 minutes. Samples were subject to SDS-PAGE using a 15% separating gel (10 µl loading) and were visualized by Coomassie staining (beads protein input loading control (A) and (B) upper panels) or immunoblot analysis using α-VAMP2 antibody ((A) middle panel, (B) lower panel). The smear of immunoreactivity around 110kDa corresponds to the SDS-resistant ternary SNARE complex containing Sx4-GST/His-SNAP23/VAMP-PrA. Samples of Sx4-GST beads (A) were also subjected to immunoblot analysis using α-SNAP23 and α-Sx4 antibodies to confirm their presence in the SDS-resistant complex.

4.3.2 Monomeric Syntaxin 4 interacts specifically with VAMP2 *in vitro*

At the end of chapter 3, I hypothesised the existence of 2 distinct pools of Syntaxin 4 in adipocytes under basal conditions; one in complex with SNAP23, one in complex with VAMP2 (section 3.4). This hypothesis was based on results obtained using PLA. There are many precedents for preformed t-SNARE complexes existing prior to SNARE complex formation (Dun et al., 2010; Kawanishi et al., 2000) but the notion of an interaction between a v-SNARE and a syntaxin is perhaps more heretical. A direct interaction between Syntaxin 4 and VAMP2 has previously been demonstrated *in vitro* (Calakos et al., 1994), but it is important to note that the constructs used in that study were tagged at

their N-terminus and may not be representative of their *in vivo* counterparts. Figure 4-2 (A) provides evidence of a time-dependent interaction between Sx4-GST and VAMP2-PrA harbouring tags at their C-termini, replacing their transmembrane domains. To further test whether there is a direct interaction between the cytosolic domains of Syntaxin 4 and VAMP2 a dot blot assay was performed (section 2.5) as an alternative approach to the pull-down assay used in Figure 4-2 (A). Successive dilutions of the indicated proteins (Figure 4-3) were spotted and allowed to dry onto nitrocellulose membranes which were subsequently probed with either VAMP2-PrA or PrA prior to immunodection using α-VAMP2 antibody. As shown in Figure 4-3 the strongest signal obtained was between Sx4-GST and VAMP2-PrA with all of the negative controls (controlling for interactions between tags) being substantially weaker.

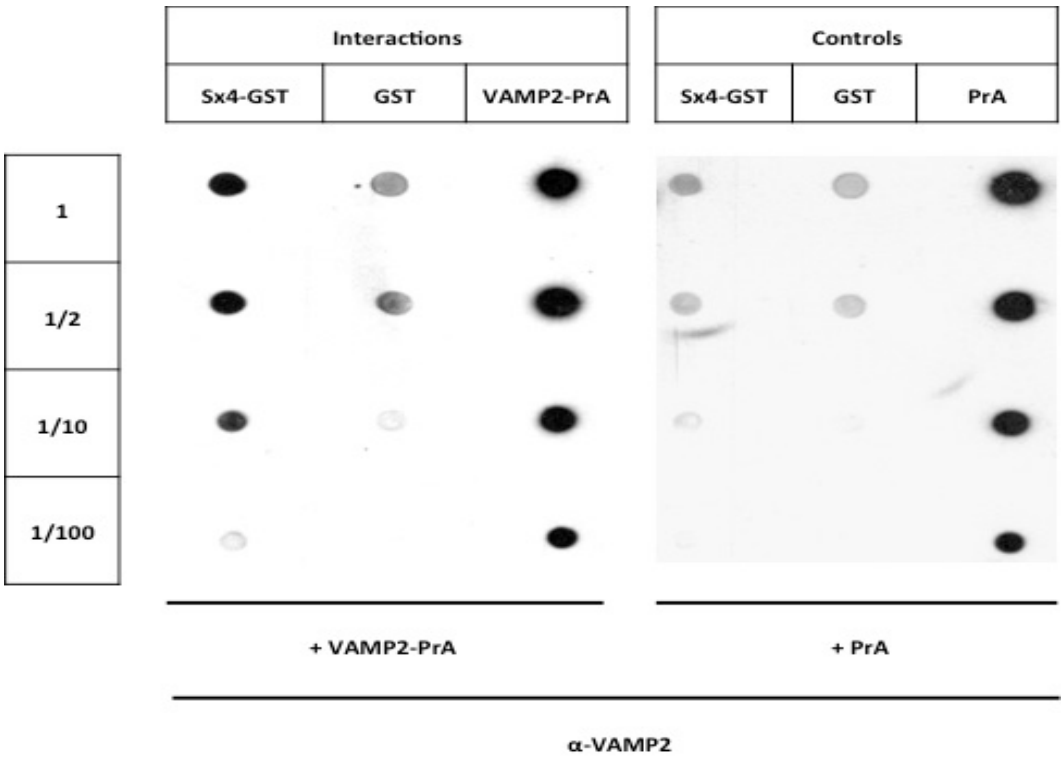

Figure 4-3: Sx4-GST interacts with VAMP2-PrA *in vitro*-Dot blot assay.

Membrane was prepared by dotting 2 µl of a series of successive dilutions in PBS (the protein amount of undiluted sample was ~5µg) of purified, dialysed Sx4-GST, VAMP2-PrA, GST or PrA as indicated and left to dry at room temperature. Following incubation with blocking solution and subsequent washes as described in section 2.5, the membrane was incubated for 2 hours at 4°C with gentle mixing in 3ml PBS containing ~10 molar excess of either VAMP2-PrA or PrA as indicated. Following this incubation, the filter was washed with PBS and subject to immunoblot analysis using α-VAMP2 antibody.

The final approach used to investigate the direct interaction between the cytosolic domains of Sytaxin 4 and VAMP2 was to carry out a pull-down assay complementary to that presented in Figure 4-2 (A) i.e. with VAMP2-PrA immobilized to IgG-Sepharose beads as bait incubated with a molar excess of purified cytosolic domain of Syntaxin 4. The Syntaxin 4 cytosolic domain was prepared by using thrombin protease to cleave the GST tag from a GST-Sx4 fusion expressed in, and purified from, BL21 *E. coli* cells (Figure 4-4).

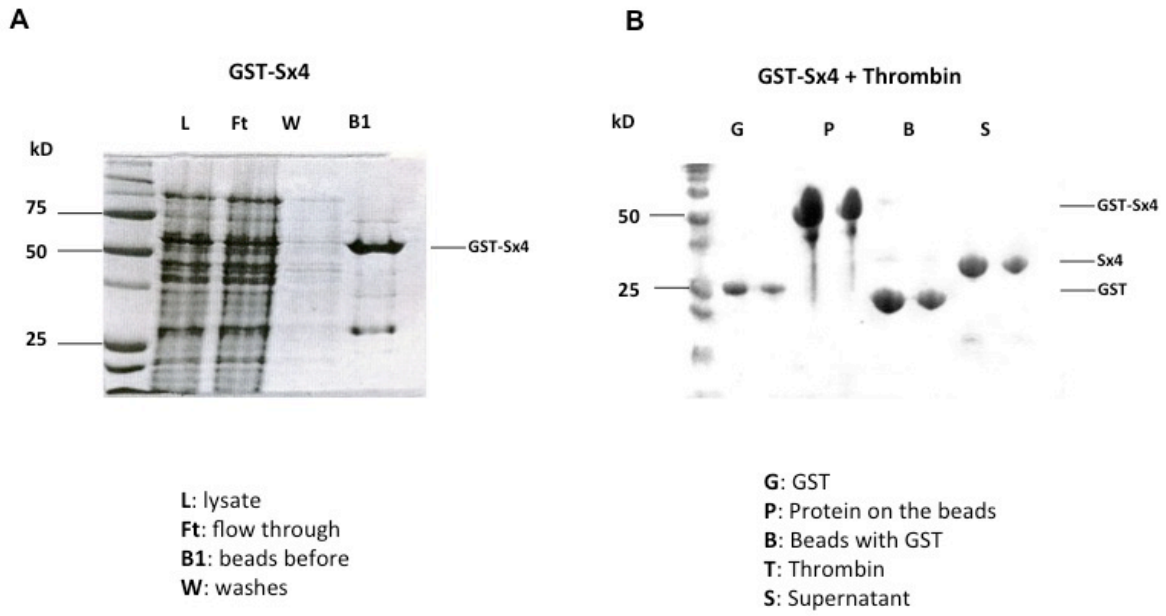

Figure 4-4: Purification of bacterially-expressed GST-Sx4, and thrombin cleavage.

(A): Plasmid pET41a: GST-Sx4 was used to recombinantly produce N-terminally GST-tagged cytosolic domain of Syntaxin 4. This was achieved by transforming the plasmid into BL21 cells and inducing protein production with IPTG in 3L of culture as outlined in methods (sections 2.3.1 and 2.3.2). Glutathione-Sepharose beads were then used to purify the GST-tagged protein (section 2.3.5). Purity of the protein was analyzed at various stages by SDS-PAGE on a 15% agarose gel (10 µl loading) followed by Commassie staining. Soluble protein ("lysate" sample) was bound to glutathione-Sepharose beads. The amount of protein not bound and bound to the column ("flow through" and "beads before" samples) are shown. Finally beads were thoroughly washed using PBS ("washes" sample represents the first wash). Circled band of a molecular weight approximately 50kDa of B1 sample corresponds to GST-Sx4. (B): GST-Sx4 protein bound to the beads (P) was treated with thrombin as described in section 2.3.7. After termination of the reaction protein bound to the beads (B) were separated from unbound material (S) by centrifugation as described in section 2.3.7. All prepared samples as well as an aliquot of GST protein (control) were heated to 95°C for 5 minutes after the addition of equal volume of 2xLSB. Samples were subject to SDS-PAGE through a 15% gel followed by Coomassie staining (10 and 5µl loading per sample). The circled single bands of a molecular weight approximately 30kDa of the supernatant sample correspond to cleaved Syntaxin 4. Positions of molecular weight markers are indicated.

Figure 4-5 demonstrates that VAMP2-PrA pulls down the cytosolic domain of Syntaxin 4 in time-dependent manner, and that this interaction is mediated through the VAMP2 sequence (as only background levels of Syntaxin 4 are pulled down by PrA alone even after prolonged incubation times).

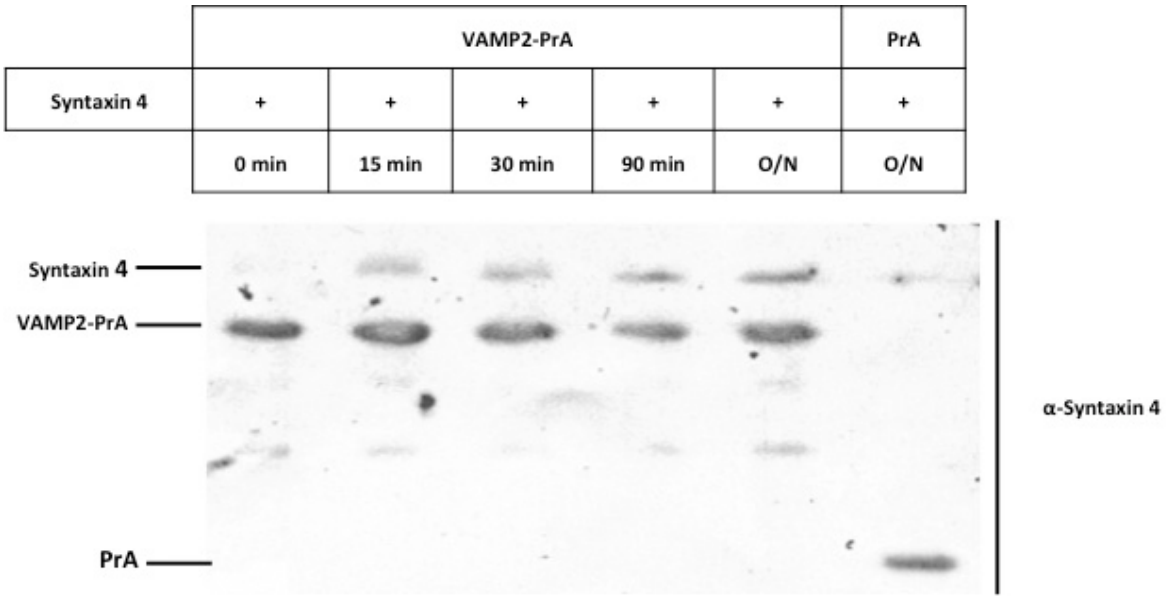

Figure 4-5: Cytosolic domain of Syntaxin 4 binds directly to the cytosolic domain of VAMP2-PrA.

10 µg of VAMP2-PrA or PrA (negative control) bound to IgG-Sepharose beads (10µl bed volume) were incubated in 1ml PBS (as described in section 2.4) containing the cytosolic Syntaxin 4 in ~10x molar excess. Following incubation on a rotating wheel for the indicated times at 4˚C the beads were washed extensively using the appropriate buffer (section 2.3.6) prior to final resuspension in 50µl 2xLSB and heating to 95˚C for 5 minutes. Eluted proteins were subject to SDS-PAGE through a 15% separating gel (10 µl loading) and were visualized by immunoblot analysis using α-Synatxin 4 antibody.

While the experiments described above (Figure 4-2, Figure 4-3 and Figure 4-5) demonstrate that Syntaxin 4 interacts directly with VAMP2, at least *in vitro*, before any functional significance of this interaction could be inferred, it was necessary to establish the specificity of this interaction. This was especially important as, due to the coiled-coil nature of the SNARE domain, SNARE proteins are notorious for promiscuous interactions, both *in vitro*, and also when overexpressed *in vivo* (Lang and Jahn, 2008). To address this, Sx4-GST (alongside GST as a negative control) was immobilized on glutathione-Sepharose beads and incubated with molar excess either of VAMP2-PrA, the PrA moiety

alone, or Snc2-PrA. Snc2 is a v-SNARE from the yeast *Saccharomyces cerevisiae* (Paumet et al., 2001). The Snc2-PrA used here is analogous to the VAMP2-PrA used in that it consists of the cytosolic domain of Snc2 tagged at its C-terminus with a PrA moiety (Carpp et al., 2006), and was expressed in, and purified from, BL21 *E. coli* cells (Figure 4-6(A)). Figure 4-6 (B) shows that Sx4-GST pulls down VAMP2-PrA but not Snc2-PrA, demonstrating a degree of specificity of the interaction between the cytosolic domains of Syntaxin 4 and VAMP2. It is worth mentioning that from Figure 4-2 it is apparent that GST interacts with VAMP2. Of course the amount of VAMP2 that is pulled down due to the GST tag is significantly less than the amount of VAMP2 that interacts with Syntaxin 4 as can be deducted from the comparison of the relative bands. These findings suggest that this unspecific binding between VAMP2 and GST should not be considered as a potential caveat regarding VAMP2/Syntaxin 4 interaction whenever GST tag is present.

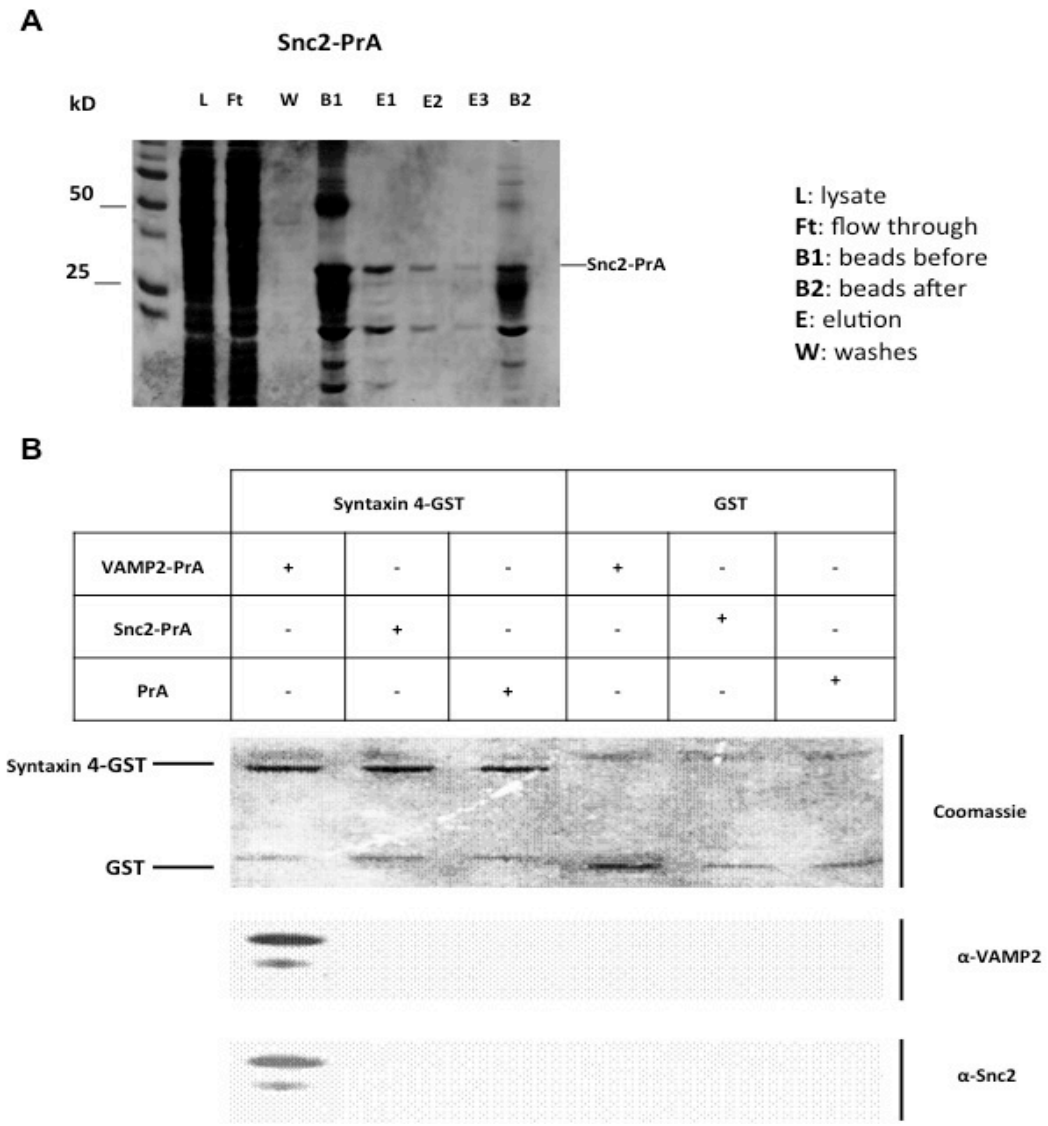

Figure 4-6: Sx4-GST/VAMP2-PrA interaction *in vitro* is specific.

(A): Purification of Snc2-PrA. The plasmid pETDUET-1:Snc2-PrA was used to produce C-terminally PrA-tagged Snc2 protein by transforming the plasmid into BL21 cells and inducing protein production with IPTG in 6L of culture as outlined in methods (sections 2.3.1 and 2.3.2). IgG-Sepharose beads were then used to purify the PrA-tagged protein (section 2.3.6). Purity of the protein was analyzed at various stages by SDS-PAGE on a 15% agarose gel (10 µl loading) followed by Commassie staining. Soluble protein (L) was bound to IgG-Sepharose beads. The protein amounts not bound and bound to the column (Ft and B1) are shown. After extensive washes of the beads (section 2.3.6) using the suitable washing buffer ("W" sample represents the first wash) proteins were eluted using the appropriate buffer (section 2.3.6) *via* 3 successive elutions (E1-E3). Protein remaining on the beads after the elution is shown (B2). Circled bands correspond to Snc2-PrA eluted protein. (B): Sx4-GST interacts with VAMP2-PrA but not an analogous protein harbouring the cytosolic domain of the yeast v-SNARE Snc2-PrA *in vitro*. 10µg of either Sx4-GST or the GST moeity alone bound to glutathione-Sepharose beads (10µl bed volume) were incubated in 1ml PBS (as described in section 2.4) containing either VAMP2-PrA or Snc2-PrA or PrA (negative control) in ~10x molar excess for two hours on a rotating wheel at 4˚C, after which time the beads were washed thoroughly using the appropriate buffer (section 2.3.6) prior to final resuspension in 50 µl 2xLSB and heating to 95˚C for 5 minutes. Eluted proteins were subject to SDS-PAGE through a 15% separating gel and visualized by Coomassie staining (protein input loading control-upper panel) (10 µl loading) or immunoblot analysis using α-VAMP2 or α-Snc2 antibodies (5 µl loading) (lower panel).

To assess whether the interaction between Syntaxin 4 and VAMP2 is facilitated by homo dimer/oligomerization (clustering) of the former (Sieber et al., 2007), rather than a binary interaction between the two different SNAREs, a further pull-down assay was performed. Sx4-GST (or GST as a negative control) immobilized to glutathione-Sepharose beads was incubated with molar excess (untagged) cytosolic Syntaxin 4 in the presence or absence of the (untagged) cytosolic domain of VAMP2 (also in molar excess over the immobilized Sx4-GST). The untagged cytosolic domain of VAMP2 was obtained by thrombin cleavage of a GST-VAMP2 fusion protein expressed in, and purified from, BL21 *E. coli* cells (Figure 4-7). From Figure 4-8 it appears that the ability of the cytosolic domain of Syntaxin 4 to bind itself is actually reduced by the presence of VAMP2 providing some evidence against the likelihood of the Syntaxin 4/VAMP2 interactions described above being facilitated by Syntaxin 4 clustering.

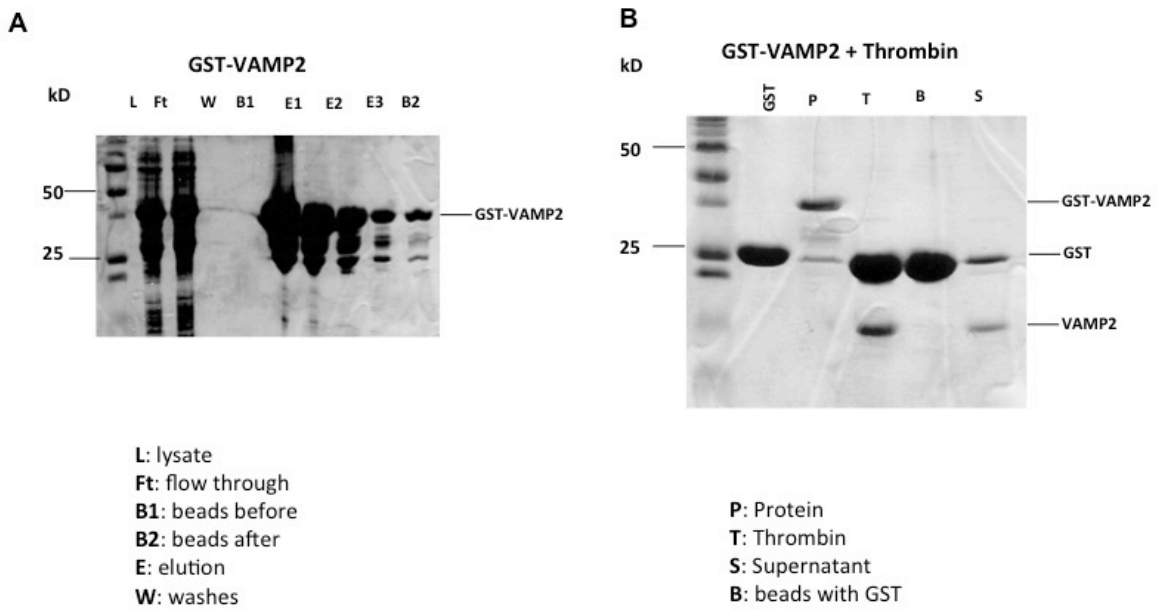

Figure 4-7: Purification and GST moiety cleavage of bacterially-expressed GST-VAMP2.

(A): Plasmid pET41a: GST-VAMP2 was used to produce N-terminally GST-tagged cytosolic domain of VAMP2 by transforming the plasmid into BL21 cells and inducing protein production with IPTG in 6L of culture as outlined in methods (sections 2.3.1 and 2.3.2). Glutathione-Sepharose beads were then used to purify the GST-tagged protein (section 2.3.5). Purity of the protein was analyzed at various stages by SDS-PAGE on a 15% agarose gel (10 µl loading) followed by Commassie staining. Soluble protein (L) was bound to glutathione-Sepharose beads. The protein amounts not bound and bound to the column (Ft and B1) are shown. After extensive washes of the beads using PBS ("W" sample represents the first wash) proteins were eluted using the appropriate buffer (section 2.3.5) *via* 3 successive elutions (E1-E3). The remaining protein on the beads after the elution is shown (B2). Circled bands correspond to GST-VAMP2 eluted protein. (B): Dialysed GST-VAMP2 protein (P) was treated with thrombin as described in section 2.3.7 (T). After the termination of the reaction cleavage products were incubated with the appropriate volume of glutathione-Sepharose beads as outlined in methods (section 2.3.7). Unbound protein (S) and were separated from protein bound to the beads (B = beads with GST moiety remaining bound) by centrifugation. All samples as well as an aliquot of GST protein (as a control to mark the migration of the cleaved GST-moeity) were heated to 95°C for 5 minutes after the addition of equal volume of 2xLSB. Samples were subject to SDS-PAGE through a 15% gel followed by Coomassie staining (10 µl loading). The band of a molecular weight approximately 15kDa in the supernatant sample corresponds to cleaved VAMP2. Positions of molecular weight markers are indicated.

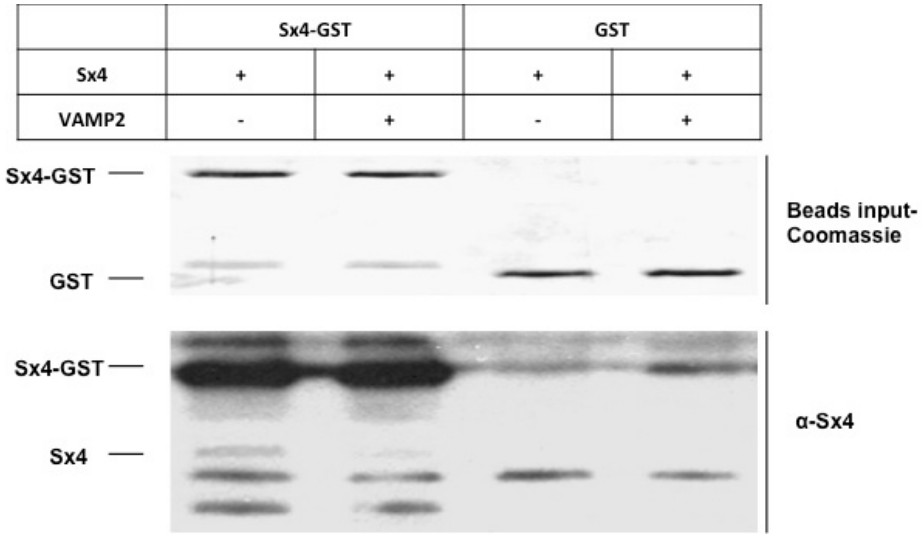

Figure 4-8: VAMP2 interacts with monomeric Sx4-GST *in vitro.*

10µg of either Sx4-GST or GST bound to glutathione-Sepharose beads (10µl bed volume) were incubated in 1ml PBS (as described in section 2.4) containing ~10x molar excess cytosolic Syntaxin 4 and VAMP2, or cytosolic Syntaxin 4 alone, for two hours on a rotating wheel at 4°C, after which time the beads were washed thoroughly using PBS prior to final resuspension in 50µl 2xLSB and heating to 95°C for 5 minutes. Eluted proteins were subject to SDS-PAGE through a 15% separating gel and visualized by Coomassie staining (protein/beads input loading control-upper panel) (10 µl loading) or immunoblot analysis using α-Syntaxin 4 antibody (5 µl loading) (lower panel).

Finally, to further investigate if this interaction can be detected between other syntaxins and their cognate v-SNAREs, in other words whether it has a more universal character or not, an additional GST pull down assay was performed. This time Tlg2-GST (the cognate yeast syntaxin protein of Snc2) was immobilized to glutathione-Sepharose beads. The recombinant Tlg2-GST was expressed in, and purified from, BL21 *E. coli* cells (Figure 4-9 (A)). GST was also immobilized to the beads and used as a negative control. Beads (carrying either Tlg2-GST or GST) were incubated for the indicted times with molar excess either of Snc2-PrA or just PrA (negative control). After extensive washing of the beads, samples prepared were subjected to SDS-PAGE analysis followed either by Coomasie staining or immunodetection using antibody against Snc2 (Figure 4-9 (B)). The results of this assay revealed a time depended interaction between these two proteins. The previous data proposes that the observed interaction between Syntaxin 4 and VAMP2 might have a more universal character and might exist between various syntaxins and their cognate v-SNAREs in different pathways and species. Of course these observations provide only some indications. Further and more detailed investigation is required before this conclusion can be drawn.

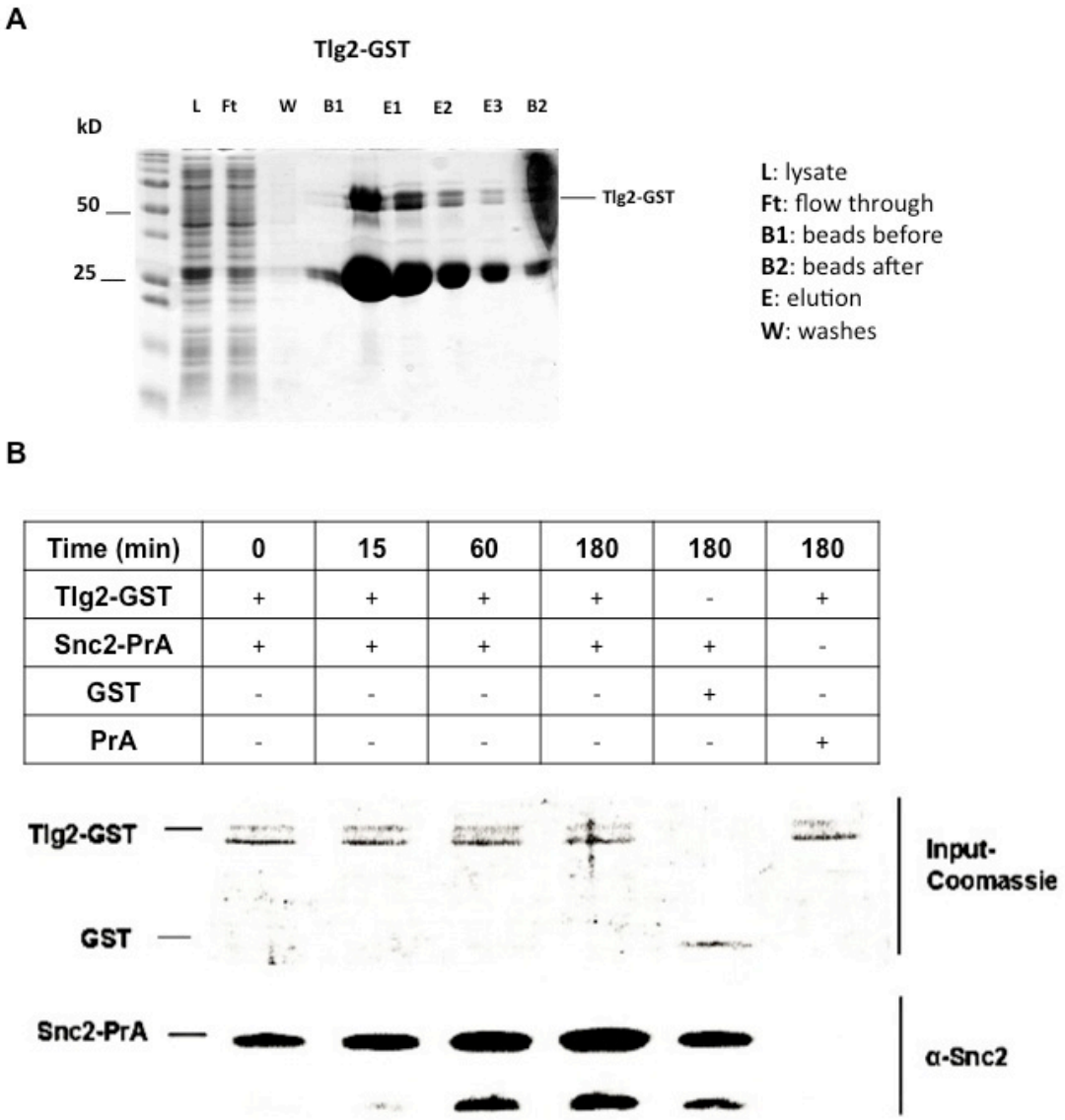

Figure 4-9: Yeast homologues of Syntaxin 4 and VAMP2 (Tlg2 and Snc2 respectively) interact with each other *in vitro*.

(A): Purification of Tlg2-GST. Plasmid pETDUET1: Tlg2-GST was used to recombinantly produce C-terminally GST-tagged cytosolic domain of Tlg2. This was achieved by transforming the plasmid into BL21 cells and inducing protein production with IPTG in 6L of culture as outlined in methods (sections 2.3.1 and 2.3.2). Glutathione-Sepharose beads were then used to purify the GST-tagged protein (section 2.3.5). Purity of the protein was analyzed at various stages by SDS-PAGE on a 15% agarose gel (10 µl loading) followed by Commassie staining. Soluble protein (lysate samples) was bound to glutathione-Sepharose beads. The protein amounts not bound and bound to the column (flow through and beads before samples) are shown. After extensive washes of the beads using PBS (washes sample represents the first wash) proteins were eluted using the appropriate buffer (section 2.3.5) *via* 3 successive elutions (elution 1-3 samples). The remaining protein on the beads after the elution is shown (Beads after samples). Circled bands correspond to Tlg2-GST eluted protein. (B): Tlg2-GST interacts with Snc2-PrA *in vitro*. 10µg of either Tg2-GST or GST (negative control) bound to glutathione-Sepharose beads (10µl bed volume) were incubated in 1ml PBS (as described in section 2.4) containing either Snc2-PrA or PrA (negative control) in ~10x molar excess each for the indicated times on a rotating wheel at 4˚C, after which the beads were washed thoroughly using PBS prior to final resuspension in 50 µl 2xLSB and heating to 95˚C for 5 minutes. Eluted proteins were subject to SDS-PAGE through a 15% separating gel and visualized by Coomassie staining (protein input loading control-upper panel) (10 µl loading) or immunoblot analysis using α-Snc2 antibody (5 µl loading) (lower panel).

4.3.3 The cytosolic domains of Syntaxin 4 and VAMP2 interact *via* their SNARE motifs

In order to further dissect the interaction between Syntaxin 4 and VAMP2 truncations of these proteins were designed, produced and purified (Figure 4-10 D and F). All the truncated forms of the proteins were produced in BL21 *E. coli* cells (sections 2.3.1, 2.3.2 and 2.3.3). Figure 4-11 shows samples analyzed by SDS-PAGE followed by Coomassie staining from each step in the purification process of N-terminally GST-tagged cytosolic Syntaxin 4 that lacks the Habc domain (GST-Sx4 (ΔHabc)) (A) and N-terminally GST-tagged cytosolic VAMP2 that lacks the first 30 amino acids (GST-VAMP2 (ΔN30)) (B). The GST tag was cleaved from both constructs using thrombin (Figure 4-11 C) to generate soluble, purified preparations of Syntaxin 4 and VAMP2 SNARE motifs. The purified proteins were used in dot blot assays (section 2.5) to demonstrate a direct interaction between the SNARE motifs of Syntaxin 4 and (Figure 4-12).

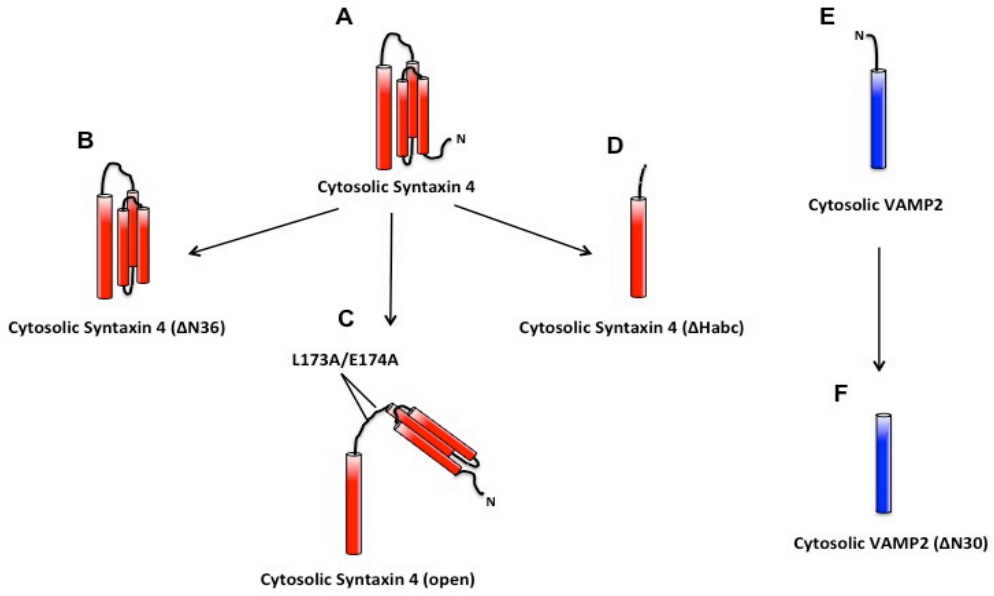

Figure 4-10: Syntaxin 4 and VAMP2 cytosolic domain mutants

Representation of Syntaxin 4 and VAMP2 cytosolic domain mutants used in this study. (A): Wild-type Syntaxin 4 that lacks the transmembrane domain. (B): Syntaxin 4 cytosolic domain that lacks the first 36 N-terminal amino acids (Aran et al., 2009). (C): Syntaxin 4 cytosolic domain that harbours two single amino acid subsitutions (L173A/E174A) at the linker area that keep Syntaxin 4 in its "open" conformation (Aran et al., 2009). (D): Truncation of cytosolic Syntaxin 4 that lacks the Habc domain. (E): Wild-type VAMP2 that lacks the transmembrane domain. (E): VAMP2 cytosolic domain that lacks the first 30 N-terminal amino acids.

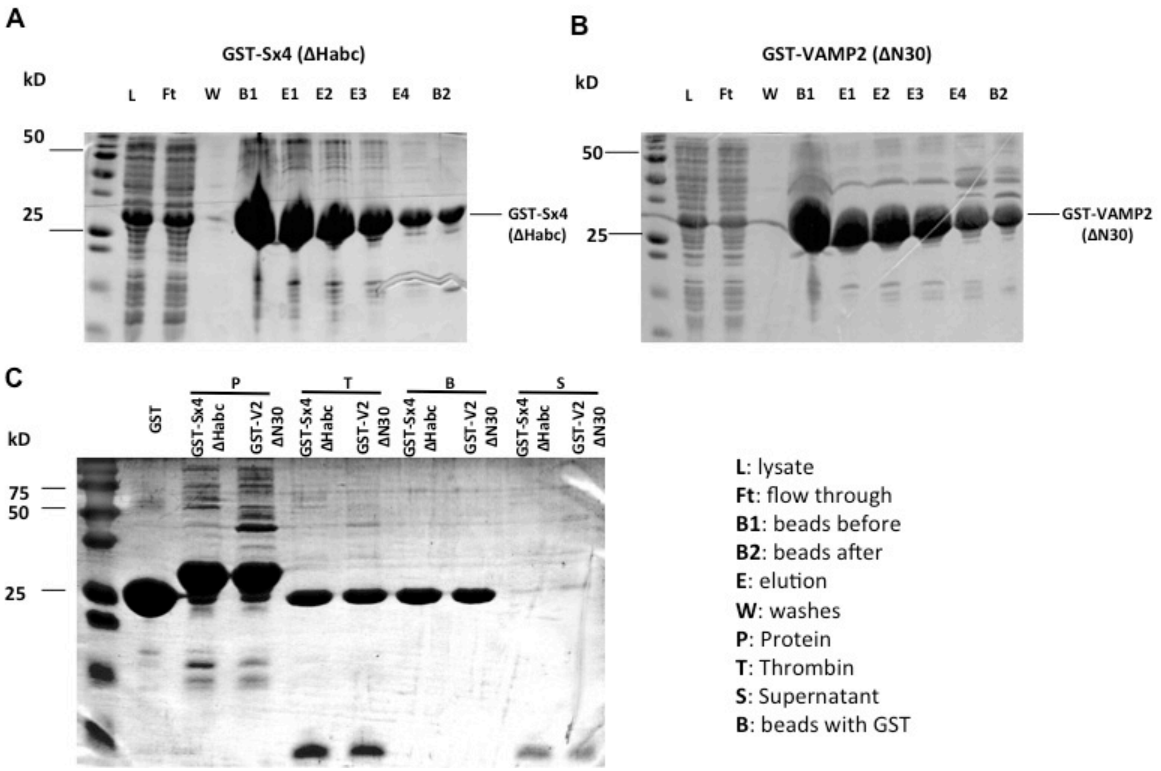

Figure 4-11: Purification and GST moiety cleavage of bacterially-expressed GST-Sx4(ΔHabc) and GST-VAMP2(ΔN30).

Plasmid pGEX4T1: GST-Sx4(ΔHabc) (A) and pGEX4T1: GST-VAMP2(ΔN30) were used to recombinantly produce N-terminally GST-tagged cytosolic domain of Syntaxin 4 that lacks the Habc domain and N-terminally GST-tagged cytosolic domain of VAMP2 that lacks the 30 first amino acids respectively. This was achieved by transforming the plasmids into BL21 cells and inducing protein production with IPTG in 6L of culture per construct as outlined in methods (sections 2.3.1 and 2.3.2). Glutathione-Sepharose beads were used to purify the GST-tagged proteins (section 2.3.5). Purity of the proteins was analyzed at various stages by SDS-PAGE on a 15% agarose gel (10 μl loading) followed by Coomassie staining. Soluble proteins (L) were bound to glutathione-Sepharose beads. The protein amounts not bound and bound to the column (Ft and B1) are shown. After extensive washes of the beads using PBS ("W" sample represents the first wash) proteins were eluted using the appropriate buffer (section 2.3.5) *via* 3 successive elutions (E1-E3 samples). The remaining protein on the beads after the elution is shown (B2). Circled bands correspond to GST-Sx4(ΔHabc) (A) and GST-VAMP2(ΔN30) (B) eluted proteins repsectively. (C): Dialysed GST-Sx4(ΔHabc) and GST-VAMP2(ΔN30) proteins (P samples) were treated with thrombin as described in section 2.3.7 (T samples). After the termination of the reaction cleavage products were incubated with the appropriate volume of glutathione-Sepharose beads as outlined in methods (section 2.3.7). Unbound protein (S samples) and bound protein to the beads (beads with GST samples; B) were separated by centrifugation. All prepared samples as well as an aliquot of GST protein (control) were heated up to 95°C for 5 minutes after the addition of equal volume of 2xLSB. Samples were subject to SDS-PAGE through a 15% gel followed by Coomassie staining (10 μl loading). The single band of a molecular weight approximately 10kDa in the supernatant sample correspond to cleaved Sx4(ΔHabc) VAMP2(ΔN30) as illustrated. Positions of molecular weight markers are indicated.

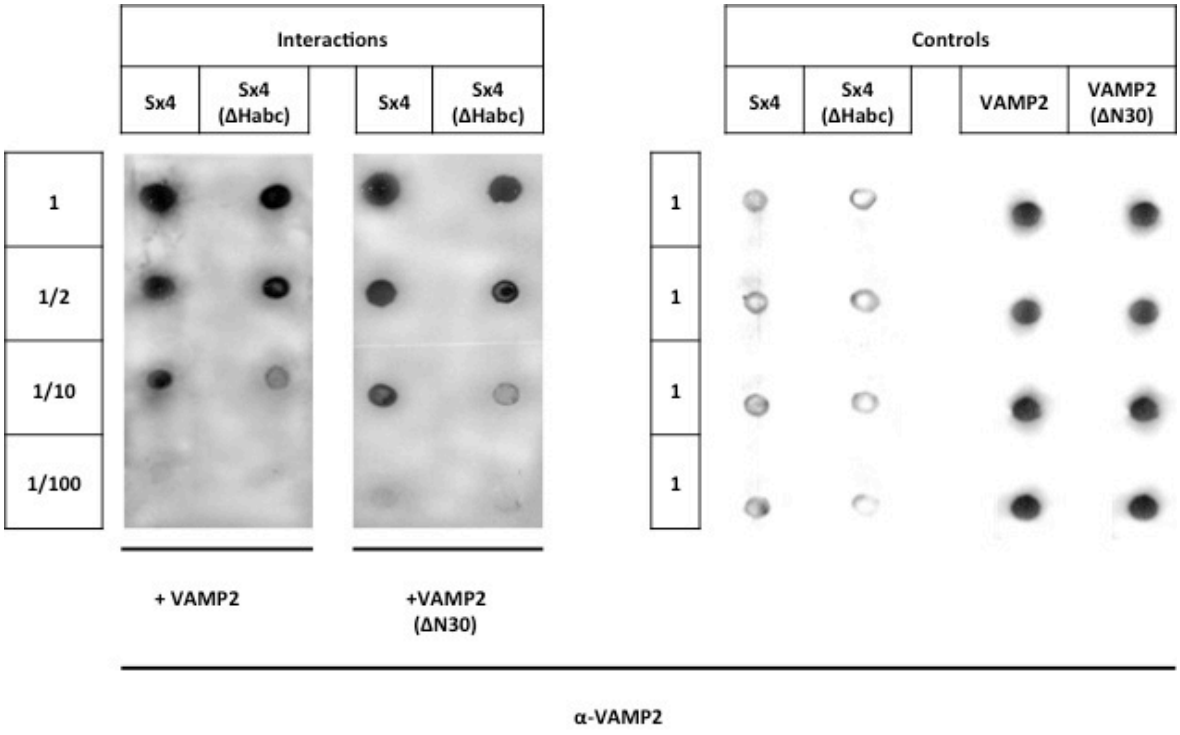

Figure 4-12: Syntaxin 4/VAMP2 interaction *in vitro* is SNARE domain related.

Membranes were prepared by dotting 2 μl of a series of successive dilutions in PBS (the protein amount of undiluted sample was ~5μg) of purified, dialysed Sx4 and Sx4(ΔHabc) as indicated as well as VAMP2 and VAMP2(ΔN30) (positive controls) and left to dry at room temperature. Membranes after were treated with blocking solution and then washed as described in section 2.5 and incubated for 2 hours at 4 ^{o}C under gentle agitation in the presence of 3ml PBS solution containing ~10 molar excess of either VAMP2 or VAMP2(ΔN30) or no protein at all (negative and positive controls) as indicated. Following the incubation unbound proteins were washed with PBS and finally membranes were subject to immunoblot analysis using α-VAMP2 antibody.

4.3.4 Syntaxin 4's interaction with VAMP2 is inhibited by its Habc domain

Like all syntaxins, Syntaxin 4 possesses an N-terminal Habc domain that, through analogy with other family members, and through biochemical evidence, is thought to regulate the availability of Syntaxin 4's SNARE domain to participate in SNARE complexes (Aran et al., 2009; Ungar and Hughson, 2003). Given that the interaction between Syntaxin 4 and VAMP2 occurs *via* their SNARE domains (Figure 4-12), it is reasonable to hypothesize that this interaction might also be regulated by the Habc domain of Syntaxin 4. To test this hypothesis, 3 different mutant versions of Sx4-GST were assessed for their ability to bind the cytosolic domain of VAMP2. One of these mutants lacks the first N-terminal amino acids (ΔN36) (Figure 4-10 B), another has been shown to be locked in an open conformation due to the substitution of two amino acids-L173A/E174A of the

flexible linker segment (open)(Aran et al., 2009) (Figure 4-10 C). The design of this mutant was based on Syntaxin 1A in which mutation of both Leu165 and Glu166, within the hinge region between the SNARE motif and the Habc domain of Sx1a, to alanine residues results in a protein that is unable to adopt the closed conformation (Dulubova et al., 1999). The last mutant that was used above lacks the entire Habc domain (ΔHabc). Figure 4-13 documents the expression and purification of C-terminally GST-tagged Syntaxin 4 (ΔN36) (A) and C-terminally GST-tagged cytosolic Syntaxin 4 that carries the two single amino acid substitutions that mentioned above, which force the protein to remain in its open conformation (Sx4-GST (open)) (B). Expression and purification of the wild-type and ΔHabc versions have been documented earlier (Figure 4-1 and Figure 4-11 A)

Sx4-GST (ΔN36), Sx4-GST (open), Sx4-GST (ΔHabc) and wild-type-Sx4-GST (purified as documented in Figure 4-13 A and B, Figure 4-11 A and Figure 4-1 B respectively) were all immobilized independently onto glutathione-Sepharose and assessed for their ability to bind the cytosolic domain of VAMP2 (GST-moiety alone was also included in this analysis as a negative control). Data obtained from these experiments are presented in Figure 4-14, Figure 4-15 and Figure 4-16 and summarised in Figure 4-17. Both the open version of Sx4 and that lacking the Habc domain bind the cytosolic domain of VAMP2 at a faster rate than the wild-type or the ΔN36 mutant, which like wild-type Sx4-GST has been characterised to preferentially adopt a closed conformation in which the Habc domain is unavailable (Aran et al., 2009). Collectively, these data are consistent with a model in which the Habc domain of Syntaxin 4 has an inhibitory effect on the interaction between Syntaxin 4 and VAMP2; likely through formation of a closed conformation (Aran et al., 2009).

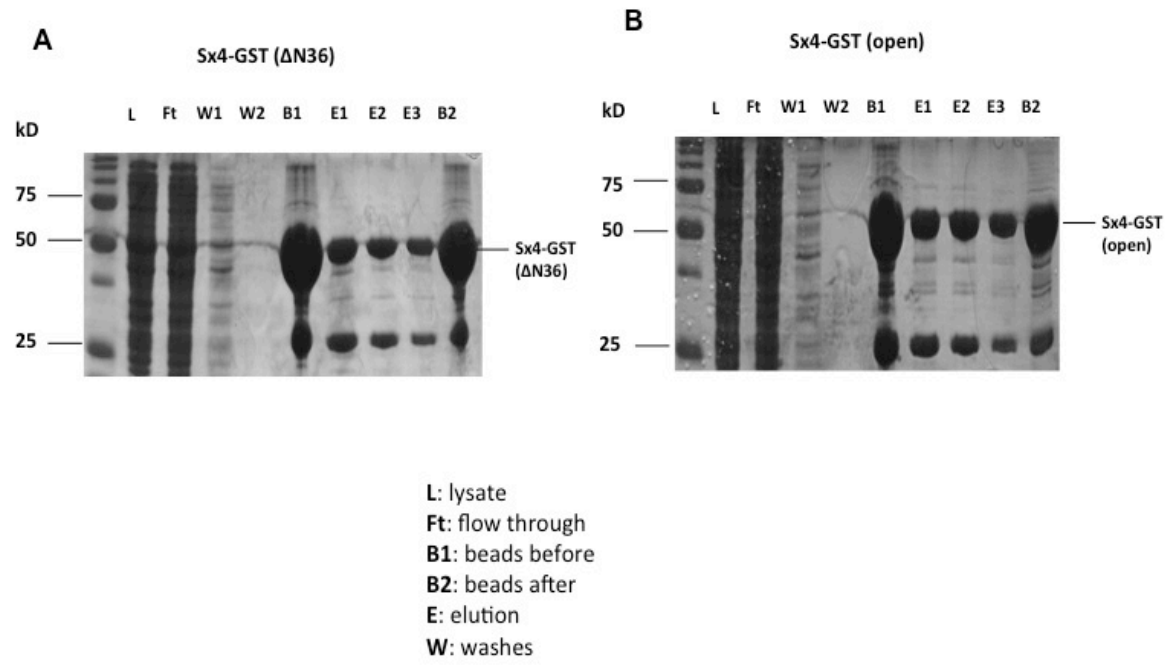

Figure 4-13: Purification of bacterially expressed mutants of Syntaxin 4.

pETDUET:Sx4-GST(ΔN36) and pETDUET:Sx4-GST(open) plasmids (Table 2.5) were used to produce C-terminally GST-tagged mutant versions of the cytosolic domain of Syntaxin 4 lacking the 36 first amino acids (ΔN36; A) or harbouring two mutations in the hinge region (L173A/E174A) ('open'; B) respectively. This was achieved by transforming the constructs into BL21 cells and inducing protein production in 6L cultures with IPTG prior to glutathione affinity purification to isolate GST proteins as outlined in methods (sections 2.3.1, 2.3.2, 2.3.3 and 2.3.5). Purity of the proteins was analyzed at various stages by SDS-PAGE on a 15% agarose gel (10µl loading) followed by Commassie staining. Soluble protein (L) was bound to glutathione-Sepharose beads. The protein fractions not bound and bound to the column (Ft and B1) are shown. After multiple washes with PBS ("W' represents the first wash) of the beads proteins were eluted using the appropriate buffer (section 2.3.5) 3 times successively (E1-E3). The remaining protein on the beads after the elution is shown (B2). Circled bands represent the corresponding eluted protein from the beads. Positions of molecular weight markers are indicated.

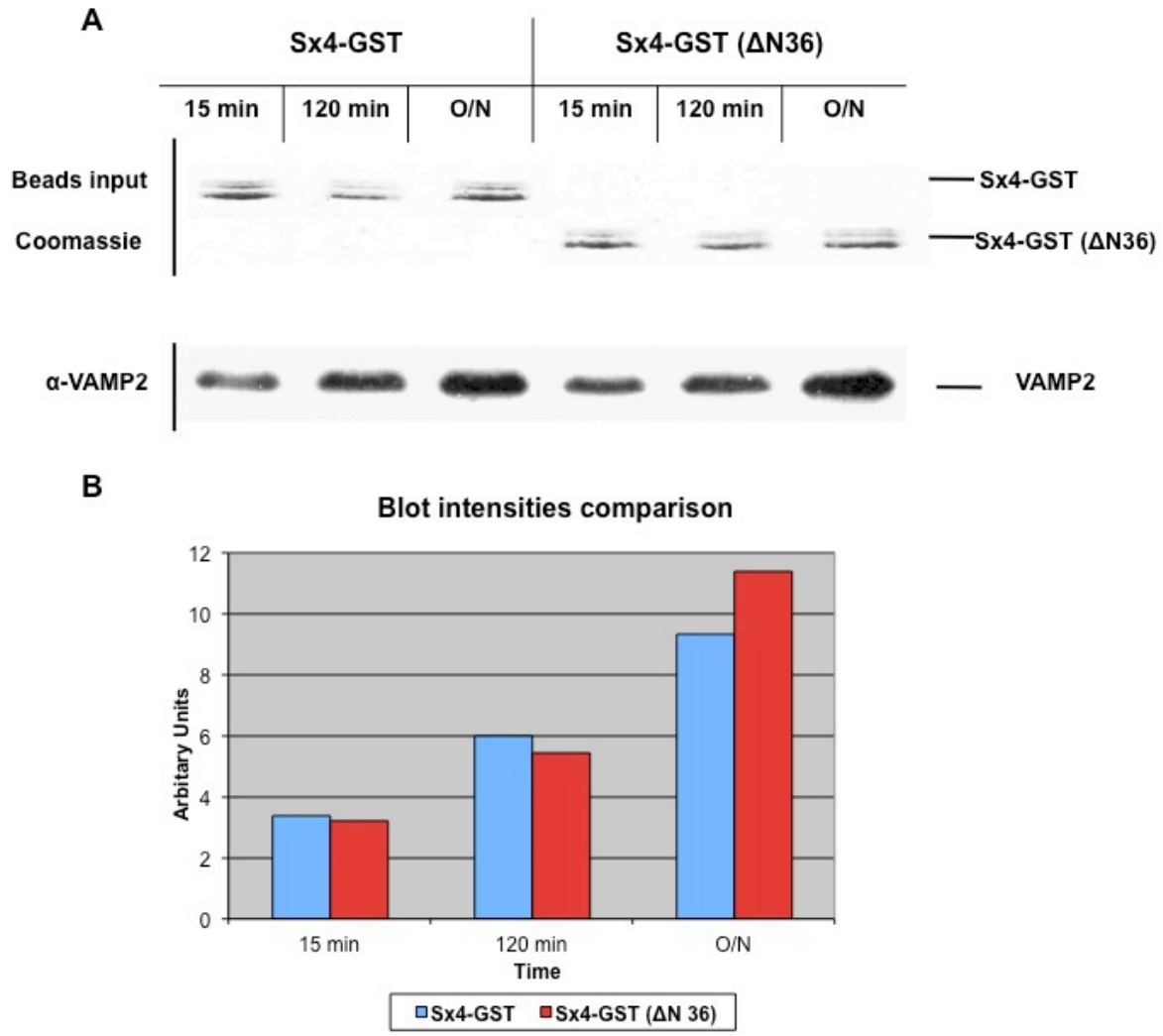

Figure 4-14: Sx4-GST (ΔN36) interacts as efficiently as wild-type Sx4-GST with the cytosolic domain of VAMP2.

(A): 10μg of either Sx4-GST or Sx4-GST(ΔN36) bound to glutathione-Sepharose (10μl bed volume) were incubated in 1ml PBS (as described in section 2.4) containing cytosolic domain of VAMP2 in ~10x molar excess for the indicated times on a rotating wheel at 4˚C, after which the beads were washed thoroughly using PBS prior to final resuspension in 50 μl 2xLSB and heating to 95˚C for 5 minutes. Eluted proteins were subject to SDS-PAGE through a 15% separating gel and visualized by Coomassie staining (protein input loading control-upper panel) (10 μl loading) or immunoblot analysis using α-VAMP2 antibody (5 μl loading) (lower panel). (B): Histogram comparing band intensities (analysed by densitometry using image j software) of VAMP2 pulled down by the two different constructs at same time point.

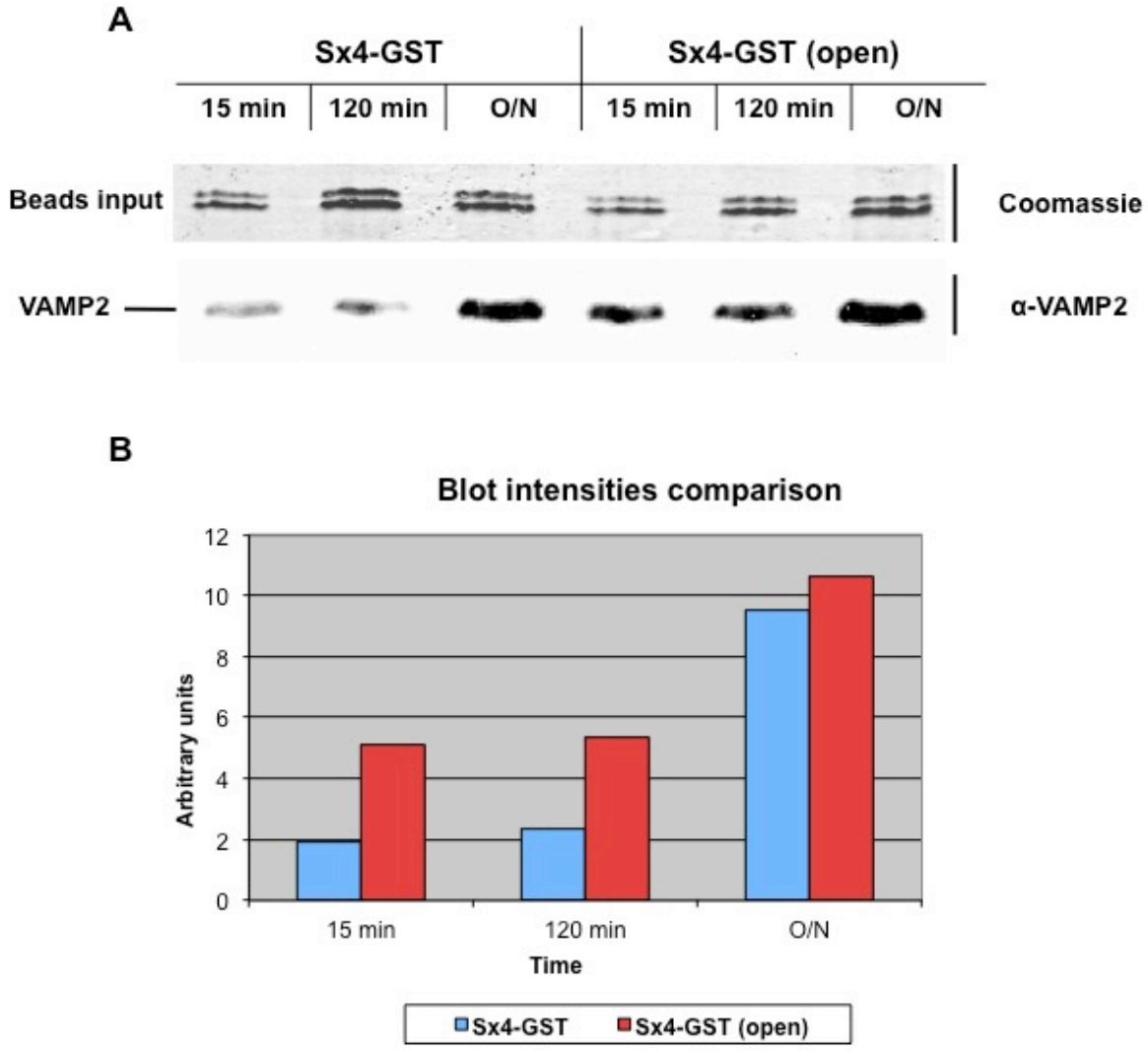

Figure 4-15: Sx4-GST (open) mutant interacts more efficiently than wild-type Sx4-GST with the cytosolic domain of VAMP2.

A): 20μg of either Sx4-GST or Sx4-GST (open) bound to glutathione-Sepharose beads (10 μl bed volume) were incubated in 1ml PBS (as described in section 2.4) containing cytosolic domain of VAMP2 in ~10x molar excess for the indicated times on a rotating wheel at 4˚C, after which the beads were washed thoroughly using PBS prior to final resuspension in 50μl 2xLSB and heating to 95˚C for 5 minutes. Eluted proteins were subject to SDS-PAGE through a 15% separating gel and visualized by Coomassie staining (protein input loading control-upper panel) (10 μl loading) or immunoblot analysis using α-VAMP2 antibody (5 μl loading) (lower panel). (B): Histogram comparing the intensities of the blot bands in panel (A) in pairs of same time point's samples. The bands were analysed by densitometry using image j software.

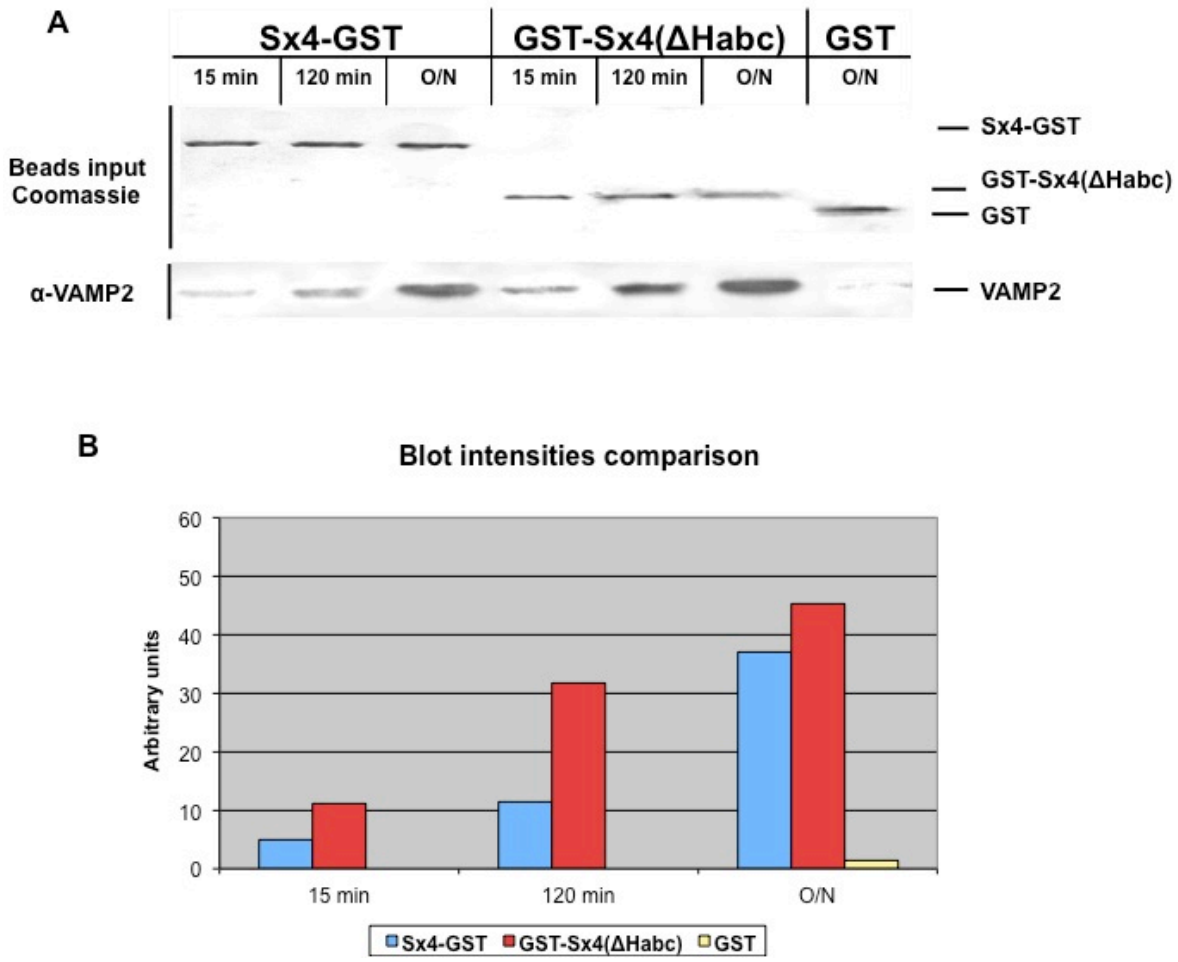

Figure 4-16: Sx4-GST (ΔHabc) interacts more efficiently than wild-type Sx4-GST with the cytosolic domain of VAMP2.

(A): 10μg of either Sx4-GST, Sx4-GST(ΔHabc) or GST (negative control) bound to glutathione-Sepharose beads (10 μl bed volume) were incubated in 1ml PBS (as described in section 2.4) containing cytosolic domain of VAMP2 in ~10x molar excess for the indicated times on a rotating wheel at 4˚C, after which the beads were washed thoroughly using PBS prior to final resuspension in 50μl 2xLSB and heating to 95˚C for 5 minutes. Eluted proteins were subject to SDS-PAGE through a 15% separating gel and visualized by Coomassie staining (protein input loading control-upper panel) (10 μl loading) or immunoblot analysis using α-VAMP2 antibody (5 μl loading) (lower panel). (B): Histogram comparing the intensities of the blot bands in panel (A) in pairs of same time point samples. The bands were analysed by densitometry using image j software.

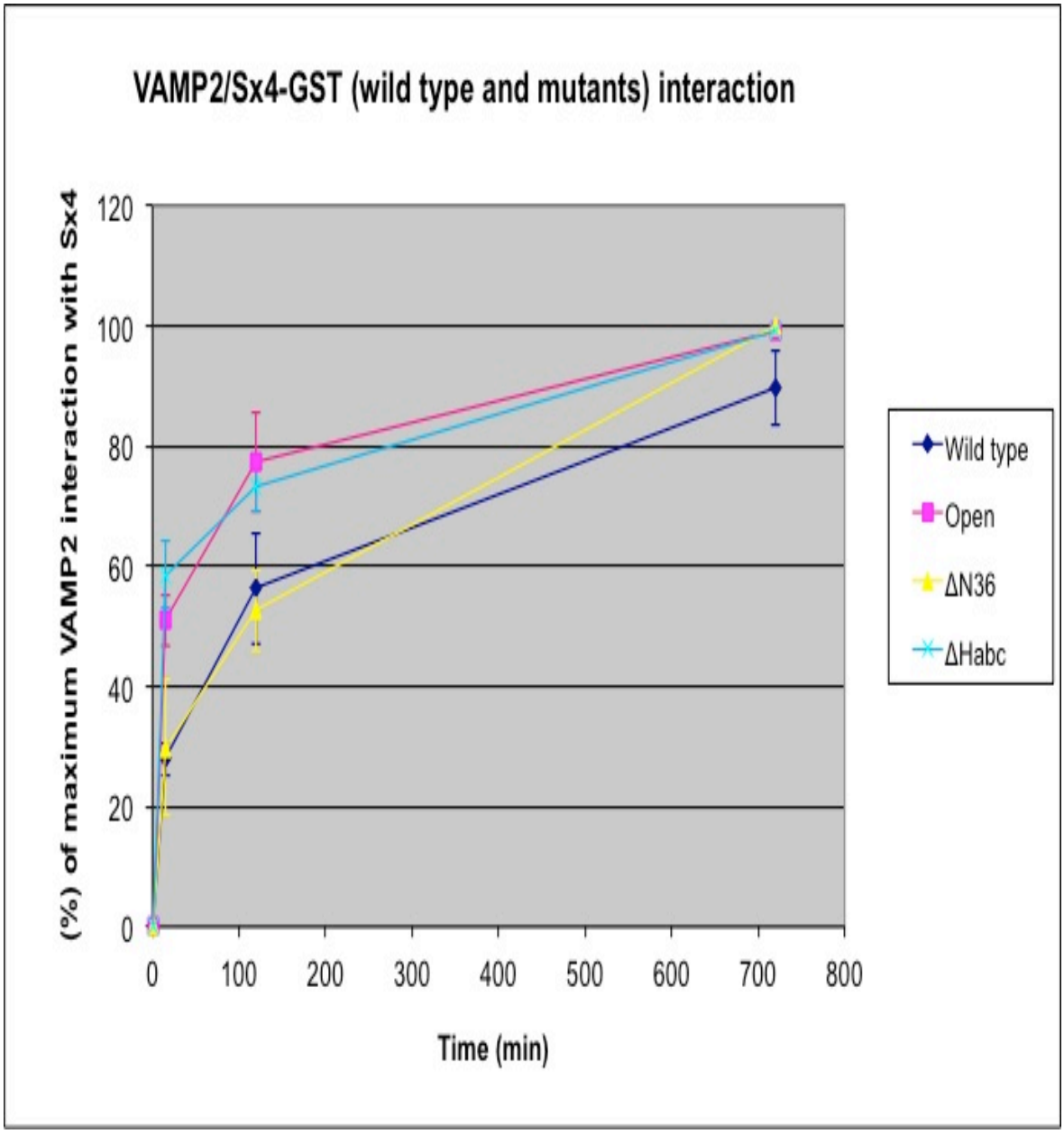

Figure 4-17: Summary of comparisons of the cytosolic domain of VAMP2 interactions with Syntaxin 4 and mutant versions thereof.

Graphical representation of data obtained assaying comparing the ability of various versions of Sx4-GST wild-type and mutants as described to pull down the cytosolic portion of VAMP2 (as in Figure 4-14 Figure 4-15 and Figure 4-16). The proportion of VAMP2 pulled down the different versions of Sx4-GST (expressed as percentage of maximum binding) is plotted as a function of time. Error bars represent the standard deviation of maximum signal intensity's percentage variable (VAMP2) of three independent experiments (appendix Figure 8-49, Figure 8-50, Figure 8-51).

4.3.5 Enhanced interaction between VAMP2 and Syntaxin 4 upon insulin stimulation

To further investigate the VAMP2/Syntaxin 4 interaction, I tested whether it is influenced by insulin-stimulation. For this purpose, the ability of recombinant VAMP2 to pull-down endogenous Sytnaxin 4 for cell lysates prepared from 3T3-L1 adipocytes either treated with insulin or not (basal cells) was assessed. His-tagged VAMP2 (produced in bacteria as outlined in Figure 4-18) immobilised on Ni-Agarose was incubated with adipocyte lysate prepared from cells treated with 100nM insulin for the indicated times, or not. Immonoblot analysis using antibodies either against Syntaxin 4 or SNAP23 was subsequently used to assess the amount of Syntaxin 4 and SNAP23 pulled down from the various lysates (Figure 4-19). This analysis revealed that insulin-stimulation increases binding between His-VAMP2 and Syntaxin 4 gradually at least up to a period of 10-20 min. No interaction between Snc2-PrA, used here as a negative control, and Syntaxin 4 was detected (Figure 4-19). Strong evidence was provided from the results of a functional opening of Syntaxin 4 -due to insulin- based on protein's amount that was pulled down by His-VAMP2 considering the inhibitory effect that Habc domain has on the interaction (Figure 4-17). Finally, as it appears from the results Syntaxin 4 interacts with His-VAMP2 directly and not in the form of ternary SNARE complex since neither SNAP23 nor a signal at the molecular weight that corresponds to the SNARE complex were detected.

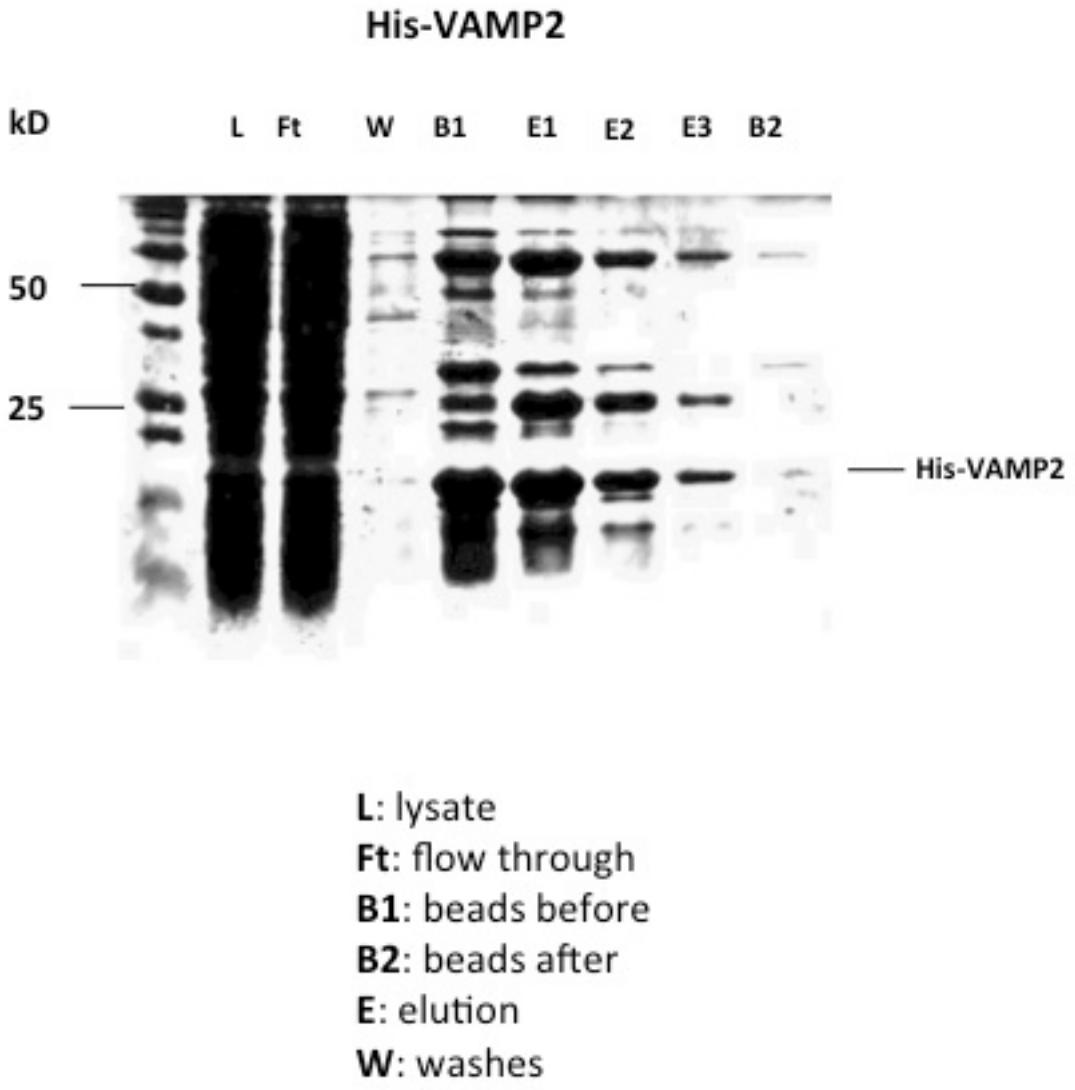

Figure 4-18: Purification of N-terminally His-tagged cytosolic VAMP2 protein

Plasmid pQE30: His-VAMP2 was used to recombinantly produce N-terminally His-tagged cytosolic domain of VAMP2 by transforming the plasmid into BL21 cells and inducing protein production with IPTG in 9L of culture as outlined in methods (sections 2.3.1 and 2.3.2). Ni-Agarose beads were then used to purify the His-tagged protein (section 2.3.4). Purity of the protein was analyzed at various stages by SDS-PAGE on a 15% agarose gel (10 µl loading) followed by Commassie staining. Soluble protein (lysate samples) was bound to Ni-Agarose beads. The protein amounts not bound and bound to the column (flow through and beads before samples) are shown. After extensive washes of the beads using the suitable washing buffer (section 2.3.4) (washes sample represents the first wash) proteins were eluted using the appropriate buffer (section 2.3.4) *via* 3 successive elutions (elution 1-3 samples). The remaining protein on the beads after the elution is shown (Beads after samples). Circled bands correspond to His-VAMP2 eluted protein.

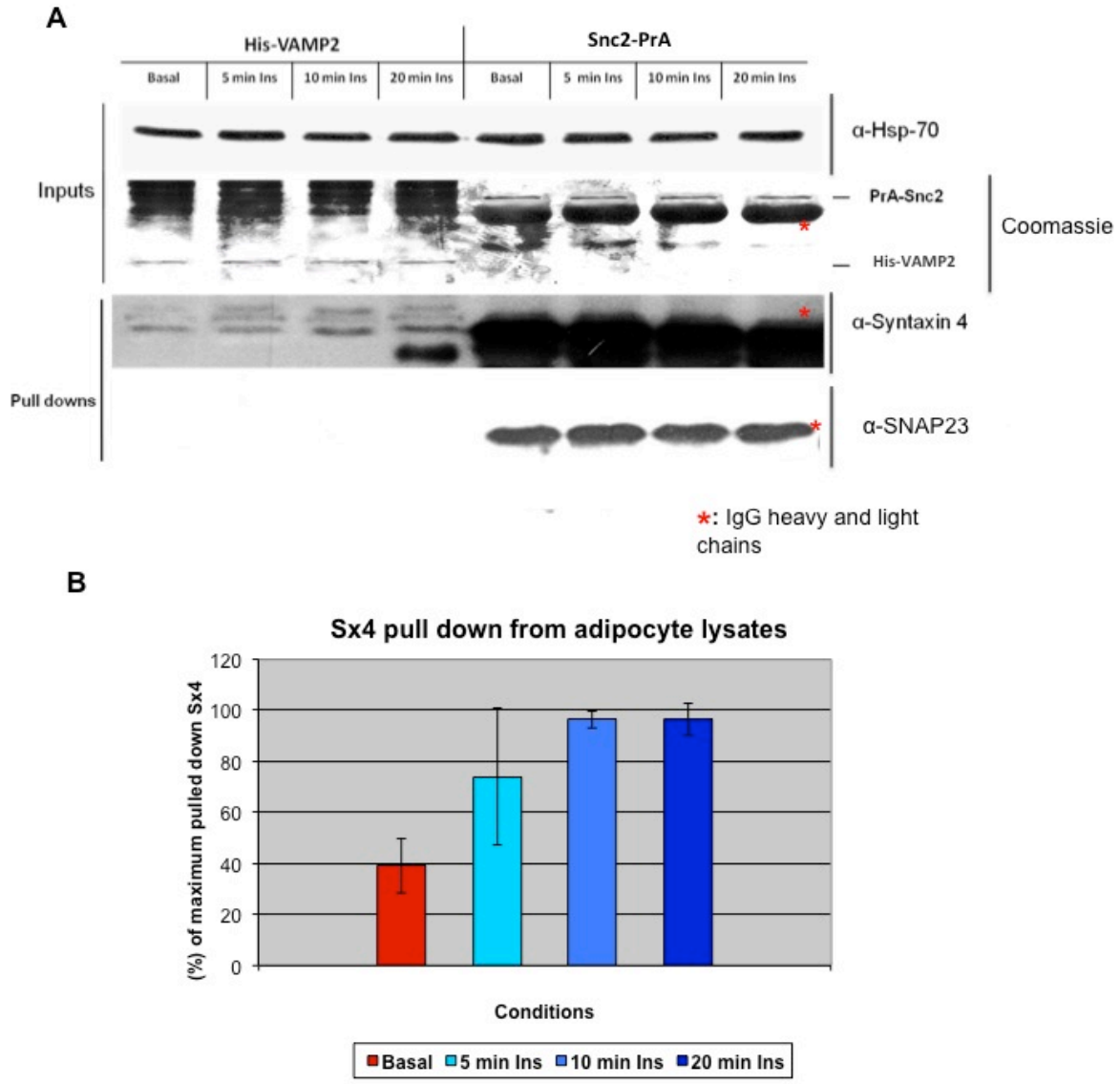

Figure 4-19: His-VAMP2 pulls down Syntaxin 4 but not SNAP23 from Adipocyte lysates

10 µg of either N-terminally his-tagged VAMP2 (His-VAMP2) or C-terminally PrA-tagged Snc2 (Snc2-PrA) (negative control) bound to Ni-Agarose and IgG-Sepharose beads corespondingly (5 and 50 µl bed volume respectively) were incubated with 3T3L1 adipocyte lysates prepared from cells that either have been treated with 100 nM of insulin for the indicated times or not as outlined in methods (sections 2.6.5 and 2.6.6). Lysates were subject to immunoblot analysis using α-Hsp-70 antibody to control for equal protein input (upper panel) (20µl loading). Following incubation on a rotating wheel at 4˚C for two hours beads were washed extensively using adipocytes lysis buffer prior to the addition of 50µl 2xLSB and heating to 60˚C for 10 minutes. Eluted proteins were subject to SDS-PAGE through a 15% separating gel and were visualized by Coomassie staining (beads protein input loading control-middle panel) (10 µl loading) or iimmunoblot analysis using either α-Syntaxin 4 or α-SNAP23 antibody (5 µl loading) (lower panel). The bands were analyzed by densitometry using image j software and normalized to both beads bound and basal condition adipocyte lysate protein inputs (histograms). Error bars represent standard deviation of three independent experiments' mean value (appendix Figure 8-55).

4.3.6 SNAP23 binds directly to the cytosolic domain of Syntaxin 4 but not to that of VAMP2 *in vitro*

Formation of several fusogenic SNARE complexes is preceded by assembly of t-SNARE complexes including that required for the externalization of GLUT4 in insulin responsive cells, where Syntaxin 4 and SNAP23 form an intermediate complex prior to development of the ternary SNARE complex (Araki et al., 1997; Dun et al., 2010). Figure 4-20 demonstrates that this binary interaction can be reconstituted *in vitro* using N-terminally His-tagged SNAP23 (His-SNAP23; produced as described in Figure 4-1 C) to pull-down the cytosolic domain of Syntaxin 4 (produced as described in Figure 4-4).

Having demonstrated direct interaction between the cytosolic domains of Syntaxin 4 and VAMP2, and Syntaxin 4 and SNAP23, I went on to investigate the remaining last possible pairwise association between the SNARE proteins involved in inulin-regulated GLUT4 delivery to the plasma membrane; namely between VAMP2 and SNAP23. Figure 4-21demonstrates that no interaction was detected between immobilised His-SNAP23 and cytosolic VAMP2 (produced as described in Figure 4-7). It is important to note that Figure 4-20 and Figure 4-21 provide confidence that the proteins used in this experiment are capable to acting with their physiological partners *in vitro*.

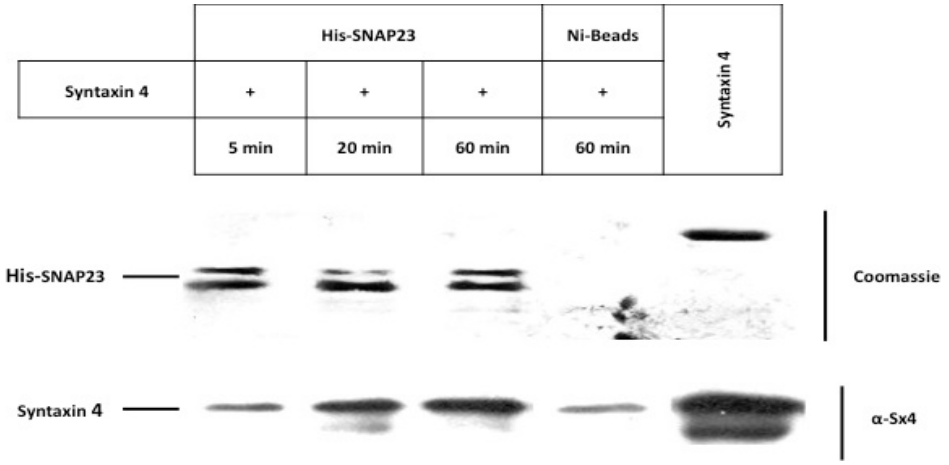

Figure 4-20: His-SNAP23 binds directly to the cytosolic domain of Syntaxin 4 *in vitro*.

30 µg His-SNAP23 (produced as described in Figure 4-1) bound to Ni-Agarose beads or empty beads (10 µl bed volume) were incubated in 1ml PBS containing cytosolic domain of Sx4 (produced as described in section 2.4) in ~10x molar excess for the indicated times on a rotating wheel at 4˚C, after which the beads were washed thoroughly using the appropriate buffer (section 2.3.4) prior to final resuspension in 50 µl 2xLSB and heating to 95˚C for 5 minutes. Eluted proteins, as well as an aliquot of Sx4 protein (positive control) were subject to SDS-PAGE through a 15% separating gel and visualized by Coomassie staining (protein input loading control-upper panel) (10 µl loading) or immunoblot analysis using α-Syntaxin 4 antibody (5 µl loading) (lower panel).

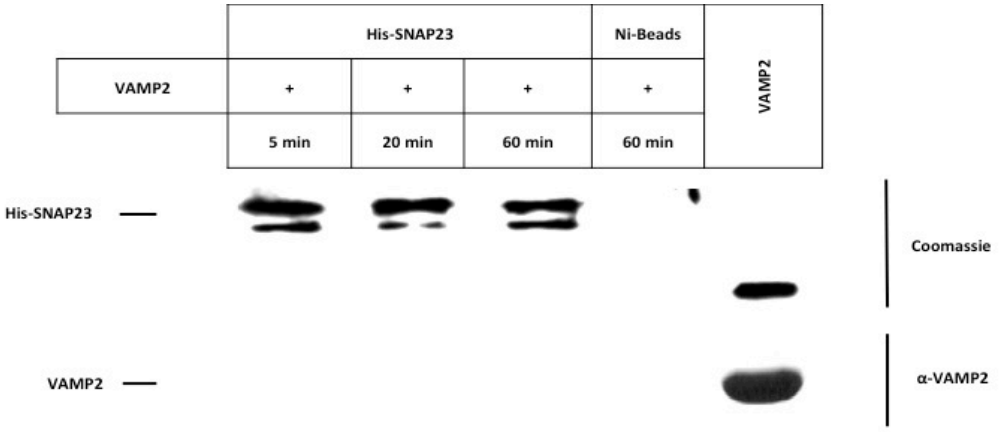

Figure 4-21: No detectable direct interaction between His-SNAP23 and the cytosolic domain of VAMP2 *in vitro*.

50 µg of His-SNAP23 (produced as described in Figure 4-1) bound to Ni-Agarose beads or empty beads (10 µl bed volume) were incubated in 1ml PBS containing cytosolic domain of VAMP2 (produced as described in Figure 4-7) in ~10x molar excess for the indicated times on a rotating wheel at 4˚C, after which the beads were washed thoroughly using the appropriate buffer (section 2.3.4) prior to final resuspension in 50µl 2xLSB and heating to 95˚C for 5 minutes. Eluted proteins, as well as an aliquot of VAMP2 protein (positive control), were subject to SDS-PAGE through a 15% separating gel and visualized by Coomassie staining (protein input loading control-upper panel) (10 µl loading) or immunoblot analysis using α-VAMP2 antibody (5 µl loading) (lower panel).

4.3.7 Syntaxin 4/SNAP23 and Syntaxin 4/VAMP2 interactions have opposite effects on the rate of SNARE complex formation *in vitro*

It has been demonstrated that formation of the intermediate t-SNARE complex mediates assembly of fusogenic SNARE complexes in many systems (Kawanishi et al., 2000; Rodkey et al., 2008; Scott et al., 2004) and it has been shown that formation of a binary SNAP23/Syntaxin 4 complex facilitates formation of the functional SNARE complex responsible for fusion of GLUT4 vesicles with the plasma membrane (Kawanishi et al., 2000; St-Denis et al., 1999). To test the hypothesis that the Syntaxin 4's interaction with SNAP23 enhances SNARE complex formation, the effect of preincubating Sx4-GST with His-tagged SNAP23 on its ability to form SDS-resistant SNARE complexes, containing SNAP23 and VAMP2 was investigated. This was achieved by preincubating Sx4-GST immobilised on glutathione-Sepharose beads with purified SNAP23 to allow formation of the binary t-SNARE complex, the ability of this to form SNARE complexes was then compared to that of Sx4-GST alone. Figure 4-22 (panel A) shows that there is a time-dependant increase in the amount of the SNARE complex formed (shown by increasing band strengths of the α-VAMP2 immunoblots at a molecular weight corresponding to the sum of the three SNARE proteins molecular weights ~110 kDa) under both conditions. Pre-incubation of His-SNAP23 with Syntaxin 4-GST (T samples) resulted in a marked increase in the level and rate of SNARE complex assembly relative to that seen when all the SNARE proteins added at the same time (A samples).

To examine any possible effect of the binary VAMP2/Syntaxin 4 interaction on the kinetics of ternary SNARE complex a similar experiment was performed. In this case His-tagged SNAP23 (His-SNAP23) immobilized to Ni-Agarose beads was incubated with solutions containing cytosolic Syntaxin 4 and VAMP2 in molar excess, which had either been preincubated overnight or not. Figure 4-23 indicates that the Syntaxin 4/VAMP2 interaction has an inhibitory effect on the rate of SNARE complex formation.

Both the experiments described above (Figure 4-22 and Figure 4-23 were repeated three times and the results were analysed statistically. These data are summarised in Figure 4-24 that shows the positive effect of the

SNAP23/Syntaxin 4 interaction (panel A) and the inhibitory effect of the VAMP2/Syntaxin 4 interaction on SNARE complex formation.

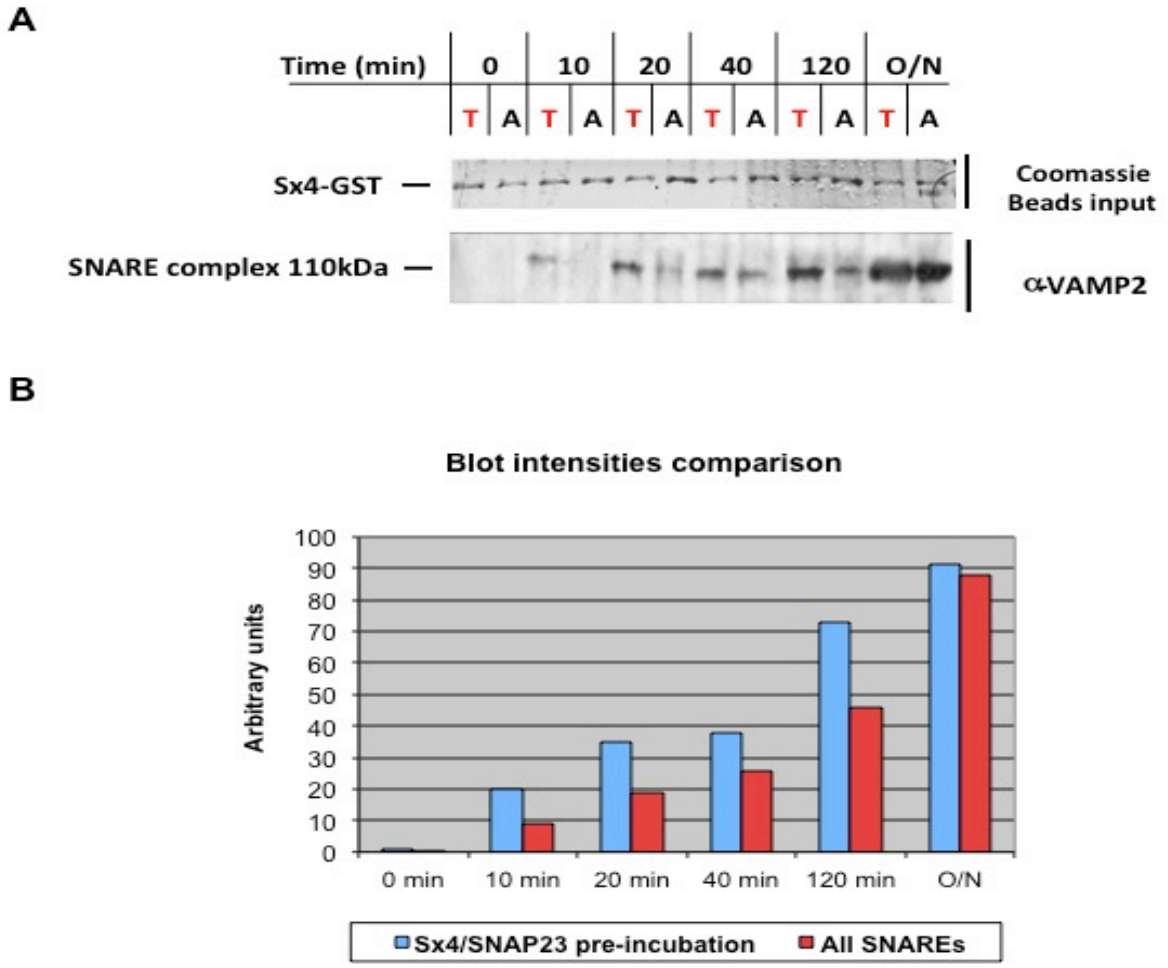

Figure 4-22: Interaction between Syntaxin 4 and SNAP23 facilitates SNARE complex formation.

(A): 10 µg Sx4-GST bound to glutathione-Sepharose beads (10µl bed volume) were pre-incubated for two hours with 1ml PBS containing His-SNAP23 in ~10x molar excess (T samples) or not (A samples). After pre-incubation VAMP2-PrA and VAMP2-PrA/His-SNAP23 (both in ~10x molar excess) were added to T and A samples respectively. Samples were incubated for the indicated times on a rotating wheel at 4°C, after which the beads were washed thoroughly using PBS prior to final resuspension in 50µl 2xLSB and heating to 95°C for 5 minutes. Samples were subjected to SDS-PAGE through a 15% separating gel and visualized by Coomassie staining (protein input loading control-upper panel) (10 µl loading) or immunoblot analysis using α-VAMP2 antibody (5 µl loading) (lower panel). The smear of bands of a molecular weight around 110 kDa corresponds to the SDS-resistant ternary SNARE complex made of Sx4-GST/His-SNAP23/VAMP-PrA. N.B. recombinant proteins used in this experiment were prepared as described in section 2.3.5 (Sx4-GST), section 2.3.4 (His-SNAP23) and section 2.3.6 (VAMP2-PrA). (B): Histogram comparing intensities of the blot bands in panel (A) in pairs of same time point's samples. The bands were analyzed by densitometry using image j software.

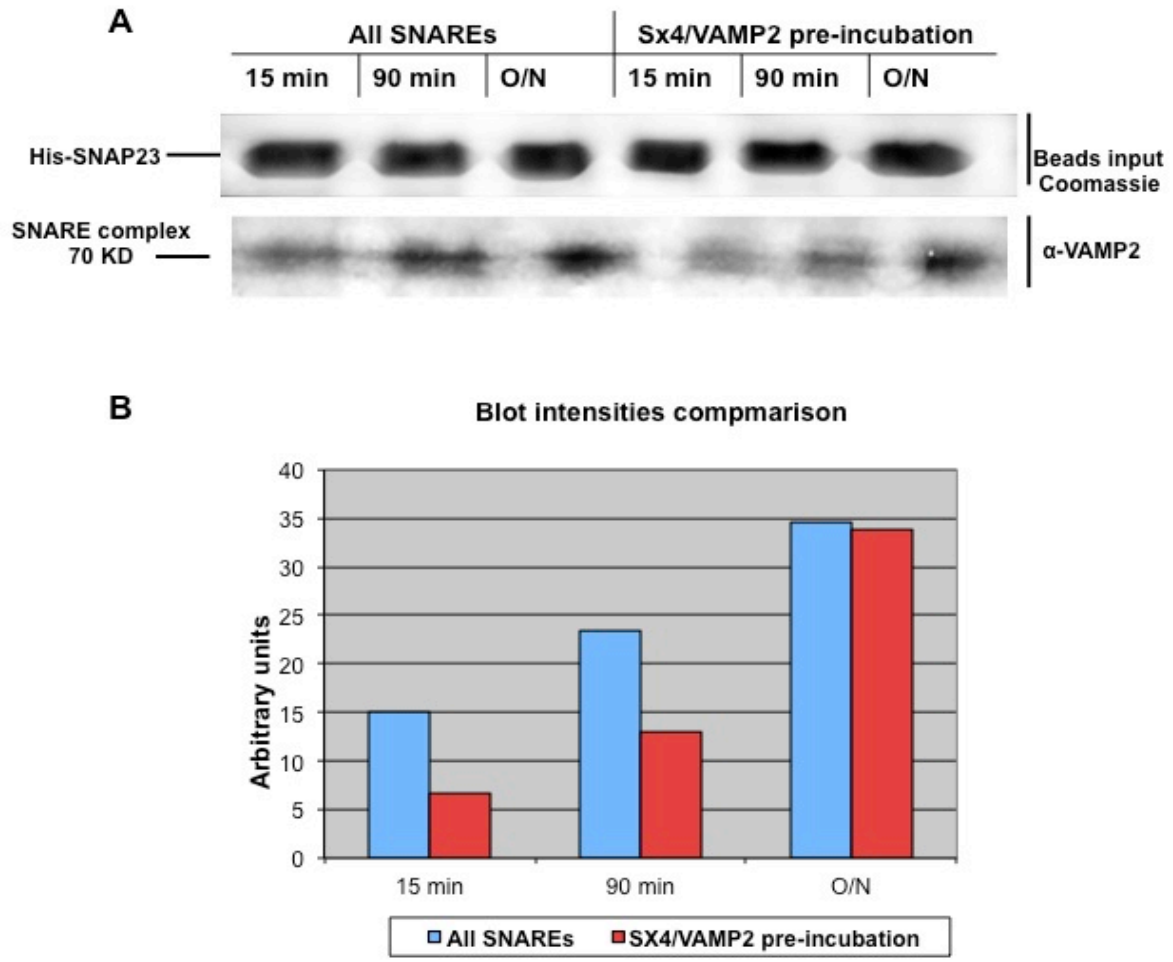

Figure 4-23: VAMP2/Sx4 interaction inhibits SNARE complex formation.

(A): 50 µg His-SNAP23 bound to Ni-Agarose beads (10µl bed volume) were incubated for the indicated times with 1ml PBS solution containing VAMP2/Sx4 in ~10x molar excess that has been pre-incubated for two hours or not as indicated. After incubation on a rotating wheel at 4˚C, beads were washed thoroughly using the appropriate buffer (section 2.3.4) prior to final resuspension in 50 µl 2xLSB and heating to 95˚C for 5 minutes. Eluted proteins were subjected to SDS-PAGE through a 15% separating gel and visualized by Coomassie staining (protein input loading control-upper panel) (10 µl loading) or immunoblot analysis using α-VAMP2 antibody (5 µl loading) (lower panel). The smear of bands of a molecular weight around 70 kDa corresponds to the SDS-resistant ternary SNARE complex made of Sx4/His-SNAP23/VAMP. N.B. recombinant proteins used in this experiment were prepared as described in sections 2.3.5 and 2.3.7 (cytosolic Syntaxin 4), section 2.3.4 (His-SNAP23) and sections 2.3.5 and 2.3.7 (cytosolic VAMP2). (B): Histogram comparing the intensities of the blot bands in panel (A) in pairs of same time points samples. The bands were analyzed by densitometry using image j software.

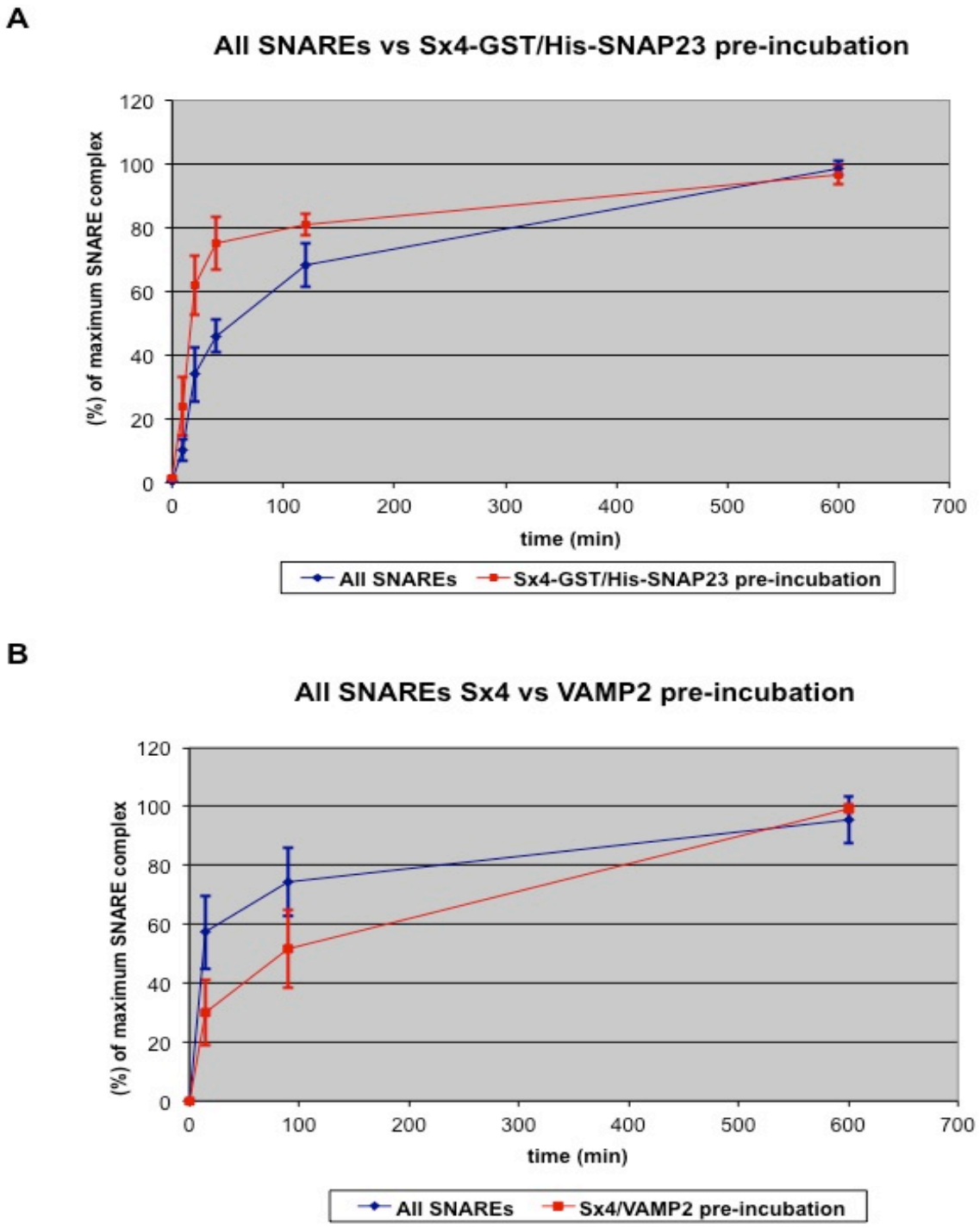

Figure 4-24: SNARE complex formation graphs

SNARE complex assembly assays with Sx4-GST/His-SNAP23, Sx4/VAMP2 pre-incubations or not were set up as described (section 2.4). Graphs show SNARE complex formation (expressed as percentage of maximum complex amount) as a function of time. Panel (A) illustrates the effect of Sx4-GST/His-SNAP23 interaction while panel (B) Sx4/VAMP2 interaction on the rate complex formation. Error bars represent the standard deviation of maximum signal intensity's percentage variable (SNARE complex) of three independent experiments (appendix Figure 8-52 Figure 8-53).

4.4 Discussion

Externalization of facilitative glucose transporter GLUT4 from intracellular depots to the plasma membrane upon insulin stimulation is important for whole-body glucose homeostasis. Fusion of GLUT4-containing vesicles with the plasma membrane is a crucial step in insulin-regulated glucose transport (Bryant et al., 2002). This fusion event is mediated by the SNARE proteins, Syntaxin 4, SNAP23 (t-SNAREs located to plasma membrane) and VAMP2 (v-SNARE anchored to the GLUT4-carrying vesicles) (Bryant and Gould, 2011), through formation of a ternary complex (Polgar et al., 2002) *via* their SNARE domains that provides the mechanical force to overcome the energy barrier required for fusion of the opposing lipid bilayers (Pobbati et al., 2006). The work presented in this chapter characterised interactions between these SNARE proteins using *in vitro* approaches. Bacterially expressed SNARE proteins were used to establish an *in vitro* complex assembly assay which demonstrates that the SNARE complex formed between Syntaxin 4, VAMP2 and SNAP-23 is extremely stable (Figure 4-2), as has been reported for several SNARE complexes (Hayashi et al., 1994; Polgar et al., 2002).

The recombinant SNARE proteins were also used to demonstrate a direct physical interaction between the SNARE motifs of Syntaxin 4 and VAMP2 (Figure 4-3 and Figure 4-5). This is an important finding as it gives credence to the hypothesis I proposed in chapter 3 based on the data obtained from the PLA studies in which a pool of Syntaxin 4 exists in complex with VAMP2 in the absence of SNAP23 *in vivo*. These data are consistent with a previous study which showed that both Syntaxin 1A and Syntaxin 4 can interact individually with VAMP2 *in vitro* (Calakos et al., 1994). The VAMP2 binding site on Syntaxin 1A was shown to lie between amino acid residues 194 and 267 of Syntaxin 1A, a region corresponding almost exactly to its SNARE domain (Calakos et al., 1994). This is consistent with my demonstration that the Syntaxin 4/VAMP2 interaction occurs *via* the SNARE domains of the two proteins (Figure 4-12). The syntaxin's Habc domain inhibited the VAMP2/Syntaxin 4 interaction (Figure 4-14 -Figure 4-17), making it tempting to speculate that the ability of Syntaxin 4 to adopt two distinct conformations, open and closed, may regulate formation of this complex. Regarding this observation pull down assays using adipocyte lysates from insulin stimulated or

not cells provided serious indications for a structural “opening” of Syntaxin 4 upon insulin indication (Figure 4-19).

Finally as far as Syntaxin 4/VAMP2 interaction is concerned I provided strong evidence that it is a specific (Figure 4-6), it is not an artifact due to syntaxin’s polymerization (clustering) (Figure 4-8) and it might have a universal character since it seems to be able to happen between syntaxins and their cognate v-SNAREs in other species and different pathways (Figure 4-9). This last observation might be of great biological significance since it is possible this interaction to further orchestrate the regulated trafficking of vesicles within the cells by facilitating docking of the vesicles to specific target organelles.

I demostrated that, in contrast to the t-SNARE complex between Syntaxin 4/SNAP23 which facilitates formation of the assembled SNARE complex (Figure 4-22), the interaction of Syntaxin 4 with VAMP2 has an inhibitory effect (Figure 4-23). In the previous chapter, I used PLA between all possible pairwise combination of the 3 SNARE proteins and Munc18c (SM) to argue for the existence of two distinct pools of Syntaxin 4 under basal conditions: one with complex with SNAP23, which generally accepted and well characterised (Kawanishi et al., 2000; St-Denis et al., 1999) and one in complex with VAMP2 and Munc18c. The inhibitory nature of VAMP2/Syntaxin 4 interaction upon SNARE complex formation shown in this chapter makes it tempting to speculate a role for the regulatory protein Munc18c in releasing this inhibition. This possibility is explored in the following chapter.

Chapter 5

In vitro analyses of the Munc18c phosphomimetic mutant Y521E

5.1 Introduction

5.1.1 Role of Munc18c in insulin-regulated GLUT4 translocation to the plasma membrane

Fusion of GLUT4 vesicles with the plasma membrane is a key terminal step in insulin-regulated glucose transport into fat and muscle cells. This fusion event is mediated by the SNARE proteins, Syntaxin 4, SNAP23 (t-SNAREs located to plasma membrane) and VAMP2 (v-SNARE anchored to the GLUT4 carrying vesicles) (Bryant et al., 2002), through formation of a highly stable (SDS-resistant) (Hayashi et al., 1994) ternary complex *via* their SNARE domains which provides the mechanical force to overcome the energy barrier for bilayer fusion (Pobbati et al., 2006). SNARE complex formation is regulated by a host of accessory proteins including members of the Sec1p/Munc18 or SM-family (Toonen and Verhage, 2003). The SM protein that regulates Syntaxin 4/SNAP23/VAMP2 mediated delivery of GLUT4 to the cell surface in response to insulin is Munc18c (James, 2005; Tellam et al., 1997; Thurmond et al., 1998; Thurmond et al., 2000). As with all SM proteins, the precise role of Munc18c remains elusive with apparently conflicting evidences supporting seemingly contradictory models (Bryant and Gould, 2011). Some studies suggest that Munc18c plays an inhibitory role in insulin-stimulated translocation of GLUT4 to the cell surface of adipocytes (Tamori et al., 1998; Thurmond et al., 1998) whereas others have indicated that Munc18c is required for the fusion of GLUT4 vesicle with the plasma membrane upon insulin stimulation (D'Andrea-Merrins et al., 2007). For example, studies using mutant versions of Munc18c in 3T3-L1 adipocytes indicate the SM protein is required for delivery of GLUT4 to the plasma membrane in response to insulin (Oh et al., 2005; Thurmond et al., 2000) whereas adipocytes derived from mesennchymal embryonic fibroblasts from Munc18c knockout mice show increased sensitivity to insulin-stimulated GLUT4 externalization, suggesting an inhibitory role for Munc18c (Kanda et al., 2005). More recently, *in vitro* studies have demonstrated that Munc18c inhibits the fusion of artificial liposomes mediated by Syntaxin 4, SNAP23 and VAMP2 (Brandie et al., 2008), further supporting models in which Munc18c exerts an inhibitory role on GLUT4 delivery to the plasma membrane.

5.1.2 Munc18c interaction with SNARE proteins

The apparently contradictory data regarding the role of Munc18c on GLUT4 translocation upon insulin-stimulation may stem from a common feature of SM proteins, namely the ability to interact with its cognate syntaxin (in this case Syntaxin 4) through a variety of different binding modes (Bryant and Gould, 2011). Many syntaxins appear to adopt two distinct conformations, a closed conformer (non-permissive for SNARE complex formation) with the Habc domain folded back on to the SNARE domain and an open one (SNARE complex formation permissive) with the Habc domain away from the SNARE domain (MacDonald et al., 2010) (discussed in Section 1.2.2.1). SM proteins have been shown to bind both of these conformations (Burgoyne and Morgan, 2007). In mode-1, the central cavity of the arch-shaped SM protein cradles its cognate syntaxin in the closed conformation (Dulubova et al., 1999), whereas in mode-2 the N-terminus of the syntaxin inserts into a hydrophobic "pocket" of its associated SM protein (Khvotchev et al., 2007); mode-2 binding is compatible with the syntaxin being in either its open, or closed conformation, whereas mode-1 binding can only occur when the syntaxin is in its closed conformation (Burgoyne and Morgan, 2007). In addition, a third binding mode of SM proteins with the assembled SNARE complex has been demonstrated, and SM proteins have also been shown to bind the pre-assembled t-SNARE binary complexes (Carr et al., 1999; D'Andrea-Merrins et al., 2007; Rodkey et al., 2008) and non-syntaxin, v-SNAREs (Carpp et al., 2006; Peng and Gallwitz, 2004), although little is known about how these interactions are facilitated. It is well-established that Munc18c interacts with the N-terminus of Syntaxin 4 (binding mode-1) (Burkhardt et al., 2008), and also with the binary t-SNARE complex (Syntaxin 4/SNAP23) and the ternary SNARE complex (Syntaxin 4/SNAP23/VAMP2) (Latham et al., 2006). Munc18c also interacts directly with the v-SNARE VAMP2 (Brandie et al., 2008). Although no definitive evidence exists to support the notion that Munc18c interacts with Syntaxin 4 in its closed conformation (binding mode-1) (Christie et al., 2012) as was shown for Syntaxin 1A and Munc18a (the corresponding neuronal proteins) *via* crystallographic studies (Misura et al., 2000), modeling studies indicate that such an interaction is possible, if not likely given that the regions of intramolecular interactions between the Habc domain and the SNARE motif of Syntaxin 1A were found to be highly conserved between the two different syntaxins (D'Andrea-Merrins et al., 2007). This has been tested experimentally.

Mutations predicted to create a constitutively 'open' version of Syntaxin 4, based on those chracterised in Syntaxin 1A, create a protein that is more susceptible to limited proteolysis than the wild-type protein, a characteristic of the Syntaxin 1A 'open' mutant (Aran et al., 2009). Furthermore *in vitro* binding assays revealed a binding mode between Syntaxin 4 and Munc18c distinct to binding mode-2 (Aran et al., 2009) that is not observed using the putatively 'open' Syntaxin 4, mutant – further supporting the contention that Syntaxin 4 is able to adopt a closed conformation akin to that characterised for Syntaxin 1A and subsequently interact with Munc18c *via* binding mode-1.

5.1.3 Phosphorylation of Munc18c

The central role that SM proteins play in regulating SNARE-mediated membrane fusion, combined with the dependence of insulin-regulated translocation of GLUT4 to the plasma membrane on SNARE proteins, makes Munc18c an attractive candidate as a regulator of insulin-stimulated glucose transport into fat and muscle cells. This could be achieved by insulin alleviating a negative regulation of Syntaxin 4. Munc18c becomes tyrosine phosphorylated in response to insulin treatment of adipocytes at two discrete sites, Tyr219 and Tyr521 (Oh and Thurmond, 2006; Schmelzle et al., 2006). *In vitro* phosphorylation studies revealed that the insulin receptor itself is responsible for Tyr521 phosphorylation (Aran et al., 2011; Jewell et al., 2011). The kinase responsible for Tyr219 phosphorylation remains to be identified. Evidence for functional significance of tyrosine phosphorylation comes from the observation that phospho-resistant mutants of Munc18c fail to rescue defective insulin-stimulated GLUT4 translocation of Munc18c knockdown adipocytes (in contrast to wild-type and phosphomimetic constructs) (Jewell et al., 2011). Furthermore, studies in MIN6 beta cells indicate that Munc18c phosphorylation facilitates vesicles exocytosis in response to glucose stimulation of these cells (Oh and Thurmond, 2006). *In vitro* binding studies indicate that phosphorylation of Munc18c on Tyr521 abrogates its binding to Syntaxin 4 (Aran et al., 2011). These data collectively make it attractive to speculate that phosphorylation of Munc18c in response to an external signal results in its dissociation from Syntaxin 4, lifting its inhibitory effect (Jewell et al., 2008; Umahara et al., 2008). Quite interestingly phosphorylated Munc18c upon insulin stimulation, which has abolished its interaction from Syntaxin 4, seems to bind to Doc2beta a cytoplasmic C2 domain

containing protein(Ke et al., 2007). Thus, tyrosine phosphorylation of Munc18c is emerging as a potential regulatory mechanism in insulin-regulated GLUT4 trafficking.

5.2 Aims of this chapter

In chapter 4 I presented data in support of a model in which Syntaxin 4 interacts with VAMP2 (in the absence of SNAP23 and/or Munc18c) and suggested this interaction is inhibitory to SNARE complex formation. PLA studies presented in chapter 3 argued for the existence of two functionally distinct pools of Syntaxin 4, one responsible for the delivery of GLUT4 to the cell surface in the absence of insulin (i.e. basal conditions), the other in response to insulin. In the model that I proposed in chapter 3, the Syntaxin 4 that is involved in insulin-stimulated delivery of GLUT4 to the cell surface is that found in association with VAMP2 and Munc18c (but not SNAP23 and/or Munc18c) under basal conditions. In this chapter I have used *in vitro* approaches to test the hypothesis that the tyrosine phosphorylation of Munc18c on residue 521 facilitates Syntaxin 4/SNAP23/VAMP2 SNARE complex formation by releasing the inhibitory interaction between Syntaxin 4 and VAMP2.

To this end, I produced recombinant versions of Syntaxin 4, SNAP23 and VAMP2 as well as Munc18c (wild-type and phospho-mimetic; Y521E) and characterised their abilities to form complexes under the various conditions described.

5.3 Results

5.3.1 Production and purification of Wild-Type and Phosphomimetic Munc18c

To investigate the effects of Munc18c phosphorylation on Tyr521 in response to insulin, I took advantage of published studies that have characterized the phosphomimetic mutant (Y521E) (Aran et al., 2011; Jewell et al., 2011). It has been shown that this mutant rescues the defective GLUT4 trafficking phenotype of adipocytes in which endogenous Munc18c has been knocked down, as well as its wild-type counterpart whereas the equivalent phosphoresistant mutant (Y521A) does not (Jewell et al., 2011). Furthermore, introduction of this mutation abrogates binding of Munc18c *in vitro* (Aran et al., 2011), in support of

the above hypothesis. Three different versions of Munc18c were produced here; a wild-type version harbouring a His-tag at its C-terminus, a wild-type version harbouring a His-tag at its N-terminus and an N-terminally His-tagged phosphomimetic (Y521E) mutant version (Aran et al., 2011). Plasmids encoding these were transformed into the *E. coli* strain BL21, and expression of the proteins was induced by addition of IPTG (sections 2.3.1 and 2.3.2). The His-tagged proteins were then purified using Ni-Agarose beads, and eluted using imidazole buffer (section 2.3.4). Figure 5-1 documents various stages of the purification process of all 3 proteins (Figure 5-1 A-C). In each case a major component of the eluate was of the predicted molecular weight for Munc18c (~68kD), but due to high level of other proteins in each elution sample (as evidenced by the multiple bands) the identity of this species (indicated in Figure 5-1) was further investigated by immunoblot analysis using antibodies against Munc18c. The empty vector pET28b was also transformed into BL21 cells, and the resultant transformants were used as a negative control for the Ni-Agarose purifications shown in Figure 5-1 D. Lysate prepared from 3T3-L1 adipocytes was included in the immunoblot analysis as a positive control for the antibody used. Figure 5-1 E demonstrates that each of the 3 versions of Munc18c have been successfully produced in, and purified from, *E. coli* as an anti-Munc18c immunoreactive band of the predicted molecular weight that is not produced by cells containing empty vector alone.

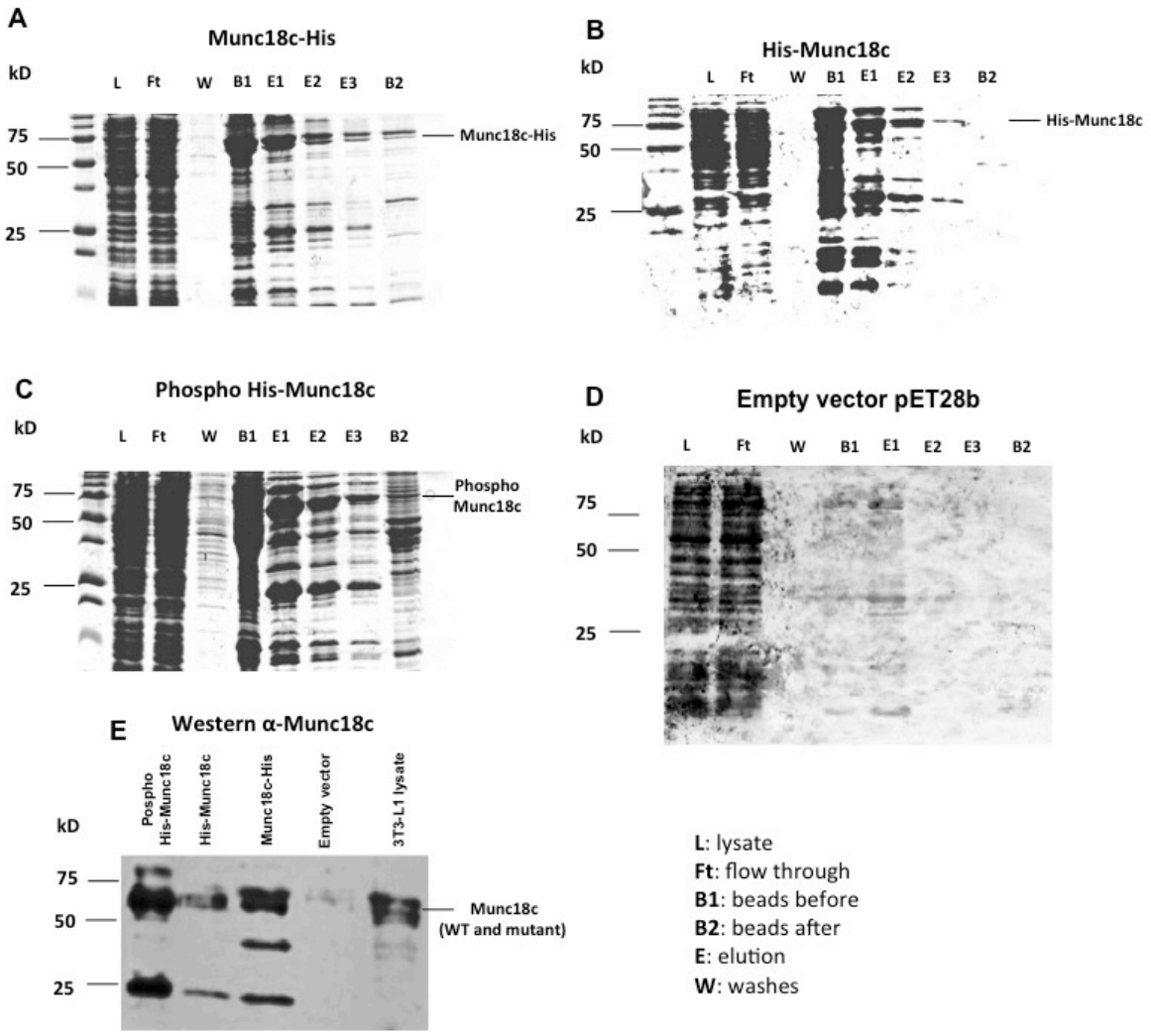

Figure 5-1: Munc18c wild-type and mutant proteins purification.

Appropriate constructs (Table 2.5) were used to produce C-terminally (A), N-terminally (B) His-tagged wild-type Munc18c and N-terminally His-tagged Munc18c (Y521E) phosphomimetic mutant (C). This was achieved by transforming the constructs into BL21 cells and inducing protein production in 10 L cultures with IPTG prior to Ni-affinity chromatography to isolate His-tagged proteins as outlined in methods (sections 2.3.1, 2.3.2 and 2.3.4). Transformants harbouring the empty vector pET28b were used as a negative control (D). Purity of the proteins was analyzed at various stages by SDS-PAGE on a 15% agarose gel (10 µl loading) followed by Commassie staining. Soluble protein (Lysate samples) was bound to Ni-Agarose beads as described (section 2.3.4). The protein fractions not bound and bound to the column (Flow through and beads before samples respectively) are shown. After multiple washes (washes samples represent the first wash) of the beads proteins were eluted using the appropriate buffer (section 2.3.4) 3 times successively (Elution 1-3 samples). The remaining protein on the beads after the elution is shown (Beads after). (E): The identity of the eluted and dialysed proteins was confirmed by immunoblot analysis using antibody against Munc18c. Transformants of the empty vector pET28b and lysates prepared from 3T3-L1 cells (section 2.6.6) were used as negative and positive control respectively (5µl loading). Positions of molecular weight markers are indicated.

5.3.2 Characterisation of bacterially-produced Munc18c

For these studies, it was important to assess whether the Munc18c produced in bacteria would function in the same way(s) as the endogenous SM protein in insulin-sensitive cells. Interaction of Munc18c with Syntaxin 4 has been well characterised (Aran et al., 2009; Hu et al., 2003). This interaction was therefore used as a measure of functionality of the purified His-tagged wild-type Munc18c constructs. For this purpose, purified Sx4-GST (section 4.3.1) was immobilised on glutathione-Sepharose and incubated with a molar excess of either N- or C-terminally His-tagged Munc18c (section 5.3.1). Following extensive washing, SDS-PAGE and immunoblot analysis with antibodies against Munc18c was used to assess the binding of the Munc18c constructs. Figure 5-2 A demonstrates that both the N- and C-terminally His tagged Munc18c proteins bind to Sx4-GST, but not to GST alone or Tlg2-GST (Tlg2 is a yeast syntaxin) that were also immobilized on glutathione-Sepharose and included in this analysis to control for non-specific binding. The reciprocal experiment was also performed by incubating His-tagged Munc18c (either N- or C-terminally tagged) immobilised on Ni-Agarose beads with molar excess Syntaxin 4. For this experiment the cytosolic domain of the syntaxin alone was used by taking advantage of a thrombin-cleavage site between the GST- and Syntaxin 4 derived sequences in the recombinant protein (Figure 4-4). Binding of Syntaxin 4 to the immobilised Munc18c proteins was assessed as above, but this time using an antibody that specifically recognises Syntaxin 4. Figure 5-2 B demonstrates that both the N- and C-terminally tagged versions of wild-type Munc18c bind the cytosolic domain of Syntaxin 4 in a time-dependent manner. Specificity in this instance is evidenced from the observation that no significant binding of cleaved Sx4 to empty beads was observed. The data presented in Figure 5-2 indicate that the two versions (N- and C-terminally His tagged) of wild-type Munc18c expressed in, and purified from *E. coli* are folded in such a manner to bind the cytosolic domain of Syntaxin 4 in a specific manner.

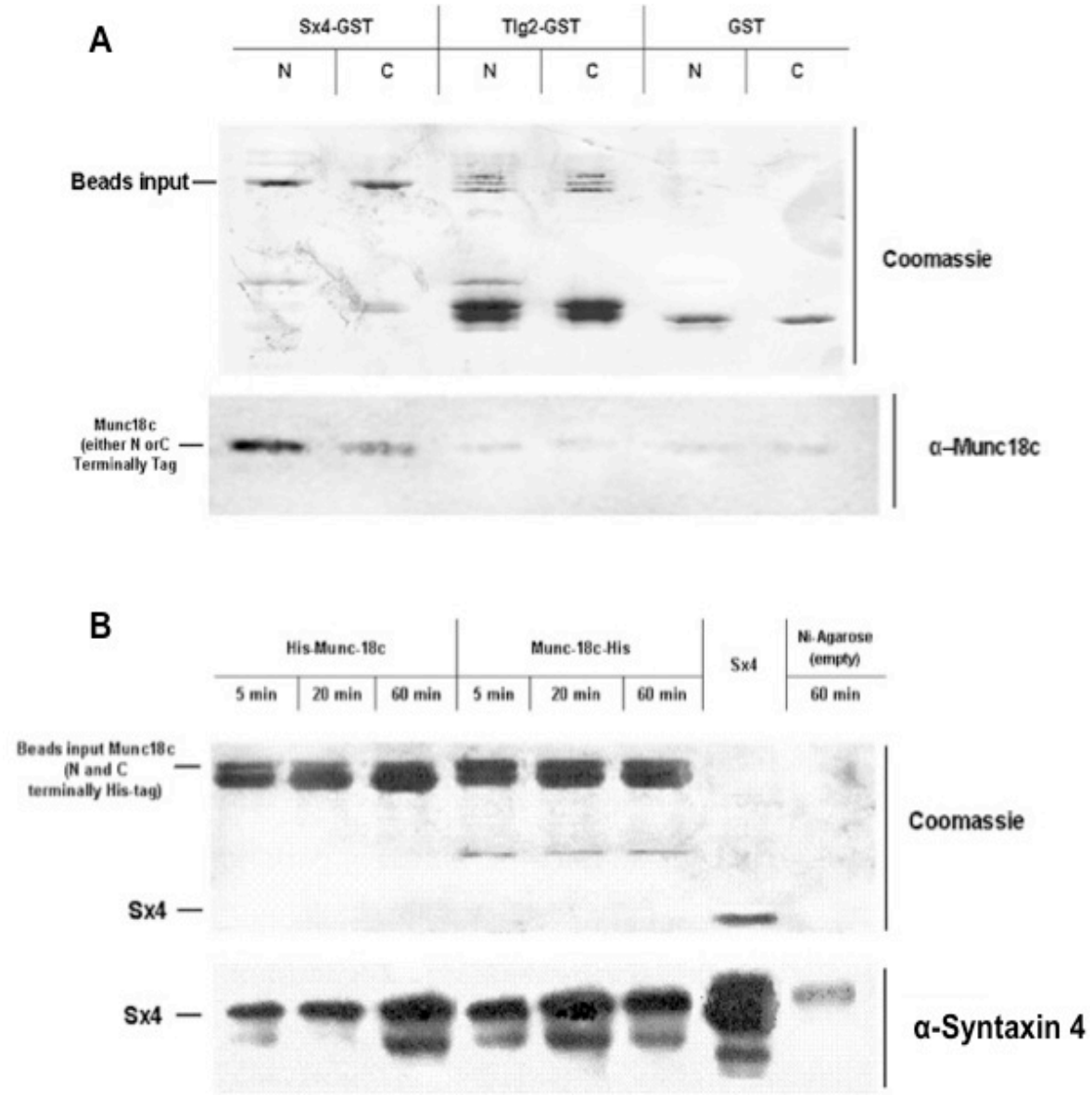

Figure 5-2: Analysis of interaction between N- and C-terminally His-tagged Munc18c and the cytosolic domain of Syntaxin 4

(A) 10 µg of Sx4-GST, Tlg2-GST and GST bound to glutathione-Sepharose beads (10 µl bed volume) were incubated in 1ml PBS (as described in section 2.4) containing either N- or C-terminally His-tagged Munc18c in ~10x molar excess (N and C respectively). Following incubation on a rotating wheel for two hours at 4˚C the beads were washed extensively using PBS prior to final resuspension in 50µl 2xLSB and heating to 95˚C for 5 minutes. Eluted proteins were subject to SDS-PAGE through a 15% separating gel (10 µl loading) and were visualized by Coomassie staining (to assess levels of input proteins immobilized on beads; upper panel) or immunoblot analysis using α-Munc18c antibody (lower panel). (B): 100µg of either N-terminally or C-terminally His-tagged Munc18c bound to Ni-Agarose beads (10µl bed volume) were incubated in 1ml PBS (as described in section 2.4) for the indicated times containing the cytosolic domain of Syntaxin 4 in ~10x molar excess. Following incubation on a rotating wheel at 4˚C the beads were washed extensively using the appropriate buffer (section 2.3.4) prior to final resuspension in 50µl 2xLSB and heating to 95˚C for 5 minutes. Eluted proteins were subject to SDS-PAGE using a 15% separating gel (10 µl loading) and were visualized by Coomassie staining (protein input loading control-upper panel) or immunoblot analysis using an α-Synatxin 4 antibody (lower panel)

5.3.3 Phosphomimetic His-Munc18c (Y521E) displays reduced interaction with VAMP2 *in vitro* compared to its wild-type counterpart

In common with other SM proteins (Carpp et al., 2006; Peng and Gallwitz, 2004), Munc18c binds directly to its cognate v-SNARE VAMP2 *in vitro* (Brandie et al., 2008); an interaction that is abrogated upon Munc18c phosphorylation at tyrosine 521 residue by the insulin receptor (Aran et al., 2011). This observation was used to assess the integrity of the His-tagged phosphomimetic Munc18c mutant (Y521E) whose purification is documented in section 5.3.1. For this purpose a pull-down assay was performed comparing the abilities of N-terminally His-tagged wild-type and phosphomimetic (Y521E) Munc18c to bind VAMP2 *in vitro*. Both Munc18c species were immobilized on Ni beads and their ability to bind the cytosolic domain of VAMP2 assessed as previously described (Aran et al., 2011). Figure 5-3 indicates that the phosphomimetic Munc18c binds less efficiently to VAMP2's cytosolic domain compared to wild-type Munc18c, providing evidence that the mutant used in these studies displays the same characteristics as preparations made from the same construct that were used to gain insight into the consequences of tyrosine phosphorylation on residue 521 (Aran et al., 2011).

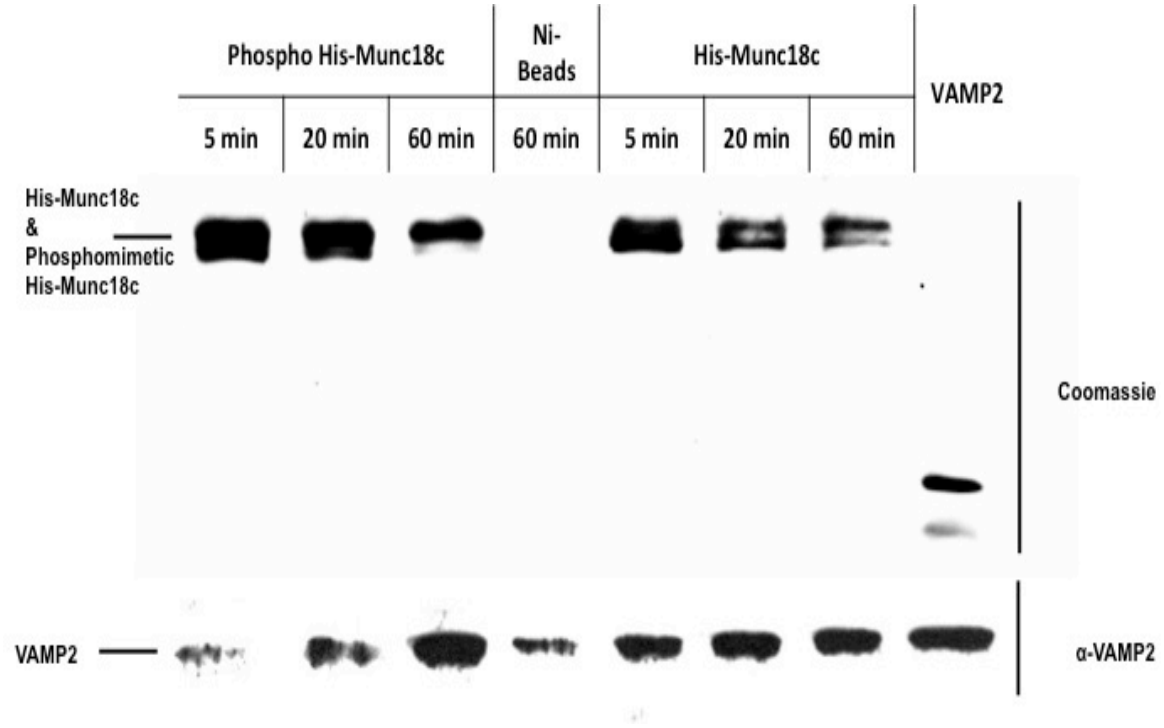

Figure 5-3:Phosphomimetic His-Munc18c (Y521E) interacts less well with the cytosolic domain of VAMP2 *in vitro* than does its wild-type counterpart.

100 µg of either N-terminally Munc18c or N-terminally Munc18c Y521E phosphomimetic mutant His-tagged bound to Ni-Agarose beads (10µl bed volume) and empty Ni-Agarose beads (negative control) were incubated in 1ml PBS (as described in section 2.4) containing the cytosolic domain of VAMP2 in ~10x molar excess for the indicated times on a rotating wheel at 4˚C, after which the beads were washed thoroughly using the appropriate buffer (section 2.3.4) prior to final resuspension in 50µl 2xLSB and heating to 95˚C for 5 minutes. Eluted proteins as well as an aliquot of the VAMP2 protein sample (positive control) were subject to SDS-PAGE through a 15% separating gel and visualized by Coomassie staining (protein input loading control-upper panel) (10 µl loading) or immunoblot analysis using α-VAMP2 antibody (5 µl loading) (lower panel)

5.3.4 Neither Munc18c nor the phopshomimetic Munc18c (Y521E) mutant bind SNAP23 *in vitro*

While it is clear that Munc18c interacts with both its cognate syntaxin and its v-SNARE (Syntaxin 4 and VAMP2) (Aran et al., 2009; Brandie et al., 2008), no evidence exists for a direct interaction between Munc18c and the third member of the Syntaxin 4 SNARE complex, SNAP23. Indeed, no published evidence exists for a direct interaction between any SM protein and a SNAP23/25 homologue. For the interpretation of the PLA data presented in chapter 3 it was important to ascertain that neither wild-type, nor the phosphomimetic Munc18c(Y521E) mutant binds SNAP23 in the absence of the other SNARE complex proteins. In order to check this thoroughly, an *in vitro* pull-down assay was performed. Both His-Munc18c and Phosphomimetic (Y521E) His-Munc18c were immobilised on Ni-

Agarose beads *via* their His-tags and incubated with a molar excess of recombinant SNAP23. The recombinant SNAP23 was prepared from a GST-SNAP23 fusion expressed in, and purified from, BL21 *E. coli* cells (sections 2.3.1, 2.3.2 and 2.3.5) and subsequent cleavage of the GST-tag using thrombin (section 2.3.7) (Figure 5-4).

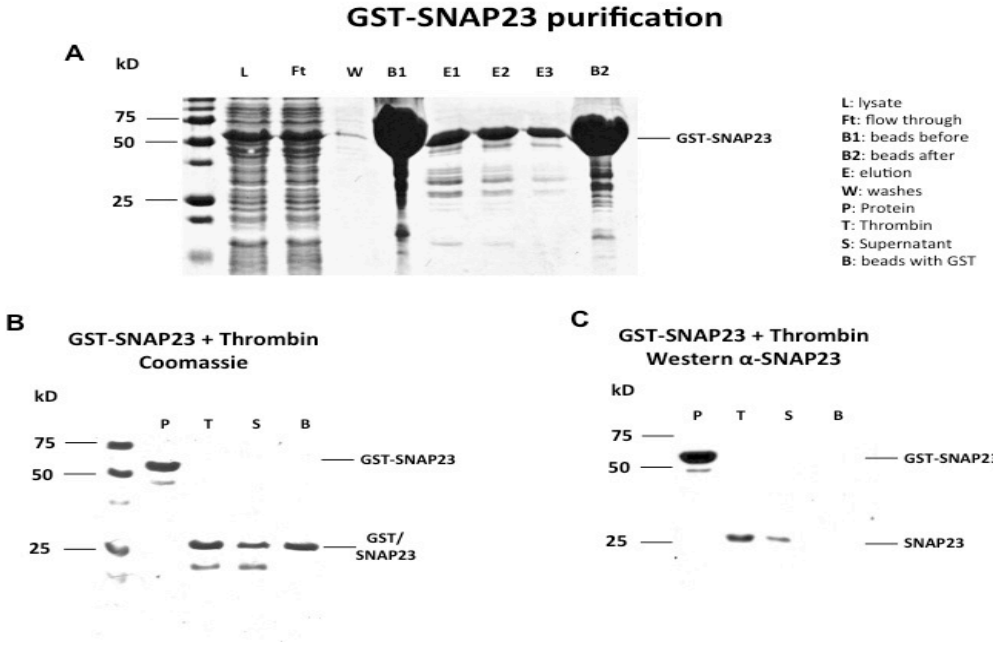

Figure 5-4: Purification and GST moiety cleavage of bacterially-expressed GST-SNAP23

(A): Plasmid pET41a: GST-SNAP23 was used to recombinantly produce N-terminally GST-tagged SNAP23. This was achieved by transforming the plasmid into BL21 cells and inducing protein production with IPTG in 6L of culture as outlined in methods (sections 2.3.1 and 2.3.2). Glutathione-Sepharose beads were then used to purify the GST-tagged protein (section 2.3.5). Purity of the protein was analyzed at various stages by SDS-PAGE on a 15% agarose gel (10 µl loading) followed by Commassie staining. Soluble protein (lysate samples) was bound to glutathione-Sepharose beads as described (section 2.3.5). The protein amounts not bound and bound to the column (flow through and beads before samples) are shown. After extensive washes of the beads using PBS (washes sample represents the first wash) proteins were eluted using the appropriate buffer (section 2.3.5) *via* 3 successive elutions (elution 1-3 samples). The remaining protein on the beads after the elution is shown (Beads after samples). Circled bands correspond to GST-SNAP23 eluted protein. (B): Dialysed GST-SNAP23 protein (p samples) was treated with thrombin as described in section 2.3.7 (thrombin samples). After the termination of the reaction cleavage products were incubated with the appropriate volume of glutathione-Sepharose beads as outlined in methods (section 2.3.7). Unbound protein (supernatant samples) and bound protein to the beads (beads with GST samples) were separated by centrifugation. All prepared samples were heated up to 95°C for 5 minutes after the addition of equal volume of 2xLSB. Samples were subject to SDS-PAGE through a 15% gel followed by either Coomassie staining (10 µl loading) (left panel) or immunodetetion analysis (5 µl loading) using antibody against SNAP23 (C). The single band of a molecular weight approximately 25kDa in the supernatant samples corresponds to cleaved SNAP23. Positions of molecular weight markers are indicated.

Following extensive washing material bound to beads carrying wild-type or phosphomimetic (Y521E) Munc18c, samples prepared were subject to SDS-PAGE and Coomassie blue staining or immunoblot analysis with an antibody against SNAP23. Figure 5-5 demonstrates that is no interaction was detected between SNAP23 and either of the Munc18c species. It is important to note that while it is possible that the lack of interaction between the Munc18c proteins and SNAP23 is due to some aberrant property of the bacterially produced SNAP23 used here, evidence to argue against this comes from the observation that the same SNAP23 is capable of forming SNARE complexes (Figure 4-2) which function in membrane fusion (Brandie et al., 2008).

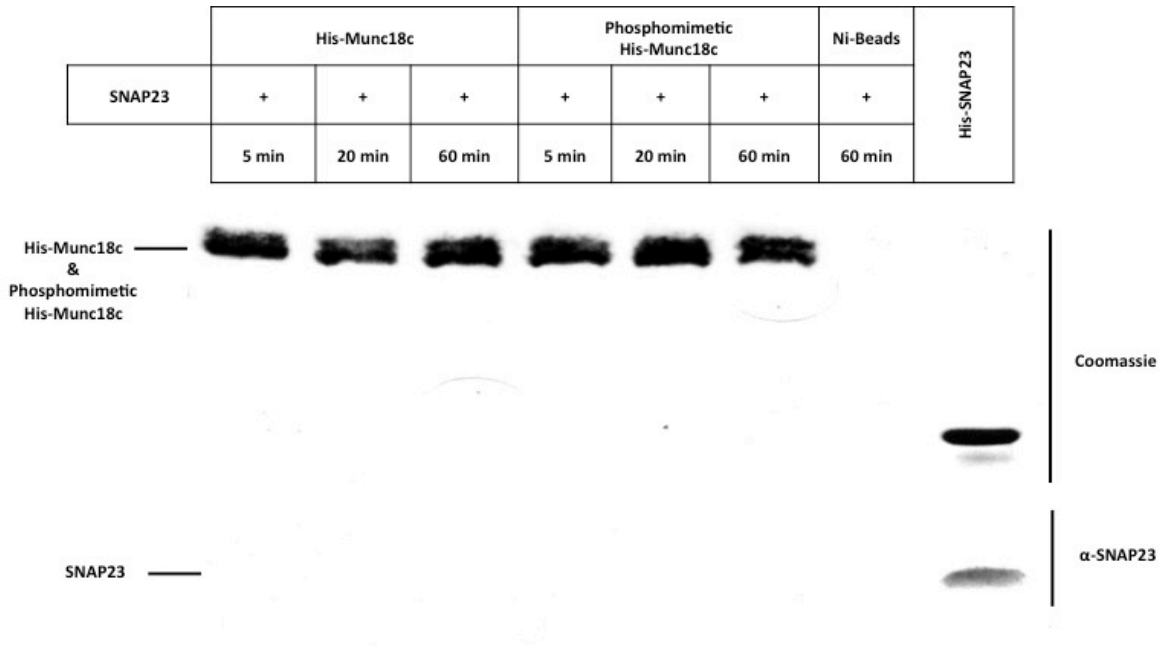

Figure 5-5: Neither His-Munc18c nor phosphomimetic His- Munc18c interact with SNAP-23 *in vitro*

10µg of either N-terminally wild-type or N-terminally phosphomimetic (Y521E) mutant His-tagged Munc18c bound to Ni-Agarose beads (10µl bed volume) and empty Ni-Agarose beads (negative control) were incubated in 1ml PBS (as described in section 2.4) containing the cytosolic domain of SNAP23 in ~10x molar excess. Following incubation for the indicated times on a rotating wheel at 4˚C the beads were washed extensively using the appropriate buffer (section 2.3.4) prior to final resuspension in 50µl 2xLSB and heating to 95˚C for 5 minutes. Eluted proteins as well as an aliquot of the SNAP23 were subject to SDS-PAGE through a 15% separating gel and then visualized by Coomassie staining (protein input loading control-upper panel) (10 µl loading) or analyzed by immunoblotting using α-SNAP23 antibody (5 µl loading) (lower panel)

5.3.5 Pull-down assays from adipocyte lysates using Syntaxin 4-GST and His-VAMP2

Co-immmunoprecipitation analyses revealed a reduction in interactions between Munc18c and Syntaxin 4 in response to glucose-stimulation of MIN16 beta cells (Jewell et al., 2008). To investigate whether insulin-stimulation of adipocytes has a similar effect on Munc18c/Syntaxin 4 interactions, a pull-down approach was undertaken from lysates of 3T3-L1 adipocyte cells either treated with insulin or not (basal cells). Initially both C-terminally GST-tagged Syntaxin 4 (Sx4-GST) and GST (as negative control) bound to glutathione-Sepharose were incubated with lysates prepared from adipocytes (as described in section 2.6.6), that had been treated with 100 nM of insulin for the indicated times or not. Following incubation at 4^{o}C for two hours, beads were washed extensively and bound material subject to SDS-PAGE followed by commassie staining and immonoblot analysis using an antibody against Munc18c. Figure 5-6 demonstrates that considerably less Munc18c is pulled down by Sx4-GST from a lysate that has been treated with insulin for 5 minutes compared to the amount that is pulled down from the lysate of non-stimulated (basal) cells. The amount of Munc18c pulled down by Sx4-GST increases the longer cells are treated with insulin, up to the basal level after 20 minutes. Taken in combination with the observation that insulin triggers Munc18c phosphorylation (Aran et al., 2011; Jewell et al., 2011) these data support the notion that insulin stimulated phosphorylation of Munc18c abrogates binding to Syntaxin 4 (Jewell et al., 2008; Oh and Thurmond, 2006). The effect of insulin on Munc18c/VAMP2 interactions was investigated using the same approach. Both His-VAMP2 and Snc2-PrA (a yeast v-SNARE protein to which Munc18c does not bind (Carpp et al., 2006), used here as a negative control) recombinant proteins bound to Ni-Agarose and IgG-Sepharose beads respectively were incubated with adipocyte lysates prepared from cells treated with insulin for the indicated times, or not, as above. Immunoblot analysis of this approach using antibody against Munc18c revealed that insulin-stimulation initially reduces binding between His-VAMP2 and Munc18c, but this is progressively restored, 20 min after the addition of insulin to the initial levels observed under basal conditions. No interaction between Snc2-PrA and Munc18c was detected (Figure 5-7). This is consistent with *in vitro* data that indicate a disruption of VAMP2/Munc18c interaction as a result of Munc18c phosphorylation triggered by insulin (Aran et al., 2011).

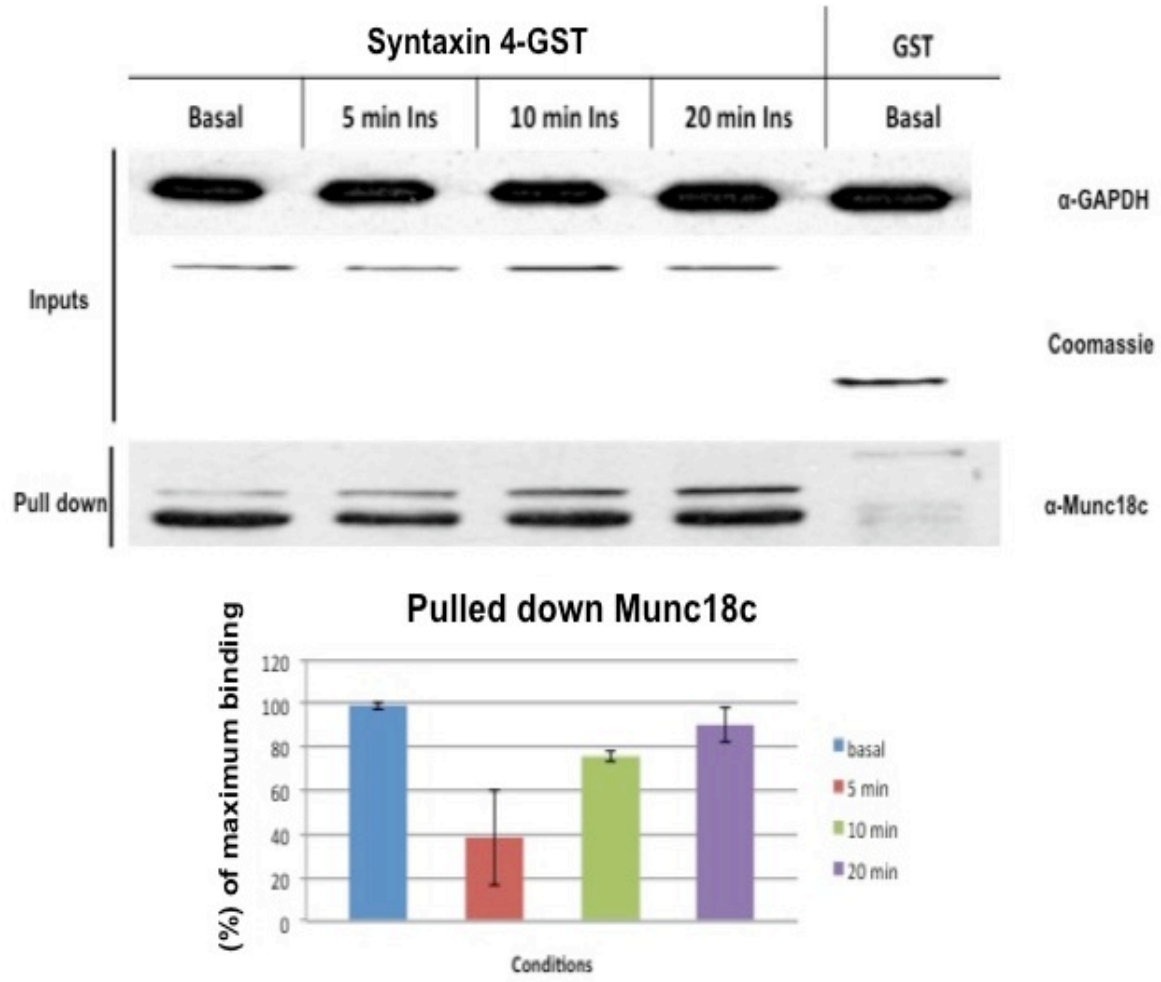

Figure 5-6: Influence of insulin-treatment on pull down of Munc18c by Syntaxin 4-GST from adipocyte lysates

10µg of either C-terminally GST-tagged Syntaxin 4 (Sx4-GST) or GST (negative control) bound to Glutathione-Sepharose beads (10µl bed volume) were incubated with 3T3L1 adipocyte lysates prepared from cells that either have been treated with 100nM of insulin for the indicated times or not as outlined in methods (sections 2.6.5 and 2.6.6). Lysates were subject to immunoblot analysis using α-GAPDH antibody to control for equal protein input (upper panel) (20µl loading). Following incubation on a rotating wheel at 4˚C for two hours beads were washed extensively using adipocytes lysis buffer prior to final resuspension in 50µl 2xLSB and heating to 60˚C for 10 minutes. Eluted proteins were subject to SDS-PAGE through a 15% separating gel and visualised by Coomassie staining (beads protein input loading control-middle panel) (10 µl loading) or immuneblot analysis using α-Munc18c antibody (5 µl loading) (lower panel). The bands were analysed by densitometry using image j software and normalised to both beads bound and basal adipocyte lysate protein inputs (histogram). Error bars represent standard deviation of three independent experiments' mean value (appendix Figure 8-54).

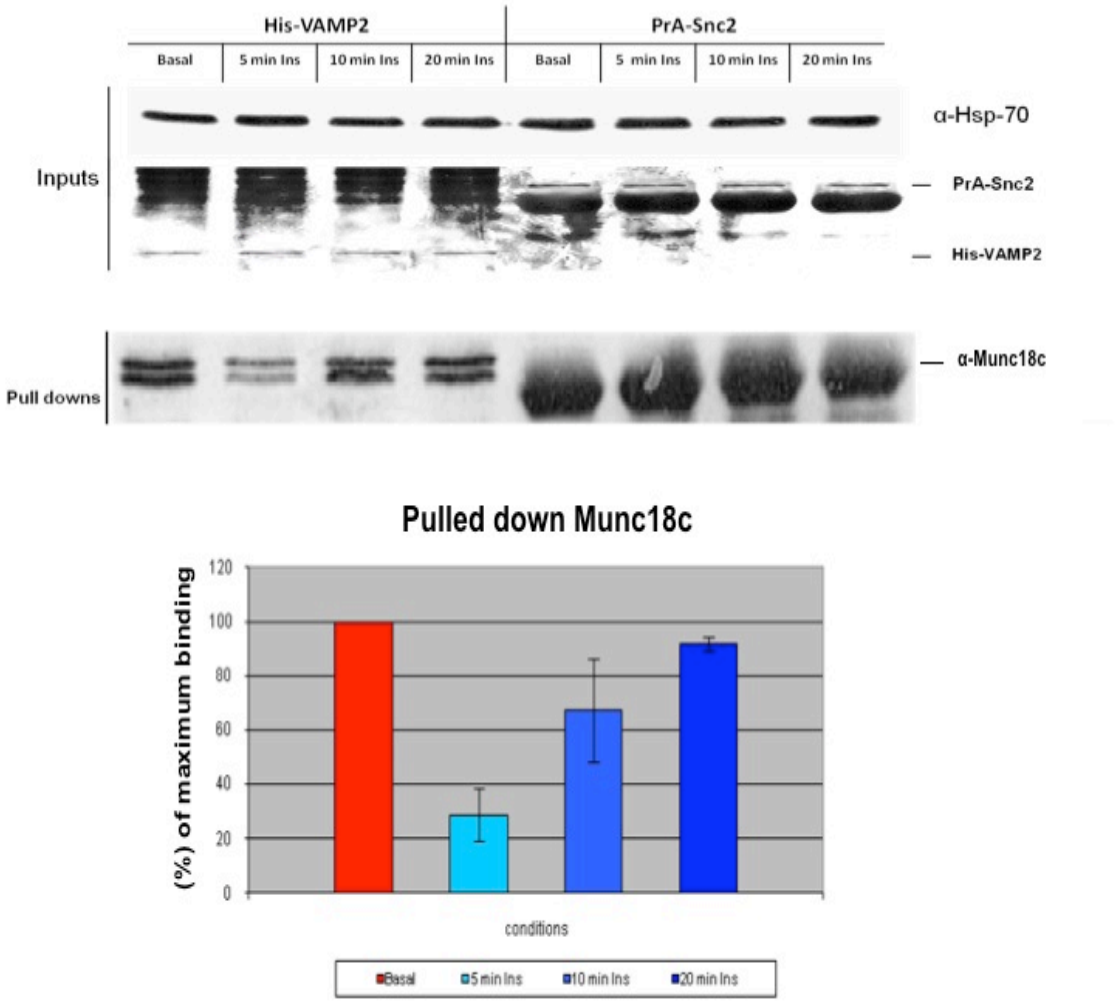

Figure 5-7: His-VAMP2 pulls down Munc18c from Adipocyte lysates

10µg of either N-terminally his-tagged VAMP2 (His-VAMP2) or C-terminally PrA-tagged Snc2 (Snc2-PrA) (negative control) bound to Ni-Agarose and IgG-Sepharose beads corespondingly (5 and 50µl bed volume respectively) were incubated with 3T3L1 adipocyte lysates prepared from cells that either have been treated with 100nM of insulin for the indicated times or not as outlined in methods (sections 2.6.5 and 2.6.6). Lysates were subject to immunoblot analysis using α-Hsp-70 antibody to control for equal protein input (upper panel) (20µl loading). Following incubation on a rotating wheel at 4°C for two hours beads were washed extensively using adipocytes lysis buffer prior to the addition of 50µl 2xLSB and heating to 60°C for 10 minutes. Eluted proteins were subject to SDS-PAGE through a 15% separating gel and were visualized by Coomassie staining (beads protein input loading control-middle panel) (10 µl loading) or immunoblot analysis using α-Munc18c antibody (5 µl loading) (lower panel). The bands were analysed by densitometry using image j software and normalized to both beads bound and basal condition adipocyte lysate protein inputs (histograms). Error bars represent standard deviation of three independent experiments' mean value (appendix Figure 8-56).

5.3.6 Phosphomimetic His-Munc18c (Y521E) facilitates SNARE complex formation *in vitro* in contrast to its wild-type counterpart that has an inhibitory role

The precise role of Munc18c in SNARE-mediated delivery of GLUT4 to the plasma membrane remains elusive. Munc18c has an inhibitory effect on Syntaxin 4/SNAP23/VAMP2-mediated liposome fusion *in vitro* (Brandie et al., 2008). To investigate whether this is a direct effect on SNARE complex assembly rather than on the fusion *per se* I followed SNARE complex assembly assay (section 2.4) in the absence and presence of Munc18c. For this purpose, Sx4-GST immobilised on glutathione-Sepharose beads was pre-incubated with N-terminally His-tagged Munc18c or not. The beads were then washed in assay buffer to remove any Munc18c that had bound non-specifically prior to addition of the other SNARE proteins (SNAP23-His and VAMP2-PrA). Rate of SNARE complex assembly was monitored by taking samples of the assay at various time points, Figure 5-8 shows that, in the absence of His-Munc18c, there is a time-dependent increase in the amount of the SNARE complex formed (shown by increasing band strengths of the α-His_6 western blots at a molecular weight corresponding to the sum of the three SNARE proteins molecular weights ~110kDa). Preincubation of His-Munc18c with Syntaxin 4-GST resulted in a marked reduction in the level and rate of SNARE complex assembly relative to that seen in the absence of His-Munc18c. These data corroborate the *in vitro* liposome fusion studies outlined above and are consistent with a model in which Munc18c inhibits formation of Sx4-containing SNARE complexes (Brandie et al., 2008). It is attractive to speculate that insulin might alleviate this inhibition with a possible mechanism for this being through phosphorylation. The effect of phosphorylation on the observed inhibitory action of Munc18c on Sytaxin 4- SNARE complex assembly was therefore investigated through addition of the phosphomimetic mutant to the SNARE complex assembly assay. For this purpose Sx4-GST was preincubated with phosphomimetic (Y521E) His-Munc18c or not and the effect of this on SNARE complex assembly assessed as described above. Figure 5-9 indicates that, in contrast to its wild-type counterpart (Figure 5-8) His-Munc18c (Y521E) stimulates SNARE complex assembly. Given the abrogation of Syntaxin 4 binding observed upon both tyrosine phosphorylation of Munc18c and the introduction of the Y521E phosphomimetic Munc18c mutation (Aran et al., 2011; Oh and Thurmond, 2006) these data suggest that this effect represents not only a release of

repression exerted by Munc18c but a concomitant stimulation of activity that drives complex formation.

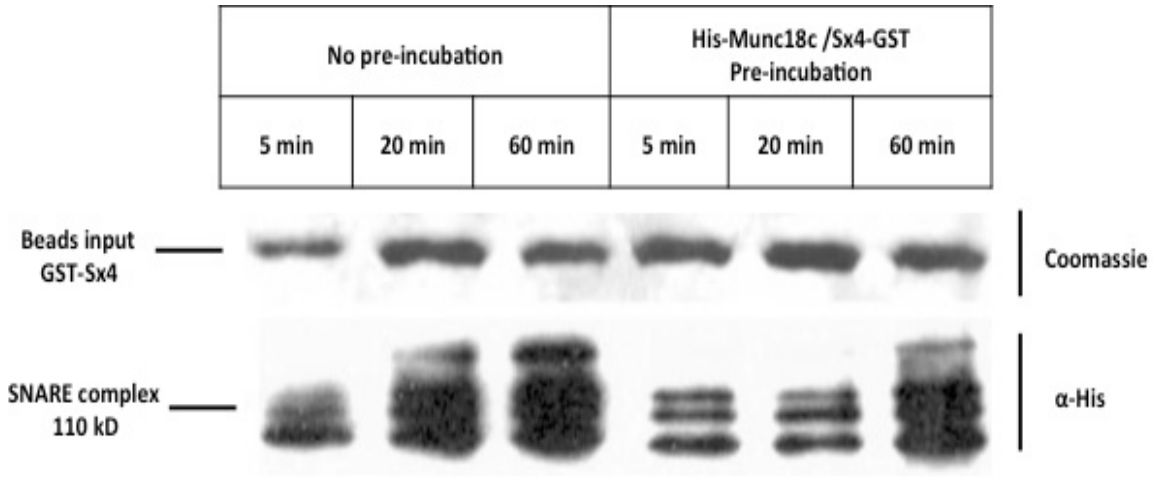

Figure 5-8: Syntaxin 4/ Munc18c interaction inhibits SNARE complex formation

50 µg Sx4-GST, bound to glutathione-Sepharose (10µl bed volume) were incubated in 1ml PBS (as described in section 2.4) containing either N-terminally His-tagged Munc18c in ~10x molar excess or not. Following incubation on a rotating wheel for two hours at 4˚C beads were washed extensively using PBS. After the washes beads were incubated in 1ml PBS (as described in section 2.4) containing N-terminally His-tagged SNAP23 and C-terminally PrA-tagged VAMP2 each in ~10x molar excess. Following incubation for the indicated times on a rotating wheel at 4˚C the beads were washed extensively using PBS prior to final resuspension in 50µl 2xLSB and heating to 95˚C for 5 minutes. Samples were subject to SDS-PAGE using a 15% separating gel (10 µl loading) and were visualised by Coomassie staining (beads protein input loading control-upper panel) or immunoblot analysis using α-His_6 antibody (lower panel). The smear of bands of a molecular weight around 110kDa corresponds to the SDS-resistant ternary SNARE complex made of Sx4-GST/His-SNAP23/VAMP-PrA (Figure 4-2)

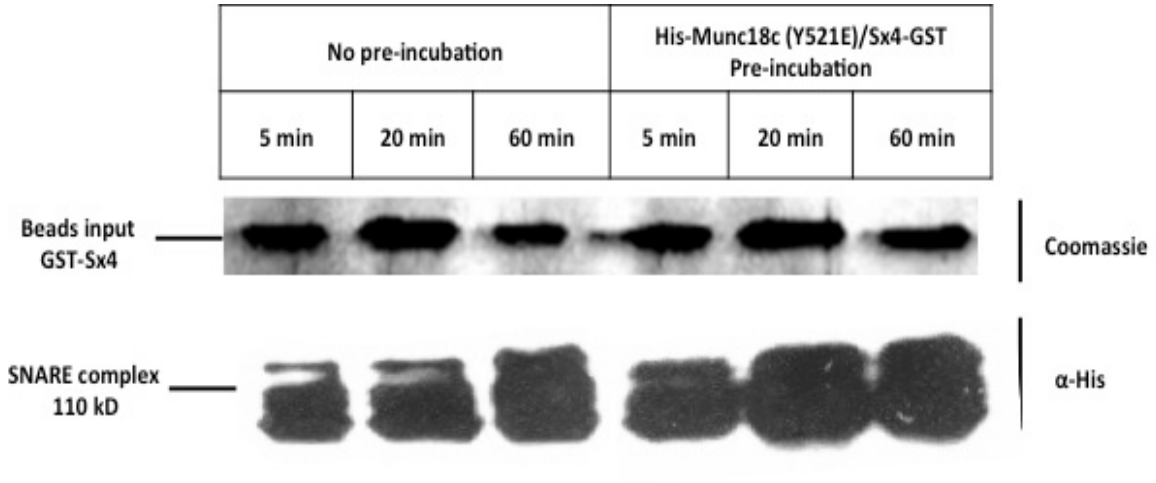

Figure 5-9: Munc18c (Y521E) facilitates the complex formation

50 µg of Sx4-GST, bound to glutathione-Sepharose beads (10µl bed volume) were incubated in 1ml PBS (as described in section 2.4) containing either N-terminally His-tagged Munc18c (Y521E) phosphomimetic mutant in ~10x molar excess or not. Following incubation on a rotating wheel for two hours at 4˚C beads were washed extensively using PBS. After the washes beads were incubated in 1ml PBS (as described in section 2.4) for the indicated times containing N-terminally His-tagged SNAP23 and C-terminally PrA-tagged VAMP2 each in ~10x molar excess. Following incubation on a rotating wheel at 4˚C for the indicated times beads were washed extensively using PBS prior to the addition of 50µl 2xLSB and heating to 95˚C for 5 minutes. Samples were subject to SDS-PAGE using a 15% separating gel (10 µl loading) and were visualised by Coomassie staining (beads protein input loading control-upper panel) or immunoblot analysis using α-His_6 antibody (lower panel). The smear of bands of a molecular weight around 110kDa corresponds to the ternary SNARE complex made of Sx4-GST/His-SNAP23/VAMP-PrA (Figure 4-2)

5.3.7 His-Munc18c (Y521E) phosphomimetic mutant releases the inhibitory effect of Syntaxin 4 and VAMP2 interaction

In chapter 4 I presented data to indicate that a previously uncharacterised interaction between Syntaxin 4 and VAMP2 has an inhibitory effect on SNARE complex rate formation. I also presented PLA results (chapter 3) that support a model in which there are two pools of Syntaxin 4 in adipocytes under basal conditions - with the one being responsible for insulin-stimulated GLUT4 vesicle fusion to the plasma membrane being in association with VAMP2 and Munc18c under basal conditions. Such an inhibitory interaction (Syntaxin 4/VAMP2) would have to be released upon insulin stimulation in order to have externalization of GLUT4, and it is tempting to hypothesise that phosphorylation of Munc18c might be the key factor in that releases. Once again I monitored SNARE complex *assembly in vitro* to test this hypothesis. In this case Sx4-GST bound to glutathione-Sepharose was pre-incubated with VAMP2-PrA in the absence and the presence of either N-terminally His-tagged Munc18c or N-terminally His-

tagged Munc18c (Y521E) phosphomimetic mutant prior to addition of His-SNAP23. Extent of SNARE complex formation was monitored by taking samples of the assay at various time points, with the level of complex assembly in each sample visualised using the α-His_6 antibody as above. Figure 5-10 indicates that the inhibition of SNARE complex formation due to VAMP2-PrA/Sx4-GST interaction is alleviated by the His-Munc18c (Y521E) phosphomimetic mutant, but not its wild-type counterpart. These data support a model in which tyrosine phosphorylation of Munc18c in response to insulin releases an inhibitory effect of the VAMP2/Syntaxin 4 interaction thus increasing the rate of SNARE complex formation and stimulating delivery of GLUT4 to the cell surface.

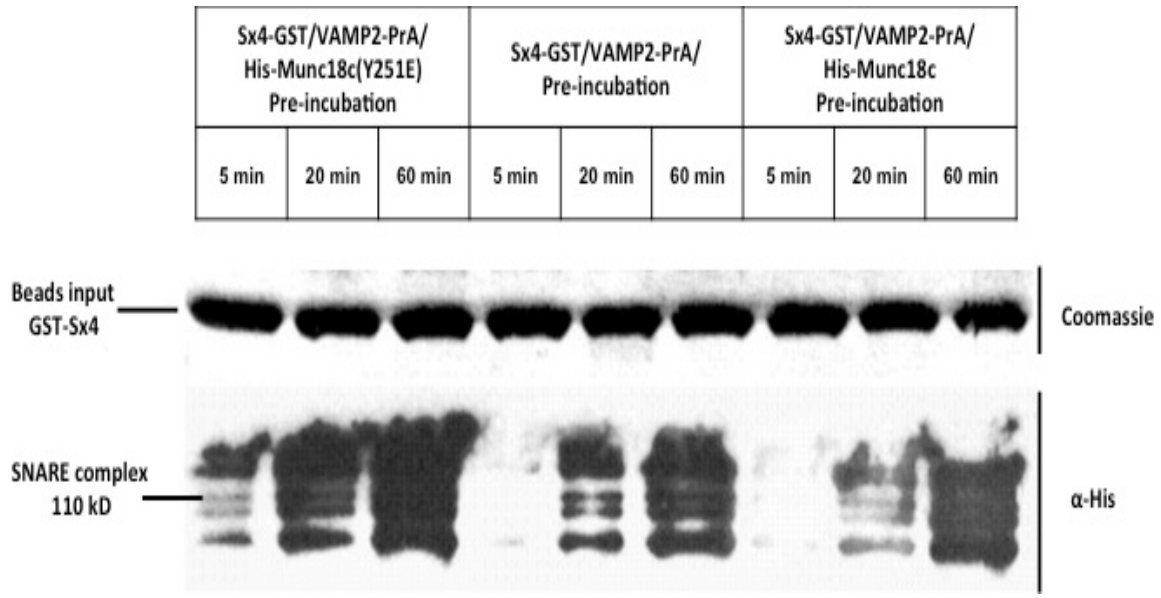

Figure 5-10: Munc18c (Y521E) releases Sx4/VAMP2 inhibitory interaction

50 µg Sx4-GST, bound to glutathione-Sepharose (10µl bed volume) were incubated in 1ml PBS (as described in section 2.4) containing VAMP2-PrA in ~10x molar excess either in absence or in presence of N-terminally His-tagged Munc18c or N-terminally His-tagged Munc18c (Y521E) phosphomimetic mutant in ~10x molar excess. Following incubation on a rotating wheel for two hours at 4°C N-terminally His-tagged SNAP23 was added in ~10x molar excess. After the final incubation on a rotating wheel at 4°C for the indicated times beads were washed extensively using PBS prior to final resuspension in 50µl 2xLSB and heating to 95°C for 5 minutes. Samples were subject to SDS-PAGE using a 15% separating gel (10 µl loading) and visualised by Coomassie staining (beads protein input loading control-upper panel) or immunoblot analysis using α-His_6 antibody (lower panel). The smear of bands of a molecular weight around 110 kDa corresponds to the SDS-resistant ternary SNARE complex made of Sx4-GST/His-SNAP23/VAMP-PrA (Figure 4-2).

5.4 Discussion

Insulin stimulates delivery of GLUT4 to the cell surface from an intracellular store in fat and muscle cells. Fusion of GLUT4-containing vesicles with the plasma membrane is SNARE-dependent and regulated by the SM protein Munc18c (Bryant and Gould, 2011). In this chapter, insulin-induced tyrosine phosphorylation of Munc18c (on residue 521) was investigated as a potential regulatory mechanism by which SNARE complex assembly can be regulated (Aran et al., 2011; Jewell et al., 2008; Jewell et al., 2011). For this study I used a Munc18c mutant (Y521E) that mimics its insulin-induced phosphorylation state (Aran et al., 2011; Jewell et al., 2011). This mutant has a reduced ability to bind both Syntaxin 4 and VAMP2, compared to its wild-type counterpart (Aran et al., 2011)(Figure 5-3). Correlation of these data with that obtained using pull-down assays from lysates prepared from adipocyte cells previously treated with insulin or suggest that phosphorylation of Munc18c upon insulin-stimulation negatively affects its ability to bind Syntaxin 4 and VAMP2. Quite interestingly this effect seems to decline as time passes and the binding ability of Munc18c regarding Syntaxin 4 and VAMP2 is restored after 20 min back to the levels prior to insulin-stimulation (Figure 5-6 and Figure 5-7).

In vitro SNARE complex formation studies presented here demonstrated an inhibitory role for Munc18c (Figure 5-8) consistent with data obtained using liposome fusion assays (Brandie et al., 2008). In contrast, the phosphomimetic mutant facilitates SNARE complex formation (Figure 5-9). This was surprising given that Munc18c phosphorylation abrogates its binding to Syntaxin 4 (Aran et al., 2009) and warrant further investigation since it suggests an additional positive role of Munc18c on SNARE complex assembly upon insulin stimulation.

Further mechanistic insight into how Munc18c phosphorylation might regulate SNARE complex assembly in response to insulin presented here build on the inhibitory interaction of Syntaxin 4 with VAMP2 on ternary SNARE complex formation introduced in chapter 4. This inhibitory interaction must be released in order to have translocation of GLUT4 to the plasma membrane. Phosphorylation of Munc18c (which PLA studies indicate is associated with the Syntaxin 4-VAMP2 pool under basal conditions; chapter 3) emerges as an appealing explanation for how this might be achieved. Use of the

phosphomimetic (Y521E) Munc18c mutant in this study support this contention in that its presence was able to release the inhibitory effect of the Syntaxin 4/VAMP 2 interaction on SNARE complex formation in contrast to wild-type Munc18c (Figure 5-10). Taken together, the findings of this chapter support the notion that phosphorylation of Munc18c on Tyr-521 acts as a regulatory step of GLUT4 vesicle fusion with plasma membrane upon insulin stimulation by regulating SNARE complex assembly.

Chapter 6

Insights into insulin-regulated traffic from Proximity Ligation Assay analyses between SNARE proteins and markers of internal GLUT4 vesicles

6.1 Introduction

6.1.1 Intracellular sequestration of GLUT4 trafficking

Translocation of Glucose transporter 4 (GLUT4) from intracellular storage compartments to the plasma membrane upon insulin stimulation is central to whole body glucose homeostasis and represents a specialised form of regulated membrane traffic (Stockli et al., 2011). The trafficking itinerary followed by GLUT4 during its insulin-dependent translocation to the plasma membrane and its subsequent internalization back into intracellular stores takes GLUT4 through numerous, distinct, membrane-bound compartments including early endosomes, intermediated transport vesicles, recycling endosomes, the *trans*-Golgi network (TGN) and GLUT4 Storage Vesicles (GSVs), which are defined as the specialized intracellular vesicles containing the pool of GLUT4 that translocates to the plasma membrane in response to insulin (Kandror and Pilch, 2011). GSVs are unlikely to be a static population of vesicles due to the dynamic nature of the endosomal system, and instead current working models of GLUT4 traffic under basal conditions suggest that GLUT4 continually traffics in two interconnected cycles. The first moving rapidly between the plasma membrane and recycling endosomes and the second cycling more slowly through recycling endosomes, *trans*-Golgi network and GSVs (Bryant et al., 2002).

6.1.2 Two major intracellular GLUT4 storage compartments

Although intracellular GLUT4 populates a wide variety of membrane-bound compartments, the majority (60-75%) is found in small diameter (~50nm) vesicles and tubules as determined by morphological and biochemical methods (Hashiramoto and James, 2000). Insulin results in movement of GLUT4 out of this pool concomitant with an increase in the amount of GLUT4 at the plasma membrane. Biochemical studies utilizing sucrose gradient centrifugation have revealed that this intracellular store of GLUT4 vesicles is made up of an overlapping mixture of at least two vesicle populations discussed in section 1.4.4, one that contains the protein cellugyrin (cellugyrin-positive) and the other that does not (cellugyrin-negative), but does contain another marker of GSVs, sortilin (Kupriyanova and Kandror, 2000). Cellugyrin-negative vesicles contain five to six times more GLUT4 than cellugyrin-positive vesicles and are likely the

source of GLUT4 that is translocated to cell surface upon insulin stimulation (Kupriyanova et al., 2002). Cellugyrin-positive vesicles on the other hand have been suggested to provide an intracellular location for GLUT4, even in the presence of insulin (Kupriyanova et al., 2002). This model has been formulated by Kandror and colleagues (Kandror and Pilch, 2011), based on evidences discussed in Section 1.4.4 indicating the existence of two independent pools of small GLUT4 containing vesicles: cellugyrin-positive vesicles that retain intracellular localization after insulin-stimulation and may represent the source of GLUT4 that cycles through the cell surface under basal conditions, and cellugyrin-negative/sortilin positive vesicles that respond to insulin and translocate GLUT4 to plasma membrane.

6.1.3 Two functionally distinct pathway deliver GLUT4 to the plasma membrane

The existence of two independent pools of internal GLUT4 vesicles that vary in responsiveness to insulin raises the possibility of the presence of two pathways for delivery of GLUT4 to the plasma membrane. TIRF microscopy studies in adipocytes revealed that under basal conditions GLUT4 delivered to the plasma membrane (*via* cycle-1, Figure 1-13) exists as clusters retained at the fusion site (Stenkula et al., 2010). In contrast, insulin stimulation does not accelerate this basal exocytosis *per se* but does disperse GLUT4 away from the fusion site into the plasma membrane (Stenkula et al., 2010). The possibility that GLUT4 is delivered to the plasma membrane *via* two different pathways under basal and insulin-stimulated conditions is also supported by evidence from studies with transgenic mice overexpressing GLUT4, where the amount of GLUT4 at the plasma membrane under basal conditions is increased by a factor of four in cells overexpressing GLUT4 compared to wild-type adipocytes. The corresponding increase after insulin-stimulation is only by a factor of two (Carvalho et al., 2004). In addition, studies on the role of microtubules in GLUT4 traffic revealed a requirement for basal mobility of GLUT vesicles, but found that they are not essential for GLUT4 translocation after insulin stimulation (Eyster et al., 2006). These, and other, findings supporting the existent of two different mechanisms by which is delivered to the plasma membrane: one being responsible for its delivery under basal conditions, the other upon insulin stimulation.

6.2 Aims of this chapter

In chapter 3 I provided evidence for the existence of two different pools of Syntaxin 4 in adipose cells. Combining this observation with the model discussed above where there are two different internal GLUT4 carrying vesicles; cellugyrin-positive and cellugyrin-free (sortilin positive) that are potentially involved in two functionally distinct pathways of GLUT4 delivery to the cell surface (cellugyrin-positive vesicles being involved in GLUT4 cycling through the cell surface under basal conditions and cellugyrin-free vesicles responsible for its insulin-stimulated plasma membrane delivery -sections 6.1.2 and 6.1.3), it is tempting to speculate that the two pools of Syntaxin 4 are functionally different. In this chapter I used PLA to test the hypothesis that the two separate pools of Syntaxin 4, identified in chapter 3 mediate different pathways from internal vesicles to the cell surface under basal and insulin-stimulated conditions.

6.3 Results

6.3.1 Selection of Primary Antibodies for PLA between Syntaxin 4, SNAP23, VAMP2, Munc18c, cellugyrin and sortilin

As discussed in section 3.3.2 the choice of appropriate primary antibodies is essential for the success of PLA. Antibodies against cellugyrin and sortillin (raised in mouse and rabbit respectively) were purchased in order to perform PLA in combination with the antibodies against the three SNARE proteins (Syntaxin 4, SNAP23 and VAMP2) and the SM protein (Munc18c) described in section 3.3.2 covering all possible pairwise associations between these two markers of internal GLUT4-containing vesicles and the SNARE/SM proteins. In order to check the specificity of these new primary antibodies, immunoblot analysis against adipose cell lysate was performed. Figure 6-1 illustrates that the primary antibodies, against cellugyrin and sortilin used for this study are specific in that they recognise a single band of the appropriate molecular weight (~29 kDa for cellugyrin, ~95kDa for sortilin).

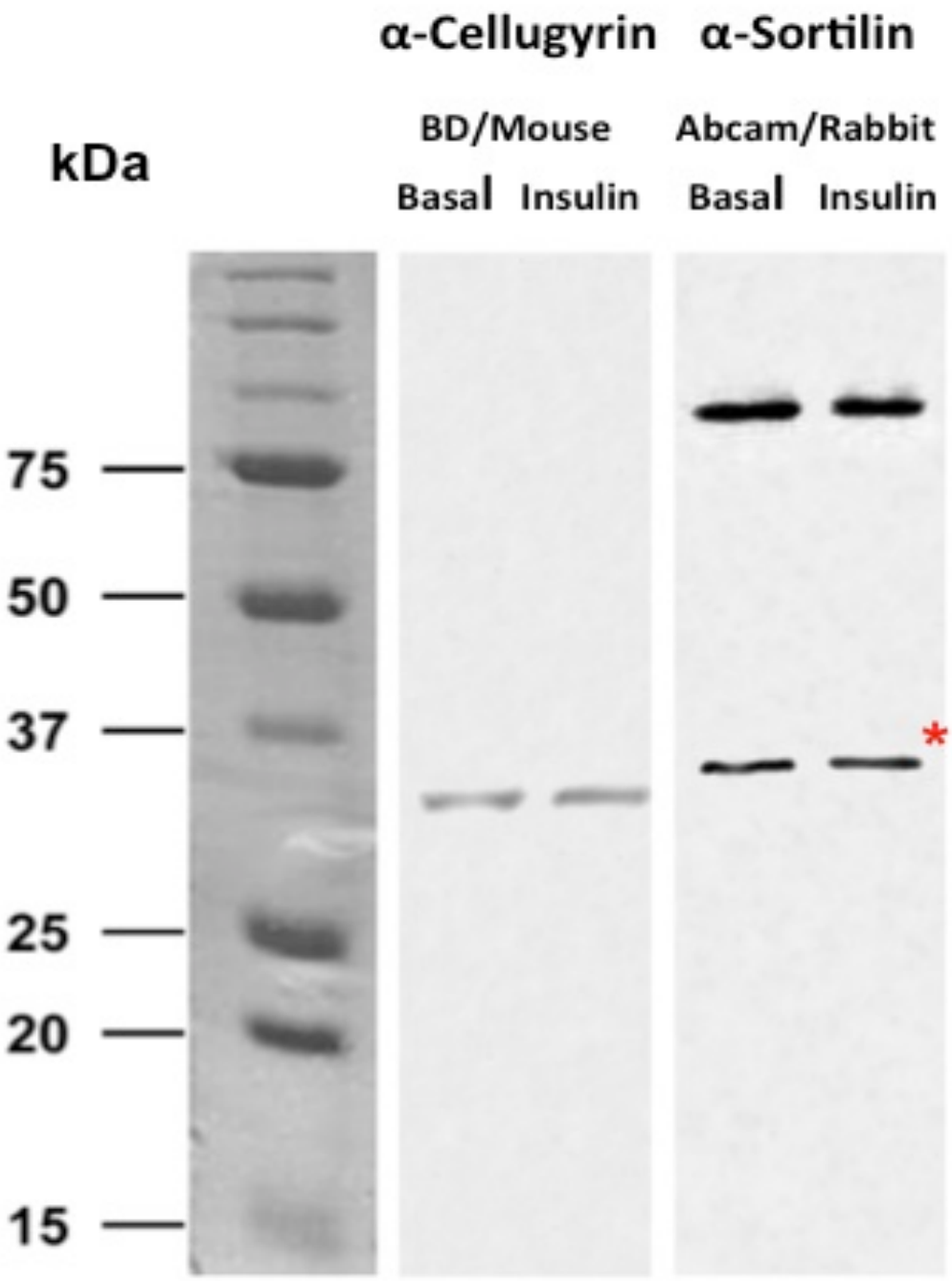

Figure 6-1: Immunoblot analysis characterisation of primary antibodies against cellugyrin and sortilin used for PLA

Cell lysate (~10 mg/ml) prepared from 3T3-L1 adipocytes treated with insulin (100 nM for 30min) (insulin) or not (basal) (section 2.6.6) were subject to SDS-PAGE (15 µl per well) and immunoblot analysis using the commercially available antibodies indicated (for more information consult section 2.1.4). The red asterisk indicates additional detected bands, which possibly correspond to cleavage product of sortilin.

6.3.2 PLA for cellugyrin/sortilin in 3T3-L1 cells

Previous studies discussed above and in section 1.4.4 have concluded that cellugyrin and sortilin populate different vesicle pools in 3T3-L1 adipocytes (Kandror and Pilch, 2011). Here, I set out to use PLA to investigate this *in situ*. This approach is feasible as PLA is able to visualize any pair of proteins in proximity of less than 10 nm and is not restricted to visualisation of interactions. Given that fusogenic GLUT4 vesicles have a diameter of around 50nm (Bryant et al., 2002), it seemed reasonable to expect a positive signal from two proteins present in the same vesicle (an assertion that is backed up by controls later in this chapter – Figure 6-3 Figure 6-4 and Figure 6-6. No signal was obtained from PLA performed using primary antibodies against cellugyrin and sortilin both under basal conditions and after insulin-stimulation in both fibroblasts and adipocytes (Figure 6-2) consistent previous findings indicating that cellugyrin and sortilin are not located in the same vesicle but rather populate different pools of GLUT4 carrying vesicles (section 6.1.2).

While the data presented in Figure 6-2 are consistent with the idea that cellugyrin and sortilin populate different pools of intracellular, GLUT4-carrying vesicles, they can not exclude the possibility that they are in the same vesicle, but still separated by a distance of greater than 10 nm (the theoretical limit of resolution of PLA used here).

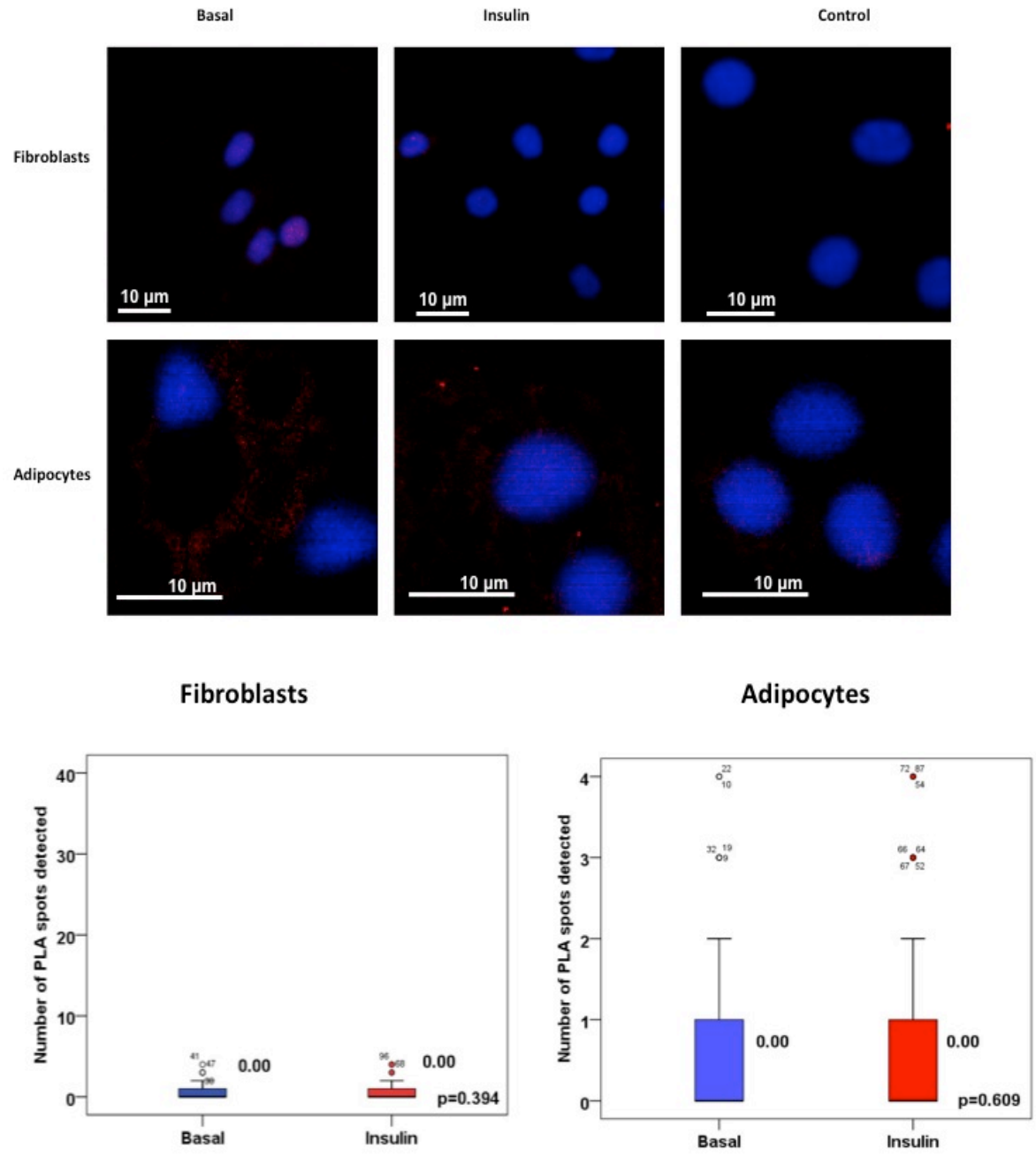

Figure 6-2: cellugyrin/sortilin PLA

PLA using antibodies against sortilin and cellugyrin was performed in 3T3-L1 fibroblasts and adipocytes treated with insulin (100 nM for 5 min) or not (basal) (section 2.6.5). Red spots correspond to a positive PLA signal. Blue: DAPI stained nuclei. The control shown represents the omission of the primary antibody against cellugyrin. Statistical analysis of PLA results was performed using blobfinder and SPSS software (Mann-Whitney U test) (see appendix Figure 8-19 Figure 8-20 Figure 8-21). The numbers in the boxes illustrate the median value (30 to 95 cells per experiment). Images are representative of three independent experiments.

6.3.3 PLA for cellugyrin/VAMP2 and sortilin/VAMP2 in 3T3-L1 cells

In order to validate the notion that PLA can be used to detect proteins that are present in the same internal GLUT4-containing vesicles, I performed PLA with both cellugyrin and sortilin in combination with VAMP2, which is predicted to be on both cellugyrin-positive and cellugyring-negative vesicles (Jedrychowski et al., 2010). Positive PLA signals were obtained in both cases (Figure 6-3 and Figure 6-4). Statistical analyses of PLAs performed with cellugyrin/VAMP2 (Figure 6-3) and sortilin/VAMP2 (Figure 6-4) in both fibroblasts and adipocytes in the presence and absence of insulin revealed a significant decrease in the number of positive dots for the former, concomitant with a significant increase in the number of positive dots for the latter upon insulin-stimulation. It is very appealing to speculate that these changes may be interrelated and reflect insulin-regulated traffic between cellugyrin-positive and cellugyrin-negative (sortilin-positive) vesicles (discussed in section 6.4 below).

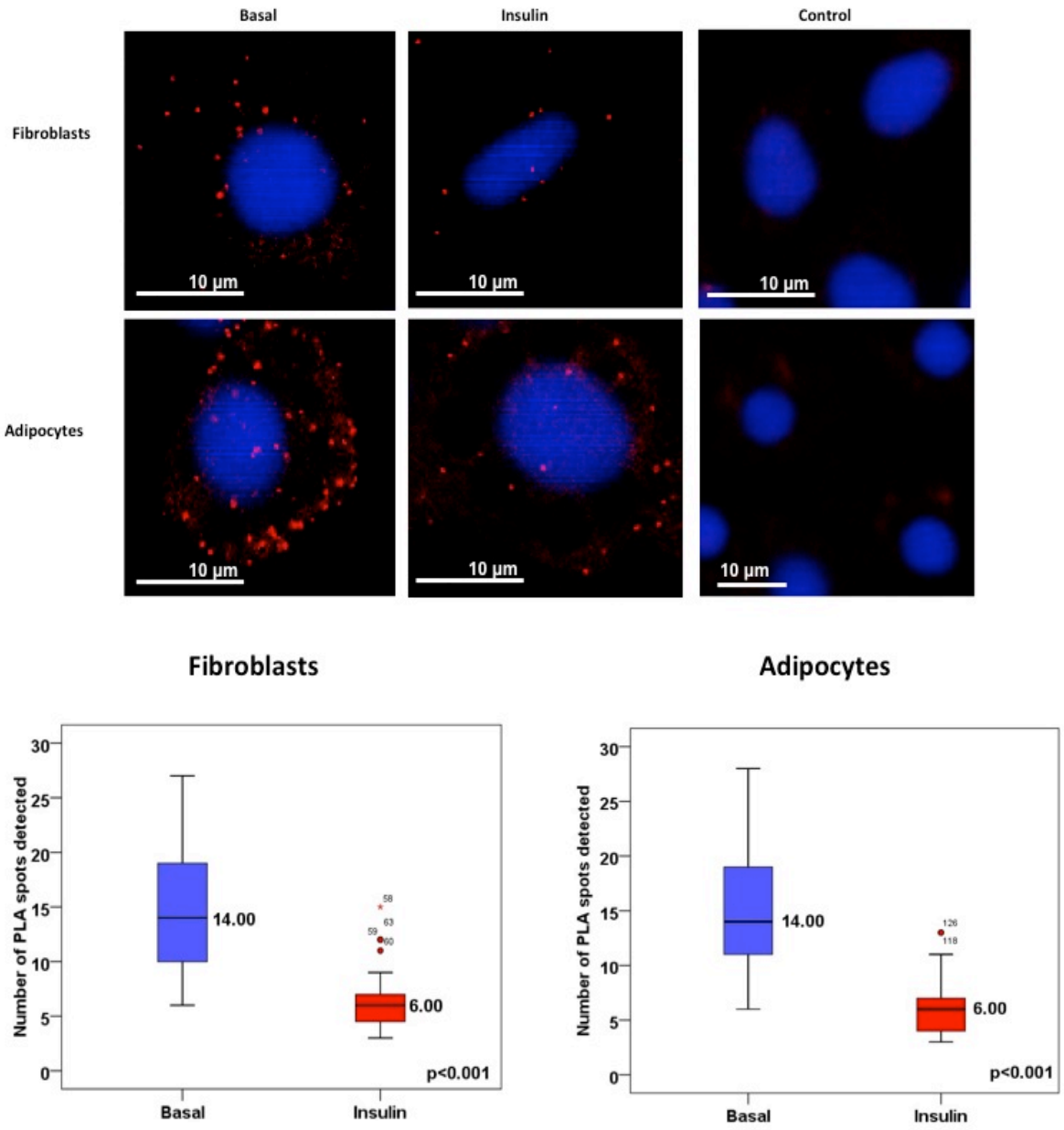

Figure 6-3: cellugyrin/VAMP2 PLA

PLA using antibodies against cellugyrin and VAMP2 (Abcam rabbit) was performed in 3T3-L1 fibroblasts and adipocytes treated with insulin (100 nM for 5 min) or not (basal) (section 2.6.5). Red spots correspond to a positive PLA signal. Blue: DAPI stained nuclei. The control shown represents the omission of the primary antibody against VAMP2. Statistical analysis of PLA results was performed using blobfinder and SPSS software (Mann-Whitney U test) (see appendix Figure 8-22 Figure 8-23 Figure 8-24). The numbers in the boxes illustrate the median value (30 to 95 cells per experiment). Images are representative of three independent experiments.

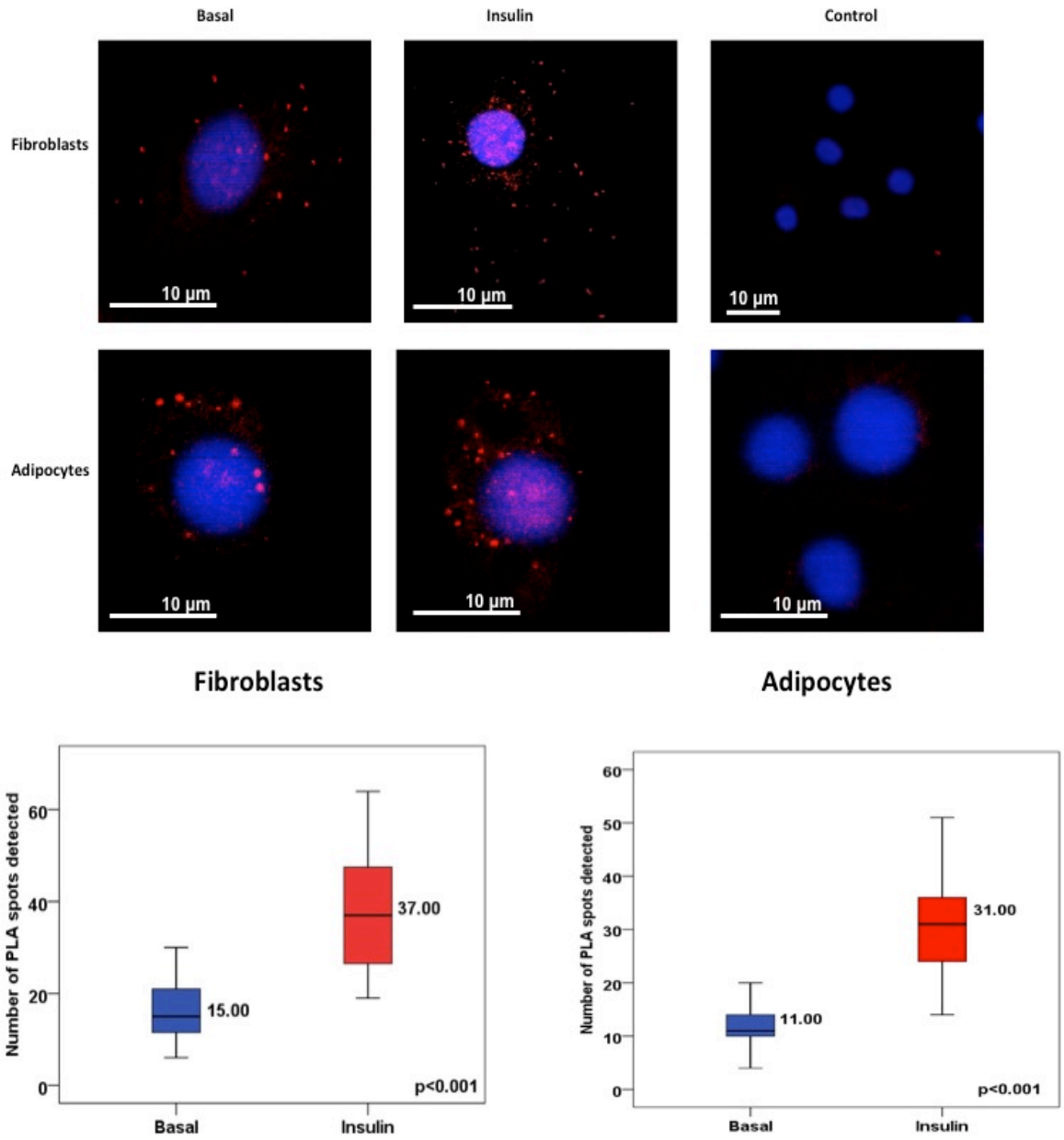

Figure 6-4: sortilin/VAMP2 PLA

PLA using antibodies against sortilin and VAMP2 (SySy mouse) was performed in 3T3-L1 fibroblasts and adipocytes treated with insulin (100 nM for 5 min) or not (basal) (section 2.6.5). Red spots correspond to positive PLA signals. Blue: DAPI stained nuclei. The control shown represents the omission of the primary antibody against VAMP2. Statistical analysis of PLA results was performed using blobfinder and SPSS software (Mann-Whitney U test) (see appendix Figure 8-25 Figure 8-26 Figure 8-27). The numbers in the boxes illustrate the median value (30 to 95 cells per experiment). Images are representative of three independent experiments.

6.3.4 PLA for cellugyrin/Munc18c and sortilin/Munc18c in 3T3-L1 cells

In chapter 3, I presented evidence to suggest that there are two distinct pools of Syntaxin 4 of 3T3-L1 cells; one in complex with SNAP23 (not in association with Munc18c or VAMP2) and the other in complex with VAMP2 and Munc18c (and not in association with SNAP23). These two pools can be distinguished by the presence/absence of Munc18c and with this in mind, I performed PLA to look at associations of Munc18c with both cellugyrin and sortilin Figure 6-5 and Figure 6-6). As would be expected from the model that the sortilin-positive (cellugyrin-negative) vesicles are source of (if not the) vesicles that translocate to the cell surface in response to insulin, levels of sortilin at the plasma membrane of adipocytes increase following insulin-stimulation, whereas those of cellugyrin do not (Kandror and Pilch, 2011). I reasoned that these observations might provide a way to use the ability to resolve the two different Syntaxin 4 pools (by their association, or lack thereof, with Munc18c) and to investigate potential functional differences between Sytaxin 4 that is in complex SNAP23 and that in complex with VAMP2 (under basal conditions). Figure 6-5 and Figure 6-6 demonstrate that whereas Munc18c is found in close proximity to sortillin, there is no detectable associations between cellugyrin and Munc18c. These data are consistent with a model in which the pool of Syntaxin 4 that is in complex with Munc18c (and VAMP2) under basal conditions is associated with sortillin-positive (cellugyrin-negative vesicles; i.e. the source of the insulin-sensitive pool of GLUT4. In contrast, the cellugyrin-positive vesicles have no Munc18c associated with them.

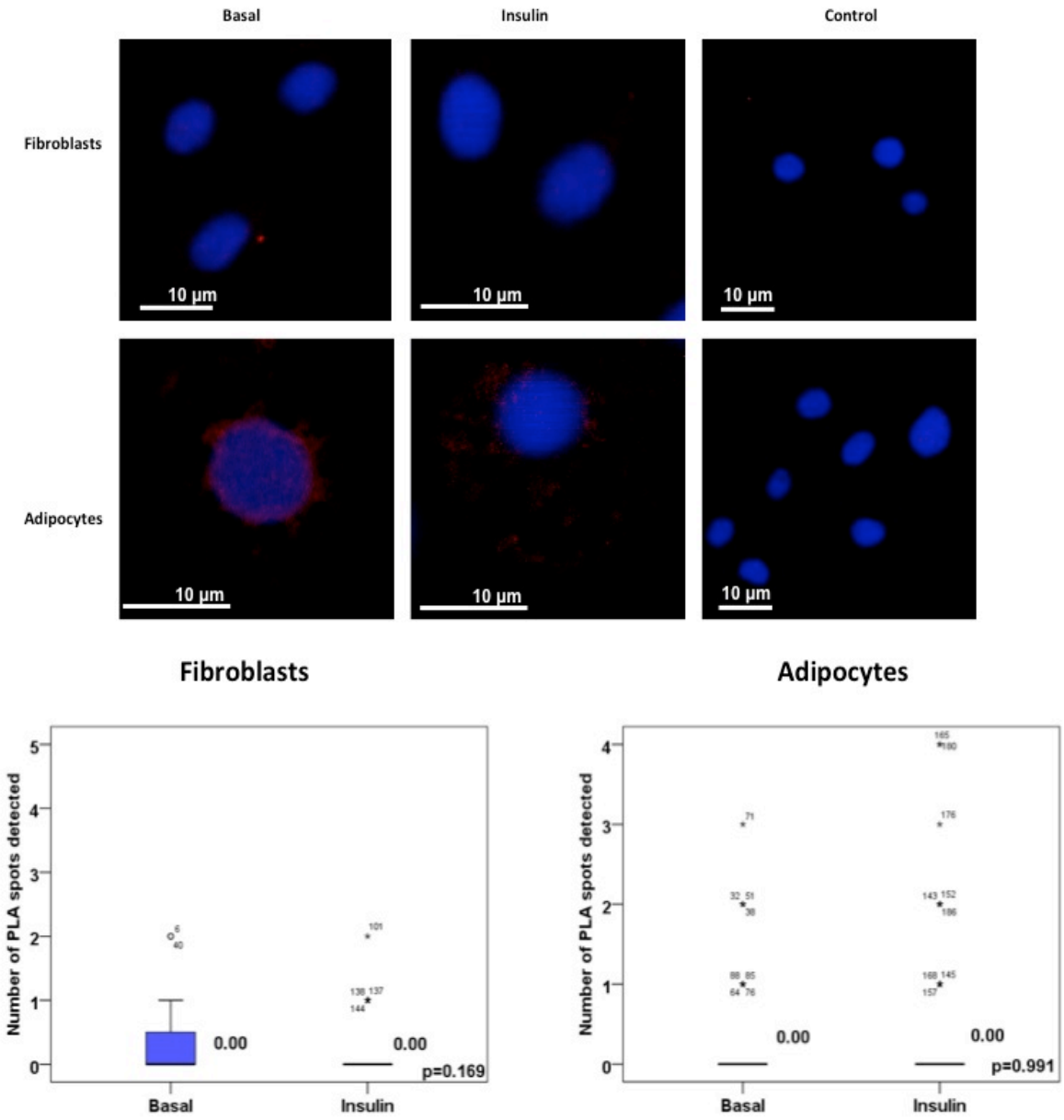

Figure 6-5: cellugyrin/Munc18c PLA

PLA using antibodies against cellugyrin and Munc18c (Abcam rabbit) was performed in 3T3-L1 fibroblasts and adipocytes treated with insulin (100 nM for 5 min) or not (basal) (section 2.6.5). Red spots correspond to positive PLA signals. Blue: DAPI stained nuclei. T he control shown represents the omission of the primary antibody against Munc18c. Statistical analysis of PLA results was performed using blobfinder and SPSS software (Mann-Whitney U test) (see appendix Figure 8-28, Figure 8-29 Figure 8-30). The numbers in the boxes illustrate the median value (30 to 95 cells per experiment). Images are representative of three independent experiments.

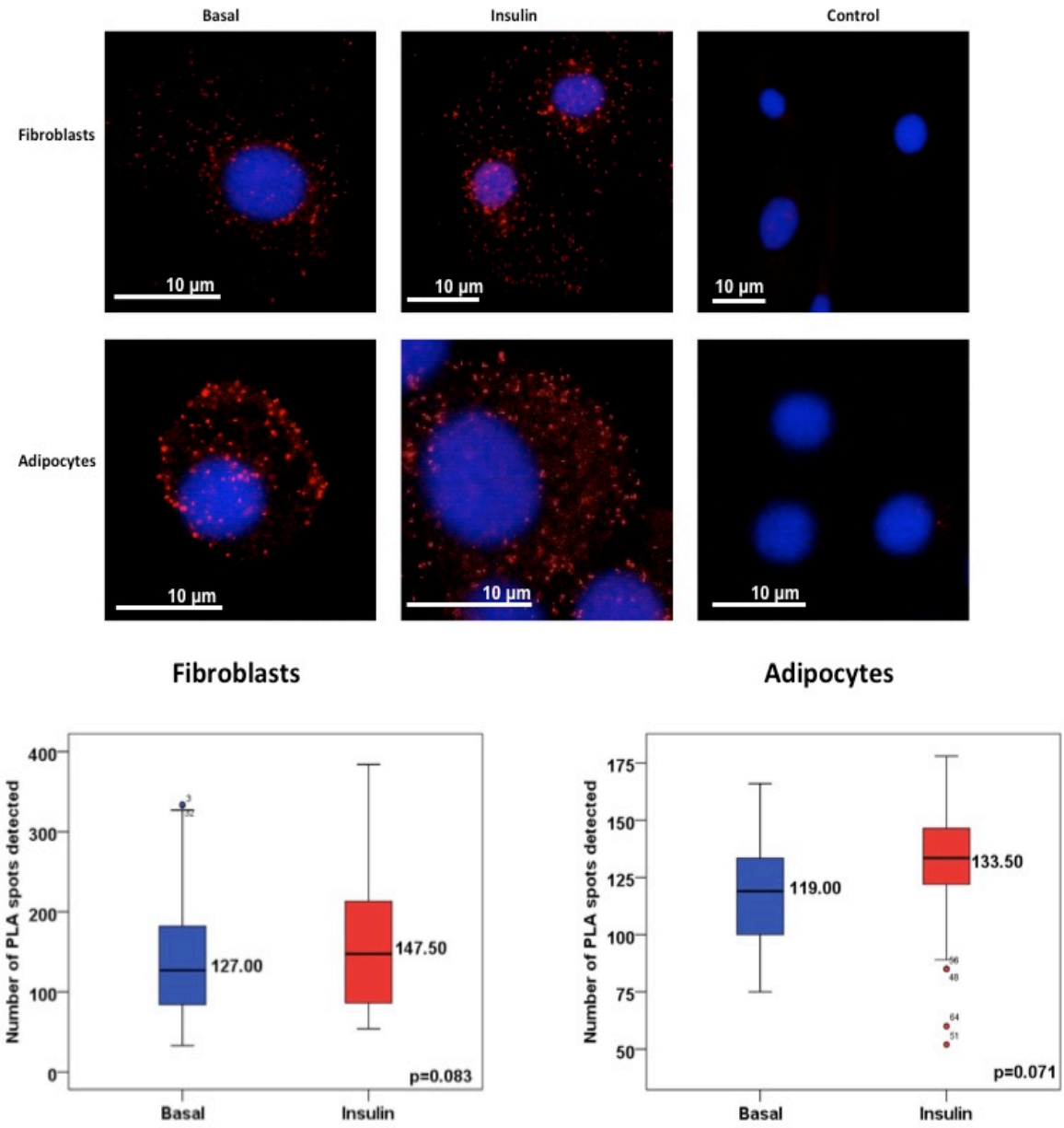

Figure 6-6: sortilin/Munc18c PLA

PLA using antibodies against sortilin and Munc18c (Abnova mouse) was performed in 3T3-L1 fibroblasts and adipocytes treated with insulin (100 nM for 5 min) or not (basal) (section 2.6.5). Red spots correspond to positive PLA signals. Blue: DAPI stained nuclei. The control shown represents the omission of the primary antibody against Munc18c. Statistical analysis of PLA results was performed using blobfinder and SPSS software (Mann-Whitney U test) (see appendix Figure 8-31 Figure 8-32 Figure 8-33). The numbers in the boxes illustrate the median value (30 to 95 cells per experiment). Images are representative of three independent experiments.

6.3.5 PLA for cellugyrin/Syntaxin 4 in 3T3-L1 cells and cellugyrin/SNAP23

The lack of association of Munc18c with cellugyrin (Figure 6-5) indicates that these vesicles are not a direct source of Munc18c-dependent delivery of GLUT4 to the plasma membrane. To investigate this further, PLA was carried out between cellugyrin/Syntaxin 4 and cellugyrin/SNAP23 (Figure 6-7 and Figure 6-8). Both Syntaxin 4 and SNAP23 are found in close proximity to cellugyrin under basal conditions; albeit at low levels, particularly in the case of Syntaxin 4. Addition of insulin reduced both associations to almost zero (N.B. this reduction was statistically significant in both cases). Collectively, the data presented in Figure 6-7 and Figure 6-8 demonstrate an association of both Syntaxin 4 and SNAP23 with cellugyrin (a marker of internal GLUT4 vesicles that do not respond to insulin) (Kandror and Pilch, 2011), and that both of these associations decrease upon insulin-stimulation.

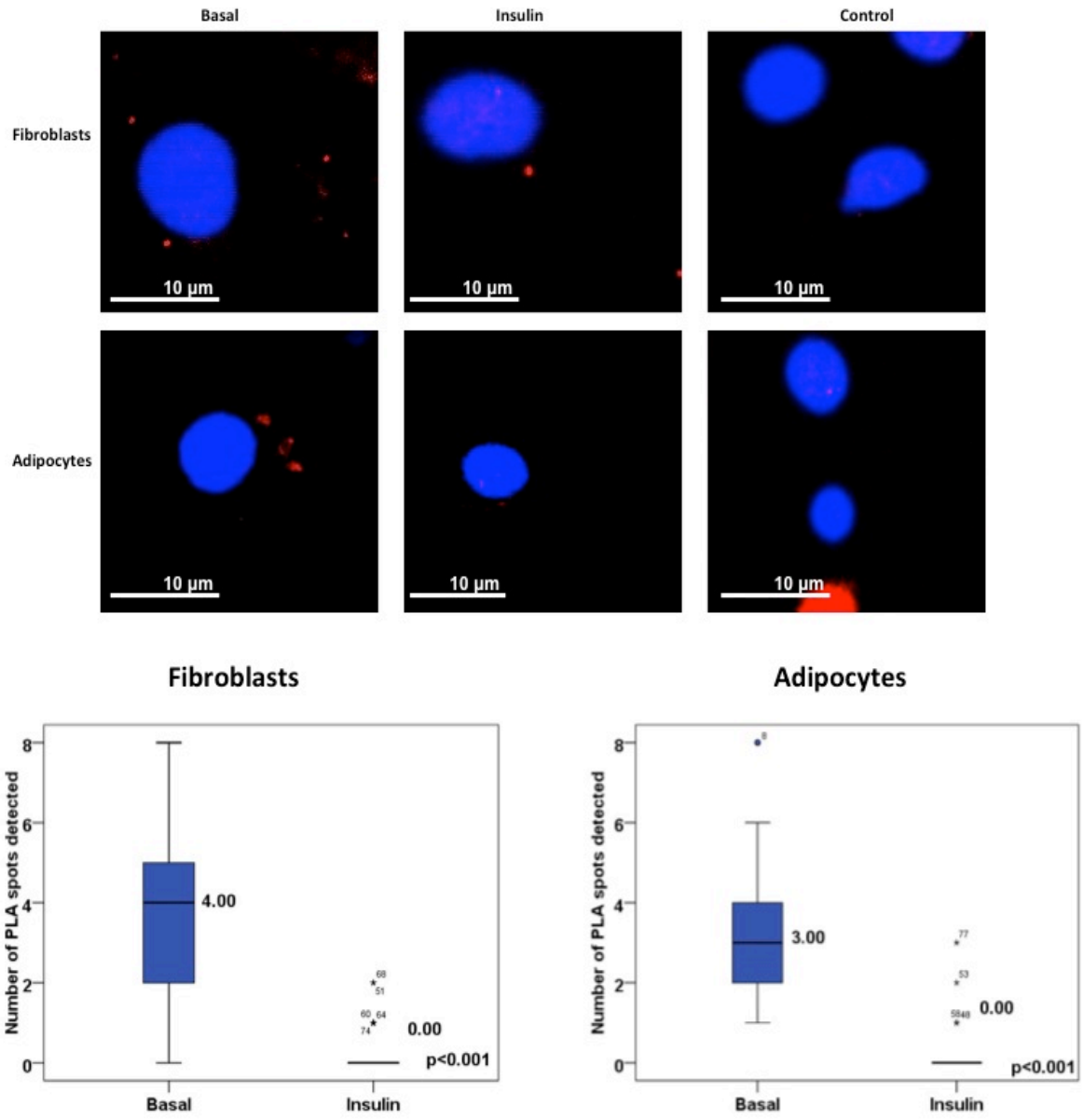

Figure 6-7: cellugyrin/Syntaxin 4 PLA

PLA using antibodies against Syntaxin 4 (SySy rabbit) and cellugyrin was performed in 3T3-L1 fibroblasts and adipocytes treated with insulin (100 nM for 5 min) or not (basal) (section 2.6.5). Red spots correspond to positive PLA signals. Blue: DAPI stained nuclei. The control shown represents the omission of the primary antibody against Syntaxin 4. Statistical analysis of PLA results was performed using blobfinder and SPSS software (Mann-Whitney U test) (see appendix Figure 8-34 Figure 8-35 Figure 8-36). The numbers in the boxes illustrate the median value (30 to 95 cells per experiment). Images are representative of three independent experiments.

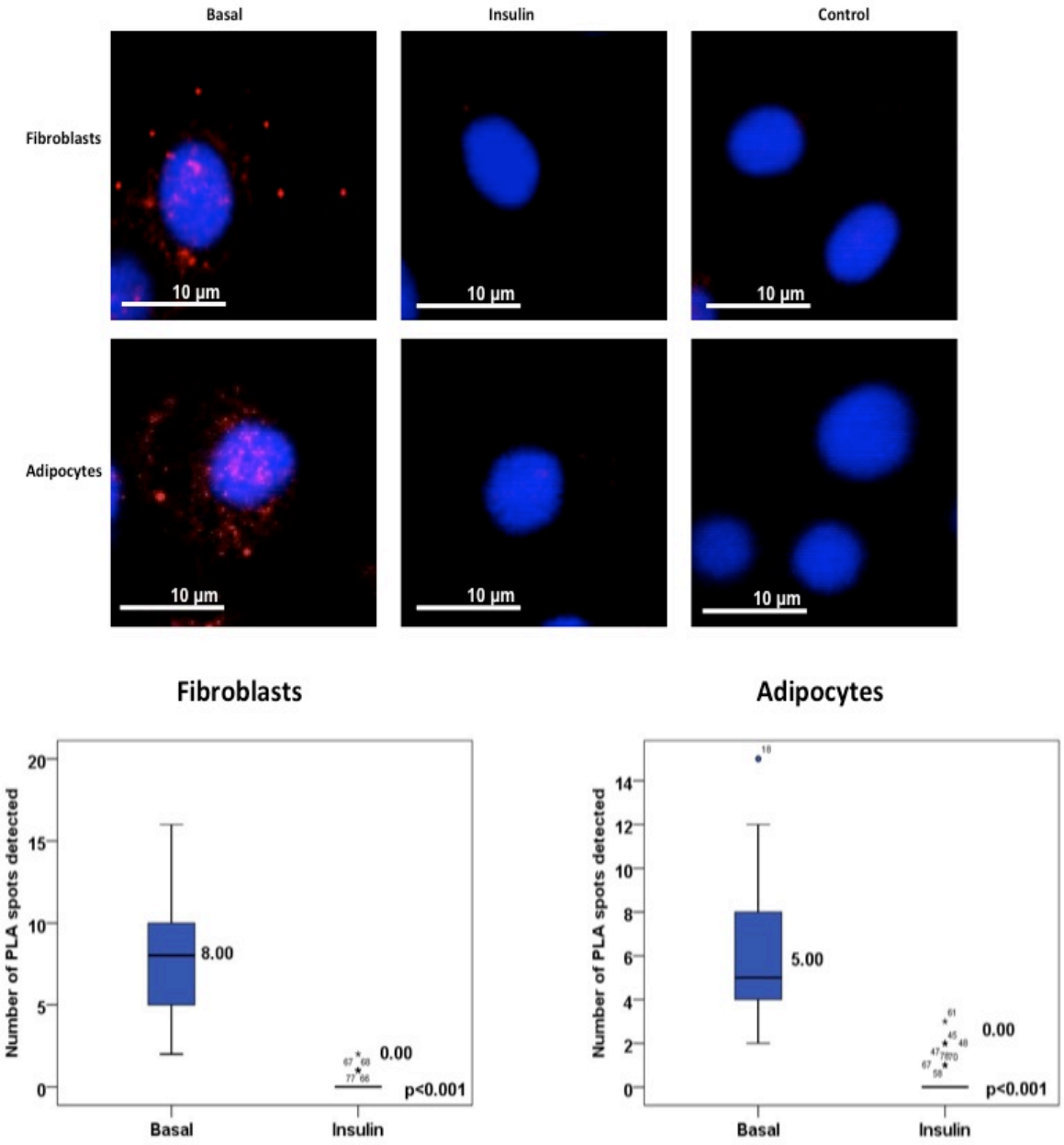

Figure 6-8: cellugyrin/SNAP23 PLA

PLA using antibodies against SNAP23 (SySy rabbit) and cellugyrin was performed in 3T3-L1 fibroblasts and adipocytes treated with insulin (100 nM for 5 min) or not (basal) (section 2.6.5). Red spots correspond to positive PLA signals. Blue: DAPI stained nuclei. The control shown represents the omission of the primary antibody against SNAP23. Statistical analysis of PLA results was performed using blobfinder and SPSS software (Mann-Whitney U test) (see appendix Figure 8-37 Figure 8-38 Figure 8-39). The numbers in the boxes illustrate the median value (30 to 95 cells per experiment). Images are representative of three independent experiments.

6.3.6 PLA for sortilin/Syntaxin 4 3T3-L1 cells and sortilin/SNAP23

To complete the PLA investigations of associations of Munc18c and the SNARE proteins that facilitate GLUT4 delivery to the plasma membrane with markers of internal stores of GLUT4 (cellugyrin and sortilin), PLA was used to investigate associations between Syntaxin 4/sortilin and SNAP23/sortilin under both basal and insulin-stimulated conditions (Figure 6-9 and Figure 6-10). A relatively small number of associations (compared to other associations of sortilin, e.g. with VAMP2) were observed of sortilin with either Syntaxin 4 or SNAP23 under basal conditions in both adipocytes and fibroblasts; both of which increased significantly upon insulin-stimulation. These data are consistent with a model in which sortilin-positive vesicles deliver GLUT4 to the plasma membrane in response to insulin.

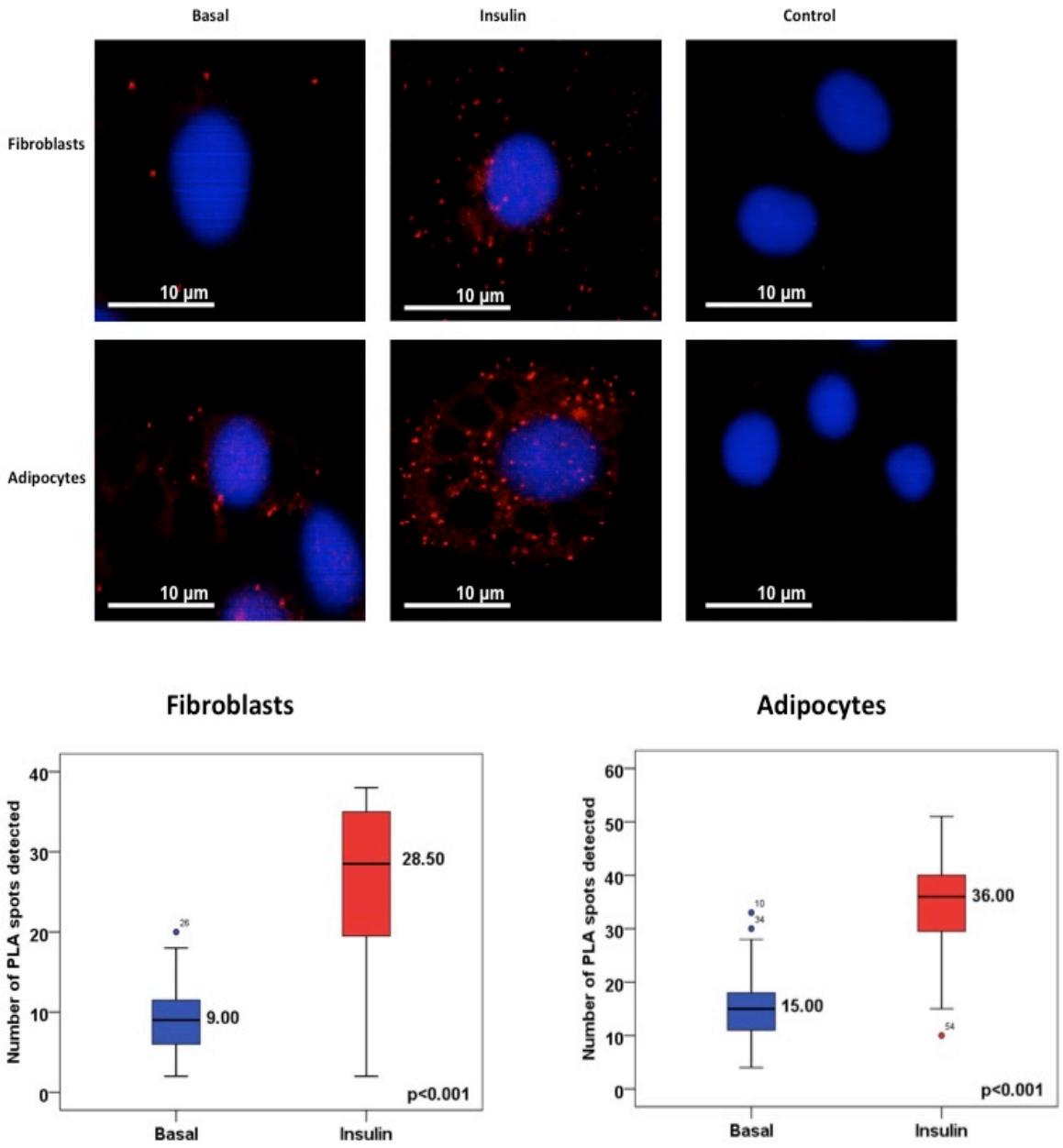

Figure 6-9: sortilin/Syntaxin 4 PLA

PLA using antibodies against sortilin and Syntaxin 4 (BD mouse) was performed in 3T3-L1 fibroblasts and adipocytes treated with insulin (100 nM for 5 min) or not (basal) (section 2.6.5). Red spots correspond to positive PLA signals. Blue: DAPI stained nuclei. The control shown represents the omission of the primary antibody against Syntaxin 4. Statistical analysis of PLA results was performed using blobfinder and SPSS software (Mann-Whitney U test) (see appendix Figure 8-40 Figure 8-41 and Figure 8-42). The numbers in the boxes illustrate the median value (30 to 95 cells per experiment). Images are representative of three independent experiments.

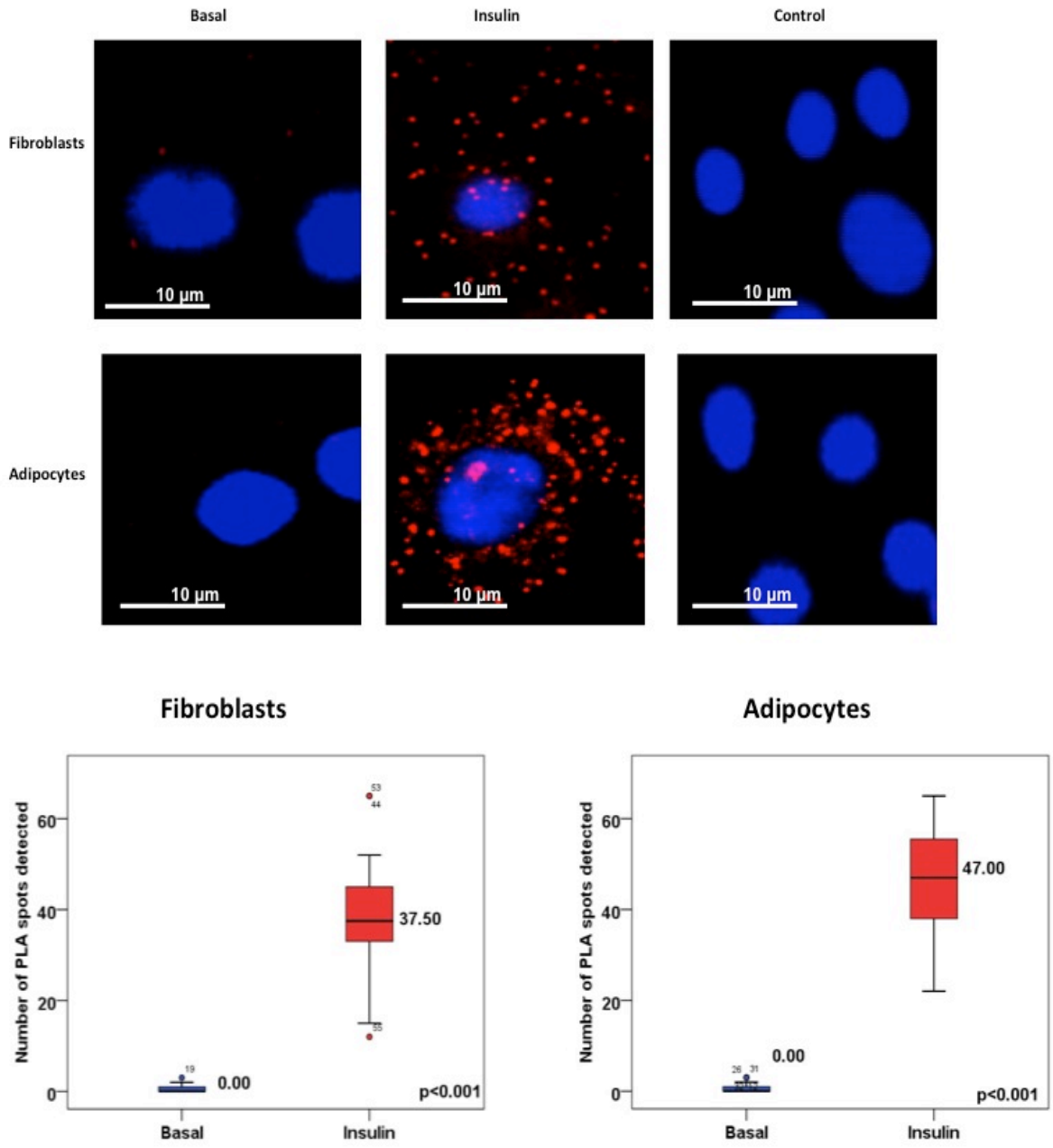

Figure 6-10: sortilin/SNAP23 PLA

PLA using antibodies against sortilin and SNAP23 (Santa Cruz mouse) was performed in 3T3-L1 fibroblasts and adipocytes treated with insulin (100 nM for 5 min) or not (basal) (section 2.6.5). Red spots correspond to positive PLA signals. Blue: DAPI stained nuclei. The control shown represents the omission of the primary antibody against sortilin. Statistical analysis of PLA results was performed using blobfinder and SPPS software (Mann-Whitney U test) (see appendix Figure 8-43 Figure 8-44 Figure 8-45). The numbers in the boxes illustrate the median value (30 to 95 cells per experiment). Images are representative of three independent experiments.

6.4 Discussion.

On its way to and from the cell surface, GLUT4 traffics through several distinct intracellular compartments that are organized into two interrelated endosomal cycles (Bryant et al., 2002). Intracellular GLUT4 carrying vesicles can be divided into 2 distinct categories: cellugyrin-positive and cellugyrin-negative (sortilin-positive) that are the source of GLUT4 delivered to the cell surface under basal and insulin-stimulated conditions respectively (discussed in sections 6.1.2 and 6.1.3). In this chapter PLA was used to investigate whether the two distinct Syntaxin 4 pools (described in chapter 3) are similarly functionally distinct, working on the hypothesis that if they are perhaps one is responsible for facilitating delivery of GLUT4 to the plasma membrane under basal conditions (from cellugyrin-negative vesicles) and the other in response to insulin (from cellugyrin-negaitve/sortilin-positive vesicles). It is important to remember that a positive PLA signal does not necessarily mean that two proteins interact directly, but can arise under any circumstances where they are in close proximity, such as present in the same membrane vesicle. Figure 6-11 summarises changes observed upon insulin-stimulation of pairwise PLA associations between the 2 markers of internal GLUT4 membranes cellugyrin and sortilin and the proteins that regulate GLUT4 delivery to the cell surface, namely Syntaxin 4, SNAP23, VAMP2 and Munc18c.

	Fibroblasts & Adipocytes
	Basal-Insulin
CG/SORT	same (no signal)
CG/VAMP2	Decrease
SORT/VAMP2	Increase
CG/MUNC18c	Same (no signal)
SORT/MUNC18c	Same (signal)
CG/Sx4	Decrease
CG/SNAP23	Decrease
SORT/Sx4	Increase
SORT/SNAP23	Increase

Figure 6-11: PLA results summary

This table summarizes the results of PLA performed on 3T3-L1 cells (both fibroblast and adipocytes) between the protein pairs listed in the column on the left with statistically-significant changes in response to insulin are listed in the column on the right. N.B. there was complete agreement regarding changes of data obtained in both adipocytes and fibroblasts.

Data from PLA performed between cellugyrin and sortilin support previous studies that found these two proteins populate two different populations of GLUT4 vesicles (Jedrychowski et al., 2010; Kupriyanova and Kandror, 2000; Kupriyanova et al., 2002). There is evidence to indicate some overlap between cellugyrin and sortilin's localization (Jedrychowski et al., 2010), this likely represents large diameter membrane compartments (e.g. recycling endosomes, TGN) in which the two proteins could be separated enough not to give a positive PLA signal and do not provide a direct source of GLUT4 to be delivered to the cell surface.

The increased PLA signal between sortilin and VAMP2 from basal to insulin-stimulated conditions taken in combination with the abolished PLA signal between VAMP2 and cellugyrin under the same transition of conditions raises the possibility of a shift in traffic of the v-SNARE between the two pools of GLUT4 carrying vesicles, from cellugyrin-positive under basal conditions to sortilin-

positive (cellugyrin-negative) after the addition of insulin. This is an interesting observation that provides evidence for a role of insulin in GSV formation in addition to its better-characterised, and more widely-studied role in translocation of GLUT4 from GSVs to the plasma membrane. Use of total internal reflection microscopy provided evidence for the formation of distinct classes of GLUT4 vesicles from the recycling compartment upon insulin stimulation, assigning an additional role to insulin (Lampson et al., 2001).

The two distinct pools of Syntaxin 4 reported in Chapter 3 can be distinguished by the association, or lack thereof, with the SM protein Munc18c (chapter 3). PLA between sortilin/Munc18c and cellugyrin/Munc18c illustrates that Munc18c localises with the insulin-responsive (cellugyrin-negative, sortilin-positive) vesicles but not with cellugyrin-positive vesicles. Given that Syntaxin 4 is found associated with both cellugyrin and sortilin (it is tempting to speculate that the Sytaxin 4 on the cellugyrin-negative (sortilin-positive) vesicles represents the pool that is in complex with Munc18c (and therefore also VAMP2; section 3.4), while Syntaxin 4 on the cellugyrin-positive (sortilin-negative) vesicles is that not associated with Munc18c (inferred by the lack of association between cellugyrin and Munc18c), but with SNAP23 (Section 6.3.5 and Figure 6-8 PLA between SNAP23 and cellugyrin under basal conditions).

As far the cellugyrin positive vesicles are concerned there is no direct evidence to support the above claim, that are associated with Syntaxin 4/SNAP23 pool, since this assumption was based on the absence of any positive PLA signal. Nevertheless the decrease of the PLA signal after the addition of insulin for both cellugyrin/Syntaxin 4 and cellugyrin/SNAP23 associations, in combination with the concomitant increase of sortilin/Syntaxin 4 and Sortilin/SNAP23 associations under the same conditions, suggests that cellugyrin positive vesicles are more likely to associate to Syntaxin 4 pool in complex with SNAP23 and that association is regulated by insulin in a negative way. This interpretation is consistent with the shift of VAMP2 between the two vesicle pools (from cellugyrin positive to sortilin positive) upon insulin stimulation described above.

Although the data presented here are not without caveats, and rely on one technique, they do support the hypothesis that the two Syntaxin 4 pools described in chapter 3 are functionally different and provide impetus for further

investigations. I propose that the Syntaxin 4 pool in complex with VAMP2 and Munc18c associates with the sortilin-positive (cellugyrin-negative) vesicles and it is the pool that regulates the fusion of GLUT4 carrying vesicles upon insulin stimulation. On the other hand, the Syntaxin 4 pool in complex with SNAP23 associates with cellugyrin-positive vesicles and is responsible for the basal translocation of GLUT4 to plasma membrane.

This study raises the intriguing possibility that delivery of GLUT4 to the cell surface under basal conditions is Munc18c-independent, a somewhat heretical idea that must be investigated further. Also striking is the observed increased association between sortilin and Syntaxin 4 upon insulin-stimulation (while sortilin/Munc18c associations remain the same). Given my contention that Munc18c and Syntaxin 4 are part of the same complex, and sortilin is unlikely to be associated with the other Syntaxin 4 pool (the one in complex with SNAP23) these data are somewhat confusing. The possible explaination is that after the addition of insulin the number of sortilin-positive vesicles increases to such an extent that all the available Syntaxin 4/Munc18c complexes become limiting. The remaining sortilin-positive vesicles would remain docked in proximity to Syntaxin 4 molecules waiting for SNAP23 and Munc18c to regulate their fusion to the plasma membrane. Such an explanation invokes Munc18c as a rate-limiting factor for GLUT4 translocation to the plasma membrane and may also provide an explanation for the apparently conflicting data supporting both a positive and negative role of Munc18c for membrane fusion- e.g. studies in which Munc18c was either knocked out (positive role) (Oh et al., 2005; Thurmond et al., 1998) or overexpressed (negative role) (Thurmond et al., 1998). Munc18c importance as a GLUT4 translocation rate-limiting factor will be discussed in detail in the last chapter.

Chapter 7

Discussion

Translocation of the facilitative glucose transporter GLUT4 from perinuclear depots to the plasma membrane is important for whole-body glucose homeostasis (Bryant et al., 2002). Fusion of GLUT4 vesicles with the plasma membrane is a key terminal step in insulin-regulated glucose transport. This fusion event is mediated by the SNARE proteins, Syntaxin 4, SNAP23 (t-SNAREs located to the plasma membrane) and VAMP2 (v-SNARE anchored to the GLUT4 carrying vesicles), (Thurmond et al., 1998) through formation of a very stable (SDS-resistant) (Hayashi et al., 1994) quaternary complex of SNARE domains that provides mechanical force to overcome the energy barrier for membrane fusion (Pobbati et al., 2006). The whole process is regulated by a number of accessory proteins among which Munc18c (member of the Sec1p/Munc18 -SM- family) plays a predominant role (Tamori et al., 1998). Munc18c interacts directly with both Syntaxin 4 and VAMP2- as well as with the assembled SNARE complex through a series of different binding modes (Aran et al., 2009; Latham et al., 2006). The precise role of Munc18c remains elusive, although a number of molecular mechanisms for its action, as well as other members of the SM protein family have been suggested. One potential role of SM/syntaxin interaction is to release the inhibitory effect of the syntaxin's Habc domain through a conformational switch. Transition of a syntaxin from its "closed" to an "open" form could then trigger the formation of the SNARE complex (Dulubova et al., 1999). Although it has long been established that insulin stimulates delivery of GLUT4-containing vesicles to the plasma membrane and that this delivery is regulated by the formation of Syntaxin 4-containing complexes, which are regulated by Munc18c, it is not known whether insulin directly regulates Syntaxin 4-containing SNARE complex formation. In this thesis, I have used a combination of *in situ* and *in vitro* approaches to investigate whether or not this is the case and to gain molecular insight into how this might be achieved.

In chapter 3, I directly tested the hypothesis that insulin regulates Syntaxin 4-containing SNARE complex assembly by using *in situ* Proximity Ligation Assay (PLA) to study the effects of insulin stimulation on pairwise associations between Syntaxin 4, SNAP23, VAMP2 and Munc18c in 3T3-L1 adipocytes and fibroblasts. This technique can provide quantified data comparing associations between the same pair(s) of proteins under different conditions. In order to optimise conditions for PLA, I performed preliminary experiments in fibroblast, as they

are quicker to grow than adipocytes and easier to visualise. It was necessary for me to check their response to insulin regarding GLUT4 translocation since they appear to have low expression of the insulin receptor (IR) (Reed and Lane, 1980). For this purpose GLUT4 surface immunostaining was performed on 3T3-L1 fibroblasts virally infected to stably express double-tagged (HA and GFP) GLUT4. From the results obtained (Figure 3-2) it is evident that fibroblasts do translocate ectopically expressed HA-GLUT4-GFP to the cell surface in response to insulin. This is likely to occur through the insulin like growth factor receptor 1 (IGF1-R) (Vigneri et al., 2010). I used PLA to visualize all six possible pairwise associations between Syntaxin 4, SNAP23, VAMP2 and Munc18c. These studies agreed with previous findings obtained from *in vitro* binding and co-immunoprecipitation studies that had characterised interactions of Syntaxin 4 with Munc18c and SNAP23 (D'Andrea-Merrins et al., 2007; Latham et al., 2006; Pevsner et al., 1994; St-Denis et al., 1999)(Figure 3-4 and Figure 3-7). Additionally association of Munc18c with VAMP2 corroborates the direct interaction between these 2 proteins that has been shown *in vitro* (Brandie et al., 2008). It is important to note that a positive PLA signal between these two proteins does not exclude the possibility of (a) bridging protein(s). Bearing this possibility in mind, the Munc18c/VAMP2 interaction is consistent with the "bridging hypothesis", proposed by Peng and Gallwitz which suggests that the binding of specific v- and t-SNAREs on opposite membrane could involve SM proteins (Peng and Gallwitz, 2004). Considering this hypothesis, a model in which Munc18c guides GLUT4 vesicles *via* its interaction with VAMP2 towards to the Syntaxin 4 on target membrane is very appealing. Based on the table that summarises PLA results from both adipocytes and fibroblasts (Figure 3-10 A) the only observed increases in associations upon insulin-stimulation are between SNAP23/Munc18c and SNAP23/VAMP2, and since there is no evidence for direct interaction of SNAP23 with either Munc18c or VAMP2, but Munc18c does bind assembled Syntaxin 4/SNAP23/VAMP2 complex (Latham et al., 2006), it is likely that the formation of SNARE complexes increases upon insulin-stimulation. Thus, this study provides the strongest evidence to date to that insulin stimulation drives SNARE complex formation. Examination of the changes in associations between the six protein pairs upon insulin stimulation (described in detail in section 3.4 (Figure 3-10 B) supports a model in which there are two separate pools of Syntaxin 4 under basal conditions (i.e. in the absence of

insulin): one in complex with SNAP23 but not with Munc18c, and the other in complex with both VAMP2 and Munc18c. This raised a plethora of questions regarding the physiological significance of such two separate pools. Indeed, suggestion of a complex between VAMP2 and Syntaxin 4 in the absence of SNAP23 was rather unorthodox and for this reason its existence was further examined using different methods.

In chapter 4 I examined interactions between the proteins used in the PLA studies and their influence on SNARE complex assembly using *in vitro* approaches. Firstly, I established a SNARE complex assembly assay using bacterially-expressed proteins to form a complex between the cytosolic domains of Syntaxin 4, VAMP2 and SNAP-23 *in vitro*. This complex is extremely stable as demonstrated by its resistance to extreme denaturing conditions (boiling, SDS) (Figure 4-2) as has previously been reported for several SNAREs complexes including the one being examined here (Hayashi et al., 1994; Polgar et al., 2002). I used the same bacterially-expressed proteins (and derivatives thereof) to demonstrate a direct, and specific, interaction between the SNARE domains of Syntaxin 4 and VAMP2 (Figure 4-3 Figure 4-5 Figure 4-6), a finding that is consistent with previously published data (Calakos et al., 1994), as well as with my suggestion of an interaction between Syntaxin 4 and VAMP2 *in vivo* under basal conditions (from my PLA studies; Figure 3-8). This interaction could potentially play a role in docking transport (in this case, GLUT4-containing) vesicles to specific target organelles (in this case the plasma membrane). Furthermore, pull-down assays from adipocyte lysates of insulin-stimulated versus basal cells, provided evidence of an "opening" of Syntaxin 4 upon insulin-stimulation (Figure 4-19); an observation that is consistent with a regulatory role of Syntaxin 4's N-terminal Habc domain as suggested (MacDonald et al., 2010), and the importance of mode-2 binding between a syntaxin and it cognate SM protein regarding SNARE complex regulation (Munson and Bryant, 2009).

The binary interactions of Syntaxin 4 with SNAP23 and VAMP2 have contrary effects with regard to SNARE complex assembly. I used the *in vitro* SNARE complex assembly assay to demonstrate that preforming the t-SNARE complex between Syntaxin 4 and SNAP23 enhances SNARE complex formation (Figure 4-22) in agreement with previous studies (Kawanishi et al., 2000; St-Denis et al., 1999). In contrast, the interaction of Syntaxin 4 with VAMP2 has an inhibitory

effect on the same assay (Figure 4-23). Taking into consideration the PLA studies which led me to speculate the existence of two distinct pools of Syntaxin 4 under basal conditions: one that is well-characterised, in complex with SNAP23, (Kawanishi et al., 2000; St-Denis et al., 1999) and one that is perhaps more contentious, in complex with VAMP2 and Munc18c, it is tantalizing to speculate a role Munc18c (the last member of this particular syntaxin pool) in releasing the inhibition of SNARE complex formation imposed by the Syntaxin 4/VAMP2 interaction in the absence of SNAP23.

In the following chapter (chapter 5) I used *in vitro* binding studies (again, pull-downs and the SNARE-complex assembly assay) to directly test the hypothesis that the phosphomimetic Munc18c (Y521E) mutant (Aran et al., 2011), releases the inhibition that interaction between Syntaxin 4 and VAMP2 imposes on SNARE complex assembly. Insulin-induced tyrosine phosphorylation of Munc18c on residue 521 has been suggested as a regulatory mechanism by which interaction between Munc18c and Syntaxin 4, which is considered as non-fusogenic (Brandie et al., 2008) can be dissociated (Aran et al., 2011; Jewell et al., 2008; Jewell et al., 2011). In this study two wild-type Munc18c constructs were used (N and C-terminally His-tagged) and their functionality was assessed by their ability to interact with Syntaxin 4 specifically (Figure 5-2). No interaction was observed of either wild-type or phosphomimetic Munc18c with SNAP23 (Figure 5-5) consistent with the lack of any publish evidence for such an interaction. Use of wild-type Munc18c in binding assays with VAMP2 further confirmed their interaction (Figure 5-3) as previously reported (Brandie et al., 2008; Latham et al., 2006) . It has been recently reported that phosphorylation of Munc18c by the insulin receptor abolishes its binding to VAMP2 (Aran et al., 2011), whereas I found that the phosphomimetic mutant decreased but didn't totally abolish the interaction (Figure 5-3). This potential discrepancy could be explained by the fact that I used a tag-free VAMP2 protein as oppose to the GST-tagged protein that was used by Aran (Aran et al., 2011). Of course, these discrepancies may also be due to different levels of detection in the two studies. The pull-down assays from adipocyte lysates is consistent with the *in vitro* binding studies described above and are consistent with the hypothesis that phosphorylation of Munc18c upon insulin stimulation abrogates its ability to bind both Syntaxin 4 and VAMP2. Quite remarkably this effect seems to decline as time passes and the binding

properties of Munc18c regarding Syntaxin 4 and VAMP2 are restored after 20 min back to the levels prior to insulin stimulation (Figure 5-6 and Figure 5-7). This intriguing observation may reflect that, rather than being a continuously stimulated condition that lasts as long as insulin is present, insulin-stimulated traffic is instead poised ready to come to completion upon receipt of an insulin signal.

Consistent with its inhibitory effect on SNARE-mediated liposome fusion (Brandie et al., 2008), I found that wild-type Munc18c inhibits SNARE complex formation (Figure 5-8). In contrast, the phosphomimetic (Y521E) mutant facilitates SNARE complex formation (Figure 5-9). This was unexpected, given that Munc18c phosphorylation abolishes its binding to Syntaxin 4.

Perhaps more strikingly, presence of the phosphomimetic Munc18c mutant in complex assembly assays where VAMP2/Syntaxin 4 complexes were preformed, releases the inhibitory effect on SNARE complex rate formation, in contrast to wild-type Munc18c, which further enhances the inhibition (Figure 5-10). This makes it extremely attractive to propose a model in which insulin alleviates the inhibition exerted by a binary Syntaxin 4/VAMP2 interaction *via* tyrosine phosphorylation of Munc18c (through the pool of Syntaxin 4 in association with VAMP2 and Munc18c revealed by the PLA studies) whereas the other pool (in complex with SNAP23 is responsible for the cycling of GLUT4 through the plasma membrane under basal conditions.

As discussed in the introduction chapter (section 1.4.4) several studies support the existence of two distinct and functionally different pathways of GLUT4 translocation: one responsible for basal delivery of GLUT4 to the plasma membrane -in which cellugyrin positive/sortilin negative GLUT4 vesicles are involved- and the other for insulin-stimulated GLUT4 translocation where cellugyrin negative/sortilin positive GLUT4 vesicles respond to insulin signal and fuse with the plasma membrane (Kupriyanova and Kandror, 2000; Kupriyanova et al., 2002). In the last result chapter PLA was used to test whether the two pools of Syntaxin 4 described earlier do indeed facilitate the delivery of GLUT4 to the plasma membrane *via* these two distinct pathways, as suggested above. To this end, I investigated if there is any evidence of proximity between the two vesicle

markers (cellugyrin and sortillin) with the SNAREs (Syntaxin 4, VAMP2, SNAP23) and Munc18c.

It is important to note here that PLA does not necessarily indicate interaction between the protein pairs but rather is an indication of proximity, for example, contained within the same membrane vesicle. Figure 6-11 summarises changes in associations between cellugyrin and sortilin as well as their pairwise combinations with Syntaxin 4, SNAP23, VAMP2 and Munc18c upon treatment of cells with insulin. Data from PLA between cellugyrin and sortilin support the notion that these two proteins populate two different polls of GLUT4 vesicles as suggested previously (Jedrychowski et al., 2010; Kupriyanova and Kandror, 2000; Kupriyanova et al., 2002). There are studies that provided evidence of some overlap between cellugyrin and sortilin localization in intracellular membrane bound organelles (Jedrychowski et al., 2010), however these are likely to be large diameter vesicles (recycling endosomes, TGN) and given that the distance threshold for PLA is 10 nm would not give a PLA signal. The observed increased PLA signal between sortilin and VAMP2 on insulin-stimulation taken with the concomitant abolishment of signal between VAMP2 and cellugyrin is consistent with a shift of VAMP2 between the two pools of GLUT4 carrying vesicles from cellugyrin positive under basal conditions to sortilin positive (cellugyrin negative) after the addition of insulin. This possibility is intriguing as it attributes a role for insulin in the formation of sortilin-positive/cellugyrin-negative GLUT4 vesicles upon insulin-stimulation. Functional evidence for the formation of distinct classes of GLUT4 vesicles from the recycling compartment upon insulin stimulation has been suggested before with the use of total internal reflection microscopy (Lampson et al., 2001).

PLA of Munc18c with cellugyrin and/or sortilin indicated that the pool of Syntaxin 4 in complex with VAMP2 and Munc18c is associated with the insulin-responsive vesicles and not with the cellugyrin-positive vesicles. (Figure 6-5 and Figure 6-6). On the other hand the cellugyrin-positive vesicles (non-insulin responsive) most likely interact with the pool of Syntaxin 4 in complex with SNAP23 *via* VAMP2. In addition, the decreased PLA signal after treatment with insulin for both cellugyrin/Syntaxin 4 and cellugyrin/SNAP23 associations, in combination with the concomitant increase in sortilin/Syntaxin 4 and Sortilin/SNAP23 association under the same conditions further supports this

notion (Figure 6-7 Figure 6-8 Figure 6-9 Figure 6-10). All these data suggest that the two Syntaxin 4 pools described previously are functionally different with the Syntaxin 4 pool in complex with VAMP2 and Munc18c associated with the sortilin-positive vesicles regulating fusion of GLUT4-carrying vesicles upon insulin stimulation. The Syntaxin 4 pool in complex with SNAP23, on the other hand, associates with cellugyrin-positive vesicles and likely regulates the basal translocation of GLUT4 to plasma membrane. This model invokes the idea that basal fusion of GLUT4 carrying vesicles is Munc18c independent; a suggestion that requires further investigation.

These data raise an interesting paradox: insulin stimulates PLA between sortillin and Syntaxin 4, but not between sortillin and Munc18c. How can we rationalise this observation? One potential explanation is that the population of sortilin-positive vesicles increases upon insulin stimulation to such an extent that all the available Syntaxin 4/Munc18c complexes are saturated. This would imply that Syntaxin 4 should be in excess compared to Munc18c. Unfortunately there is no previously published data determining the relative abundances of these two proteins in adipocytes. Nonetheless PLA data is consistent to previous findings showing that Syntaxin 1A exists in 20-fold excess over Munc18-1 in PC12 cells (Schutz et al., 2005). I propose that the remaining sortilin-positive vesicles are probably docked to plasma membrane, perhaps *via* a Syntaxin 4/VAMP2 interaction, waiting for SNAP23 and phosphorylated Munc18c to regulate their fusion to the plasma membrane. This explanation underlines the importance of Munc18c concentration as a rate-limiting factor for GLUT4 translocation to plasma membrane not by controling the availability of Syntaxin 4 but rather as a regulator of the insulin responsive GLUT4/sortilin vesicles.

As mentioned above (section 1.4.5.4) the precise role of Munc18c remains elusive. Two studies have suggested that Munc18c plays an inhibitory role for insulin-stimulated translocation of GLUT4 to plasma membrane in adipocytes (Tamori et al., 1998; Thurmond et al., 1998) whereas two others have suggested that Munc18c is required for fusion of GLUT4 vesicle to plasma membrane upon insulin stimulation (Oh et al., 2005; Thurmond et al., 2000). Adipocytes derived from mesennchymal embryonic fibroblasts from Munc18c knockout mice showed increased sensitivity to insulin-stimulated GLUT4 externalization, suggesting an inhibitory role for Munc18c (Kanda et al., 2005). Consistent with the previous

finding, recent *in vitro* studies revealed that Munc18c seems to inhibit the fusion of artificial liposomes mediated by Syntaxin 4, SNAP23 and VAMP2 (Brandie et al., 2008), further supporting the idea of an inhibitory role of Munc18c regarding GLUT4 vesicles fusion to plasma membrane.

Considering all the above, Munc18c concentration emerges as a potential explanation for all these contradictory results. I predict that as the number of sortilin-positive vesicles increases upon addition of insulin, there is a decreased translocation of GLUT4 to plasma membrane as Munc18c is limiting. Expanding further this idea, higher concentrations of Munc18c than the available population of sortilin-positive GLUT4 vesicles would also result into decreased translocation of GLUT4 to plasma membrane after insulin stimulation, since 'empty' Munc18c (not VAMP2-GLUT4 vesicle bound) would bind to Syntaxin 4 resulting into a fusion futile complex. Only equal amounts of Munc18c and sortilin positive GLUT4 vesicles would maximize GLUT4 externalization to plasma membrane. Consistent with this, others have reported diminished GLUT4 translocation upon overexpression of wild-type Munc18c (Thurmond and Pessin, 2000)

All the data presented in this these obtained from PLA, *in vitro* binding and complex assembly assays can be combined into a model that is presented in Figure 7-2 and Figure 7-2. Under basal conditions there are two pools of Syntaxin 4: one in complex with SNAP23 (Figure 7-2 A), the other with VAMP2 and Munc18c (Figure 7-2 B). Cellugyrin-positive/sortilin-negative vesicles (Figure 7-2 C) translocate to the plasma membrane where VAMP2 interacts with the preformed t-SNARE complex (Syntaxin 4/SNAP23) forming a ternary SNARE complex to trigger GLUT4 vesicle fusion with the plasma membrane (Figure 7-2 A). This fusion event is independent of Munc18c. Data from the SNARE complex assembly suggests that the SNAP23/Syntaxin 4 interaction facilitates SNARE complex formation. –This is consistent with previously published data (St-Denis et al., 1999) and could explain SM protein-independent SNARE mediated membrane fusion in this case. The other pool of Syntaxin 4 is in complex with Munc18c and VAMP2. Given that Syntaxin 4 disrupts interaction of Munc18c with VAMP2 (Brandie et al., 2008), and my finding that Syntaxin 4 interacts with VAMP2 *via* their SNARE domains the most likely way for this complex to be formed is by Munc18c interacting *via* binding mode-2 with Syntaxin 4 (through

the N-terminal peptide) this could force the syntaxin to adopt its open conformation enabling VAMP2 to bind the syntaxin's exposed SNARE domain (Figure 7-2 B). Interaction of both Munc18c and VAMP2 with Syntaxin 4 are inhibitory for SNARE complex formation (Figure 4-23 Figure 5-8 and (Brandie et al., 2008)) so it is quite possible that GLUT4 vesicles remain docked at the plasma membrane *via* the Syntaxin 4/VAMP2 interaction. Upon insulin-stimulation there is a shift of VAMP2 from cellugyrin-positive/sortilin-negative to sortilin-positive/cellugyrin-negative GLUT4 vesicles (Figure 7-2 C). This shift represents an increase of the number of VAMP2 carrying sortilin-positive GLUT4 vesicles. As a result these vesicles outnumber Munc18c molecules, the majority of which are in complex with Syntaxin 4/VAMP2. This would drive the GLUT4 vesicles (sortilin-positive) to interact, *via* VAMP2, with individual Syntaxin 4 proteins, present in the plasma membrane – to form non-fusogenic/inhibitory to SNARE complex formation complexes (Figure 7-2 D). At the same time insulin signalling phosphorylates Munc18c (Figure 7-2 B) (Oh and Thurmond, 2006) a process known to facilitate GLUT4 exocytosis (Jewell et al., 2011). The data presented in Figure 5-10 suggest that this phosphorylation of Munc18c serves to lift the inhibitory action of the Syntaxin 4/VAMP2 interaction on SNARE complex assembly and thus drive membrane fusion. Following GLUT4 vesicle fusion with the plasma membrane free phosphorylated Munc18c could be directed to pre-docked sortilin-positive GLUT4 vesicles, which are bound to Syntaxin 4 *via* their VAMP2 protein to facilitate another round of SNARE complex formation and membrane fusion (Figure 7-2 D). Finally, after the effect of insulin, dephosphorylated Munc18c proteins could bind to remaining sortilin-positive GLUT4 vesicles *via* the vesicle anchored VAMP2 and lead them toward to free Syntaxin 4 molecules. Such a Syntaxin 4/Munc18c interaction would displace VAMP2 from Munc18c (Brandie et al., 2008) and subsequently free VAMP2 could bind to the SNARE domain of "open" Syntaxin 4 forming once again the second pool of Syntaxin 4 (Syntaxin 4/Munc18c/VAMP2) (Figure 7-2 B).

The model presented above is a simplified, SNARE/SM protein focused one. A number of other SNARE and Munc18c interacting proteins, such as synip and tomosyn (Min et al., 1999; Widberg et al., 2003), also play a role in regulation of SNARE complex formation. Interaction of Munc18c with its binding partner Doc2β may play a role in the above model as this association releases Munc18c

inhibition of Syntaxin 4 to facilitate exocytosis (Jewell et al., 2008; Ke et al., 2007). However, the findings presented in this thesis provide new insights into the mechanism by which SNAREs regulate GLUT4 translocation to the plasma membrane in insulin-responsive cells.

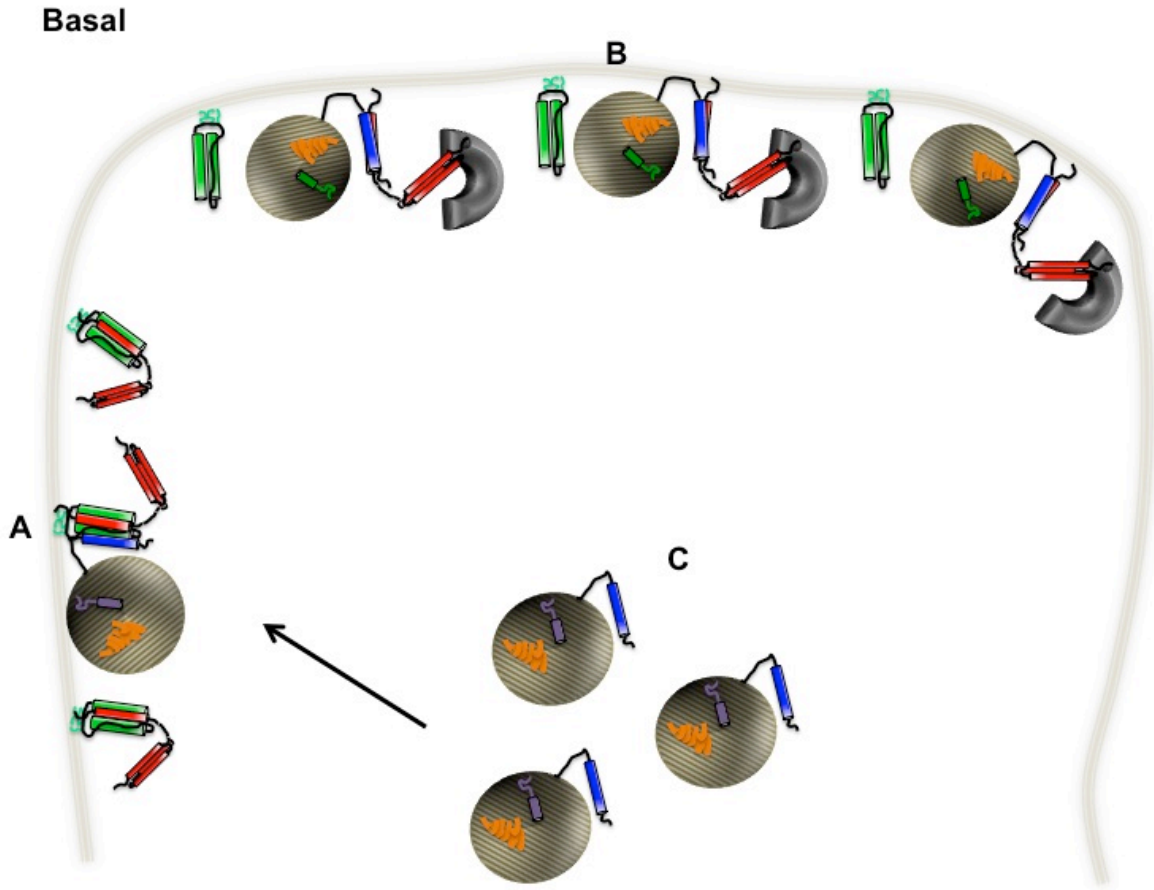

Figure 7-1: Proposed model basal conditions

A: Pool of Syntaxin 4 (red) in complex with SNAP23 (light green). B: Pool of Syntaxin 4 in complex with Munc18c (grey arch) and VAMP2 (blue) – spheres represent GLUT4 (orange) vesicles that either carry cellugyrin (purple) or sortillin (dark green) proteins. C: Under basal conditions cellugyrin positive GLUT4 vesicles fuse with plasma membrane *via* Syntaxin 4/SNAP23 t-SNARE complex in a Munc18c independent fashion and deliver GLUT4 transporter (orange) to plasma membrane.

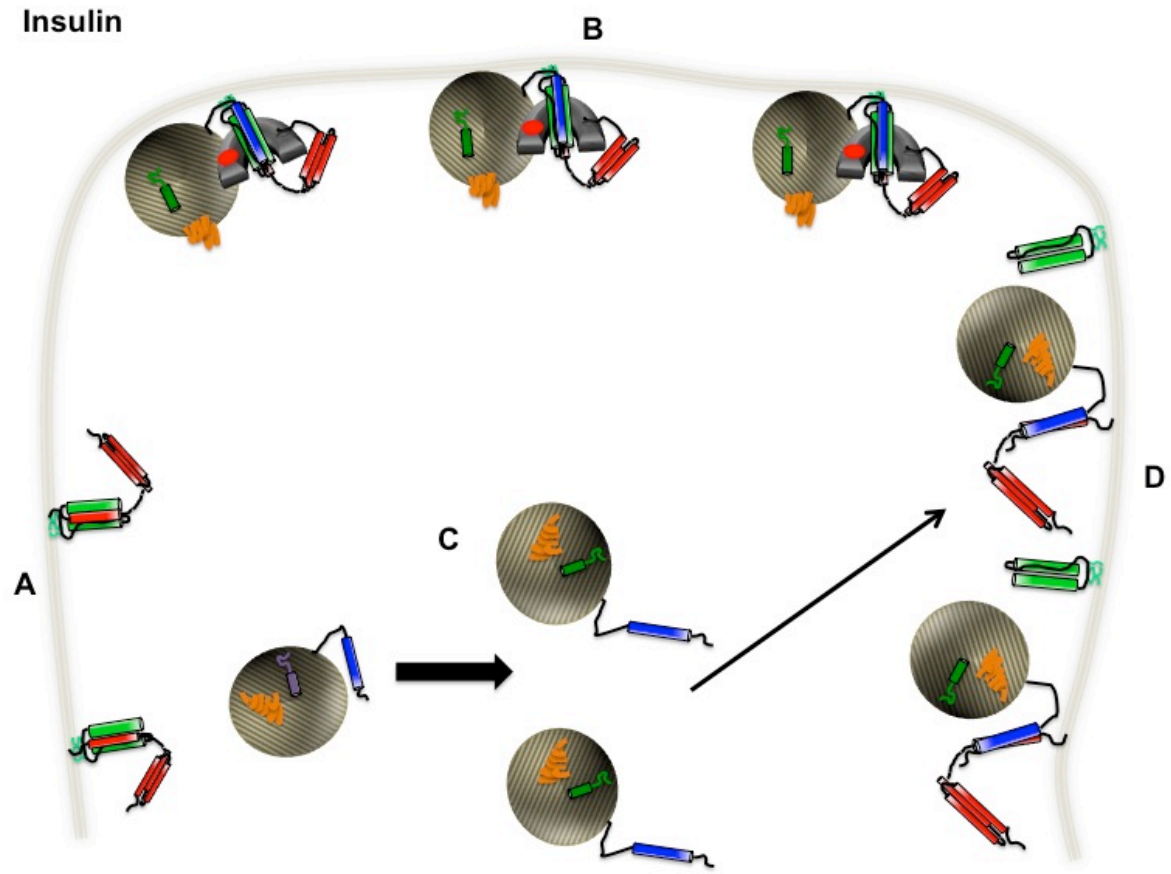

Figure 7-2: Proposed model insulin stimulation

A: Pool of Syntaxin 4 (red) in complex with SNAP23 (light green). B: Pool of Syntaxin 4 in complex with phosphorylated Munc18c (grey arch with red spot) and VAMP2 (blue) – spheres represent GLUT4 (orange) vesicles that either carry cellugyrin (purple) or sortillin (dark green) proteins. C: Upon insulin stimulation there is a shift of VAMP2 from cellugyrin to sortillin positive vesicles. B: Phosphorylated Munc18c (grey arch with red dot) facilitates SNARE complex formation and sortilin positive GLUT4 vesicles that were docked under basal conditions fuse with plasma membrane and Munc18c leaves the site of the fusion. D: Newly formed sortilin positive GLUT4 vesicles interact with distinct Syntaxin 4 molecules (this interaction is not fusogenic) waiting for free phosphorylated Munc18c to facilitate SNARE complex formation.

Appendix

8.1 Proximity Ligation Assay (PLA) raw data and statistical analysis

A Zeiss LSM Pascal Exciter confocal fluorescence microscope was used to examine PLA slides and images were taken using LSM software (Zeiss). Pictures were further studied using Blobfinder software (signal estimation) and the data were statistically analyzed using SPSS (statistical analysis software).

Fibroblasts Munc18c/Sx4

A

Test Statistics[a]

	PLA
Mann-Whitney U	341.000
Wilcoxon W	806.000
Z	-1.614
Asymp. Sig. (2-tailed)	.107

a. Grouping Variable: Conditions

B

PLA raw data

Fibroblasts Sx4/ Munc18c	Basal	Insulin
1	38	45
2	42	48
3	28	53
4	26	26
5	33	39
6	39	42
7	29	29
8	31	51
9	43	40
10	18	38
11	30	36
12	38	28
13	29	44
14	26	51
15	28	19
16	34	26
17	30	35
18	15	38
19	45	42
20	50	47
21	35	13
22	18	38
23	25	26
24	39	24
25	35	34
26	34	32
27	27	20
28	30	41
29	32	38
30	36	32

C

Descriptives

Conditions			Statistic	Std. Error
PLA	Basal	Mean	32.10	1.445
		95% Confidence Interval for Mean Lower Bound	29.14	
		95% Confidence Interval for Mean Upper Bound	35.06	
		5% Trimmed Mean	32.09	
		Median	31.50	
		Variance	62.645	
		Std. Deviation	7.915	
		Minimum	15	
		Maximum	50	
		Range	35	
		Interquartile Range	10	
		Skewness	-.033	.427
		Kurtosis	.260	.833
	Insulin	Mean	35.83	1.843
		95% Confidence Interval for Mean Lower Bound	32.06	
		95% Confidence Interval for Mean Upper Bound	39.60	
		5% Trimmed Mean	36.07	
		Median	38.00	
		Variance	101.868	
		Std. Deviation	10.093	
		Minimum	13	
		Maximum	53	
		Range	40	
		Interquartile Range	15	
		Skewness	-.315	.427
		Kurtosis	-.416	.833

Figure 8-1: PLA raw data and statistical analysis for Munc18c/Syntaxin 4 in 3T3-L1 fibroblast cells

A: Results of Mann-Whitney non-parametrical statistical tests of data from Figure 3-4. B: Raw data from Figure 3-4. C: Descriptive statistics of raw data from B.

Adipocytes Munc18c/Sx4

A

Test Statistics[a]

	PLA
Mann-Whitney U	636.500
Wilcoxon W	1302.500
Z	-.130
Asymp. Sig. (2-tailed)	.897

a. Grouping Variable: Conditions

B

PLA raw data

Adipocytes Sx4/ Munc18c	Basal	Insulin
1	20	42
2	20	67
3	21	63
4	17	22
5	17	41
6	54	72
7	32	46
8	32	22
9	19	48
10	33	31
11	25	34
12	25	33
13	24	53
14	25	57
15	24	14
16	22	17
17	28	21
18	25	28
19	22	32
20	45	15
21	32	16
22	30	34
23	37	20
24	40	15
25	32	16
26	22	14
27	37	18
28	14	25
29	34	20
30	37	20
31	20	20
32	17	29
33	42	25
34	30	25
35	24	47
36	30	26

C

Descriptives

Conditions				Statistic	Std. Error
PLA	Basal	Mean		28.00	1.479
		95% Confidence Interval for Mean	Lower Bound	25.00	
			Upper Bound	31.00	
		5% Trimmed Mean		27.48	
		Median		25.00	
		Variance		78.800	
		Std. Deviation		8.877	
		Minimum		14	
		Maximum		54	
		Range		40	
		Interquartile Range		12	
		Skewness		.842	.393
		Kurtosis		.717	.768
	Insulin	Mean		31.33	2.668
		95% Confidence Interval for Mean	Lower Bound	25.92	
			Upper Bound	36.75	
		5% Trimmed Mean		30.16	
		Median		25.50	
		Variance		256.229	
		Std. Deviation		16.007	
		Minimum		14	
		Maximum		72	
		Range		58	
		Interquartile Range		22	
		Skewness		1.063	.393
		Kurtosis		.250	.768

Figure 8-2: PLA raw data and statistical analysis for Munc18c/Syntaxin 4 in 3T3-L1 adipocyte cells.

A: Results of Mann-Whitney non-parametrical statistical tests of data from Figure 3-4. B: Raw data from Figure 3-4. C: Descriptive statistics of raw data from B.

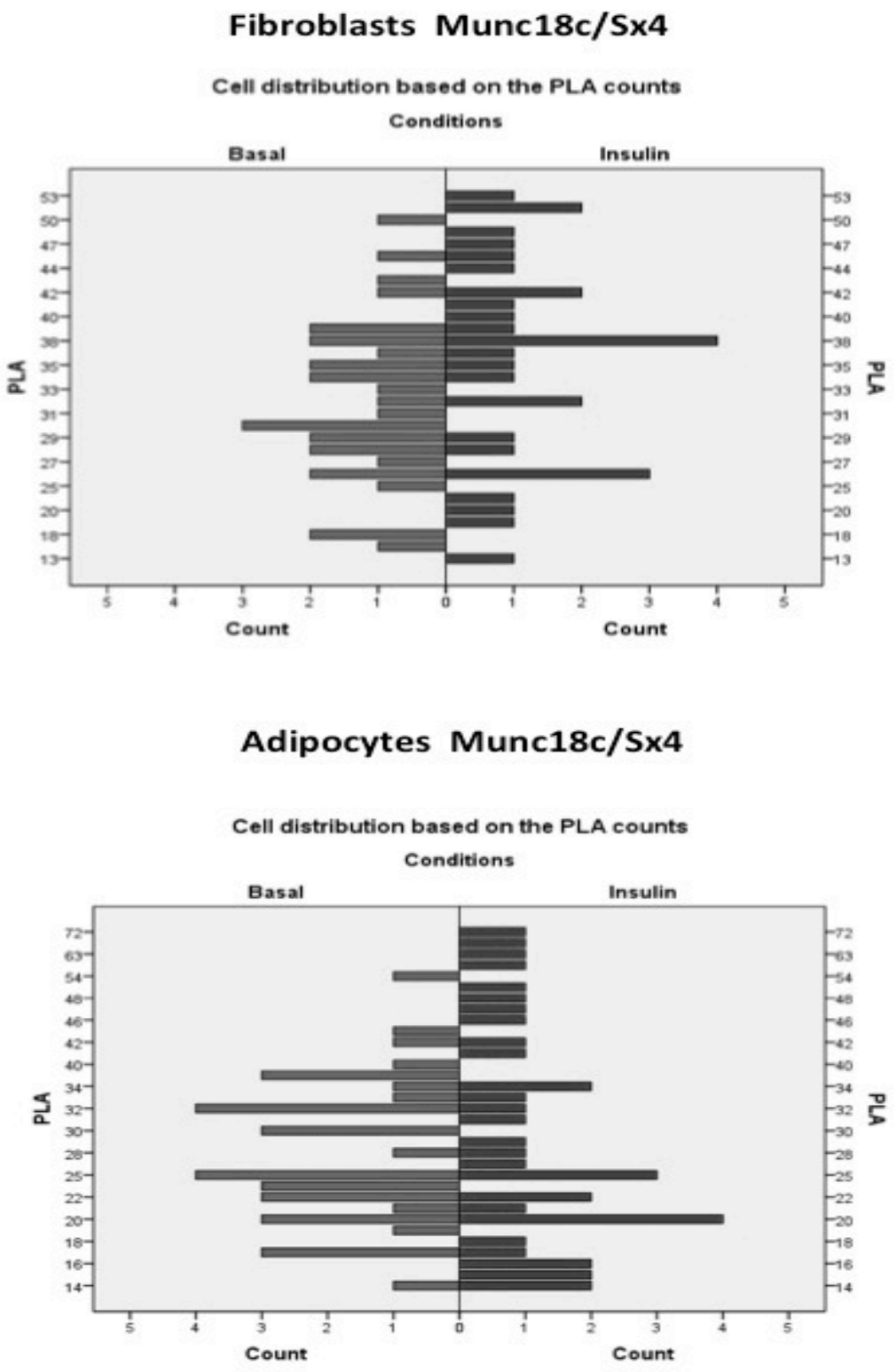

Figure 8-3: 3T3-L1 cell distribution based on PLA results for Munc18c/Syntaxin 4

Cell distribution based on PLA results for Munc18c/Syntaxin 4 (Figure 3-4) under basal conditions and upon insulin stimulation of fibroblasts (upper panel) and adipocytes (lower panel).

Fibroblasts Munc18c/VAMP2

A

Test Statistics[a]

	PLA
Mann-Whitney U	1082.000
Wilcoxon W	2357.000
Z	-.499
Asymp. Sig. (2-tailed)	.618

a. Grouping Variable: Conditions

B

PLA raw data

Fibroblasts VAMP2/ Munc18c	Basal	Insulin
1	17	24
2	14	16
3	19	21
4	25	27
5	17	23
6	14	13
7	22	14
8	32	15
9	37	35
10	24	17
11	35	16
12	55	42
13	48	32
14	39	41
15	29	49
16	45	31
17	44	38
18	38	49
19	21	29
20	10	31
21	13	19
22	12	45
23	11	28
24	18	26
25	15	20
26	35	15
27	17	24
28	15	29
29	21	22
30	28	15
31	18	15
32	12	21
33	31	45
34	22	38
35	28	23
36	36	15
37	28	24
38	23	18
39	30	17
40	30	24
41	12	18
42	15	21
43	25	17
44	14	30
45	15	17
46	21	16
47	25	
48	13	
49	32	
50	37	

C

Descriptives

Conditions				Statistic	Std. Error
PLA	Basal	Mean		24.74	1.534
		95% Confidence Interval for Mean	Lower Bound	21.66	
			Upper Bound	27.82	
		5% Trimmed Mean		24.10	
		Median		22.50	
		Variance		117.625	
		Std. Deviation		10.846	
		Minimum		10	
		Maximum		55	
		Range		45	
		Interquartile Range		17	
		Skewness		.745	.337
		Kurtosis		-.034	.662
	Insulin	Mean		25.33	1.493
		95% Confidence Interval for Mean	Lower Bound	22.32	
			Upper Bound	28.33	
		5% Trimmed Mean		24.69	
		Median		23.00	
		Variance		102.536	
		Std. Deviation		10.126	
		Minimum		13	
		Maximum		49	
		Range		36	
		Interquartile Range		14	
		Skewness		.918	.350
		Kurtosis		-.123	.688

Figure 8-4: PLA raw data and statistical analysis for Munc18c/VAMP2 in 3T3-L1 fibroblast cells

A: Results of Mann-Whitney non-parametrical statistical tests of data from Figure 3-5. B: Raw data from Figure 3-5. C: Descriptive statistics of raw data from B.

Adipocytes Munc18c/VAMP2

A

Test Statistics[a]

	PLA
Mann-Whitney U	807.000
Wilcoxon W	1587.000
Z	-.635
Asymp. Sig. (2-tailed)	.526

a. Grouping Variable: Conditions

B

PLA raw data

Adipocytes VAMP2/ Munc18c	Basal	Insulin
1	16	21
2	17	16
3	23	13
4	17	25
5	21	16
6	13	18
7	17	19
8	24	20
9	18	19
10	27	23
11	20	17
12	12	16
13	16	20
14	17	19
15	20	19
16	17	23
17	18	15
18	17	18
19	19	14
20	15	18
21	14	17
22	24	27
23	11	18
24	17	16
25	12	18
26	15	25
27	19	28
28	18	16
29	20	14
30	15	15
31	23	14
32	20	13
33	14	15
34	14	26
35	11	11
36	26	21
37	11	11
38	17	19
39	11	18
40		18
41		16
42		16
43		20
44		15
45		12

C

Descriptives

Conditions				Statistic	Std. Error
PLA	Basal	Mean		17.33	.668
		95% Confidence Interval for Mean	Lower Bound	15.98	
			Upper Bound	18.68	
		5% Trimmed Mean		17.18	
		Median		17.00	
		Variance		17.386	
		Std. Deviation		4.170	
		Minimum		11	
		Maximum		27	
		Range		16	
		Interquartile Range		6	
		Skewness		.417	.378
		Kurtosis		-.228	.741
	Insulin	Mean		17.96	.605
		95% Confidence Interval for Mean	Lower Bound	16.74	
			Upper Bound	19.18	
		5% Trimmed Mean		17.81	
		Median		18.00	
		Variance		16.498	
		Std. Deviation		4.062	
		Minimum		11	
		Maximum		28	
		Range		17	
		Interquartile Range		5	
		Skewness		.655	.354
		Kurtosis		.210	.695

Figure 8-5: PLA raw data and statistical analysis for Munc18c/VAMP2 in 3T3-L1 adipocyte cells

A: Results of Mann-Whitney non-parametrical statistical tests of data from Figure 3-5. B: Raw data from Figure 3-5. C: Descriptive statistics of raw data from B.

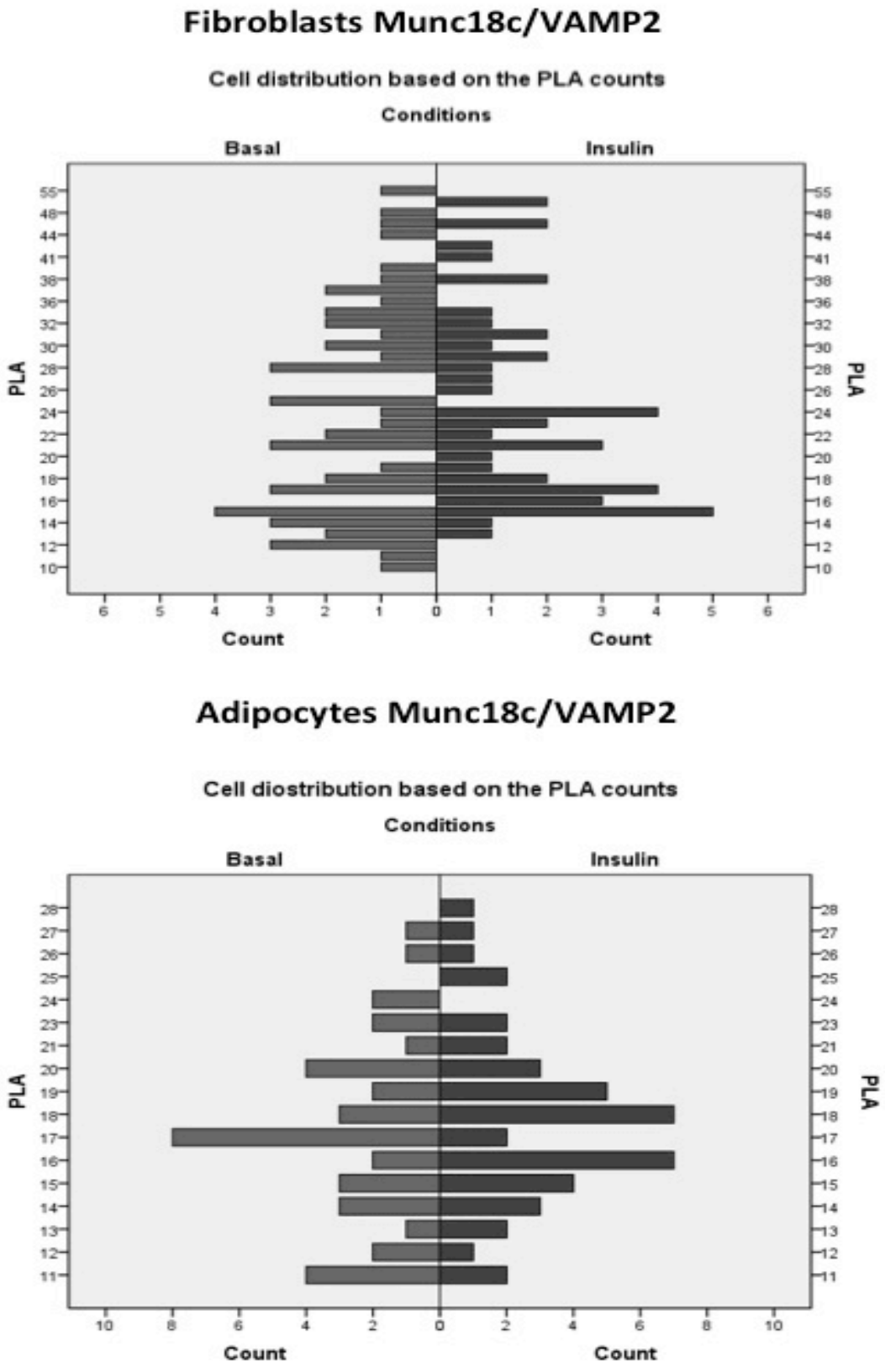

Figure 8-6: 3T3-L1 cell distribution based on PLA results for Munc18c/VAMP2

Cell distribution based on PLA results for Munc18c/VAMP2 (Figure 3-5) under basal conditions and upon insulin stimulation of fibroblasts (upper panel) and adipocytes (lower panel).

Fibroblasts SNAP23/Munc18c

A

Test Statistics[a]

	PLA
Mann-Whitney U	6.500
Wilcoxon W	867.500
Z	-7.737
Asymp. Sig. (2-tailed)	.000

a. Grouping Variable: Conditions

B

PLA raw data		
Fibroblasts SNAP23/ Munc18c	Basal	Insulin
1	16	62
2	8	24
3	18	42
4	15	41
5	10	63
6	7	30
7	12	28
8	12	23
9	4	62
10	25	58
11	14	35
12	8	34
13	17	48
14	11	46
15	16	31
16	13	36
17	17	29
18	15	46
19	18	38
20	14	64
21	30	62
22	12	82
23	9	52
24	15	52
25	6	40
26	11	43
27	18	57
28	3	56
29	14	40
30	10	45
31	8	58
32	13	48
33	9	44
34	4	45
35	13	46
36	11	39
37	4	47
38	4	52
39	7	48
40	9	49
41	17	50

C

Descriptives

Conditions				Statistic	Std. Error
PLA	Basal	Mean		12.12	.876
		95% Confidence Interval for Mean	Lower Bound	10.35	
			Upper Bound	13.89	
		5% Trimmed Mean		11.76	
		Median		12.00	
		Variance		31.460	
		Std. Deviation		5.609	
		Minimum		3	
		Maximum		30	
		Range		27	
		Interquartile Range		8	
		Skewness		.788	.369
		Kurtosis		1.573	.724
	Insulin	Mean		46.22	1.920
		95% Confidence Interval for Mean	Lower Bound	42.34	
			Upper Bound	50.10	
		5% Trimmed Mean		46.00	
		Median		46.00	
		Variance		151.076	
		Std. Deviation		12.291	
		Minimum		23	
		Maximum		82	
		Range		59	
		Interquartile Range		16	
		Skewness		.363	.369
		Kurtosis		.560	.724

Figure 8-7: PLA raw data and statistical analysis for Munc18c/SNAP23 in 3T3-L1 fibroblast cells

A: Results of Mann-Whitney non-parametrical statistical tests of data from Figure 3-6. B: Raw data from Figure 3-6. C: Descriptive statistics of raw data from B.

Adipocytes SNAP23/Munc18c

A

Test Statistics[a]

	PLA
Mann-Whitney U	.000
Wilcoxon W	3741.000
Z	-10.445
Asymp. Sig. (2-tailed)	.000

a. Grouping Variable: Conditions

B

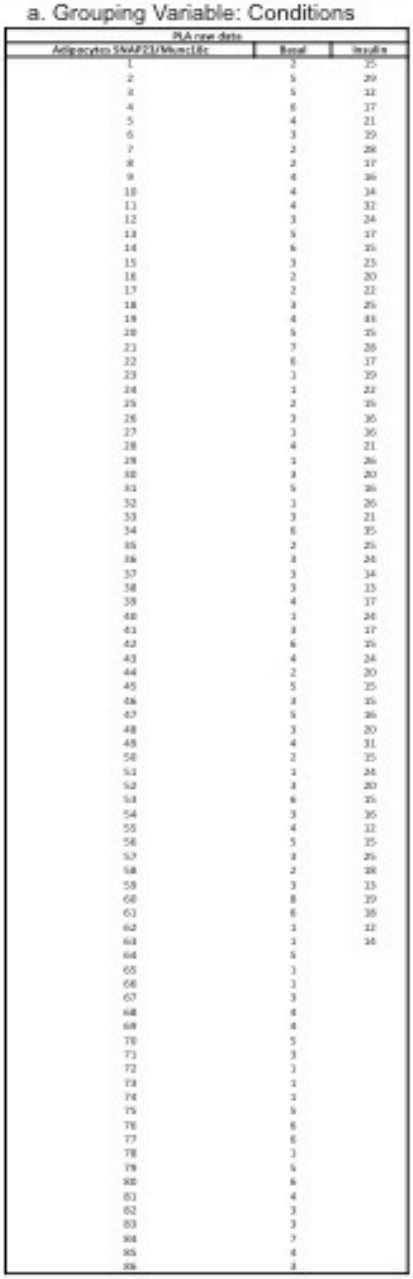

C

Descriptives

Conditions				Statistic	Std. Error
PLA	Basal	Mean		3.48	.188
		95% Confidence Interval for Mean	Lower Bound	3.10	
			Upper Bound	3.85	
		5% Trimmed Mean		3.42	
		Median		3.00	
		Variance		3.052	
		Std. Deviation		1.747	
		Minimum		1	
		Maximum		8	
		Range		7	
		Interquartile Range		3	
		Skewness		.277	.260
		Kurtosis		-.655	.514
	Insulin	Mean		19.65	.700
		95% Confidence Interval for Mean	Lower Bound	18.25	
			Upper Bound	21.05	
		5% Trimmed Mean		19.32	
		Median		18.00	
		Variance		30.908	
		Std. Deviation		5.560	
		Minimum		12	
		Maximum		35	
		Range		23	
		Interquartile Range		9	
		Skewness		.861	.302
		Kurtosis		.113	.595

Figure 8-8: PLA raw data and statistical analysis for Munc18c/SNAP23 in 3T3-L1 adipocyte cells

A: Results of Mann-Whitney non-parametrical statistical tests of data from Figure 3-6. B: Raw data from Figure 3-6. C: Descriptive statistics of raw data from B.

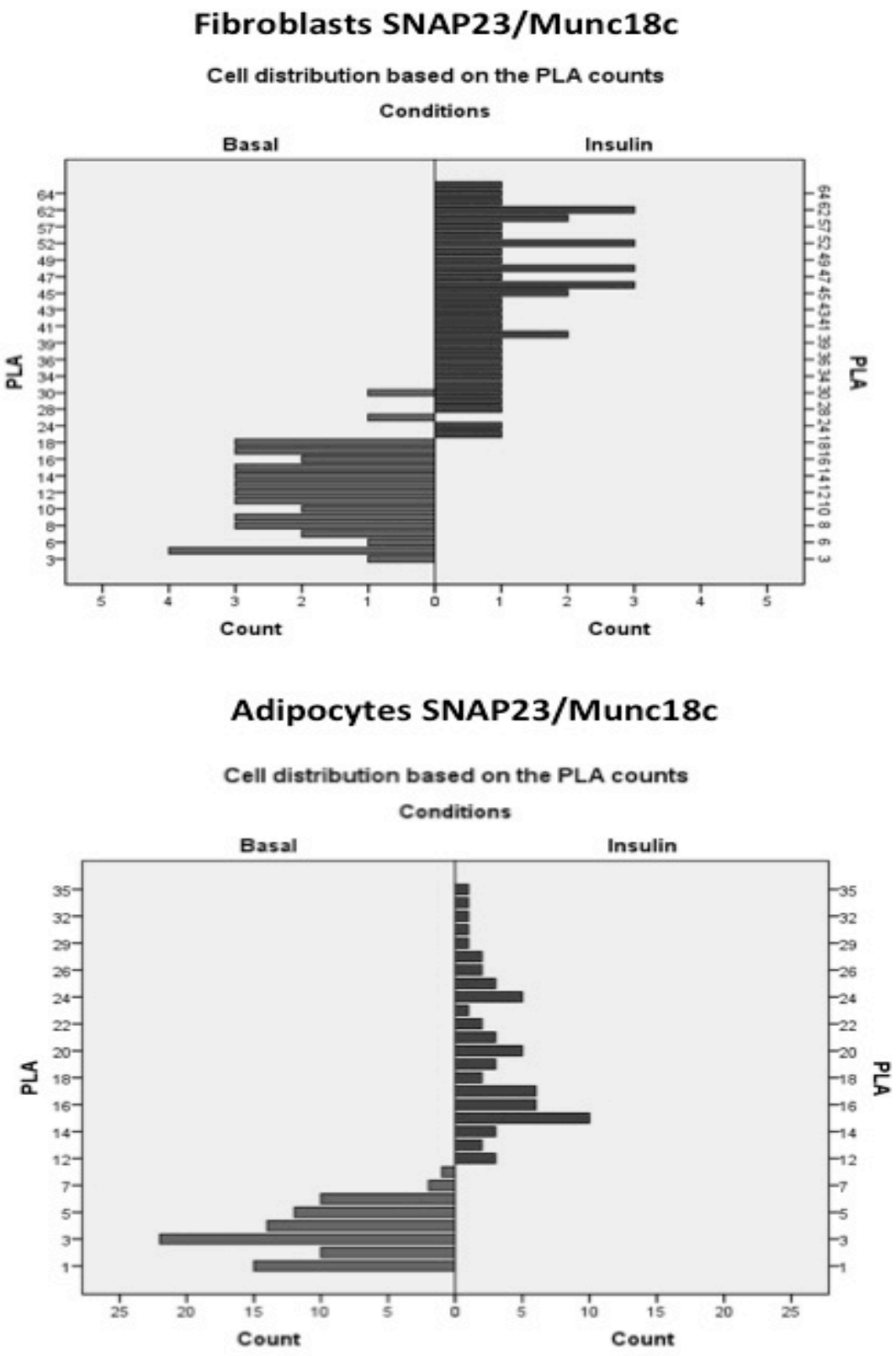

Figure 8-9: 3T3-L1 cell distribution based on PLA results for Munc18c/SNAP23

Cell distribution based on PLA results for Munc18c/SNAP23 (Figure 3-6) under basal conditions and upon insulin stimulation of fibroblasts (upper panel) and adipocytes (lower panel).

Fibroblasts SNAP23/Sx4

A

Test Statistics[a]

	PLA
Mann-Whitney U	375.500
Wilcoxon W	840.500
Z	-1.102
Asymp. Sig. (2-tailed)	.271

a. Grouping Variable: Conditions

B

PLA raw data		
Fibroblasts SNAP23/Sx4	Basal	Insulin
1	374	525
2	394	525
3	339	303
4	291	330
5	236	250
6	550	523
7	494	502
8	246	446
9	503	362
10	310	450
11	423	321
12	563	436
13	428	585
14	532	450
15	652	610
16	685	526
17	453	488
18	299	389
19	378	463
20	423	396
21	526	299
22	347	450
23	508	485
24	496	389
25	258	593
26	362	497
27	428	421
28	386	411
29	403	658
30	438	492

C

Descriptives

	Conditions			Statistic	Std. Error
PLA	Basal	Mean		424.17	20.542
		95% Confidence Interval for Mean	Lower Bound	382.15	
			Upper Bound	466.18	
		5% Trimmed Mean		420.56	
		Median		423.00	
		Variance		12659.109	
		Std. Deviation		112.513	
		Minimum		236	
		Maximum		685	
		Range		449	
		Interquartile Range		159	
		Skewness		.364	.427
		Kurtosis		-.109	.833
	Insulin	Mean		452.50	17.790
		95% Confidence Interval for Mean	Lower Bound	416.11	
			Upper Bound	488.89	
		5% Trimmed Mean		452.31	
		Median		450.00	
		Variance		9494.741	
		Std. Deviation		97.441	
		Minimum		250	
		Maximum		658	
		Range		408	
		Interquartile Range		135	
		Skewness		-.055	.427
		Kurtosis		-.234	.833

Figure 8-10: PLA raw data and statistical analysis for Syntaxin 4/SNAP23 in 3T3-L1 fibroblast cells

A: Results of Mann-Whitney non-parametrical statistical tests of data from Figure 3-7. B: Raw data from Figure 3-7. C: Descriptive statistics of raw data from B.

Adipocytes SNAP23/Sx4

A

Test Statistics[a]

	PLA
Mann-Whitney U	620.000
Wilcoxon W	1286.000
Z	-.316
Asymp. Sig. (2-tailed)	.752

a. Grouping Variable: Conditions

B

PLA raw data		
Adipocytes SNAP23/Sx4	Basal	Insulin
1	28	19
2	19	39
3	21	27
4	21	28
5	18	30
6	45	28
7	37	17
8	24	21
9	20	25
10	23	22
11	20	35
12	28	36
13	23	34
14	28	29
15	23	27
16	35	20
17	32	32
18	35	34
19	36	25
20	38	28
21	15	32
22	24	20
23	35	13
24	25	31
25	29	30
26	25	33
27	35	27
28	15	36
29	30	23
30	28	23
31	17	32
32	33	29
33	21	14
34	28	25
35	22	23
36	30	26

C

Descriptives

Conditions			Statistic	Std. Error
PLA	Basal	Mean	26.83	1.198
		95% Confidence Interval for Mean Lower Bound	24.40	
		95% Confidence Interval for Mean Upper Bound	29.26	
		5% Trimmed Mean	26.65	
		Median	26.50	
		Variance	51.629	
		Std. Deviation	7.185	
		Minimum	15	
		Maximum	45	
		Range	30	
		Interquartile Range	12	
		Skewness	.394	.393
		Kurtosis	-.349	.768
	Insulin	Mean	27.03	1.044
		95% Confidence Interval for Mean Lower Bound	24.91	
		95% Confidence Interval for Mean Upper Bound	29.15	
		5% Trimmed Mean	27.19	
		Median	27.50	
		Variance	39.228	
		Std. Deviation	6.263	
		Minimum	13	
		Maximum	39	
		Range	26	
		Interquartile Range	9	
		Skewness	-.332	.393
		Kurtosis	-.293	.768

Figure 8-11: PLA raw data and statistical analysis for Syntaxin 4/SNAP23 in 3T3-L1 adipocyte cells

A: Results of Mann-Whitney non-parametrical statistical tests of data from Figure 3-7. B: Raw data from Figure 3-7. C: Descriptive statistics of raw data from B.

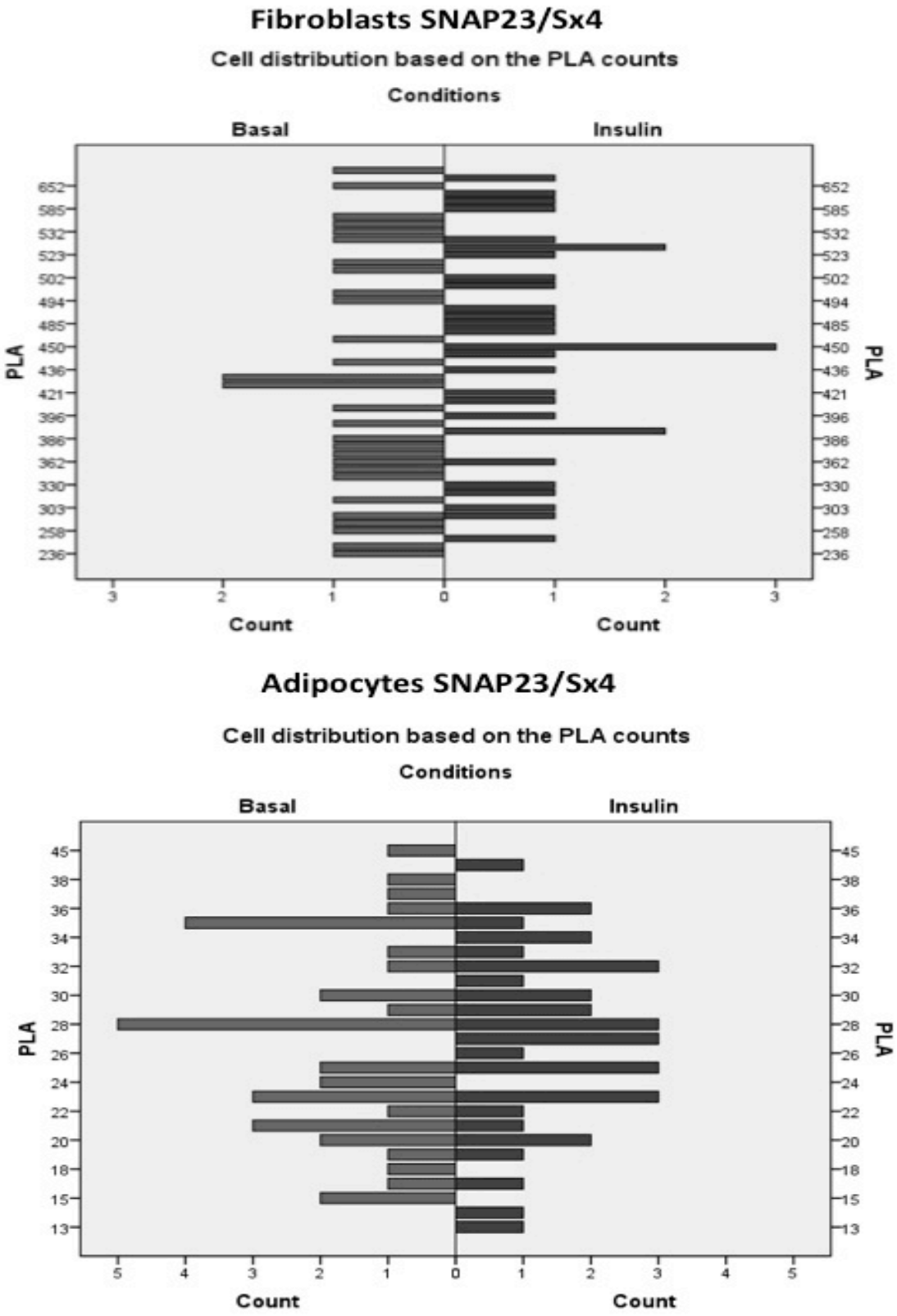

Figure 8-12: 3T3-L1 cell distribution based on PLA results for Syntaxin 4/SNAP23

Cell distribution based on PLA results for Syntaxin 4/SNAP23 (Figure 3-7) under basal conditions and upon insulin stimulation of fibroblasts (upper panel) and adipocytes (lower panel).

Fibroblasts VAMP2/Sx4

A

Test Statistics[a]

	PLA
Mann-Whitney U	396.000
Wilcoxon W	861.000
Z	-.798
Asymp. Sig. (2-tailed)	.425

a. Grouping Variable: Conditions

B

PLA raw data		
Fibroblasts VAMP2/Sx4	Basal	Insulin
1	201	401
2	201	316
3	242	509
4	105	284
5	329	210
6	90	229
7	282	373
8	261	322
9	226	220
10	237	292
11	138	347
12	249	385
13	305	181
14	271	260
15	247	399
16	449	339
17	247	463
18	259	273
19	150	356
20	380	386
21	270	266
22	288	300
23	352	288
24	428	311
25	382	221
26	348	198
27	296	165
28	199	201
29	489	148
30	399	256

C

Descriptives

Conditions				Statistic	Std. Error
PLA	Basal	Mean		277.33	17.773
		95% Confidence Interval for Mean	Lower Bound	240.98	
			Upper Bound	313.68	
		5% Trimmed Mean		276.44	
		Median		265.50	
		Variance		9476.506	
		Std. Deviation		97.347	
		Minimum		90	
		Maximum		489	
		Range		399	
		Interquartile Range		129	
		Skewness		.191	.427
		Kurtosis		-.136	.833
	Insulin	Mean		296.63	16.080
		95% Confidence Interval for Mean	Lower Bound	263.75	
			Upper Bound	329.52	
		5% Trimmed Mean		293.63	
		Median		290.00	
		Variance		7756.930	
		Std. Deviation		88.073	
		Minimum		148	
		Maximum		509	
		Range		361	
		Interquartile Range		140	
		Skewness		.418	.427
		Kurtosis		-.161	.833

Figure 8-13: PLA raw data and statistical analysis for Syntaxin 4/VAMP2 in 3T3-L1 fibroblast cells

A: Results of Mann-Whitney non-parametrical statistical tests of data from Figure 3-8. B: Raw data from Figure 3-8. C: Descriptive statistics of raw data from B.

Adipocytes VAMP2/Sx4

A

Test Statistics[a]

	PLA
Mann-Whitney U	512.000
Wilcoxon W	1178.000
Z	-1.535
Asymp. Sig. (2-tailed)	.125

a. Grouping Variable: Conditions

B

PLA raw data		
Adipocytes VAMP2/Sx4	Basal	Insulin
1	25	10
2	19	22
3	20	26
4	25	20
5	29	22
6	20	23
7	34	28
8	11	15
9	22	32
10	19	27
11	16	25
12	17	27
13	21	13
14	30	26
15	21	23
16	18	27
17	20	20
18	19	16
19	28	19
20	17	19
21	15	10
22	12	27
23	10	20
24	12	29
25	15	18
26	37	29
27	20	28
28	19	28
29	26	27
30	21	25
31	24	18
32	27	24
33	25	27
34	25	26
35	20	28
36	28	23

C

Descriptives

Conditions				Statistic	Std. Error
PLA	Basal	Mean		21.31	1.032
		95% Confidence Interval for Mean	Lower Bound	19.21	
			Upper Bound	23.40	
		5% Trimmed Mean		21.11	
		Median		20.00	
		Variance		38.333	
		Std. Deviation		6.191	
		Minimum		10	
		Maximum		37	
		Range		27	
		Interquartile Range		8	
		Skewness		.392	.393
		Kurtosis		.181	.768
	Insulin	Mean		22.97	.912
		95% Confidence Interval for Mean	Lower Bound	21.12	
			Upper Bound	24.82	
		5% Trimmed Mean		23.27	
		Median		24.50	
		Variance		29.913	
		Std. Deviation		5.469	
		Minimum		10	
		Maximum		32	
		Range		22	
		Interquartile Range		8	
		Skewness		-.828	.393
		Kurtosis		.083	.768

Figure 8-14: PLA raw data and statistical analysis for Syntaxin 4/VAMP2 in 3T3-L1 adipocyte cells

A: Results of Mann-Whitney non-parametrical statistical tests of data from Figure 3-8. B: Raw data from Figure 3-8. C: Descriptive statistics of raw data from B.

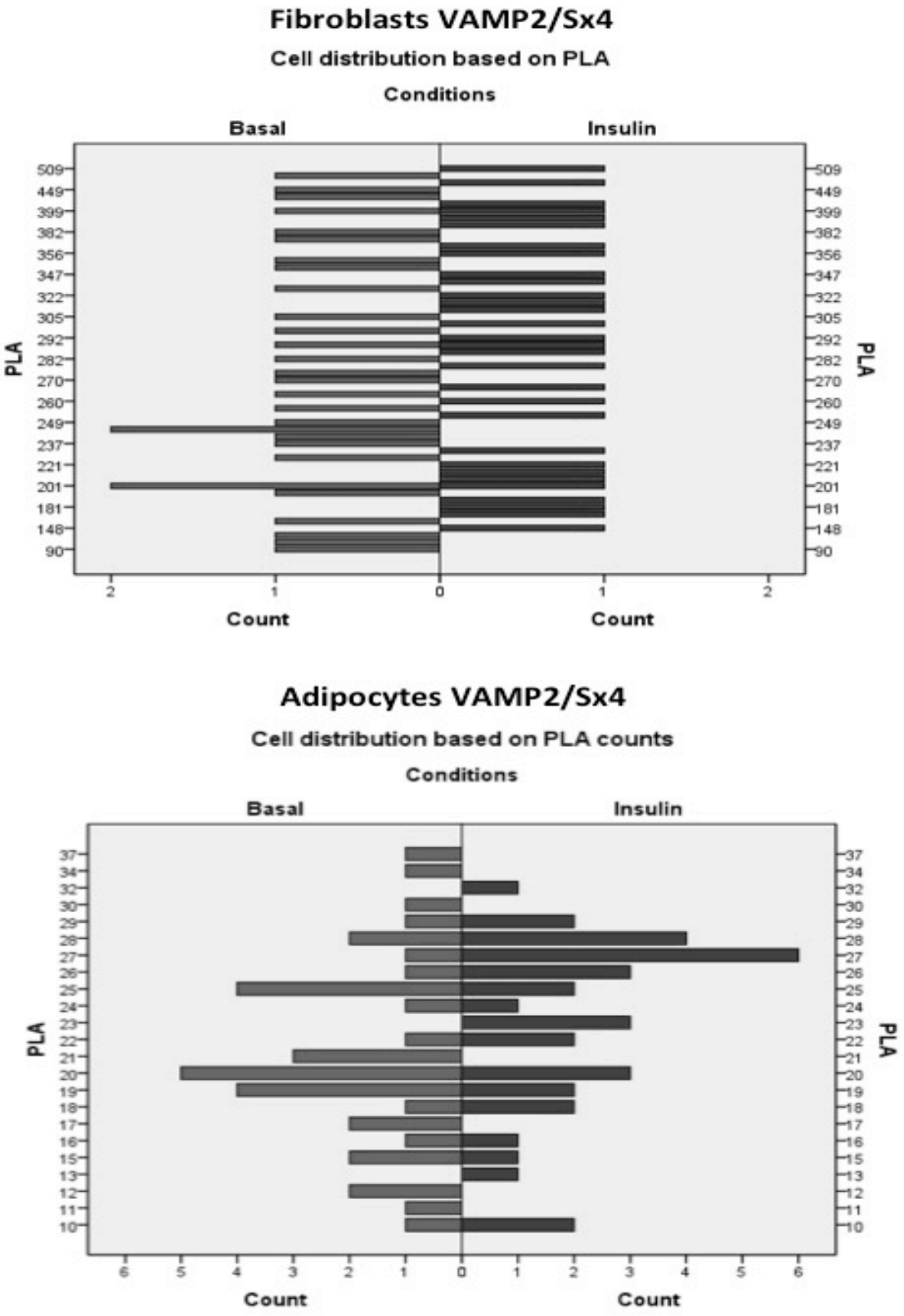

Figure 8-15: 3T3-L1 cell distribution based on PLA results for Syntaxin 4/VAMP2

Cell distribution based on PLA results for Syntaxin 4/VAMP2 (Figure 3-8) under basal conditions and upon insulin stimulation of fibroblasts (upper panel) and adipocytes (lower panel).

Fibroblasts VAMP2/SNAP23

A

Test Statistics[a]

	PLA
Mann-Whitney U	6.000
Wilcoxon W	996.000
Z	-8.031
Asymp. Sig. (2-tailed)	.000

a. Grouping Variable: Conditions

B

PLA raw data

Fibroblasts VAMP2/ SNAP23	Basal	Insulin
1	30	37
2	13	25
3	9	33
4	8	33
5	12	78
6	4	50
7	29	40
8	9	38
9	10	49
10	14	58
11	20	40
12	1	59
13	1	64
14	14	41
15	14	42
16	8	38
17	5	110
18	8	55
19	3	45
20	7	72
21	2	90
22	5	100
23	9	60
24	4	58
25	12	62
26	17	74
27	12	43
28	14	48
29	7	35
30	9	85
31	15	28
32	8	53
33	10	52
34	4	68
35	13	55
36	16	43
37	12	32
38	7	56
39	2	89
40	1	25
41	3	50
42	10	55
43	7	56
44	12	52

C

Descriptives

Conditions				Statistic	Std. Error
PLA	Basal	Mean		9.77	.963
		95% Confidence Interval for Mean	Lower Bound	7.83	
			Upper Bound	11.71	
		5% Trimmed Mean		9.21	
		Median		9.00	
		Variance		40.784	
		Std. Deviation		6.386	
		Minimum		1	
		Maximum		30	
		Range		29	
		Interquartile Range		8	
		Skewness		1.230	.357
		Kurtosis		2.494	.702
	Insulin	Mean		54.00	2.954
		95% Confidence Interval for Mean	Lower Bound	48.04	
			Upper Bound	59.96	
		5% Trimmed Mean		52.84	
		Median		52.00	
		Variance		384.047	
		Std. Deviation		19.597	
		Minimum		25	
		Maximum		110	
		Range		85	
		Interquartile Range		22	
		Skewness		.958	.357
		Kurtosis		.780	.702

Figure 8-16: PLA raw data and statistical analysis for SNAP23/VAMP2 in 3T3-L1 fibroblast cells

A: Results of Mann-Whitney non-parametrical statistical tests of data from Figure 3-9. B: Raw data from Figure 3-9. C: Descriptive statistics of raw data from B.

Adipocytes VAMP2/SNAP23

A

Test Statistics[a]

	PLA
Mann-Whitney U	11.500
Wilcoxon W	677.500
Z	-7.174
Asymp. Sig. (2-tailed)	.000

a. Grouping Variable: Conditions

B

PLA raw data		
Adipocytes VAMP2/ SNAP23	Basal	Insulin
1	28	17
2	28	49
3	15	34
4	7	52
5	20	39
6	16	22
7	17	49
8	7	48
9	24	34
10	3	38
11	13	30
12	15	45
13	8	37
14	8	40
15	4	67
16	7	33
17	9	33
18	10	32
19	7	45
20	25	55
21	6	40
22	8	36
23	8	37
24	15	35
25	20	30
26	6	31
27	12	35
28	11	45
29	13	40
30	12	40
31	8	85
32	9	35
33	19	60
34	15	68
35	9	37
36	13	40

C

Descriptives

Conditions				Statistic	Std. Error
PLA	Basal	Mean		12.64	1.090
		95% Confidence Interval for Mean	Lower Bound	10.43	
			Upper Bound	14.85	
		5% Trimmed Mean		12.30	
		Median		11.50	
		Variance		42.752	
		Std. Deviation		6.538	
		Minimum		3	
		Maximum		28	
		Range		25	
		Interquartile Range		8	
		Skewness		.901	.393
		Kurtosis		.149	.768
	Insulin	Mean		41.47	2.186
		95% Confidence Interval for Mean	Lower Bound	37.03	
			Upper Bound	45.91	
		5% Trimmed Mean		40.71	
		Median		38.50	
		Variance		172.028	
		Std. Deviation		13.116	
		Minimum		17	
		Maximum		85	
		Range		68	
		Interquartile Range		13	
		Skewness		1.322	.393
		Kurtosis		2.757	.768

Figure 8-17: PLA raw data and statistical analysis for SNAP23/VAMP2 in 3T3-L1 adipocyte cells

A: Results of Mann-Whitney non-parametrical statistical tests of data from Figure 3-9. B: Raw data from Figure 3-9. C: Descriptive statistics of raw data from B.

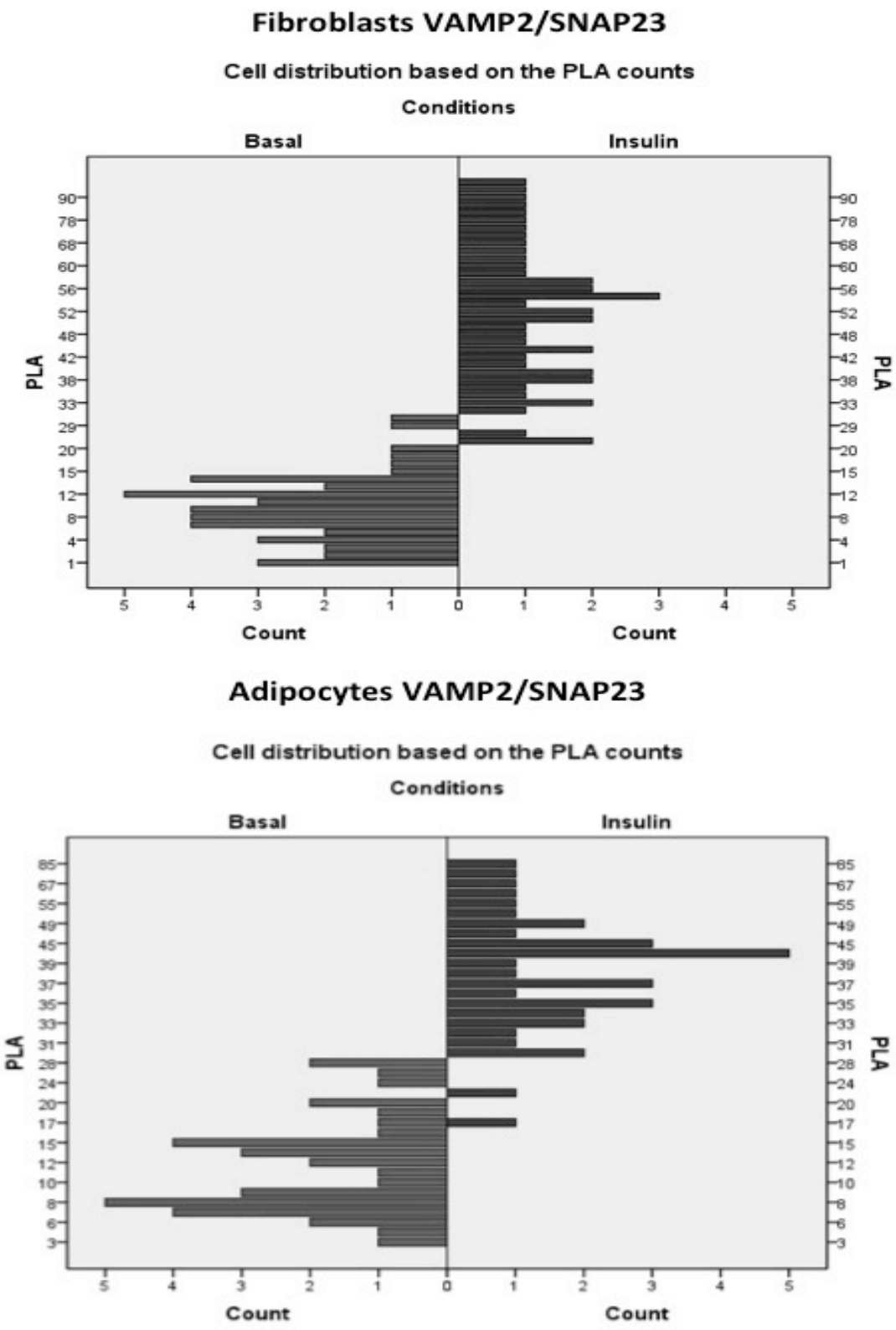

Figure 8-18: 3T3-L1 cell distribution based on PLA results for SNAP23/VAMP2

Cell distribution based on PLA results for SNAP23/VAMP2 (Figure 3-9) under basal conditions and upon insulin stimulation of fibroblasts (upper panel) and adipocytes (lower panel).

Fibroblasts Cellugyrin/Sortilin

A

Test Statistics[a]

	PLA
Mann-Whitney U	1736.500
Wilcoxon W	3881.500
Z	-.853
Asymp. Sig. (2-tailed)	.394

a. Grouping Variable: conditions

B

PLA raw data

Fibroblasts Cellugyrin/Sortilin	Basal	Insulin
1	0	1
2	1	1
3	2	1
4	1	2
5	0	1
6	1	0
7	0	0
8	0	0
9	0	1
10	2	1
11	1	2
12	1	1
13	0	0
14	1	0
15	0	0
16	0	0
17	1	0
18	1	0
19	2	1
20	0	0
21	0	0
22	1	0
23	1	0
24	0	0
25	1	0
26	0	0
27	0	0
28	1	0
29	0	2
30	0	1
31	0	0
32	1	1
33	1	0
34	0	1
35	0	0
36	0	1
37	0	0
38	3	4
39	2	1
40	1	0
41	4	0
42	1	0
43	1	0
44	0	2
45	0	0
46	0	0
47	3	0
48	0	0
49	0	0
50	1	1
51	0	0
52	0	0
53	0	1
54	1	0
55	0	0
56	1	1
57	0	0
58	0	0
59		1
60		0
61		1
62		1
63		0
64		0
65		2

C

Descriptives

	conditions			Statistic	Std. Error
PLA	Basal	Mean		.66	.117
		95% Confidence Interval for Mean	Lower Bound	.42	
			Upper Bound	.89	
		5% Trimmed Mean		.54	
		Median		.00	
		Variance		.791	
		Std. Deviation		.890	
		Minimum		0	
		Maximum		4	
		Range		4	
		Interquartile Range		1	
		Skewness		1.679	.314
		Kurtosis		3.208	.618
	Insulin	Mean		.54	.103
		95% Confidence Interval for Mean	Lower Bound	.33	
			Upper Bound	.74	
		5% Trimmed Mean		.44	
		Median		.00	
		Variance		.690	
		Std. Deviation		.831	
		Minimum		0	
		Maximum		4	
		Range		4	
		Interquartile Range		1	
		Skewness		1.900	.297
		Kurtosis		4.328	.586

Figure 8-19: PLA raw data and statistical analysis for Cellugyrin/Sortilin in 3T3-L1 fibroblast cells

A: Results of Mann-Whitney non-parametrical statistical tests of data from Figure 6-2. B: Raw data from Figure 6-2. C: Descriptive statistics of raw data from B.

Adipocytes Cellugyrin/Sortilin

A

Test Statistics[a]

	PLA
Mann-Whitney U	1066.000
Wilcoxon W	2147.000
Z	-.512
Asymp. Sig. (2-tailed)	.609

a. Grouping Variable: Conditions

B

PLA raw data

Adipocytes Cellugyrin/ Sortilin	Basal	Insulin
1	0	0
2	0	0
3	0	0
4	1	1
5	2	3
6	0	3
7	0	2
8	0	4
9	3	1
10	4	0
11	1	0
12	1	1
13	0	1
14	0	0
15	0	0
16	1	2
17	0	0
18	0	3
19	3	1
20	0	3
21	2	3
22	4	2
23	0	0
24	0	0
25	0	0
26	0	4
27	0	1
28	0	1
29	0	0
30	0	0
31	0	0
32	3	0
33	1	0
34	1	0
35	1	1
36	1	0
37	0	1
38	0	0
39	0	2
40	0	0
41	0	4
42	0	0
43	0	0
44	2	0
45	2	0
46	1	0
47		0
48		0
49		0

C

Descriptives

Conditions				Statistic	Std. Error
PLA	Basal	Mean		.74	.169
		95% Confidence Interval for Mean	Lower Bound	.40	
			Upper Bound	1.08	
		5% Trimmed Mean		.61	
		Median		.00	
		Variance		1.308	
		Std. Deviation		1.144	
		Minimum		0	
		Maximum		4	
		Range		4	
		Interquartile Range		1	
		Skewness		1.566	.350
		Kurtosis		1.582	.688
	Insulin	Mean		.90	.183
		95% Confidence Interval for Mean	Lower Bound	.53	
			Upper Bound	1.27	
		5% Trimmed Mean		.78	
		Median		.00	
		Variance		1.635	
		Std. Deviation		1.279	
		Minimum		0	
		Maximum		4	
		Range		4	
		Interquartile Range		2	
		Skewness		1.258	.340
		Kurtosis		.330	.668

Figure 8-20: PLA raw data and statistical analysis for Cellugyrin/Sortilin in 3T3-L1 adipocyte cells

A: Results of Mann-Whitney non-parametrical statistical tests of data from Figure 6-2. B: Raw data from Figure 6-2. C: Descriptive statistics of raw data from B.

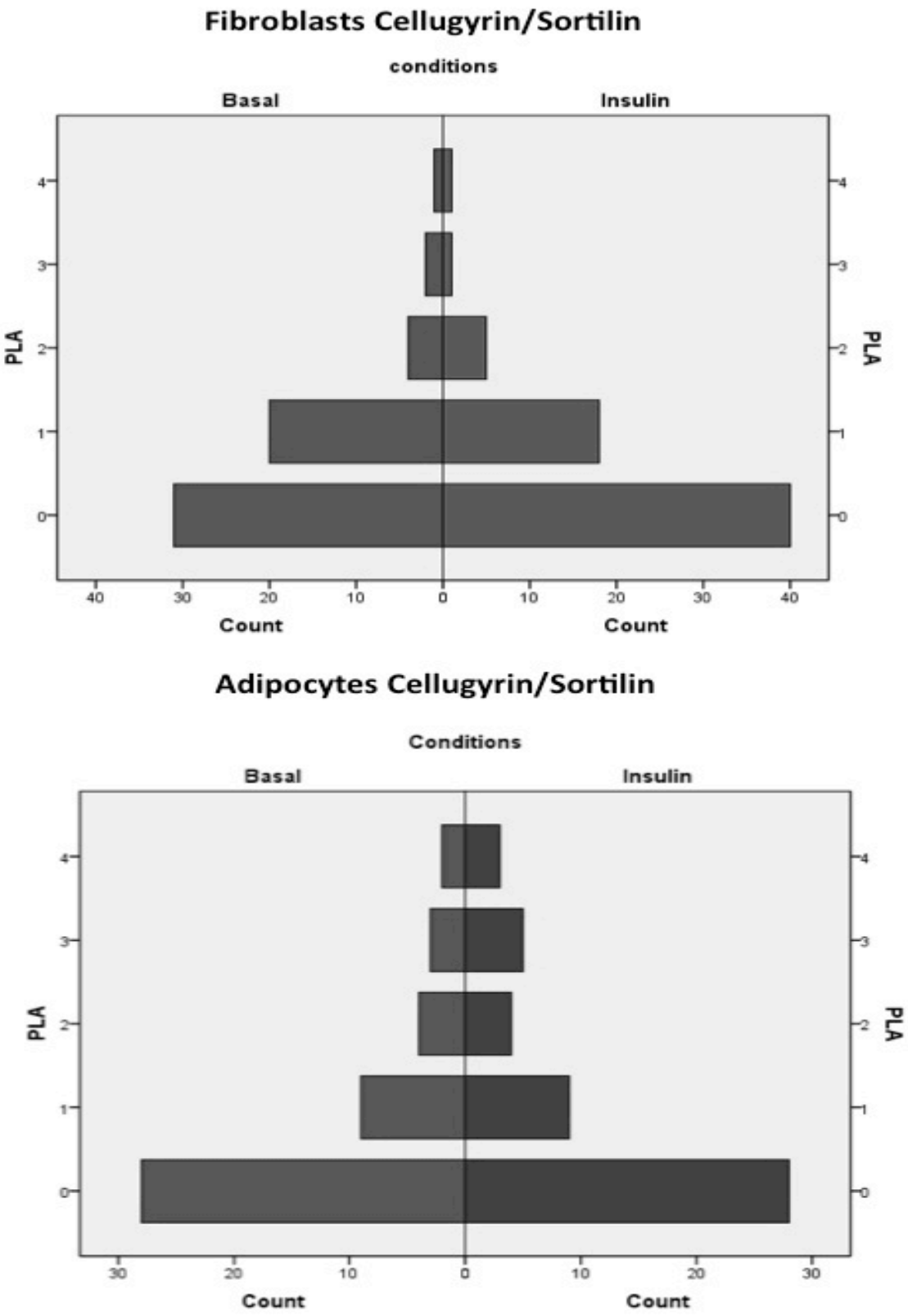

Figure 8-21: 3T3-L1 cell distribution based on PLA results for Cellugyrin/Sortilin

Cell distribution based on PLA results for Cellugyrin/Sortilin (Figure 6-2) under basal conditions and upon insulin stimulation of fibroblasts (upper panel) and adipocytes (lower panel).

Fibroblasts Cellugyrin/VAMP2

A

Test Statistics[a]

	PLA
Mann-Whitney U	202.500
Wilcoxon W	2830.500
Z	-8.558
Asymp. Sig. (2-tailed)	.000

a. Grouping Variable: Conditions

B

PLA raw data

Fibroblasts Cellugyrin/VAMP2	Basal	Insulin
1	19	3
2	19	3
3	9	5
4	17	7
5	14	15
6	15	12
7	15	11
8	23	3
9	22	6
10	11	12
11	7	4
12	19	5
13	20	4
14	11	5
15	9	5
16	22	4
17	21	4
18	13	7
19	8	4
20	13	6
21	19	5
22	14	9
23	6	3
24	16	7
25	11	4
26	9	8
27	9	7
28	7	7
29	8	5
30	7	3
31	11	4
32	14	4
33	13	7
34	24	6
35	17	5
36	27	3
37	7	4
38	20	6
39	15	9
40	8	7
41	13	7
42	10	7
43	15	4
44	19	6
45	16	5
46	22	5
47	15	7
48	11	8
49	12	6
50	10	7
51	11	8
52	15	7
53	17	5
54		5
55		6
56		5
57		7
58		7
59		9
60		5
61		9
62		7
63		5
64		6
65		6
66		6
67		6
68		4
69		4
70		7
71		5
72		6

C

Descriptives

	Conditions			Statistic	Std. Error
PLA	Basal	Mean		14.25	.710
		95% Confidence Interval for Mean	Lower Bound	12.82	
			Upper Bound	15.67	
		5% Trimmed Mean		14.08	
		Median		14.00	
		Variance		26.689	
		Std. Deviation		5.166	
		Minimum		6	
		Maximum		27	
		Range		21	
		Interquartile Range		9	
		Skewness		.378	.327
		Kurtosis		-.640	.644
	Insulin	Mean		6.04	.265
		95% Confidence Interval for Mean	Lower Bound	5.51	
			Upper Bound	6.57	
		5% Trimmed Mean		5.84	
		Median		6.00	
		Variance		5.055	
		Std. Deviation		2.248	
		Minimum		3	
		Maximum		15	
		Range		12	
		Interquartile Range		3	
		Skewness		1.423	.283
		Kurtosis		3.269	.559

Figure 8-22: PLA raw data and statistical analysis for Cellugyrin/VAMP2 in 3T3-L1 fibroblast cells

A: Results of Mann-Whitney non-parametrical statistical tests of data from Figure 6-3. B: Raw data from Figure 6-3. C: Descriptive statistics of raw data from B.

Adipocytes Cellugyrin/VAMP2

A

Test Statistics[a]

	VAR00001
Mann-Whitney U	275.000
Wilcoxon W	4835.000
Z	-10.593
Asymp. Sig. (2-tailed)	.000

a. Grouping Variable: Conditions

B

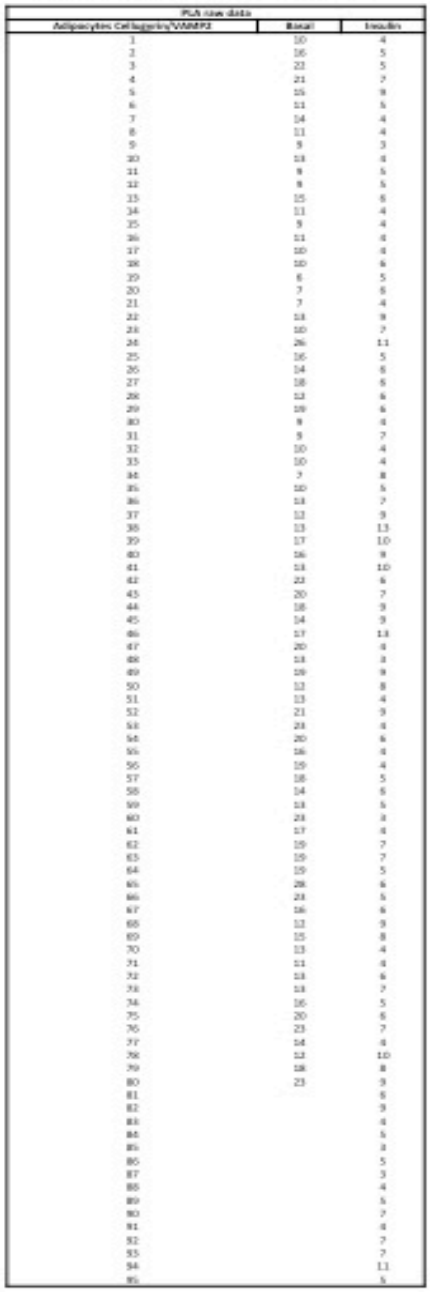

C

Descriptives

Conditions				Statistic	Std. Error
PLA	Basal	Mean		14.90	.544
		95% Confidence Interval for Mean	Lower Bound	13.82	
			Upper Bound	15.98	
		5% Trimmed Mean		14.79	
		Median		14.00	
		Variance		23.635	
		Std. Deviation		4.862	
		Minimum		6	
		Maximum		28	
		Range		22	
		Interquartile Range		8	
		Skewness		.430	.269
		Kurtosis		-.434	.532
	Insulin	Mean		6.09	.232
		95% Confidence Interval for Mean	Lower Bound	5.63	
			Upper Bound	6.56	
		5% Trimmed Mean		5.96	
		Median		6.00	
		Variance		5.108	
		Std. Deviation		2.260	
		Minimum		3	
		Maximum		13	
		Range		10	
		Interquartile Range		3	
		Skewness		.930	.247
		Kurtosis		.462	.490

Figure 8-23: PLA raw data and statistical analysis for Cellugyrin/VAMP2 in 3T3-L1 adipocyte cells

A: Results of Mann-Whitney non-parametrical statistical tests of data from Figure 6-3. B: Raw data from Figure 6-3. C: Descriptive statistics of raw data from B.

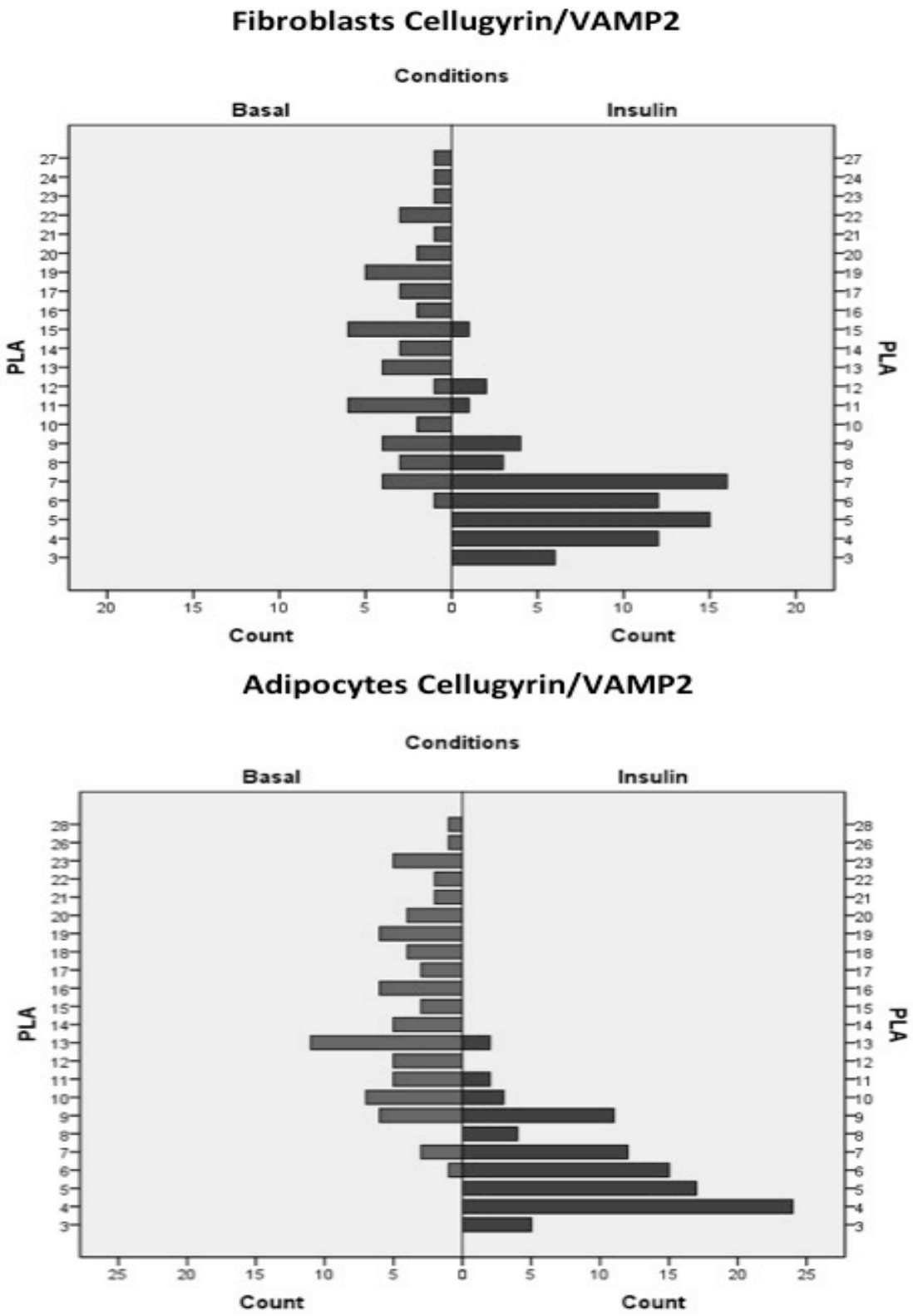

Figure 8-24: 3T3-L1 cell distribution based on PLA results for Cellugyrin/VAMP2

Cell distribution based on PLA results for Cellugyrin/VAMP2 (Figure 6-3) under basal conditions and upon insulin stimulation of fibroblasts (upper panel) and adipocytes (lower panel).

Fibroblasts Sortilin/VAMP2

A

Test Statistics[a]

	PLA
Mann-Whitney U	116.000
Wilcoxon W	1244.000
Z	-7.755
Asymp. Sig. (2-tailed)	.000

a. Grouping Variable: conditions

B

PLA raw data

Fibroblasts Sortilin/VAMP2	Basal	Insulin
1	7	23
2	11	21
3	9	19
4	13	38
5	11	52
6	8	26
7	15	50
8	21	48
9	13	64
10	21	58
11	14	46
12	12	37
13	18	34
14	20	57
15	21	57
16	23	33
17	11	22
18	13	24
19	26	28
20	24	42
21	26	33
22	11	38
23	19	25
24	15	47
25	21	58
26	15	26
27	10	48
28	8	47
29	14	33
30	25	28
31	26	37
32	17	32
33	24	32
34	17	27
35	6	23
36	12	23
37	14	26
38	28	26
39	19	25
40	26	44
41	12	37
42	7	47
43	7	51
44	24	36
45	30	61
46	20	41
47	18	40
48		42
49		42
50		59
51		37
52		52

C

Descriptives

conditions				Statistic	Std. Error
PLA	Basal	Mean		16.64	.949
		95% Confidence Interval for Mean	Lower Bound	14.73	
			Upper Bound	18.55	
		5% Trimmed Mean		16.54	
		Median		15.00	
		Variance		42.366	
		Std. Deviation		6.509	
		Minimum		6	
		Maximum		30	
		Range		24	
		Interquartile Range		10	
		Skewness		.203	.347
		Kurtosis		-1.030	.681
	Insulin	Mean		38.50	1.698
		95% Confidence Interval for Mean	Lower Bound	35.09	
			Upper Bound	41.91	
		5% Trimmed Mean		38.21	
		Median		37.00	
		Variance		149.941	
		Std. Deviation		12.245	
		Minimum		19	
		Maximum		64	
		Range		45	
		Interquartile Range		22	
		Skewness		.306	.330
		Kurtosis		-.961	.650

Figure 8-25: PLA raw data and statistical analysis for Sortilin/VAMP2 in 3T3-L1 fibroblast cells

A: Results of Mann-Whitney non-parametrical statistical tests of data from Figure 6-4. B: Raw data from Figure 6-4. C: Descriptive statistics of raw data from B.

Adipocytes Sortilin/VAMP2

A

Test Statistics[a]

	PLA
Mann-Whitney U	35.000
Wilcoxon W	1070.000
Z	-8.087
Asymp. Sig. (2-tailed)	.000

a. Grouping Variable: Conditions

B

PLA raw data

Adipocytes Sortilin/VAMP2	Basal	Insulin
1	9	22
2	12	25
3	5	32
4	10	34
5	14	38
6	12	48
7	11	51
8	10	27
9	4	22
10	18	30
11	12	34
12	16	31
13	13	36
14	10	18
15	7	19
16	9	20
17	4	24
18	12	36
19	10	44
20	10	38
21	14	35
22	16	32
23	13	19
24	15	26
25	14	28
26	10	24
27	8	25
28	19	38
29	13	40
30	11	41
31	7	14
32	6	35
33	10	38
34	15	26
35	11	31
36	7	34
37	11	39
38	14	23
39	20	28
40	19	35
41	13	15
42	10	14
43	9	26
44	11	45
45	10	32
46		33
47		35
48		22
49		30

C

Descriptives

Conditions				Statistic	Std. Error
PLA	Basal	Mean		11.42	.562
		95% Confidence Interval for Mean	Lower Bound	10.29	
			Upper Bound	12.55	
		5% Trimmed Mean		11.38	
		Median		11.00	
		Variance		14.204	
		Std. Deviation		3.769	
		Minimum		4	
		Maximum		20	
		Range		16	
		Interquartile Range		5	
		Skewness		.242	.354
		Kurtosis		.057	.695
	Insulin	Mean		30.45	1.242
		95% Confidence Interval for Mean	Lower Bound	27.95	
			Upper Bound	32.95	
		5% Trimmed Mean		30.34	
		Median		31.00	
		Variance		75.586	
		Std. Deviation		8.694	
		Minimum		14	
		Maximum		51	
		Range		37	
		Interquartile Range		12	
		Skewness		.094	.340
		Kurtosis		-.331	.668

Figure 8-26: PLA raw data and statistical analysis for Sortilin/VAMP2 in 3T3-L1 adipocyte cells

A: Results of Mann-Whitney non-parametrical statistical tests of data from Figure 6-4. B: Raw data from Figure 6-4. C: Descriptive statistics of raw data from B.

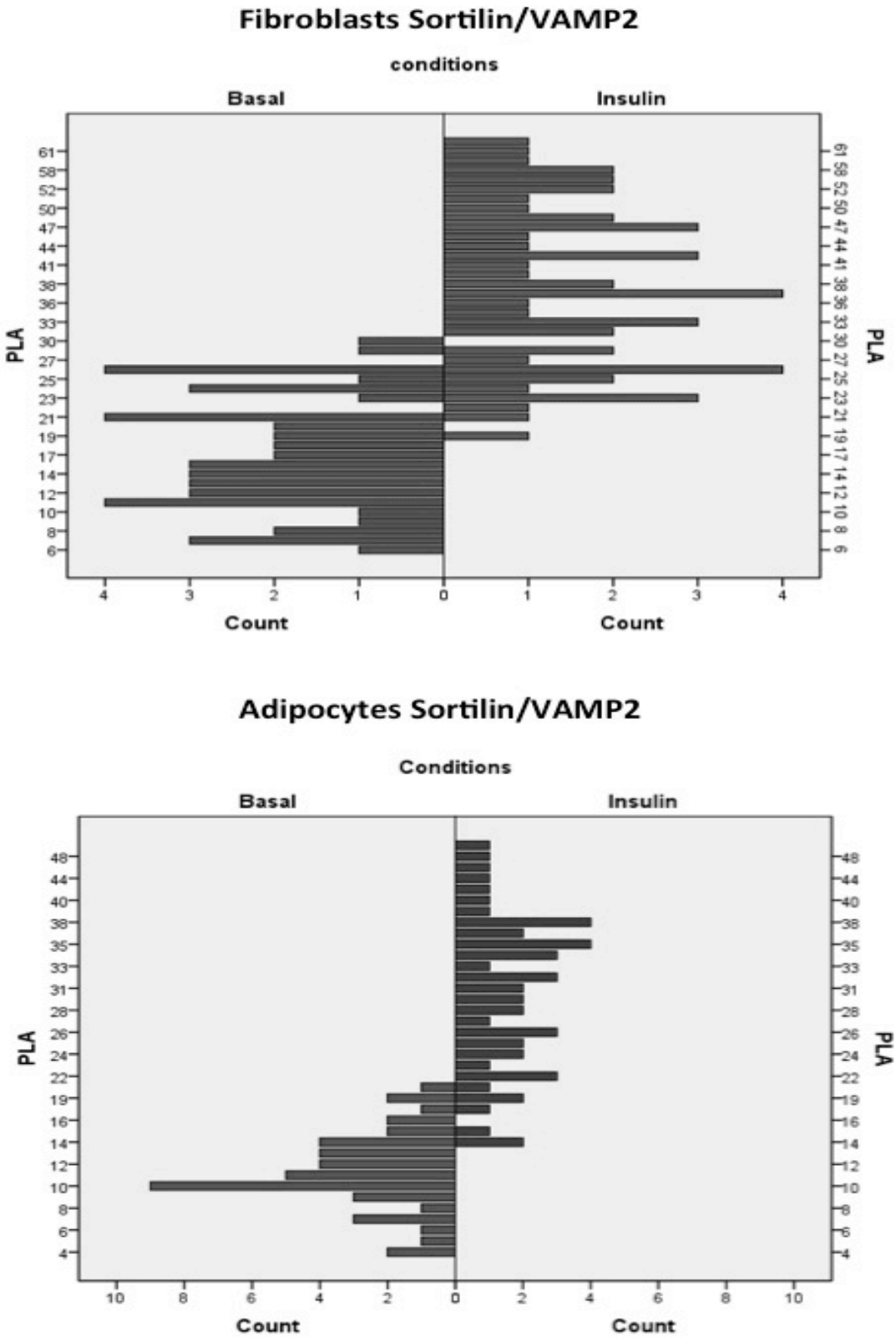

Figure 8-27: 3T3-L1 cell distribution based on PLA results for Sortilin/VAMP2

Cell distribution based on PLA results for Sortilin/VAMP2 (Figure 6-4) under basal conditions and upon insulin stimulation of fibroblasts (upper panel) and adipocytes (lower panel).

Fibroblasts Cellugyrin/Munc18c

A

Test Statistics[a]

	PLA
Mann-Whitney U	2503.000
Wilcoxon W	5824.000
Z	-1.374
Asymp. Sig. (2-tailed)	.169

a. Grouping Variable: Conditions

B

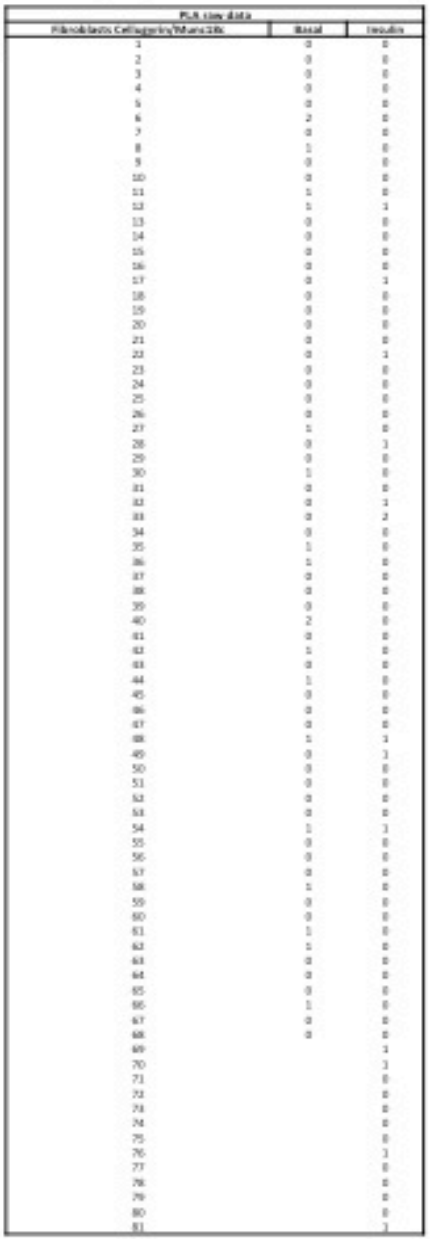

C

Descriptives

Conditions				Statistic	Std. Error
PLA	Basal	Mean		.28	.062
		95% Confidence Interval for Mean	Lower Bound	.16	
			Upper Bound	.40	
		5% Trimmed Mean		.22	
		Median		.00	
		Variance		.264	
		Std. Deviation		.514	
		Minimum		0	
		Maximum		2	
		Range		2	
		Interquartile Range		1	
		Skewness		1.665	.291
		Kurtosis		1.984	.574
	Insulin	Mean		.17	.046
		95% Confidence Interval for Mean	Lower Bound	.08	
			Upper Bound	.26	
		5% Trimmed Mean		.12	
		Median		.00	
		Variance		.170	
		Std. Deviation		.412	
		Minimum		0	
		Maximum		2	
		Range		2	
		Interquartile Range		0	
		Skewness		2.298	.267
		Kurtosis		4.751	.529

Figure 8-28: PLA raw data and statistical analysis for Cellugyrin/Munc18c in 3T3-L1 fibroblast cells

A: Results of Mann-Whitney non-parametrical statistical tests of data from Figure 6-5. B: Raw data from Figure 6-5. C: Descriptive statistics of raw data from B.

Adipocytes Cellugyrin/Munc18c

A

Test Statistics[a]

	PLA
Mann-Whitney U	4367.000
Wilcoxon W	8927.000
Z	-.011
Asymp. Sig. (2-tailed)	.991

a. Grouping Variable: Conditions

B

PLA raw data

Adipocytes Cellugyrin/Munc18c	Basal	Insulin
1	0	0
2	0	0
3	1	0
4	2	0
5	0	0
6	0	1
7	1	0
8	0	0
9	0	0
10	0	0
11	0	2
12	0	1
13	1	0
14	0	0
15	0	0
16	0	1
17	1	0
18	0	0
19	0	1
20	0	0
21	0	1
22	0	0
23	1	0
24	0	2
25	0	0
26	0	0
27	2	0
28	0	0
29	0	0
30	0	0
31	0	0
32	2	0
33	0	0
34	0	0
35	1	0
36	0	0
37	0	0
38	2	1
39	0	0
40	0	0
41	0	0
42	1	0
43	0	0
44	0	1
45	1	0
46	0	0
47	0	0
48	0	0
49	0	0
50	0	0
51	2	2
52	0	0
53	0	1
54	0	0
55	0	0
56	1	0
57	0	0
58	0	0
59	2	0
60	0	2
61	0	0
62	0	0
63	0	0
64	1	0
65	0	1
66	0	0
67	0	0
68	0	0
69	0	0
70	0	0
71	3	0
72	0	0
73	0	4
74	0	0
75	0	0
76	1	1
77	0	0
78	0	0
79	0	0
80	0	0
81	0	2
82	0	0
83	0	0
84	0	3
85	1	0
86	0	0
87	0	0
88	1	4
89	0	0
90	0	0
91	0	0
92	0	0
93		0
94		2
95		1

C

Descriptives

Conditions				Statistic	Std. Error
PLA	Basal	Mean		.30	.067
		95% Confidence Interval for Mean	Lower Bound	.17	
			Upper Bound	.44	
		5% Trimmed Mean		.21	
		Median		.00	
		Variance		.412	
		Std. Deviation		.642	
		Minimum		0	
		Maximum		3	
		Range		3	
		Interquartile Range		0	
		Skewness		2.175	.251
		Kurtosis		4.239	.498
	Insulin	Mean		.36	.085
		95% Confidence Interval for Mean	Lower Bound	.19	
			Upper Bound	.53	
		5% Trimmed Mean		.23	
		Median		.00	
		Variance		.679	
		Std. Deviation		.824	
		Minimum		0	
		Maximum		4	
		Range		4	
		Interquartile Range		0	
		Skewness		2.740	.247
		Kurtosis		7.903	.490

Figure 8-29: PLA raw data and statistical analysis for Cellugyrin/Munc18c in 3T3-L1 adipocyte cells

A: Results of Mann-Whitney non-parametrical statistical tests of data from Figure 6-5. B: Raw data from Figure 6-5. C: Descriptive statistics of raw data from B.

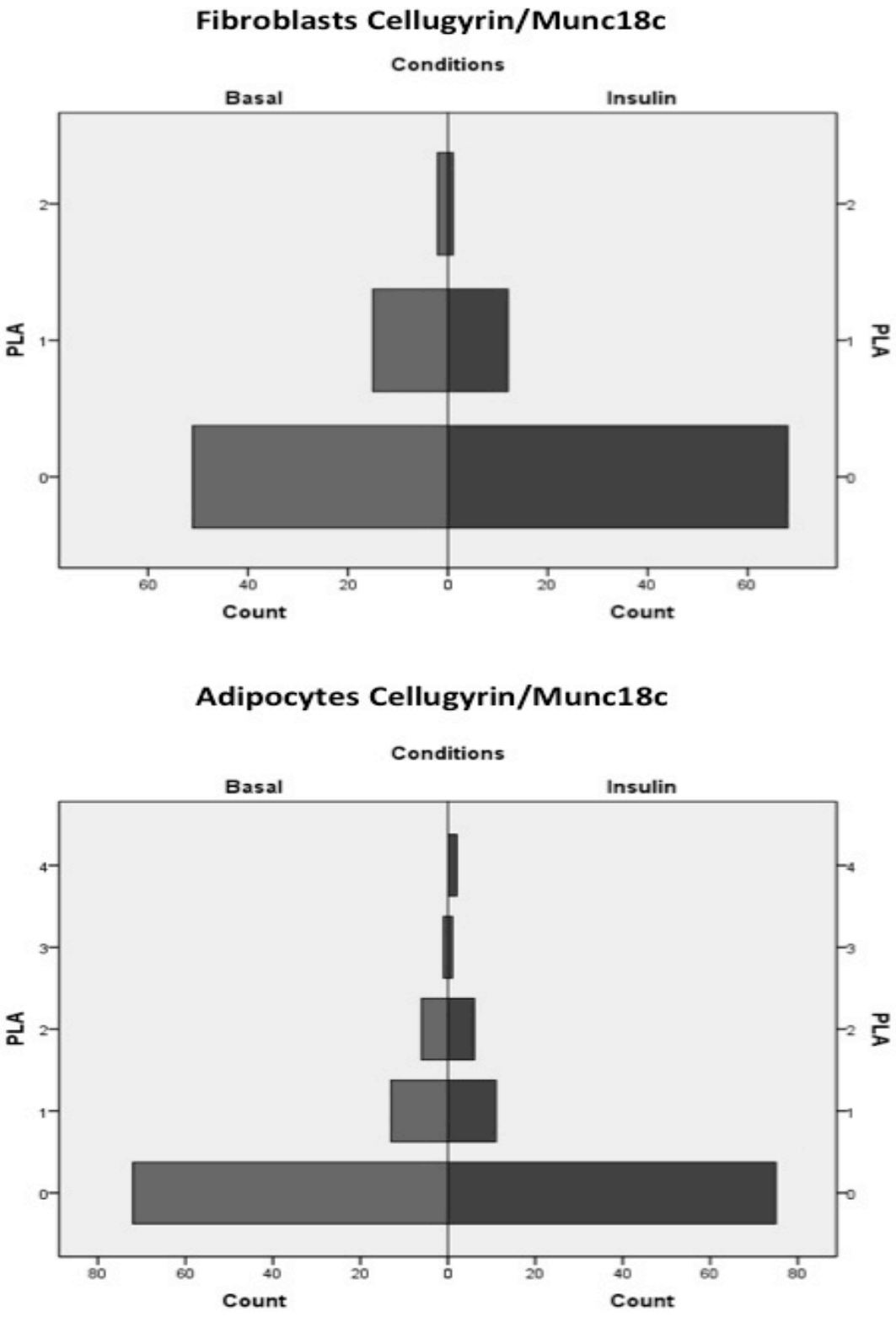

Figure 8-30: 3T3-L1 cell distribution based on PLA results for Cellugyrin/Munc18c

Cell distribution based on PLA results for Cellugyrin/Munc18c (Figure 6-5) under basal conditions and upon insulin stimulation of fibroblasts (upper panel) and adipocytes (lower panel).

Fibroblasts Sortilin/Munc18c

A

Test Statistics[a]

	PLA
Mann-Whitney U	1653.500
Wilcoxon W	3544.500
Z	-1.735
Asymp. Sig. (2-tailed)	.083

a. Grouping Variable: Conditions

B

PLA raw data

Fibroblasts Sortilin/Munc18c	Basal	Insulin
1	327	79
2	253	74
3	333	79
4	185	128
5	37	154
6	33	193
7	41	174
8	67	86
9	42	115
10	53	160
11	88	80
12	127	82
13	149	137
14	228	166
15	100	247
16	71	117
17	132	148
18	91	215
19	170	135
20	109	384
21	72	360
22	182	372
23	93	354
24	86	285
25	77	273
26	113	318
27	134	59
28	196	179
29	160	128
30	136	159
31	254	92
32	334	188
33	172	85
34	127	251
35	144	113
36	183	113
37	62	325
38	268	155
39	200	78
40	100	135
41	84	135
42	240	57
43	189	126
44	207	54
45	130	147
46	148	212
47	83	183
48	91	79
49	74	213
50	78	281
51	126	75
52	149	83
53	86	216
54	139	68
55	213	81
56	98	155
57	95	101
58	100	173
59	72	158
60	157	142
61	83	179
62		61
63		324
64		226
65		138
66		276

C

Descriptives

	Conditions			Statistic	Std. Error
PLA	Basal	Mean		137.23	9.344
		95% Confidence Interval for Mean	Lower Bound	118.54	
			Upper Bound	155.92	
		5% Trimmed Mean		132.07	
		Median		127.00	
		Variance		5326.013	
		Std. Deviation		72.980	
		Minimum		33	
		Maximum		334	
		Range		301	
		Interquartile Range		99	
		Skewness		1.005	.306
		Kurtosis		.656	.604
	Insulin	Mean		165.42	10.710
		95% Confidence Interval for Mean	Lower Bound	144.03	
			Upper Bound	186.81	
		5% Trimmed Mean		160.06	
		Median		147.50	
		Variance		7570.863	
		Std. Deviation		87.011	
		Minimum		54	
		Maximum		384	
		Range		330	
		Interquartile Range		128	
		Skewness		.909	.295
		Kurtosis		.030	.582

Figure 8-31: PLA raw data and statistical analysis for Sortilin/Munc18c in 3T3-L1 fibroblast cells

A: Results of Mann-Whitney non-parametrical statistical tests of data from Figure 6-6. B: Raw data from Figure 6-6. C: Descriptive statistics of raw data from B.

Adipocytes Sortilin/Munc18c

A

Test Statistics[a]

	PLA
Mann-Whitney U	536.000
Wilcoxon W	1356.000
Z	-2.541
Asymp. Sig. (2-tailed)	.071

a. Grouping Variable: Conditions

B

PLA raw data		
Adipocytes Sortilin/Munc18c	Basal	Insulin
1	124	156
2	112	133
3	98	128
4	75	145
5	143	173
6	135	99
7	142	96
8	95	85
9	115	134
10	124	150
11	85	52
12	158	148
13	133	132
14	106	120
15	96	165
16	145	85
17	166	130
18	154	89
19	123	93
20	102	126
21	98	134
22	86	152
23	137	143
24	128	60
25	115	178
26	134	140
27	122	145
28	94	135
29	89	126
30	133	133
31	109	142
32	140	119
33	125	124
34	121	133
35	98	148
36	106	162
37	111	143
38	118	135
39	115	133
40	120	155

C

Descriptives

Conditions				Statistic	Std. Error
PLA	Basal	Mean		118.25	3.356
		95% Confidence Interval for Mean	Lower Bound	111.46	
			Upper Bound	125.04	
		5% Trimmed Mean		117.94	
		Median		119.00	
		Variance		450.551	
		Std. Deviation		21.226	
		Minimum		75	
		Maximum		166	
		Range		91	
		Interquartile Range		35	
		Skewness		.142	.374
		Kurtosis		-.420	.733
	Insulin	Mean		129.48	4.449
		95% Confidence Interval for Mean	Lower Bound	120.48	
			Upper Bound	138.47	
		5% Trimmed Mean		131.00	
		Median		133.50	
		Variance		791.589	
		Std. Deviation		28.135	
		Minimum		52	
		Maximum		178	
		Range		126	
		Interquartile Range		26	
		Skewness		-.968	.374
		Kurtosis		.926	.733

Figure 8-32: PLA raw data and statistical analysis for Sortilin/Munc18c in 3T3-L1 adipocyte cells

A: Results of Mann-Whitney non-parametrical statistical tests of data from Figure 6-6. B: Raw data from Figure 6-6. C: Descriptive statistics of raw data from B.

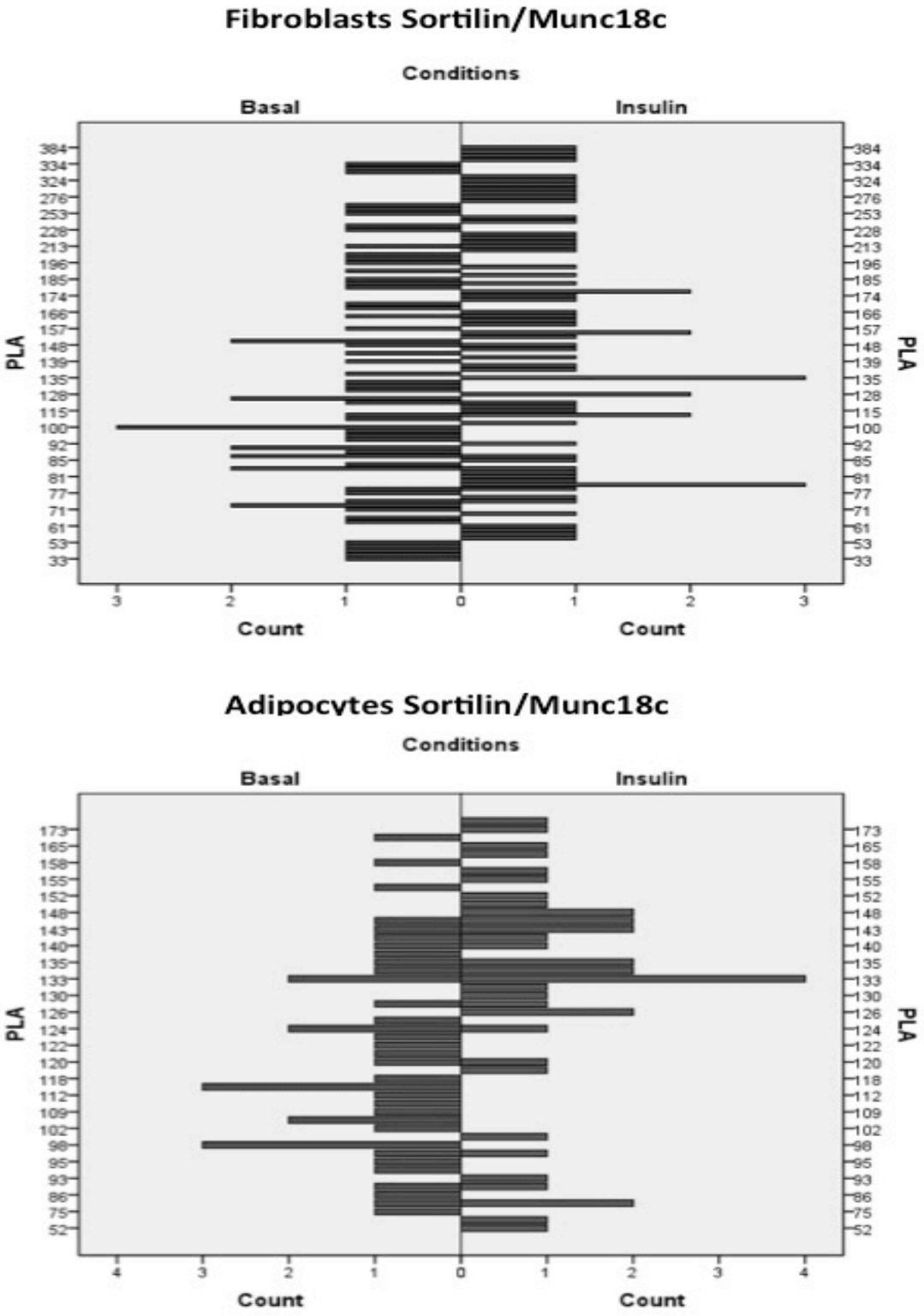

Figure 8-33: 3T3-L1 cell distribution based on PLA results for Sortilin/Munc18c

Cell distribution based on PLA results for Sortilin/Munc18c (Figure 6-6) under basal conditions and upon insulin stimulation of fibroblasts (upper panel) and adipocytes (lower panel).

Fibroblasts Cellugyrin/Sx4

A

Test Statistics[a]

	PLA
Mann-Whitney U	143.500
Wilcoxon W	923.500
Z	-6.484
Asymp. Sig. (2-tailed)	.000

a. Grouping Variable: Conditions

B

PLA raw data		
Fibroblasts Cellugyrin/Sx4	Basal	Insulin
1	3	0
2	4	0
3	2	0
4	1	0
5	5	1
6	2	0
7	3	0
8	4	0
9	5	0
10	6	1
11	0	0
12	4	2
13	4	0
14	2	0
15	4	0
16	6	0
17	0	0
18	1	0
19	2	0
20	5	1
21	8	1
22	0	0
23	4	0
24	2	0
25	5	1
26	2	0
27	3	0
28	5	0
29	1	2
30	4	0
31	4	0
32	6	0
33	5	0
34	3	1
35	7	1
36	0	0
37	0	0
38	2	0
39	8	0

C

Descriptives

Conditions				Statistic	Std. Error
PLA	Basal	Mean		3.38	.352
		95% Confidence Interval for Mean	Lower Bound	2.67	
			Upper Bound	4.10	
		5% Trimmed Mean		3.32	
		Median		4.00	
		Variance		4.822	
		Std. Deviation		2.196	
		Minimum		0	
		Maximum		8	
		Range		8	
		Interquartile Range		3	
		Skewness		.187	.378
		Kurtosis		-.548	.741
	Insulin	Mean		.28	.090
		95% Confidence Interval for Mean	Lower Bound	.10	
			Upper Bound	.46	
		5% Trimmed Mean		.20	
		Median		.00	
		Variance		.313	
		Std. Deviation		.560	
		Minimum		0	
		Maximum		2	
		Range		2	
		Interquartile Range		0	
		Skewness		1.909	.378
		Kurtosis		2.870	.741

Figure 8-34: PLA raw data and statistical analysis for Cellugyrin/Syntaxin 4 in 3T3-L1 fibroblast cells

A: Results of Mann-Whitney non-parametrical statistical tests of data from Figure 6-7. B: Raw data from Figure 6-7. C: Descriptive statistics of raw data from B.

Adipocytes Cellugyrin/Sx4

A

Test Statistics[a]

	PLA
Mann-Whitney U	36.500
Wilcoxon W	816.500
Z	-7.636
Asymp. Sig. (2-tailed)	.000

a. Grouping Variable: Conditions

B

PLA raw data		
Adipocytes Cellugyrin/Sx4	Basal	Insulin
1	2	0
2	3	0
3	2	0
4	2	0
5	3	0
6	5	0
7	5	0
8	8	0
9	5	1
10	4	0
11	2	0
12	2	0
13	2	0
14	2	2
15	3	0
16	3	0
17	3	0
18	4	0
19	5	1
20	6	0
21	1	0
22	2	0
23	1	0
24	2	0
25	2	0
26	5	0
27	3	0
28	4	0
29	3	0
30	2	0
31	3	0
32	3	0
33	2	0
34	4	0
35	1	0
36	2	0
37	2	0
38	2	3
39	3	0

C

Descriptives

Conditions				Statistic	Std. Error
PLA	Basal	Mean		3.03	.239
		95% Confidence Interval for Mean	Lower Bound	2.54	
			Upper Bound	3.51	
		5% Trimmed Mean		2.92	
		Median		3.00	
		Variance		2.236	
		Std. Deviation		1.495	
		Minimum		1	
		Maximum		8	
		Range		7	
		Interquartile Range		2	
		Skewness		1.248	.378
		Kurtosis		1.908	.741
	Insulin	Mean		.18	.096
		95% Confidence Interval for Mean	Lower Bound	-.02	
			Upper Bound	.37	
		5% Trimmed Mean		.06	
		Median		.00	
		Variance		.362	
		Std. Deviation		.601	
		Minimum		0	
		Maximum		3	
		Range		3	
		Interquartile Range		0	
		Skewness		3.746	.378
		Kurtosis		14.469	.741

Figure 8-35: PLA raw data and statistical analysis for Cellugyrin/Syntaxin 4 in 3T3-L1 adipocyte cells

A: Results of Mann-Whitney non-parametrical statistical tests of data from Figure 6-7. B: Raw data from Figure 6-7. C: Descriptive statistics of raw data from B.

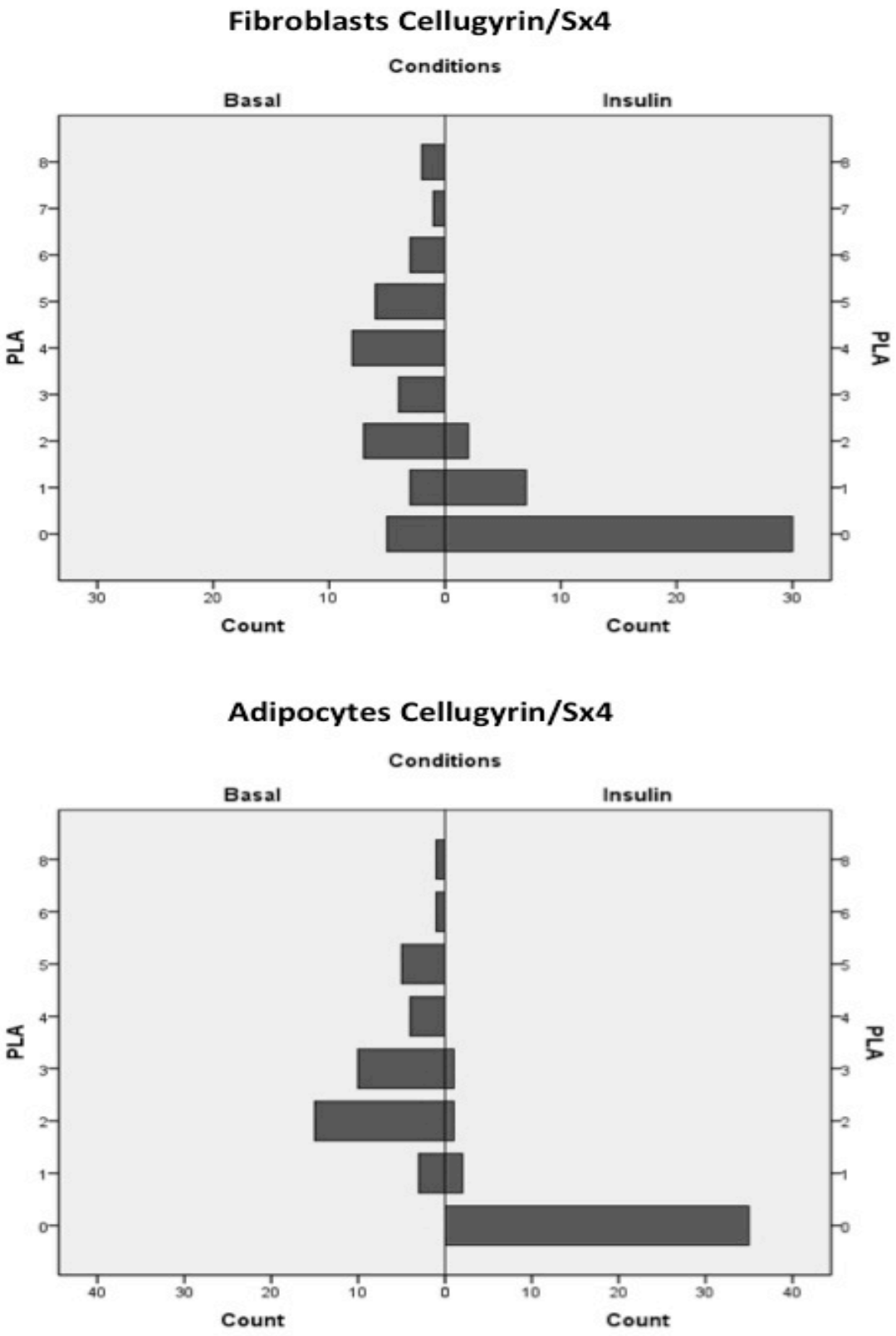

Figure 8-36: 3T3-L1 cell distribution based on PLA results for Cellugyrin/Syntaxin 4

Cell distribution based on PLA results for Cellugyrin/Syntaxin 4 (Figure 6-7) under basal conditions and upon insulin stimulation of fibroblasts (upper panel) and adipocytes (lower panel).

Fibroblasts Cellugyrin/SNAP23

A

Test Statistics[a]

	PLA
Mann-Whitney U	1.500
Wilcoxon W	821.500
Z	-7.926
Asymp. Sig. (2-tailed)	.000

a. Grouping Variable: Conditions

B

PLA raw data

Fibroblasts Cellugyrin/ SNAP23	Basal	Insulin
1	10	0
2	5	0
3	6	0
4	8	0
5	9	0
6	11	0
7	3	1
8	5	0
9	5	0
10	8	0
11	6	1
12	9	0
13	4	1
14	11	1
15	15	0
16	3	0
17	10	0
18	6	0
19	5	0
20	8	0
21	7	0
22	9	2
23	12	0
24	4	0
25	6	0
26	8	1
27	9	1
28	2	1
29	8	0
30	7	0
31	9	0
32	6	0
33	11	0
34	12	0
35	15	0
36	2	0
37	2	1
38	10	0
39	16	0
40	13	0

C

Descriptives

Conditions				Statistic	Std. Error
PLA	Basal	Mean		7.88	.572
		95% Confidence Interval for Mean	Lower Bound	6.72	
			Upper Bound	9.03	
		5% Trimmed Mean		7.78	
		Median		8.00	
		Variance		13.087	
		Std. Deviation		3.618	
		Minimum		2	
		Maximum		16	
		Range		14	
		Interquartile Range		5	
		Skewness		.329	.374
		Kurtosis		-.342	.733
	Insulin	Mean		.25	.078
		95% Confidence Interval for Mean	Lower Bound	.09	
			Upper Bound	.41	
		5% Trimmed Mean		.19	
		Median		.00	
		Variance		.244	
		Std. Deviation		.494	
		Minimum		0	
		Maximum		2	
		Range		2	
		Interquartile Range		0	
		Skewness		1.852	.374
		Kurtosis		2.819	.733

Figure 8-37: PLA raw data and statistical analysis for Cellugyrin/SNAP23 in 3T3-L1 fibroblast cells

A: Results of Mann-Whitney non-parametrical statistical tests of data from Figure 6-8. B: Raw data from Figure 6-8. C: Descriptive statistics of raw data from B.

Adipocytes Cellugyrin/SNAP23

A

Test Statistics[a]

	PLA
Mann-Whitney U	10.500
Wilcoxon W	830.500
Z	-7.843
Asymp. Sig. (2-tailed)	.000

a. Grouping Variable: Conditions

B

PLA raw data

Adipocytes Cellugyrin/ SNAP23	Basal	Insulin
1	5	0
2	8	0
3	7	0
4	4	0
5	7	2
6	5	0
7	5	2
8	5	2
9	5	2
10	5	0
11	5	0
12	4	0
13	4	0
14	5	0
15	9	0
16	11	0
17	12	0
18	15	1
19	7	0
20	2	0
21	2	3
22	5	0
23	3	0
24	3	0
25	4	0
26	4	0
27	5	1
28	8	0
29	8	0
30	4	1
31	2	0
32	8	0
33	9	0
34	9	0
35	10	0
36	12	0
37	3	0
38	6	1
39	12	0
40	6	0

C

Descriptives

Conditions				Statistic	Std. Error
PLA	Basal	Mean		6.33	.494
		95% Confidence Interval for Mean	Lower Bound	5.33	
			Upper Bound	7.32	
		5% Trimmed Mean		6.17	
		Median		5.00	
		Variance		9.763	
		Std. Deviation		3.125	
		Minimum		2	
		Maximum		15	
		Range		13	
		Interquartile Range		4	
		Skewness		.866	.374
		Kurtosis		.282	.733
	Insulin	Mean		.38	.122
		95% Confidence Interval for Mean	Lower Bound	.13	
			Upper Bound	.62	
		5% Trimmed Mean		.28	
		Median		.00	
		Variance		.599	
		Std. Deviation		.774	
		Minimum		0	
		Maximum		3	
		Range		3	
		Interquartile Range		0	
		Skewness		2.012	.374
		Kurtosis		3.132	.733

Figure 8-38: PLA raw data and statistical analysis for Cellugyrin/SNAP23 in 3T3-L1 adipocyte cells

A: Results of Mann-Whitney non-parametrical statistical tests of data from Figure 6-8. B: Raw data from Figure 6-8. C: Descriptive statistics of raw data from B.

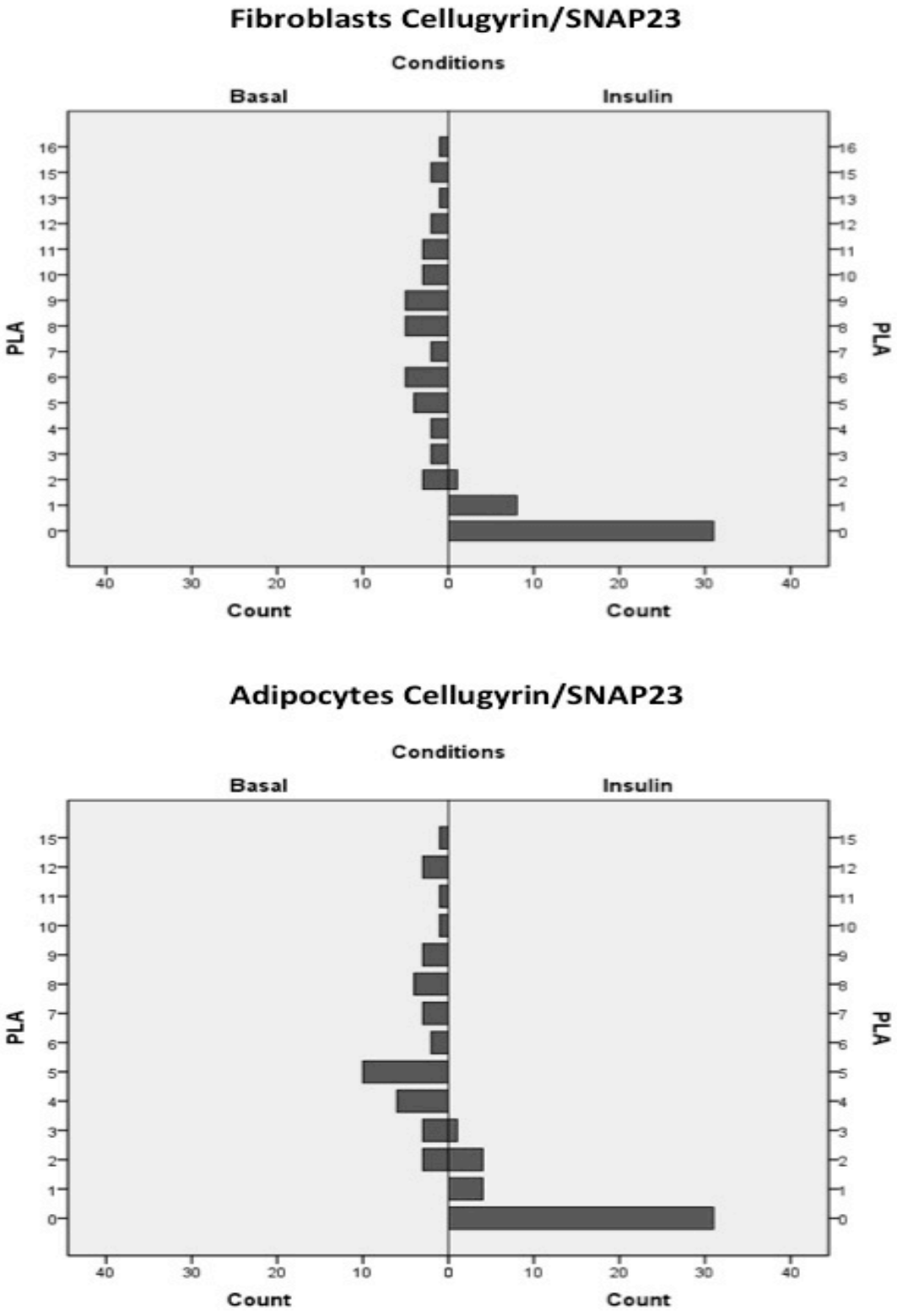

Figure 8-39: 3T3-L1 cell distribution based on PLA results for Cellugyrin/SNAP23

Cell distribution based on PLA results for Cellugyrin/SNAP23 (Figure 6-8) under basal conditions and upon insulin stimulation of fibroblasts (upper panel) and adipocytes (lower panel).

Fibroblasts Sortilin/Sx4

A

Test Statistics[a]

	PLA
Mann-Whitney U	134.500
Wilcoxon W	954.500
Z	-6.410
Asymp. Sig. (2-tailed)	.000

a. Grouping Variable: Conditions

B

PLA raw data		
Fibroblasts Sortilin/sx4	Basal	Insulin
1	6	35
2	8	38
3	4	25
4	15	26
5	12	24
6	10	32
7	18	38
8	10	19
9	5	20
10	4	22
11	9	28
12	8	36
13	6	34
14	5	32
15	3	38
16	11	35
17	15	10
18	12	9
19	7	8
20	10	35
21	9	32
22	6	38
23	4	30
24	8	31
25	11	29
26	20	28
27	15	26
28	4	8
29	10	15
30	6	16
31	3	22
32	2	30
33	8	35
34	11	2
35	14	36
36	12	16
37	11	33
38	13	35
39	10	19
40	9	28

C

Descriptives

Conditions				Statistic	Std. Error
PLA	Basal	Mean		9.10	.668
		95% Confidence Interval for Mean	Lower Bound	7.75	
			Upper Bound	10.45	
		5% Trimmed Mean		8.92	
		Median		9.00	
		Variance		17.836	
		Std. Deviation		4.223	
		Minimum		2	
		Maximum		20	
		Range		18	
		Interquartile Range		6	
		Skewness		.460	.374
		Kurtosis		-.042	.733
	Insulin	Mean		26.33	1.548
		95% Confidence Interval for Mean	Lower Bound	23.19	
			Upper Bound	29.46	
		5% Trimmed Mean		26.86	
		Median		28.50	
		Variance		95.815	
		Std. Deviation		9.789	
		Minimum		2	
		Maximum		38	
		Range		36	
		Interquartile Range		16	
		Skewness		-.810	.374
		Kurtosis		-.269	.733

Figure 8-40: PLA raw data and statistical analysis for Sortilin/Syntaxin 4 in 3T3-L1 fibroblast cells

A: Results of Mann-Whitney non-parametrical statistical tests of data from Figure 6-9. B: Raw data from Figure 6-9. C: Descriptive statistics of raw data from B.

Adipocytes Sortilin/Sx4

A

Test Statistics[a]

	PLA
Mann-Whitney U	91.500
Wilcoxon W	911.500
Z	-6.823
Asymp. Sig. (2-tailed)	.000

a. Grouping Variable: Conditions

B

PLA raw data		
Adipocytes Sortilin/Sx4	Basal	Insulin
1	9	40
2	8	38
3	11	36
4	15	39
5	12	42
6	16	51
7	14	21
8	18	27
9	17	32
10	33	35
11	25	35
12	28	30
13	22	15
14	26	10
15	20	45
16	15	50
17	14	35
18	21	38
19	15	31
20	14	30
21	9	36
22	8	38
23	8	40
24	4	40
25	5	45
26	8	41
27	6	42
28	11	19
29	15	22
30	12	29
31	18	25
32	20	35
33	14	48
34	30	29
35	11	36
36	15	24
37	16	35
38	18	38
39	15	45
40	12	40

C

Descriptives

Conditions				Statistic	Std. Error
PLA	Basal	Mean		15.20	1.060
		95% Confidence Interval for Mean	Lower Bound	13.05	
			Upper Bound	17.35	
		5% Trimmed Mean		14.89	
		Median		15.00	
		Variance		44.985	
		Std. Deviation		6.707	
		Minimum		4	
		Maximum		33	
		Range		29	
		Interquartile Range		7	
		Skewness		.755	.374
		Kurtosis		.468	.733
	Insulin	Mean		34.67	1.457
		95% Confidence Interval for Mean	Lower Bound	31.73	
			Upper Bound	37.62	
		5% Trimmed Mean		35.03	
		Median		36.00	
		Variance		84.943	
		Std. Deviation		9.216	
		Minimum		10	
		Maximum		51	
		Range		41	
		Interquartile Range		11	
		Skewness		-.648	.374
		Kurtosis		.375	.733

Figure 8-41: PLA raw data and statistical analysis for Sortilin/Syntaxin 4 in 3T3-L1 adipocyte cells

A: Results of Mann-Whitney non-parametrical statistical tests of data from Figure 6-9. B: Raw data from Figure 6-9. C: Descriptive statistics of raw data from B.

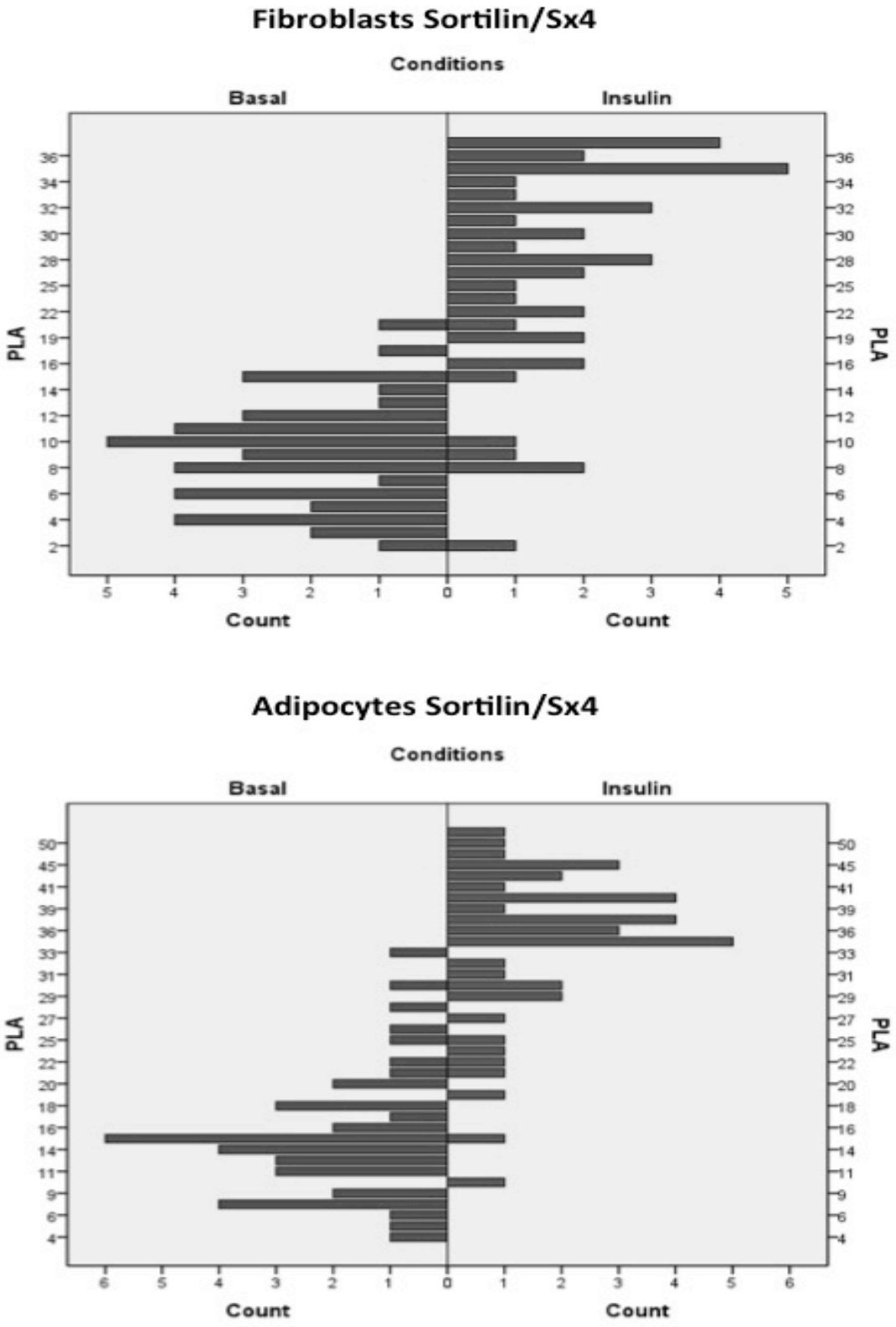

Figure 8-42: 3T3-L1 cell distribution based on PLA results for Sortilin/Syntaxin 4

Cell distribution based on PLA results for Sortilin/Syntaxin 4 (Figure 6-9) under basal conditions and upon insulin stimulation of fibroblasts (upper panel) and adipocytes (lower panel).

Fibroblasts Sortilin/SNAP23

A

Test Statistics[a]

	PLA
Mann-Whitney U	.000
Wilcoxon W	820.000
Z	-7.857
Asymp. Sig. (2-tailed)	.000

a. Grouping Variable: Conditions

B

PLA raw data		
Fibroblasts Sortilin/sx4	Basal	Insulin
1	0	38
2	1	40
3	0	35
4	0	65
5	1	45
6	0	52
7	0	35
8	2	25
9	0	24
10	0	35
11	0	38
12	2	45
13	0	65
14	0	25
15	1	12
16	1	36
17	1	45
18	0	45
19	3	48
20	0	50
21	0	50
22	0	48
23	0	35
24	0	36
25	2	37
26	2	22
27	0	29
28	0	28
29	0	35
30	0	15
31	0	18
32	1	36
33	0	39
34	1	40
35	0	38
36	0	40
37	1	31
38	0	37
39	0	42
40	0	43

C

Descriptives

Conditions				Statistic	Std. Error
PLA	Basal	Mean		.48	.124
		95% Confidence Interval for Mean	Lower Bound	.22	
			Upper Bound	.73	
		5% Trimmed Mean		.39	
		Median		.00	
		Variance		.615	
		Std. Deviation		.784	
		Minimum		0	
		Maximum		3	
		Range		3	
		Interquartile Range		1	
		Skewness		1.599	.374
		Kurtosis		1.841	.733
	Insulin	Mean		37.55	1.802
		95% Confidence Interval for Mean	Lower Bound	33.90	
			Upper Bound	41.20	
		5% Trimmed Mean		37.36	
		Median		37.50	
		Variance		129.946	
		Std. Deviation		11.399	
		Minimum		12	
		Maximum		65	
		Range		53	
		Interquartile Range		13	
		Skewness		.087	.374
		Kurtosis		.745	.733

Figure 8-43: PLA raw data and statistical analysis for Sortilin/SNAP23 in 3T3-L1 fibroblast cells

A: Results of Mann-Whitney non-parametrical statistical tests of data from Figure 6-10. B: Raw data from Figure 6-10. C: Descriptive statistics of raw data from B.

Adipocytes Sortilin/SNAP23

A

Test Statistics[a]

	PLA
Mann-Whitney U	.000
Wilcoxon W	820.000
Z	-7.853
Asymp. Sig. (2-tailed)	.000

a. Grouping Variable: Conditions

B

PLA raw data		
Adipocytes Sortilin/Sx4	Basal	Insulin
1	0	50
2	1	55
3	1	65
4	1	45
5	2	48
6	0	51
7	2	59
8	0	56
9	0	62
10	0	64
11	0	48
12	3	45
13	0	46
14	0	38
15	0	40
16	0	42
17	0	54
18	1	55
19	1	51
20	1	35
21	0	38
22	2	22
23	0	29
24	0	27
25	0	56
26	3	60
27	0	39
28	0	40
29	0	46
30	0	48
31	3	52
32	3	41
33	0	38
34	0	34
35	0	32
36	0	36
37	0	30
38	0	56
39	0	59
40	0	58

C

Descriptives

Conditions				Statistic	Std. Error
PLA	Basal	Mean		.60	.159
		95% Confidence Interval for Mean	Lower Bound	.28	
			Upper Bound	.92	
		5% Trimmed Mean		.50	
		Median		.00	
		Variance		1.015	
		Std. Deviation		1.008	
		Minimum		0	
		Maximum		3	
		Range		3	
		Interquartile Range		1	
		Skewness		1.532	.374
		Kurtosis		1.045	.733
	Insulin	Mean		46.25	1.728
		95% Confidence Interval for Mean	Lower Bound	42.76	
			Upper Bound	49.74	
		5% Trimmed Mean		46.44	
		Median		47.00	
		Variance		119.372	
		Std. Deviation		10.926	
		Minimum		22	
		Maximum		65	
		Range		43	
		Interquartile Range		18	
		Skewness		-.234	.374
		Kurtosis		-.748	.733

Figure 8-44: PLA raw data and statistical analysis for Sortilin/SNAP23 in 3T3-L1 adipocyte cells

A: Results of Mann-Whitney non-parametrical statistical tests of data from Figure 6-10. B: Raw data from Figure 6-10. C: Descriptive statistics of raw data from B.

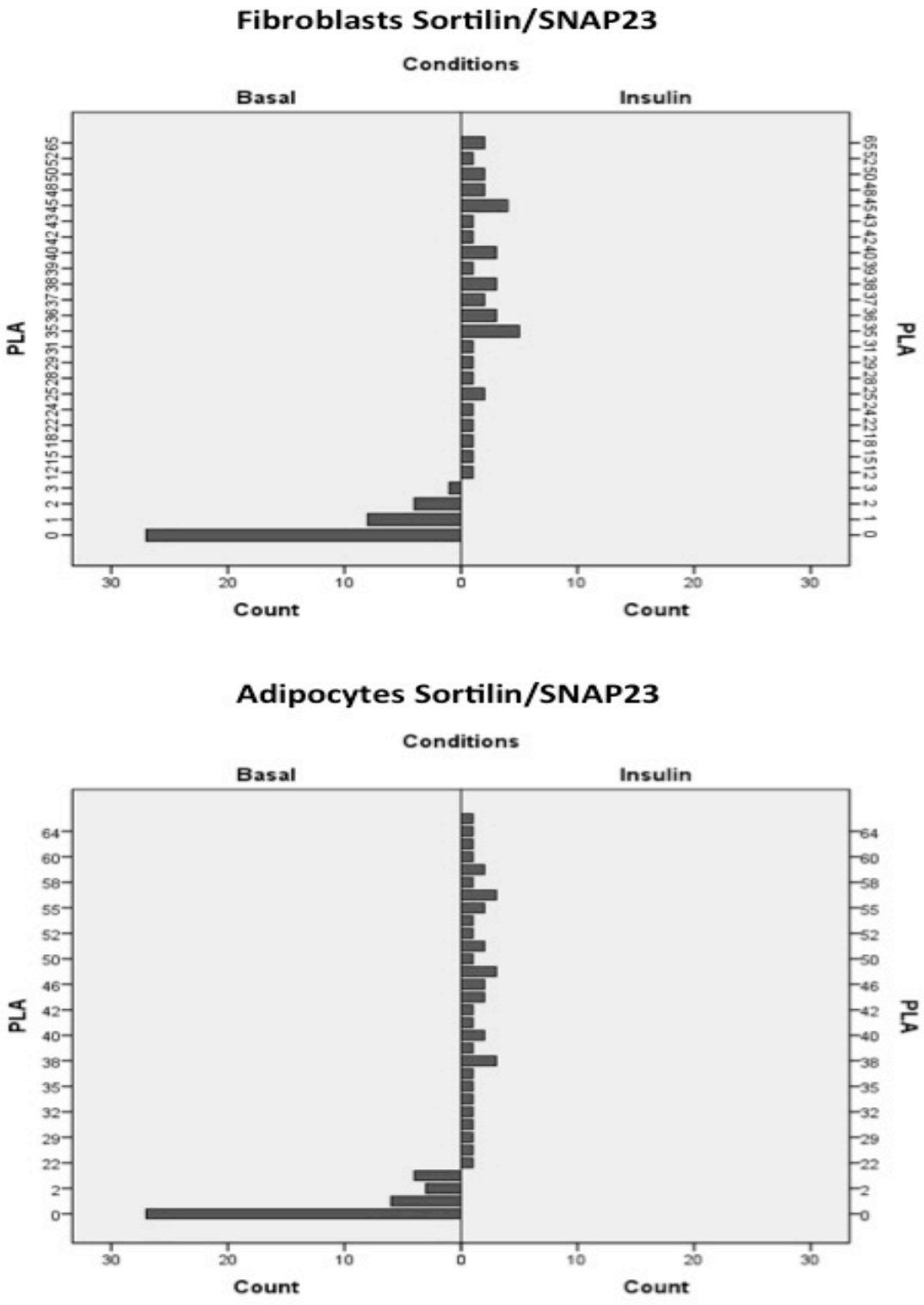

Figure 8-45: 3T3-L1 cell distribution based on PLA results for Sortilin/SNAP23

Cell distribution based on PLA results for Sortilin/SNAP23 (Figure 6-10) under basal conditions and upon insulin stimulation of fibroblasts (upper panel) and adipocytes (lower panel).

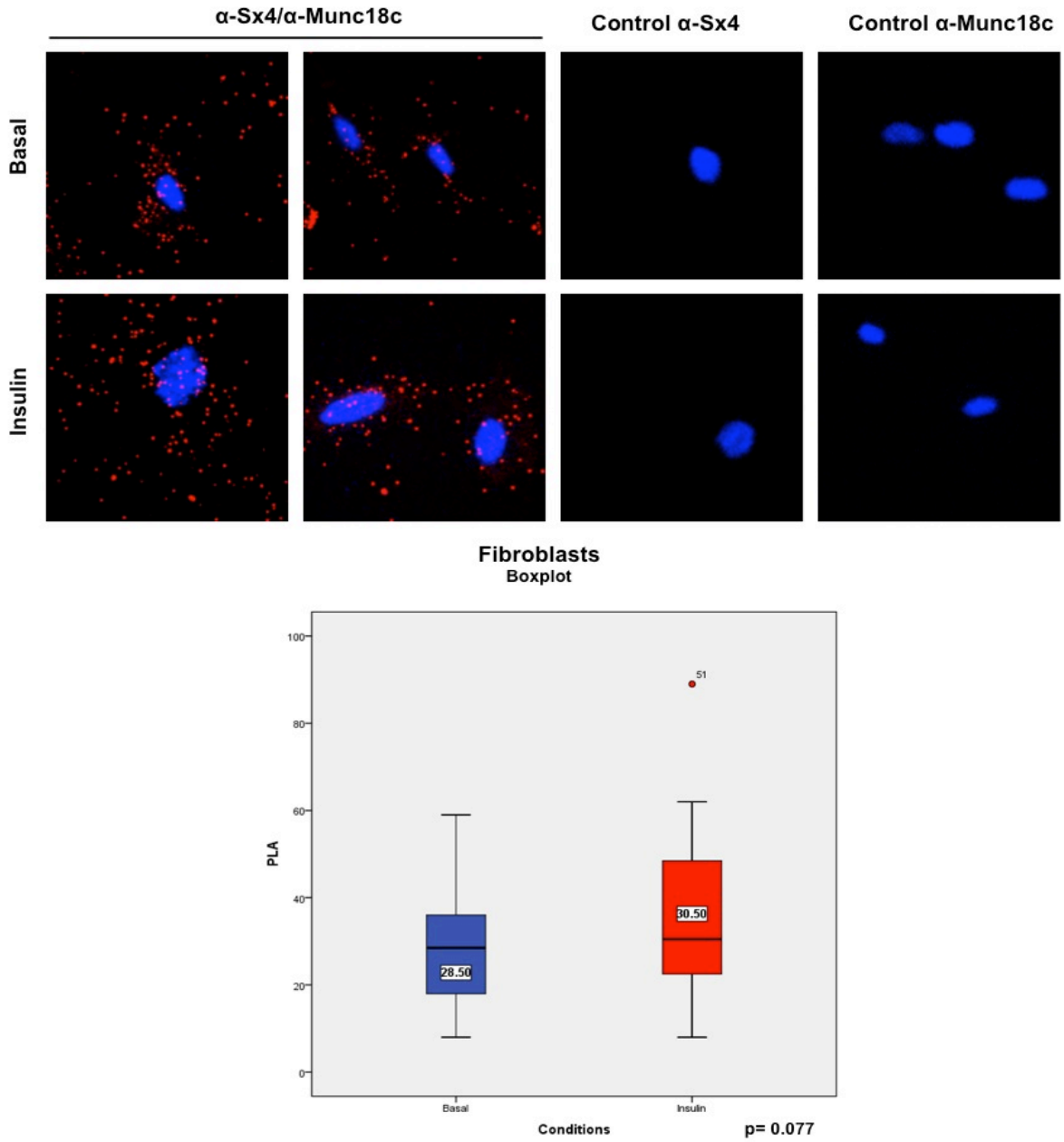

Figure 8-46: Syntaxin 4/Munc18c PLA in 3T3-L1 fibroblasts using a different combination of primary antibodies

PLA using different combination of antibodies against Syntaxin 4 and Munc18c was performed in 3T3-L1 fibroblasts and adipocytes treated with insulin (100nM for 5 min) or not (basal) (section 2.6.5). The antibody against Syntaxin 4 which was used in this experiment was produced in mouse and purchased from Abcam (catalogue# ab77037) in contrast to the antibody which was produced in mouse and purchased from BD Transduction Laboratories (catalogue# 610439) that was used in the same experiment as described in Figure 3-4. Red spots correspond to protein protein interaction couples. Blue: DAPI stained nuclei. The controls shown represent the omission of one of the primary antibody against Syntaxin 4 or Munc18c as ilustrated. Statistical analysis of the PLA results was performed using blobfinder and SPPS software (Mann-Whitney U test). The numbers in the boxes illustrate the median value (32 to 72 cells per experiment). Images are representative of three independent experiments.

Fibroblasts Munc18c/Sx4 (different antibody combination)

A

Test Statistics[a]

	PLA
Mann-Whitney U	616.000
Wilcoxon W	1436.000
Z	-1.771
Asymp. Sig. (2-tailed)	.077

a. Grouping Variable: Conditions

B

PLA raw data (Abcam-Mouse/Abcam-Rabbit)		
Fibroblasts Sx4/ Munc18c	Basal	Insulin
1	24	20
2	42	21
3	32	60
4	30	61
5	18	61
6	25	55
7	29	24
8	10	16
9	10	8
10	11	44
11	31	89
12	36	61
13	44	38
14	18	40
15	33	25
16	33	23
17	28	38
18	31	42
19	53	53
20	44	15
21	13	44
22	22	43
23	36	56
24	59	12
25	11	19
26	47	27
27	24	30
28	36	31
29	22	25
30	18	62
31	14	14
32	40	33
33	39	29
34	27	46
35	29	51
36	37	22
37	26	16
38	23	30
39	8	27
40	14	25

C

Descriptives

Conditions				Statistic	Std. Error
PLA	Basal	Mean		28.18	1.956
		95% Confidence Interval for Mean	Lower Bound	24.22	
			Upper Bound	32.13	
		5% Trimmed Mean		27.69	
		Median		28.50	
		Variance		153.020	
		Std. Deviation		12.370	
		Minimum		8	
		Maximum		59	
		Range		51	
		Interquartile Range		18	
		Skewness		.338	.374
		Kurtosis		-.243	.733
	Insulin	Mean		35.90	2.841
		95% Confidence Interval for Mean	Lower Bound	30.15	
			Upper Bound	41.65	
		5% Trimmed Mean		35.14	
		Median		30.50	
		Variance		322.862	
		Std. Deviation		17.968	
		Minimum		8	
		Maximum		89	
		Range		81	
		Interquartile Range		28	
		Skewness		.743	.374
		Kurtosis		.314	.733

Figure 8-47: PLA raw data and statistical analysis for Munc18c/Syntaxin 4 in 3T3-L1 fibroblast cells (different antibody combination)

A: Results of Mann-Whitney non-parametrical statistical tests of data from Figure 8-46. B: Raw data from Figure 8-46. C: Descriptive statistics of raw data from B.

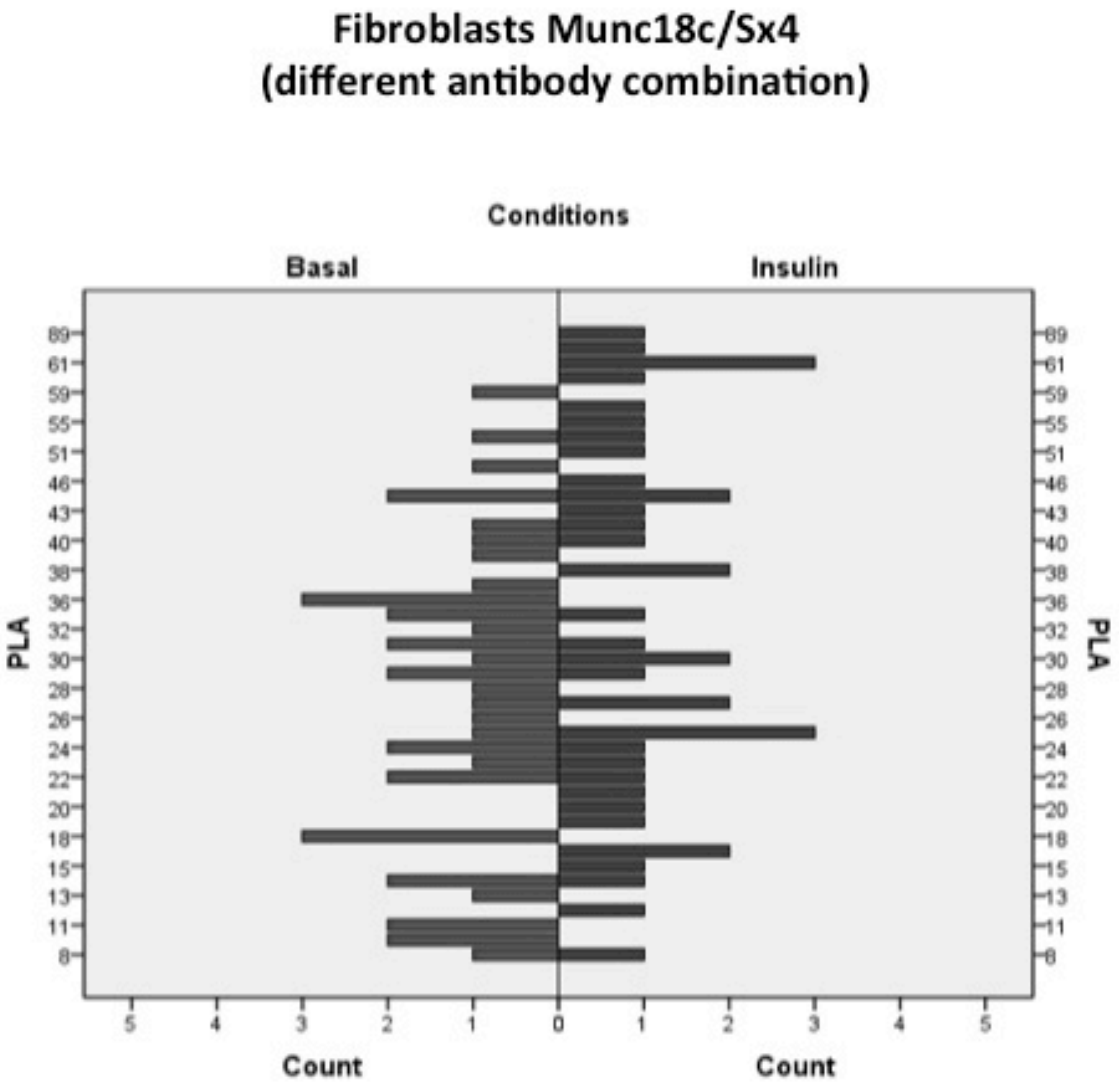

Figure 8-48: 3T3-L1 fibroblast cell distribution based on PLA results for Munc18c/Syntaxin 4 (different antibody combination)

Cell distribution based on PLA results for Munc18c/Syntaxin 4 (Figure 8-46) under basal conditions and upon insulin stimulation.

8.2 Cytosolic domain VAMP2 interactions with Syntaxin 4-GST and mutants thereof – Immunoblots and raw data

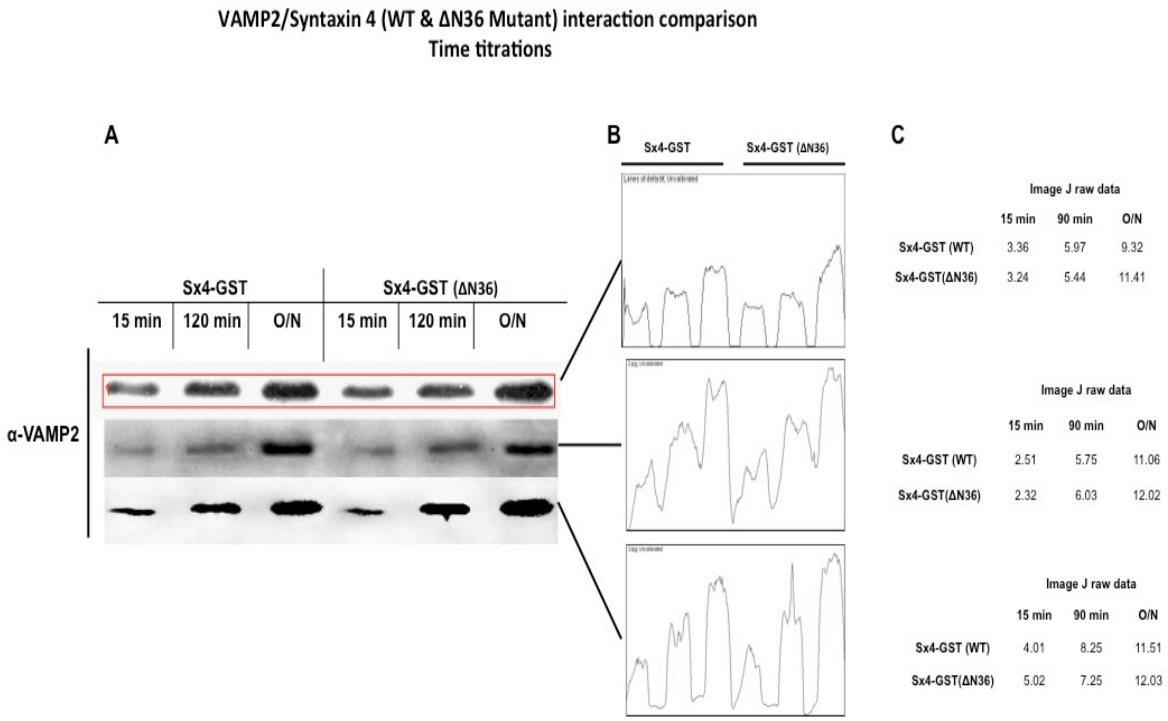

Figure 8-49: Sx4-GST(ΔN36) interacts as efficiently as wild-type Sx4-GST with the cytosolic domain of VAMP2. Raw data from three independent experiments.

A: 10µg of either Sx4-GST or Sx4-GST(ΔN36) bound to glutathione-Sepharose (10µl bed volume) were incubated in 1ml PBS (as described in section 2.4) containing cytosolic domain of VAMP2 in ~10x molar excess for the indicated times on a rotating wheel at 4˚C, after which the beads were washed thoroughly using PBS prior to final resuspension in 50µl 2xLSB and heating to 95˚C for 5 minutes. Eluted proteins were subject to SDS-PAGE through a 15% separating gel and visualized immunoblot analysis using α-VAMP2 antibody (5 µl loading- three panels each represent a single experiment). B: Plots comparing band intensities derived by densitometry using image j software of VAMP2 pulled down by the two different constructs at same time point. C: Numerical raw data from the previous blot expressed as arbitrary units, which used for statistical analysis in Figure 4-17.

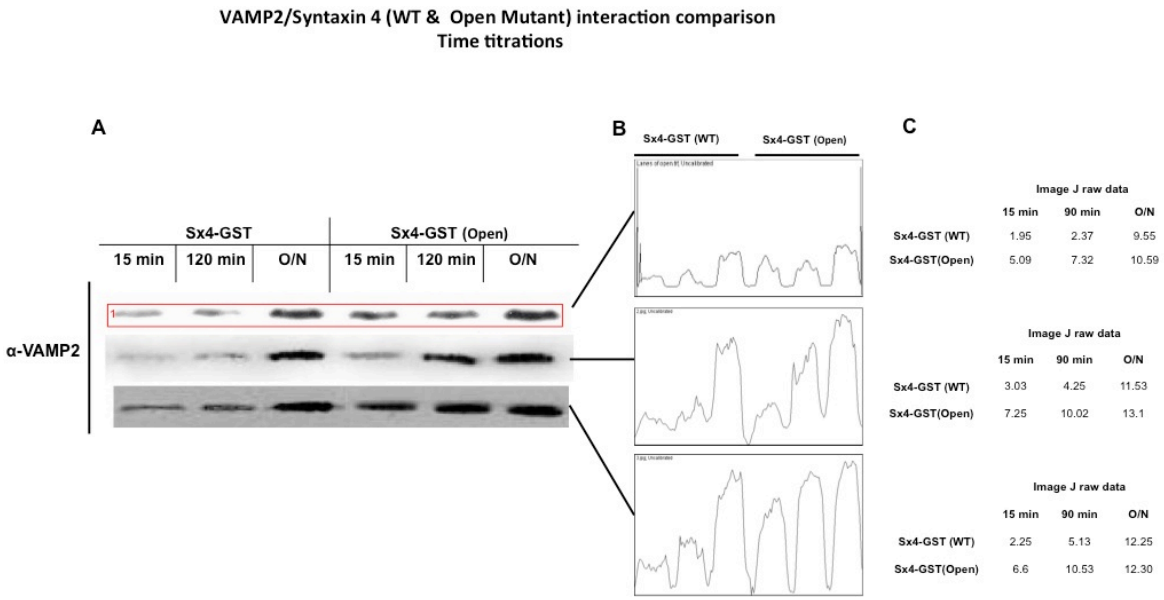

Figure 8-50: Sx4-GST(open) mutant interacts more efficiently than wild-type Sx4-GST with the cytosolic domain of VAMP2. Raw data from three independent experiments.

A: 20µg of either Sx4-GST or Sx4-GST(open) bound to glutathione-Sepharose beads (10µl bed volume) were incubated in 1ml PBS (as described in section 2.4) containing cytosolic domain of VAMP2 in ~10x molar excess for the indicated times on a rotating wheel at 4˚C, after which the beads were washed thoroughly using PBS prior to final resuspension in 50µl 2xLSB and heating to 95˚C for 5 minutes. Eluted proteins were subject to SDS-PAGE through a 15% separating gel and visualized by immunoblot analysis using α-VAMP2 antibody (5 µl loading- three panels each represent a single experiment). B: Plots comparing band intensities derived by densitometry using image j software of VAMP2 pulled down by the two different constructs at same time point. C: Numerical raw data from the previous plots expressed as arbitrary units, which used for statistical analysis in Figure 4-17.

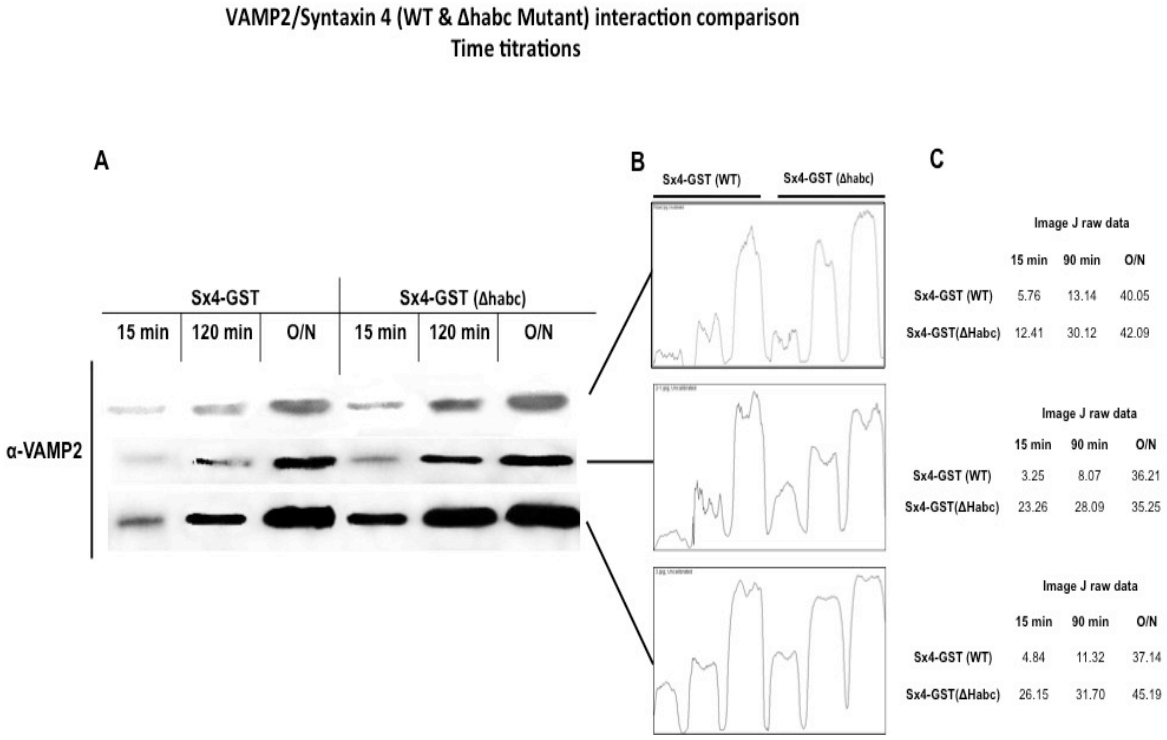

Figure 8-51: Sx4-GST(ΔHabc) interacts more efficiently than wild-type Sx4-GST with the cytosolic domain of VAMP2. Raw data from three independent experiments.

A: 10µg of either Sx4-GST, Sx4-GST(ΔHabc) or GST (negative control) bound to glutathione-Sepharose beads (10µl bed volume) were incubated in 1ml PBS (as described in section 2.4) containing cytosolic domain of VAMP2 in ~10x molar excess for the indicated times on a rotating wheel at 4˚C, after which the beads were washed thoroughly using PBS prior to final resuspension in 50µl 2xLSB and heating to 95˚C for 5 minutes. Eluted proteins were subject to SDS-PAGE through a 15% separating gel and visualized by immunoblot analysis using α-VAMP2 antibody (5 µl loading- three panels each represent a single experiment). B: Plots comparing band intensities derived by densitometry using image j software of VAMP2 pulled down by the two different constructs at same time point. C: Numerical raw data from the previous plots expressed as arbitrary units, which used for statistical analysis in Figure 4-17.

8.3 SNARE Complex formation assays – Immunoblots and raw data

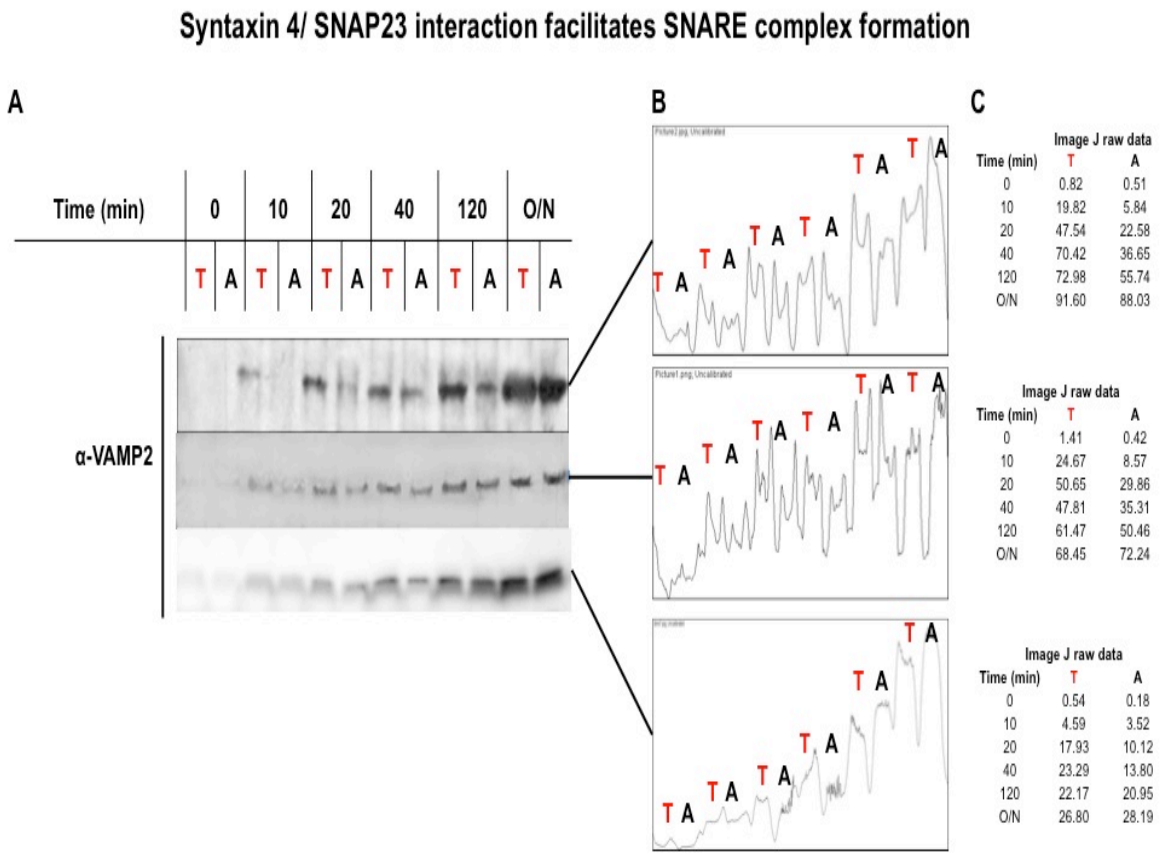

Figure 8-52: Interaction between Syntaxin 4 and SNAP23 facilitates SNARE complex formation. Raw data from three independent experiments.

A: 10 µg Sx4-GST bound to glutathione-Sepharose beads (10µl bed volume) were pre-incubated for two hours with 1ml PBS containing His-SNAP23 in ~10x molar excess (T samples) or not (A samples). After pre-incubation VAMP2-PrA and VAMP2-PrA/His-SNAP23 (both in ~10x molar excess) were added to T and A samples respectively. Samples were incubated for the indicated times on a rotating wheel at 4˚C, after which the beads were washed thoroughly using PBS prior to final resuspension in 50µl 2xLSB and heating to 95˚C for 5 minutes. Samples were subject to SDS-PAGE through a 15% separating gel and visualized by immunoblot analysis using α-VAMP2 antibody (5 µl loading -three panels each represent a single experiment). The smear of bands of a molecular weight around 110kDa and corresponds to the SDS-resistant ternary SNARE complex made of Sx4-GST/His-SNAP23/VAMP-PrA. N.B. recombinanat proteins used in this experiment were prepared as described in section 2.3.5 (Sx4-GST), section 2.3.4 (His-SNAP23) and section 2.3.6 (VAMP2-PrA). B: Plots comparing band intensities at the same time point derived by densitometry using image j software of SNARE complex formed under the two different conditions. C: Numerical raw data from the previous plots expressed as arbitrary units, which used for statistical analysis in Figure 4-24.

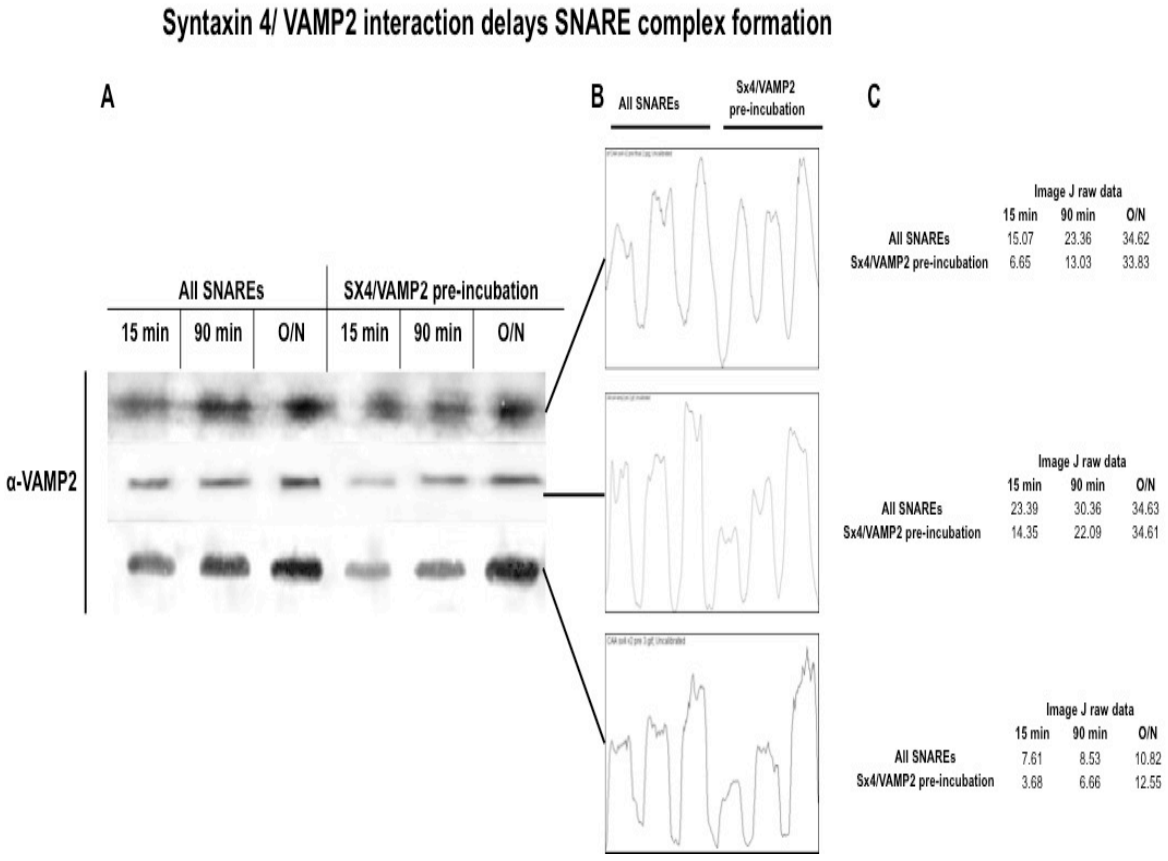

Figure 8-53: VAMP2/Sx4 interaction inhibits SNARE complex formation. Raw data from three independent experiments.

A: 50 µg His-SNAP23 bound to Ni-Agarose beads (10µl bed volume) were incubated for the indicated times with 1ml PBS solution containing VAMP2/Sx4 in ~10x molar excess that has been pre-incubated for two hours or not as indicated. After incubation on a rotating wheel at 4˚C, beads were washed thoroughly using the appropriate buffer (section 2.3.4) prior to final resuspension in 50µl 2xLSB and heating to 95˚C for 5 minutes. Eluted proteins were subject to SDS-PAGE through a 15% separating gel and visualized by immunoblot analysis using α-VAMP2 antibody (5 µl loading-three panels each represent a single experiment). The bands of a molecular weight around 70kDa correspond to the SDS-resistant ternary SNARE complex made of Sx4 /His-SNAP23/VAMP. N.B. recombinanat proteins used in this experiment were prepared as described in sections 2.3.5 and 2.3.7(cytosolic Syntaxin 4), section 2.3.4 (His-SNAP23) and sections 2.3.5 and 2.3.7 (cytosolic VAMP2). B: Plots comparing band intensities at the same time point derived by densitometry using image j software of SNARE complex formed under the two different conditions. C: Numerical raw data from the previous plots expressed as arbitrary units, which used for statistical analysis in Figure 4-24.

8.4 Pull down assays using adipocyte lysates – Immunoblots and raw data

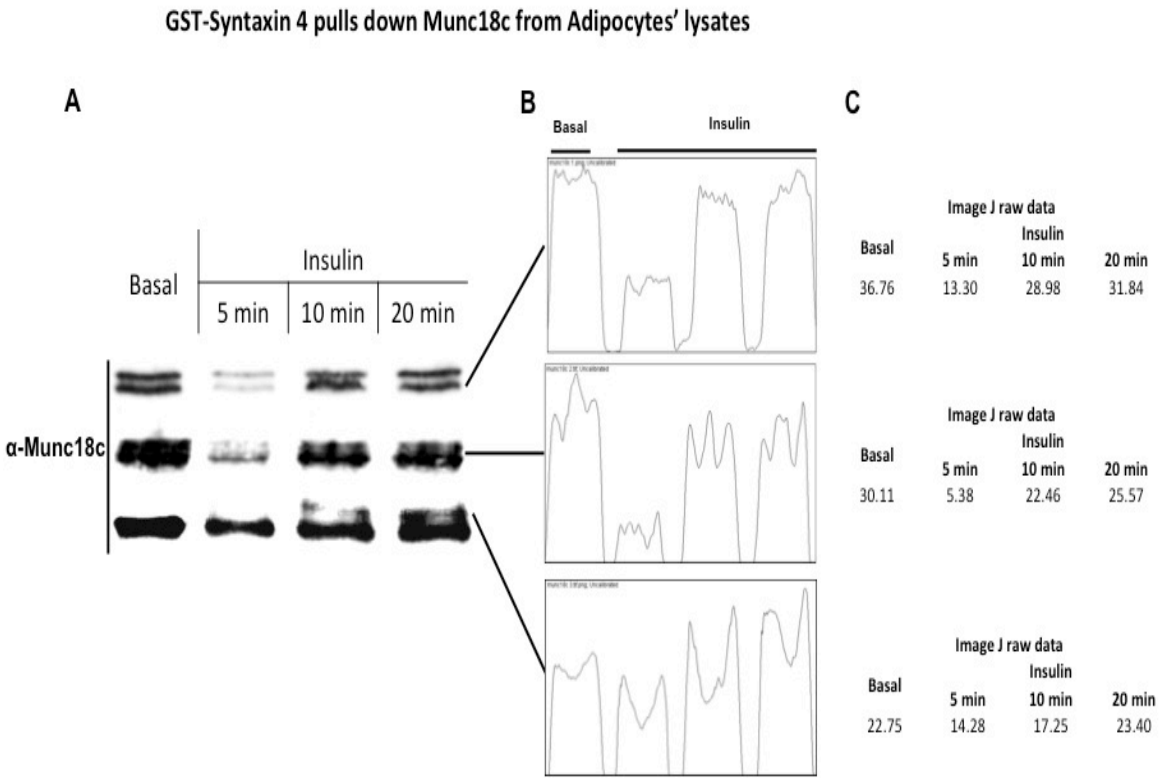

Figure 8-54: Influence of insulin-treatment on pull down of Munc18c by Syntaxin 4-GST from adipocyte lysates. Raw data from three independent experiments.

10 µg of C-terminally GST-tagged Syntaxin 4 (Sx4-GST) bound to glutathione-Sepharose beads (10µl bed volume) were incubated with 3T3L1 adipocyte lysates prepared from cells that either have been treated with 100nM of insulin for the indicated times or not as outlined in methods (sections 2.6.5 and 2.6.6). Following incubation on a rotating wheel at 4°C for two hours beads were washed extensively using adipocyte lysis buffer prior to final resuspension in 50µl 2xLSB and heating to 60°C for 10 minutes. Eluted proteins were subject to SDS-PAGE through a 15% separating gel and visualized by immuneblot analysis using α-Munc18c antibody (5 µl loading- three panels each represents a single experiment). B: Plots comparing band intensities derived by densitometry using image j software of Munc18c pulled down under different conditions as illustrated Syntaxin 4-GST. C: Numerical raw data from the previous plots expressed as arbitrary units, which used for statistical analysis in Figure 5-6 after being normalized to both beads and lysate protein input.

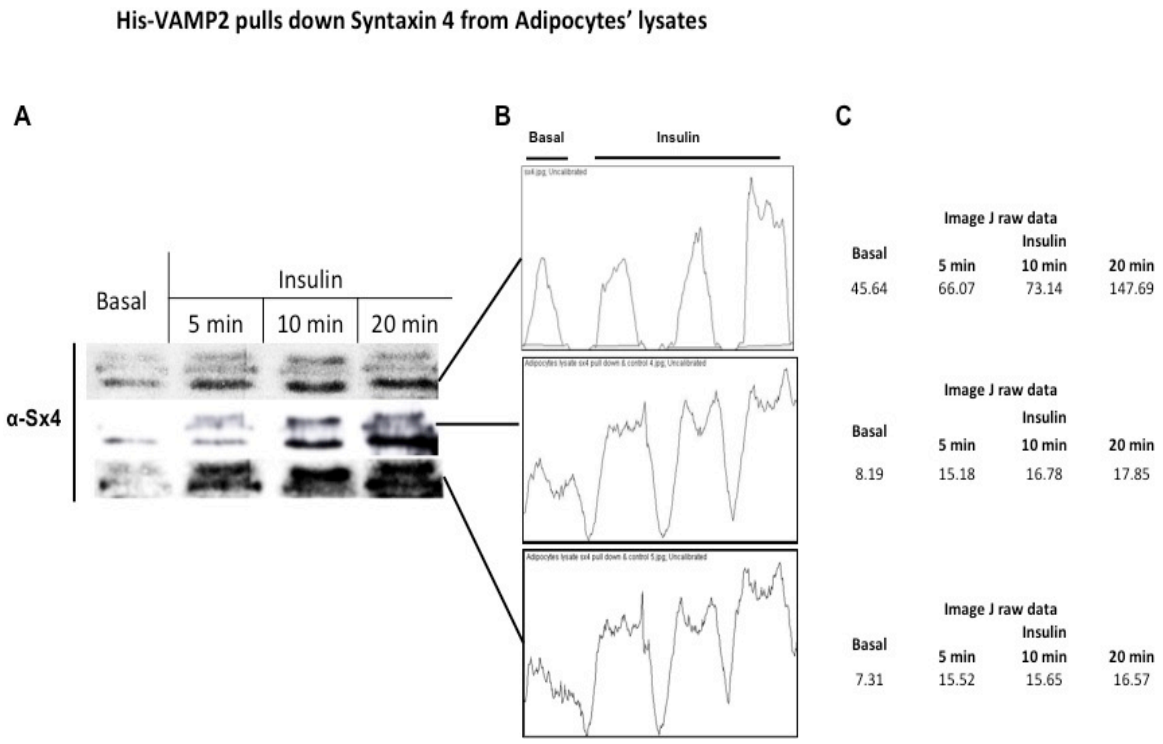

Figure 8-55: Influence of insulin-treatment on pull down of Syntaxin 4 by His-VAMP2 from adipocyte lysates. Raw data from three independent experiments.

10 µg of N-terminally his-tagged VAMP2 (His-VAMP2) bound to Ni-Agarose (5 µl bed volume) were incubated with 3T3L1 adipocyte lysates prepared from cells that either have been treated with 100nM of insulin for the indicated times or not as outlined in methods (sections 2.6.5 and 2.6.6). Following incubation on a rotating wheel at 4°C for two hours beads were washed extensively using adipocyte lysis buffer prior to the addition of 50µl 2xLSB and heating to 60°C for 10 minutes. Eluted proteins were subject to SDS-PAGE through a 15% separating gel and were visualized by immunoblot analysis using α-Syntaxin 4 antibody (5 µl loading) (lower panel-three panels each represents a single experiment). B: Plots comparing band intensities derived by densitometry using image j software of Syntaxin 4 pulled down under different conditions as illustrated by His-VAMP2. C: Numerical raw data from the previous plots expressed as arbitrary units, which used for statistical analysis in Figure 4-19 after being normalized to both beads and lysate protein inputs.

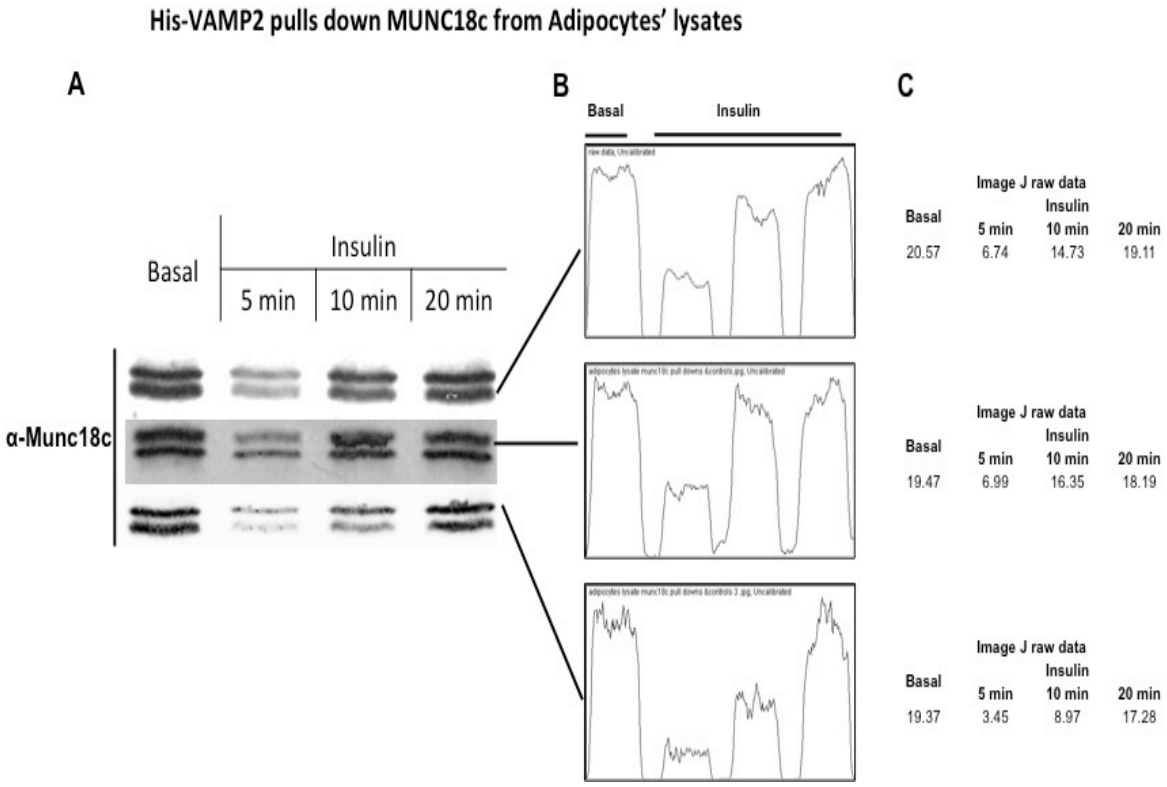

Figure 8-56: Influence of insulin-treatment on pull down of Munc18c by His-VAMP2 from adipocyte lysates. Raw data from three independent experiments.

10 µg of N-terminally his-tagged VAMP2 (His-VAMP2) bound to Ni-Agarose (5 µl bed volume) were incubated with 3T3L1 adipocyte lysates prepared from cells that either have been treated with 100nM of insulin for the indicated times or not as outlined in methods (sections 2.6.5 and 2.6.6). Following incubation on a rotating wheel at 4°C for two hours beads were washed extensively using adipocyte lysis buffer prior to the addition of 50µl 2xLSB and heating to 60°C for 10 minutes. Eluted proteins were subject to SDS-PAGE through a 15% separating gel and were visualized by immunoblot analysis using α-Munc18c antibody (5 µl loading - three panels each represents a single experiment). B: Plots comparing band intensities derived by densitometry using image j software of Munc18c pulled down under different conditions as illustrated by His-VAMP2. C: Numerical raw data from the previous plots expressed as arbitrary units, which used for statistical analysis in Figure 5-7 after being normalized to both beads and lysate protein inputs.

List of references

Aledo, J.C., Lavoie, L., Volchuk, A., Keller, S.R., Klip, A., and Hundal, H.S. (1997). Identification and characterization of two distinct intracellular GLUT4 pools in rat skeletal muscle: evidence for an endosomal and an insulin-sensitive GLUT4 compartment. Biochem J *325 (Pt 3)*, 727-732.

Alessi, D.R., James, S.R., Downes, C.P., Holmes, A.B., Gaffney, P.R., Reese, C.B., and Cohen, P. (1997). Characterization of a 3-phosphoinositide-dependent protein kinase which phosphorylates and activates protein kinase Balpha. Curr Biol *7*, 261-269.

Alexandrov, K., Horiuchi, H., Steele-Mortimer, O., Seabra, M.C., and Zerial, M. (1994). Rab escort protein-1 is a multifunctional protein that accompanies newly prenylated rab proteins to their target membranes. EMBO J *13*, 5262-5273.

Andag, U., Neumann, T., and Schmitt, H.D. (2001). The coatomer-interacting protein Dsl1p is required for Golgi-to-endoplasmic reticulum retrieval in yeast. J Biol Chem *276*, 39150-39160.

Antonin, W., Fasshauer, D., Becker, S., Jahn, R., and Schneider, T.R. (2002). Crystal structure of the endosomal SNARE complex reveals common structural principles of all SNAREs. Nature structural biology *9*, 107-111.

Araki, S., Tamori, Y., Kawanishi, M., Shinoda, H., Masugi, J., Mori, H., Niki, T., Okazawa, H., Kubota, T., and Kasuga, M. (1997). Inhibition of the binding of SNAP-23 to syntaxin 4 by Munc18c. Biochem Biophys Res Commun *234*, 257-262.

Aran, V., Brandie, F.M., Boyd, A.R., Kantidakis, T., Rideout, E.J., Kelly, S.M., Gould, G.W., and Bryant, N.J. (2009). Characterization of two distinct binding modes between syntaxin 4 and Munc18c. Biochem J *419*, 655-660.

Aran, V., Bryant, N.J., and Gould, G.W. (2011). Tyrosine phosphorylation of Munc18c on residue 521 abrogates binding to Syntaxin 4. BMC Biochem *12*, 19.

Barlowe, C. (1997). Coupled ER to Golgi transport reconstituted with purified cytosolic proteins. J Cell Biol *139*, 1097-1108.

Baumann, C.A., Ribon, V., Kanzaki, M., Thurmond, D.C., Mora, S., Shigematsu, S., Bickel, P.E., Pessin, J.E., and Saltiel, A.R. (2000). CAP defines a second signalling pathway required for insulin-stimulated glucose transport. Nature *407*, 202-207.

Baumert, M., Maycox, P.R., Navone, F., De Camilli, P., and Jahn, R. (1989). Synaptobrevin: an integral membrane protein of 18,000 daltons present in small synaptic vesicles of rat brain. EMBO J *8*, 379-384.

Bell, G.I., and Polonsky, K.S. (2001). Diabetes mellitus and genetically programmed defects in beta-cell function. Nature *414*, 788-791.

Bennett, M.K., Calakos, N., and Scheller, R.H. (1992). Syntaxin: a synaptic protein implicated in docking of synaptic vesicles at presynaptic active zones. Science *257*, 255-259.

Bock, J.B., Matern, H.T., Peden, A.A., and Scheller, R.H. (2001). A genomic perspective on membrane compartment organization. Nature *409*, 839-841.

Bonifacino, J.S., and Glick, B.S. (2004). The mechanisms of vesicle budding and fusion. Cell *116*, 153-166.

Bracher, A., and Weissenhorn, W. (2002). Structural basis for the Golgi membrane recruitment of Sly1p by Sed5p. EMBO J *21*, 6114-6124.

Bradford, M.M. (1976). A rapid and sensitive method for the quantitation of microgram quantities of protein utilizing the principle of protein-dye binding. Analytical biochemistry *72*, 248-254.

Brandie, F.M., Aran, V., Verma, A., McNew, J.A., Bryant, N.J., and Gould, G.W. (2008). Negative regulation of syntaxin4/SNAP-23/VAMP2-mediated membrane fusion by Munc18c in vitro. PLoS One *3*, e4074.

Brenner, S. (1974). The genetics of Caenorhabditis elegans. Genetics *77*, 71-94.

Brunger, A.T. (2005). Structure and function of SNARE and SNARE-interacting proteins. Q Rev Biophys *38*, 1-47.

Bryant, N.J., and Gould, G.W. (2011). SNARE proteins underpin insulin-regulated GLUT4 traffic. Traffic *12*, 657-664.

Bryant, N.J., Govers, R., and James, D.E. (2002). Regulated transport of the glucose transporter GLUT4. Nat Rev Mol Cell Biol *3*, 267-277.

Bryant, N.J., and James, D.E. (2001). Vps45p stabilizes the syntaxin homologue Tlg2p and positively regulates SNARE complex formation. EMBO J *20*, 3380-3388.

Bryant, N.J., and James, D.E. (2003). The Sec1p/Munc18 (SM) protein, Vps45p, cycles on and off membranes during vesicle transport. J Cell Biol *161*, 691-696.

Burgoyne, R.D., and Morgan, A. (2007). Membrane trafficking: three steps to fusion. Curr Biol *17*, R255-258.

Burkhardt, P., Hattendorf, D.A., Weis, W.I., and Fasshauer, D. (2008). Munc18a controls SNARE assembly through its interaction with the syntaxin N-peptide. EMBO J *27*, 923-933.

Cai, H., Reinisch, K., and Ferro-Novick, S. (2007). Coats, tethers, Rabs, and SNAREs work together to mediate the intracellular destination of a transport vesicle. Developmental cell *12*, 671-682.

Cain, C.C., Trimble, W.S., and Lienhard, G.E. (1992). Members of the VAMP family of synaptic vesicle proteins are components of glucose transporter-containing vesicles from rat adipocytes. J Biol Chem *267*, 11681-11684.

Calakos, N., Bennett, M.K., Peterson, K.E., and Scheller, R.H. (1994). Protein-protein interactions contributing to the specificity of intracellular vesicular trafficking. Science *263*, 1146-1149.

Carpp, L.N., Ciufo, L.F., Shanks, S.G., Boyd, A., and Bryant, N.J. (2006). The Sec1p/Munc18 protein Vps45p binds its cognate SNARE proteins via two distinct modes. J Cell Biol *173*, 927-936.

Carr, C.M., Grote, E., Munson, M., Hughson, F.M., and Novick, P.J. (1999). Sec1p binds to SNARE complexes and concentrates at sites of secretion. J Cell Biol *146*, 333-344.

Carroll, K.S., Hanna, J., Simon, I., Krise, J., Barbero, P., and Pfeffer, S.R. (2001). Role of Rab9 GTPase in facilitating receptor recruitment by TIP47. Science *292*, 1373-1376.

Carvalho, E., Schellhorn, S.E., Zabolotny, J.M., Martin, S., Tozzo, E., Peroni, O.D., Houseknecht, K.L., Mundt, A., James, D.E., and Kahn, B.B. (2004). GLUT4 overexpression or deficiency in adipocytes of transgenic mice alters the composition of GLUT4 vesicles and the subcellular localization of GLUT4 and insulin-responsive aminopeptidase. J Biol Chem *279*, 21598-21605.

Cavanaugh, L.F., Chen, X., Richardson, B.C., Ungar, D., Pelczer, I., Rizo, J., and Hughson, F.M. (2007). Structural analysis of conserved oligomeric Golgi complex subunit 2. J Biol Chem *282*, 23418-23426.

Chen, Y.A., and Scheller, R.H. (2001). SNARE-mediated membrane fusion. Nat Rev Mol Cell Biol *2*, 98-106.

Chernomordik, L.V., and Kozlov, M.M. (2005). Membrane hemifusion: crossing a chasm in two leaps. Cell *123*, 375-382.

Chernomordik, L.V., and Kozlov, M.M. (2008). Mechanics of membrane fusion. Nat Struct Mol Biol *15*, 675-683.

Chiang, S.H., Baumann, C.A., Kanzaki, M., Thurmond, D.C., Watson, R.T., Neudauer, C.L., Macara, I.G., Pessin, J.E., and Saltiel, A.R. (2001). Insulin-stimulated GLUT4 translocation requires the CAP-dependent activation of TC10. Nature *410*, 944-948.

Christie, M.P., Whitten, A.E., King, G.J., Hu, S.H., Jarrott, R.J., Chen, K.E., Duff, A.P., Callow, P., Collins, B.M., James, D.E., *et al.* (2012). Low-resolution solution structures of Munc18:Syntaxin protein complexes indicate an open binding mode driven by the Syntaxin N-peptide. Proc Natl Acad Sci U S A.

Conboy, M.J., and Cyert, M.S. (2000). Luv1p/Rki1p/Tcs3p/Vps54p, a yeast protein that localizes to the late Golgi and early endosome, is required for normal vacuolar morphology. Mol Biol Cell *11*, 2429-2443.

Cushman, S.W., and Wardzala, L.J. (1980). Potential mechanism of insulin action on glucose transport in the isolated rat adipose cell. Apparent translocation of intracellular transport systems to the plasma membrane. J Biol Chem *255*, 4758-4762.

D'Andrea-Merrins, M., Chang, L., Lam, A.D., Ernst, S.A., and Stuenkel, E.L. (2007). Munc18c interaction with syntaxin 4 monomers and SNARE complex intermediates in GLUT4 vesicle trafficking. J Biol Chem *282*, 16553-16566.

Dacks, J.B., and Field, M.C. (2007). Evolution of the eukaryotic membrane-trafficking system: origin, tempo and mode. J Cell Sci *120*, 2977-2985.

Deak, F., Schoch, S., Liu, X., Sudhof, T.C., and Kavalali, E.T. (2004). Synaptobrevin is essential for fast synaptic-vesicle endocytosis. Nature cell biology *6*, 1102-1108.

Delprato, A., Merithew, E., and Lambright, D.G. (2004). Structure, exchange determinants, and family-wide rab specificity of the tandem helical bundle and Vps9 domains of Rabex-5. Cell *118*, 607-617.

Dulubova, I., Khvotchev, M., Liu, S., Huryeva, I., Sudhof, T.C., and Rizo, J. (2007). Munc18-1 binds directly to the neuronal SNARE complex. Proc Natl Acad Sci U S A *104*, 2697-2702.

Dulubova, I., Sugita, S., Hill, S., Hosaka, M., Fernandez, I., Sudhof, T.C., and Rizo, J. (1999). A conformational switch in syntaxin during exocytosis: role of munc18. EMBO J *18*, 4372-4382.

Dulubova, I., Yamaguchi, T., Gao, Y., Min, S.W., Huryeva, I., Sudhof, T.C., and Rizo, J. (2002). How Tlg2p/syntaxin 16 'snares' Vps45. EMBO J *21*, 3620-3631.

Dun, A.R., Rickman, C., and Duncan, R.R. (2010). The t-SNARE complex: a close up. Cell Mol Neurobiol *30*, 1321-1326.

Eyster, C.A., Duggins, Q.S., Gorbsky, G.J., and Olson, A.L. (2006). Microtubule network is required for insulin signaling through activation of Akt/protein kinase B: evidence that insulin stimulates vesicle docking/fusion but not intracellular mobility. J Biol Chem *281*, 39719-39727.

Fasshauer, D., Antonin, W., Margittai, M., Pabst, S., and Jahn, R. (1999). Mixed and non-cognate SNARE complexes. Characterization of assembly and biophysical properties. J Biol Chem *274*, 15440-15446.

Fasshauer, D., Sutton, R.B., Brunger, A.T., and Jahn, R. (1998). Conserved structural features of the synaptic fusion complex: SNARE proteins reclassified as Q- and R-SNAREs. Proc Natl Acad Sci U S A *95*, 15781-15786.

Fernandez, I., Ubach, J., Dulubova, I., Zhang, X., Sudhof, T.C., and Rizo, J. (1998). Three-dimensional structure of an evolutionarily conserved N-terminal domain of syntaxin 1A. Cell *94*, 841-849.

Fujita, Y., Shirataki, H., Sakisaka, T., Asakura, T., Ohya, T., Kotani, H., Yokoyama, S., Nishioka, H., Matsuura, Y., Mizoguchi, A., *et al.* (1998). Tomosyn: a syntaxin-1-binding protein that forms a novel complex in the neurotransmitter release process. Neuron *20*, 905-915.

Fukuda, M. (2008). Regulation of secretory vesicle traffic by Rab small GTPases. Cell Mol Life Sci *65*, 2801-2813.

Fukuda, R., McNew, J.A., Weber, T., Parlati, F., Engel, T., Nickel, W., Rothman, J.E., and Sollner, T.H. (2000). Functional architecture of an intracellular membrane t-SNARE. Nature *407*, 198-202.

Gaisano, H.Y., Sheu, L., and Whitcomb, D. (2004). Alcoholic chronic pancreatitis involves displacement of Munc18c from the pancreatic acinar basal membrane surface. Pancreas *28*, 395-400.

Gammeltoft, S., and Van Obberghen, E. (1986). Protein kinase activity of the insulin receptor. Biochem J *235*, 1-11.

Gengyo-Ando, K., Kitayama, H., Mukaida, M., and Ikawa, Y. (1996). A murine neural-specific homolog corrects cholinergic defects in Caenorhabditis elegans unc-18 mutants. The Journal of neuroscience : the official journal of the Society for Neuroscience *16*, 6695-6702.

Gonzalo, S., and Linder, M.E. (1998). SNAP-25 palmitoylation and plasma membrane targeting require a functional secretory pathway. Mol Biol Cell *9*, 585-597.

Groffen, A.J., Jacobsen, L., Schut, D., and Verhage, M. (2005). Two distinct genes drive expression of seven tomosyn isoforms in the mammalian brain, sharing a conserved structure with a unique variable domain. J Neurochem *92*, 554-568.

Gual, P., Le Marchand-Brustel, Y., and Tanti, J.F. (2005). Positive and negative regulation of insulin signaling through IRS-1 phosphorylation. Biochimie *87*, 99-109.

Halemani, N.D., Bethani, I., Rizzoli, S.O., and Lang, T. (2010). Structure and dynamics of a two-helix SNARE complex in live cells. Traffic *11*, 394-404.

Hashiramoto, M., and James, D.E. (2000). Characterization of insulin-responsive GLUT4 storage vesicles isolated from 3T3-L1 adipocytes. Mol Cell Biol *20*, 416-427.

Hayashi, T., McMahon, H., Yamasaki, S., Binz, T., Hata, Y., Sudhof, T.C., and Niemann, H. (1994). Synaptic vesicle membrane fusion complex: action of clostridial neurotoxins on assembly. EMBO J *13*, 5051-5061.

He, B., and Guo, W. (2009). The exocyst complex in polarized exocytosis. Curr Opin Cell Biol *21*, 537-542.

Hirshman, M.F., Goodyear, L.J., Wardzala, L.J., Horton, E.D., and Horton, E.S. (1990). Identification of an intracellular pool of glucose transporters from basal and insulin-stimulated rat skeletal muscle. J Biol Chem *265*, 987-991.

Hong, W. (2005). SNAREs and traffic. Biochim Biophys Acta *1744*, 120-144.

Hu, S.H., Gee, C.L., Latham, C.F., Rowlinson, S.W., Rova, U., Jones, A., Halliday, J.A., Bryant, N.J., James, D.E., and Martin, J.L. (2003). Recombinant expression of Munc18c in a baculovirus system and interaction with syntaxin4. Protein expression and purification *31*, 305-310.

Hu, S.H., Latham, C.F., Gee, C.L., James, D.E., and Martin, J.L. (2007). Structure of the Munc18c/Syntaxin4 N-peptide complex defines universal features of the N-peptide binding mode of Sec1/Munc18 proteins. Proc Natl Acad Sci U S A *104*, 8773-8778.

James, D.E. (2005). MUNC-ing around with insulin action. J Clin Invest *115*, 219-221.

James, D.E., Brown, R., Navarro, J., and Pilch, P.F. (1988). Insulin-regulatable tissues express a unique insulin-sensitive glucose transport protein. Nature *333*, 183-185.

James, D.E., Strube, M., and Mueckler, M. (1989). Molecular cloning and characterization of an insulin-regulatable glucose transporter. Nature *338*, 83-87.

Jedrychowski, M.P., Gartner, C.A., Gygi, S.P., Zhou, L., Herz, J., Kandror, K.V., and Pilch, P.F. (2010). Proteomic analysis of GLUT4 storage vesicles reveals LRP1 to be an important vesicle component and target of insulin signaling. J Biol Chem *285*, 104-114.

Jewell, J.L., Oh, E., Bennett, S.M., Meroueh, S.O., and Thurmond, D.C. (2008). The tyrosine phosphorylation of Munc18c induces a switch in binding specificity from syntaxin 4 to Doc2beta. J Biol Chem *283*, 21734-21746.

Jewell, J.L., Oh, E., Ramalingam, L., Kalwat, M.A., Tagliabracci, V.S., Tackett, L., Elmendorf, J.S., and Thurmond, D.C. (2011). Munc18c phosphorylation by the insulin receptor links cell signaling directly to SNARE exocytosis. J Cell Biol *193*, 185-199.

Jewell, J.L., Oh, E., and Thurmond, D.C. (2010). Exocytosis mechanisms underlying insulin release and glucose uptake: conserved roles for Munc18c and syntaxin 4. Am J Physiol Regul Integr Comp Physiol *298*, R517-531.

Johnson, J.R., Ferdek, P., Lian, L.Y., Barclay, J.W., Burgoyne, R.D., and Morgan, A. (2009). Binding of UNC-18 to the N-terminus of syntaxin is essential for neurotransmission in Caenorhabditis elegans. Biochem J *418*, 73-80.

Kanda, H., Tamori, Y., Shinoda, H., Yoshikawa, M., Sakaue, M., Udagawa, J., Otani, H., Tashiro, F., Miyazaki, J., and Kasuga, M. (2005). Adipocytes from Munc18c-null mice show increased sensitivity to insulin-stimulated GLUT4 externalization. J Clin Invest *115*, 291-301.

Kandror, K.V., Coderre, L., Pushkin, A.V., and Pilch, P.F. (1995). Comparison of glucose-transporter-containing vesicles from rat fat and muscle tissues: evidence for a unique endosomal compartment. Biochem J *307 (Pt 2)*, 383-390.

Kandror, K.V., and Pilch, P.F. (2011). The sugar is sIRVed: sorting Glut4 and its fellow travelers. Traffic *12*, 665-671.

Katz, L., and Brennwald, P. (2000). Testing the 3Q:1R "rule": mutational analysis of the ionic "zero" layer in the yeast exocytic SNARE complex reveals no requirement for arginine. Mol Biol Cell *11*, 3849-3858.

Kawaguchi, T., Tamori, Y., Kanda, H., Yoshikawa, M., Tateya, S., Nishino, N., and Kasuga, M. (2010). The t-SNAREs syntaxin4 and SNAP23 but not v-SNARE VAMP2 are indispensable to tether GLUT4 vesicles at the plasma membrane in adipocyte. Biochem Biophys Res Commun *391*, 1336-1341.

Kawanishi, M., Tamori, Y., Okazawa, H., Araki, S., Shinoda, H., and Kasuga, M. (2000). Role of SNAP23 in insulin-induced translocation of GLUT4 in 3T3-L1 adipocytes. Mediation of complex formation between syntaxin4 and VAMP2. J Biol Chem *275*, 8240-8247.

Ke, B., Oh, E., and Thurmond, D.C. (2007). Doc2beta is a novel Munc18c-interacting partner and positive effector of syntaxin 4-mediated exocytosis. J Biol Chem *282*, 21786-21797.

Kee, Y., Yoo, J.S., Hazuka, C.D., Peterson, K.E., Hsu, S.C., and Scheller, R.H. (1997). Subunit structure of the mammalian exocyst complex. Proc Natl Acad Sci U S A *94*, 14438-14443.

Khan, A.H., Thurmond, D.C., Yang, C., Ceresa, B.P., Sigmund, C.D., and Pessin, J.E. (2001). Munc18c regulates insulin-stimulated glut4 translocation to the transverse tubules in skeletal muscle. J Biol Chem *276*, 4063-4069.

Khvotchev, M., Dulubova, I., Sun, J., Dai, H., Rizo, J., and Sudhof, T.C. (2007). Dual modes of Munc18-1/SNARE interactions are coupled by functionally critical binding to syntaxin-1 N terminus. The Journal of neuroscience : the official journal of the Society for Neuroscience *27*, 12147-12155.

Kimura, A., Baumann, C.A., Chiang, S.H., and Saltiel, A.R. (2001). The sorbin homology domain: a motif for the targeting of proteins to lipid rafts. Proc Natl Acad Sci U S A *98*, 9098-9103.

Kohn, A.D., Summers, S.A., Birnbaum, M.J., and Roth, R.A. (1996). Expression of a constitutively active Akt Ser/Thr kinase in 3T3-L1 adipocytes stimulates glucose uptake and glucose transporter 4 translocation. J Biol Chem *271*, 31372-31378.

Kupriyanova, T.A., and Kandror, K.V. (2000). Cellugyrin is a marker for a distinct population of intracellular Glut4-containing vesicles. J Biol Chem *275*, 36263-36268.

Kupriyanova, T.A., Kandror, V., and Kandror, K.V. (2002). Isolation and characterization of the two major intracellular Glut4 storage compartments. J Biol Chem *277*, 9133-9138.

Lampson, M.A., Schmoranzer, J., Zeigerer, A., Simon, S.M., and McGraw, T.E. (2001). Insulin-regulated release from the endosomal recycling compartment is regulated by budding of specialized vesicles. Mol Biol Cell *12*, 3489-3501.

Lang, T., and Jahn, R. (2008). Core proteins of the secretory machinery. Handb Exp Pharmacol, 107-127.

Larance, M., Ramm, G., Stockli, J., van Dam, E.M., Winata, S., Wasinger, V., Simpson, F., Graham, M., Junutula, J.R., Guilhaus, M., *et al.* (2005). Characterization of the role of the Rab GTPase-activating protein AS160 in insulin-regulated GLUT4 trafficking. J Biol Chem *280*, 37803-37813.

Latham, C.F., Lopez, J.A., Hu, S.H., Gee, C.L., Westbury, E., Blair, D.H., Armishaw, C.J., Alewood, P.F., Bryant, N.J., James, D.E., *et al.* (2006).

Molecular dissection of the Munc18c/syntaxin4 interaction: implications for regulation of membrane trafficking. Traffic *7*, 1408-1419.

Latham, C.F., Osborne, S.L., Cryle, M.J., and Meunier, F.A. (2007). Arachidonic acid potentiates exocytosis and allows neuronal SNARE complex to interact with Munc18a. J Neurochem *100*, 1543-1554.

Laufman, O., Kedan, A., Hong, W., and Lev, S. (2009). Direct interaction between the COG complex and the SM protein, Sly1, is required for Golgi SNARE pairing. EMBO J *28*, 2006-2017.

Leney, S.E., and Tavare, J.M. (2009). The molecular basis of insulin-stimulated glucose uptake: signalling, trafficking and potential drug targets. J Endocrinol *203*, 1-18.

Li, L.V., Bakirtzi, K., Watson, R.T., Pessin, J.E., and Kandror, K.V. (2009). The C-terminus of GLUT4 targets the transporter to the perinuclear compartment but not to the insulin-responsive vesicles. Biochem J *419*, 105-112, 101 p following 112.

Livingstone, C., James, D.E., Rice, J.E., Hanpeter, D., and Gould, G.W. (1996). Compartment ablation analysis of the insulin-responsive glucose transporter (GLUT4) in 3T3-L1 adipocytes. Biochem J *315 (Pt 2)*, 487-495.

MacDonald, C., Munson, M., and Bryant, N.J. (2010). Autoinhibition of SNARE complex assembly by a conformational switch represents a conserved feature of syntaxins. Biochem Soc Trans *38*, 209-212.

Malsam, J., Kreye, S., and Sollner, T.H. (2008). Membrane fusion: SNAREs and regulation. Cell Mol Life Sci *65*, 2814-2832.

Margittai, M., Fasshauer, D., Pabst, S., Jahn, R., and Langen, R. (2001). Homo- and heterooligomeric SNARE complexes studied by site-directed spin labeling. J Biol Chem *276*, 13169-13177.

Martin, L.B., Shewan, A., Millar, C.A., Gould, G.W., and James, D.E. (1998). Vesicle-associated membrane protein 2 plays a specific role in the insulin-dependent trafficking of the facilitative glucose transporter GLUT4 in 3T3-L1 adipocytes. J Biol Chem *273*, 1444-1452.

Martin, S., Tellam, J., Livingstone, C., Slot, J.W., Gould, G.W., and James, D.E. (1996). The glucose transporter (GLUT-4) and vesicle-associated membrane protein-2 (VAMP-2) are segregated from recycling endosomes in insulin-sensitive cells. J Cell Biol *134*, 625-635.

Masaki, R., Yamamoto, A., Akagawa, K., and Tashiro, Y. (1998). Important roles of the C-terminal portion of HPC-1/syntaxin 1A in membrane anchoring and intracellular localization. Journal of biochemistry *124*, 311-318.

Matsui, Y., Kikuchi, A., Araki, S., Hata, Y., Kondo, J., Teranishi, Y., and Takai, Y. (1990). Molecular cloning and characterization of a novel type of regulatory protein (GDI) for smg p25A, a ras p21-like GTP-binding protein. Mol Cell Biol *10*, 4116-4122.

Medine, C.N., Rickman, C., Chamberlain, L.H., and Duncan, R.R. (2007). Munc18-1 prevents the formation of ectopic SNARE complexes in living cells. J Cell Sci *120*, 4407-4415.

Miinea, C.P., Sano, H., Kane, S., Sano, E., Fukuda, M., Peranen, J., Lane, W.S., and Lienhard, G.E. (2005). AS160, the Akt substrate regulating GLUT4 translocation, has a functional Rab GTPase-activating protein domain. Biochem J *391*, 87-93.

Millar, C.A., Shewan, A., Hickson, G.R., James, D.E., and Gould, G.W. (1999). Differential regulation of secretory compartments containing the insulin-responsive glucose transporter 4 in 3T3-L1 adipocytes. Mol Biol Cell *10*, 3675-3688.

Min, J., Okada, S., Kanzaki, M., Elmendorf, J.S., Coker, K.J., Ceresa, B.P., Syu, L.J., Noda, Y., Saltiel, A.R., and Pessin, J.E. (1999). Synip: a novel insulin-regulated syntaxin 4-binding protein mediating GLUT4 translocation in adipocytes. Molecular cell *3*, 751-760.

Misura, K.M., Scheller, R.H., and Weis, W.I. (2000). Three-dimensional structure of the neuronal-Sec1-syntaxin 1a complex. Nature *404*, 355-362.

Mitra, P., Zheng, X., and Czech, M.P. (2004). RNAi-based analysis of CAP, Cbl, and CrkII function in the regulation of GLUT4 by insulin. J Biol Chem *279*, 37431-37435.

Molero, J.C., Jensen, T.E., Withers, P.C., Couzens, M., Herzog, H., Thien, C.B., Langdon, W.Y., Walder, K., Murphy, M.A., Bowtell, D.D., *et al.* (2004). c-Cbl-deficient mice have reduced adiposity, higher energy expenditure, and improved peripheral insulin action. J Clin Invest *114*, 1326-1333.

Montecucco, C., Schiavo, G., and Pantano, S. (2005). SNARE complexes and neuroexocytosis: how many, how close? Trends in biochemical sciences *30*, 367-372.

Munson, M., and Bryant, N.J. (2009). A role for the syntaxin N-terminus. Biochem J *418*, e1-3.

Munson, M., Chen, X., Cocina, A.E., Schultz, S.M., and Hughson, F.M. (2000). Interactions within the yeast t-SNARE Sso1p that control SNARE complex assembly. Nature structural biology *7*, 894-902.

Nielsen, E., Christoforidis, S., Uttenweiler-Joseph, S., Miaczynska, M., Dewitte, F., Wilm, M., Hoflack, B., and Zerial, M. (2000). Rabenosyn-5, a novel Rab5 effector, is complexed with hVPS45 and recruited to endosomes through a FYVE finger domain. J Cell Biol *151*, 601-612.

Novick, P., Field, C., and Schekman, R. (1980). Identification of 23 complementation groups required for post-translational events in the yeast secretory pathway. Cell *21*, 205-215.

Oh, E., Spurlin, B.A., Pessin, J.E., and Thurmond, D.C. (2005). Munc18c heterozygous knockout mice display increased susceptibility for severe glucose intolerance. Diabetes *54*, 638-647.

Oh, E., and Thurmond, D.C. (2006). The stimulus-induced tyrosine phosphorylation of Munc18c facilitates vesicle exocytosis. J Biol Chem *281*, 17624-17634.

Ohya, T., Miaczynska, M., Coskun, U., Lommer, B., Runge, A., Drechsel, D., Kalaidzidis, Y., and Zerial, M. (2009). Reconstitution of Rab- and SNARE-dependent membrane fusion by synthetic endosomes. Nature *459*, 1091-1097.

Okada, S., Ohshima, K., Uehara, Y., Shimizu, H., Hashimoto, K., Yamada, M., and Mori, M. (2007). Synip phosphorylation is required for insulin-stimulated Glut4 translocation. Biochem Biophys Res Commun *356*, 102-106.

Ostrowicz, C.W., Meiringer, C.T., and Ungermann, C. (2008). Yeast vacuole fusion: a model system for eukaryotic endomembrane dynamics. Autophagy *4*, 5-19.

Pagan, J.K., Wylie, F.G., Joseph, S., Widberg, C., Bryant, N.J., James, D.E., and Stow, J.L. (2003). The t-SNARE syntaxin 4 is regulated during macrophage activation to function in membrane traffic and cytokine secretion. Curr Biol *13*, 156-160.

Palade, G. (1975). Intracellular aspects of the process of protein synthesis. Science *189*, 867.

Pan, X., Eathiraj, S., Munson, M., and Lambright, D.G. (2006). TBC-domain GAPs for Rab GTPases accelerate GTP hydrolysis by a dual-finger mechanism. Nature *442*, 303-306.

Parlati, F., McNew, J.A., Fukuda, R., Miller, R., Sollner, T.H., and Rothman, J.E. (2000). Topological restriction of SNARE-dependent membrane fusion. Nature *407*, 194-198.

Parlati, F., Varlamov, O., Paz, K., McNew, J.A., Hurtado, D., Sollner, T.H., and Rothman, J.E. (2002). Distinct SNARE complexes mediating membrane fusion in Golgi transport based on combinatorial specificity. Proc Natl Acad Sci U S A *99*, 5424-5429.

Paumet, F., Brugger, B., Parlati, F., McNew, J.A., Sollner, T.H., and Rothman, J.E. (2001). A t-SNARE of the endocytic pathway must be activated for fusion. J Cell Biol *155*, 961-968.

Peng, R., and Gallwitz, D. (2002). Sly1 protein bound to Golgi syntaxin Sed5p allows assembly and contributes to specificity of SNARE fusion complexes. J Cell Biol *157*, 645-655.

Peng, R., and Gallwitz, D. (2004). Multiple SNARE interactions of an SM protein: Sed5p/Sly1p binding is dispensable for transport. EMBO J *23*, 3939-3949.

Pevsner, J., Hsu, S.C., Braun, J.E., Calakos, N., Ting, A.E., Bennett, M.K., and Scheller, R.H. (1994). Specificity and regulation of a synaptic vesicle docking complex. Neuron *13*, 353-361.

Pfeffer, S.R. (1999). Transport-vesicle targeting: tethers before SNAREs. Nature cell biology *1*, E17-22.

Ploug, T., van Deurs, B., Ai, H., Cushman, S.W., and Ralston, E. (1998). Analysis of GLUT4 distribution in whole skeletal muscle fibers: identification of distinct storage compartments that are recruited by insulin and muscle contractions. J Cell Biol *142*, 1429-1446.

Pobbati, A.V., Stein, A., and Fasshauer, D. (2006). N- to C-terminal SNARE complex assembly promotes rapid membrane fusion. Science *313*, 673-676.

Polgar, J., Chung, S.H., and Reed, G.L. (2002). Vesicle-associated membrane protein 3 (VAMP-3) and VAMP-8 are present in human platelets and are required for granule secretion. Blood *100*, 1081-1083.

Rand, R.P. (1981). Interacting phospholipid bilayers: measured forces and induced structural changes. Annual review of biophysics and bioengineering *10*, 277-314.

Randhawa, V.K., Bilan, P.J., Khayat, Z.A., Daneman, N., Liu, Z., Ramlal, T., Volchuk, A., Peng, X.R., Coppola, T., Regazzi, R., *et al*. (2000). VAMP2, but not VAMP3/cellubrevin, mediates insulin-dependent incorporation of GLUT4 into the plasma membrane of L6 myoblasts. Mol Biol Cell *11*, 2403-2417.

Ravichandran, V., Chawla, A., and Roche, P.A. (1996). Identification of a novel syntaxin- and synaptobrevin/VAMP-binding protein, SNAP-23, expressed in non-neuronal tissues. J Biol Chem *271*, 13300-13303.

Rea, S., Martin, L.B., McIntosh, S., Macaulay, S.L., Ramsdale, T., Baldini, G., and James, D.E. (1998). Syndet, an adipocyte target SNARE involved in the insulin-induced translocation of GLUT4 to the cell surface. J Biol Chem *273*, 18784-18792.

Reed, B.C., and Lane, M.D. (1980). Insulin receptor synthesis and turnover in differentiating 3T3-L1 preadipocytes. Proc Natl Acad Sci U S A *77*, 285-289.

Rizo, J., Chen, X., and Arac, D. (2006). Unraveling the mechanisms of synaptotagmin and SNARE function in neurotransmitter release. Trends Cell Biol *16*, 339-350.

Rizo, J., and Sudhof, T.C. (2002). Snares and Munc18 in synaptic vesicle fusion. Nat Rev Neurosci *3*, 641-653.

Rodkey, T.L., Liu, S., Barry, M., and McNew, J.A. (2008). Munc18a scaffolds SNARE assembly to promote membrane fusion. Mol Biol Cell *19*, 5422-5434.

Rothman, J.E. (1994). Mechanisms of intracellular protein transport. Nature *372*, 55-63.

Rowe, J., Calegari, F., Taverna, E., Longhi, R., and Rosa, P. (2001). Syntaxin 1A is delivered to the apical and basolateral domains of epithelial cells: the role of munc-18 proteins. J Cell Sci *114*, 3323-3332.

Rowland, A.F., Fazakerley, D.J., and James, D.E. (2011). Mapping insulin/GLUT4 circuitry. Traffic *12*, 672-681.

Sacher, M., Kim, Y.G., Lavie, A., Oh, B.H., and Segev, N. (2008). The TRAPP complex: insights into its architecture and function. Traffic *9*, 2032-2042.

Saltiel, A.R., and Kahn, C.R. (2001). Insulin signalling and the regulation of glucose and lipid metabolism. Nature *414*, 799-806.

Sano, H., Kane, S., Sano, E., and Lienhard, G.E. (2005). Synip phosphorylation does not regulate insulin-stimulated GLUT4 translocation. Biochem Biophys Res Commun *332*, 880-884.

Sano, H., Kane, S., Sano, E., Miinea, C.P., Asara, J.M., Lane, W.S., Garner, C.W., and Lienhard, G.E. (2003). Insulin-stimulated phosphorylation of a Rab GTPase-activating protein regulates GLUT4 translocation. J Biol Chem *278*, 14599-14602.

Sano, H., Roach, W.G., Peck, G.R., Fukuda, M., and Lienhard, G.E. (2008). Rab10 in insulin-stimulated GLUT4 translocation. Biochem J *411*, 89-95.

Sapperstein, S.K., Lupashin, V.V., Schmitt, H.D., and Waters, M.G. (1996). Assembly of the ER to Golgi SNARE complex requires Uso1p. J Cell Biol *132*, 755-767.

Sato, T.K., Rehling, P., Peterson, M.R., and Emr, S.D. (2000). Class C Vps protein complex regulates vacuolar SNARE pairing and is required for vesicle docking/fusion. Molecular cell *6*, 661-671.

Schiavo, G., Benfenati, F., Poulain, B., Rossetto, O., Polverino de Laureto, P., DasGupta, B.R., and Montecucco, C. (1992). Tetanus and botulinum-B neurotoxins block neurotransmitter release by proteolytic cleavage of synaptobrevin. Nature *359*, 832-835.

Schmelzle, K., Kane, S., Gridley, S., Lienhard, G.E., and White, F.M. (2006). Temporal dynamics of tyrosine phosphorylation in insulin signaling. Diabetes *55*, 2171-2179.

Schoch, S., Deak, F., Konigstorfer, A., Mozhayeva, M., Sara, Y., Sudhof, T.C., and Kavalali, E.T. (2001). SNARE function analyzed in synaptobrevin/VAMP knockout mice. Science *294*, 1117-1122.

Schutz, D., Zilly, F., Lang, T., Jahn, R., and Bruns, D. (2005). A dual function for Munc-18 in exocytosis of PC12 cells. The European journal of neuroscience *21*, 2419-2432.

Scott, B.L., Van Komen, J.S., Irshad, H., Liu, S., Wilson, K.A., and McNew, J.A. (2004). Sec1p directly stimulates SNARE-mediated membrane fusion in vitro. J Cell Biol *167*, 75-85.

Seabra, M.C., and Coudrier, E. (2004). Rab GTPases and myosin motors in organelle motility. Traffic *5*, 393-399.

Semerdjieva, S., Shortt, B., Maxwell, E., Singh, S., Fonarev, P., Hansen, J., Schiavo, G., Grant, B.D., and Smythe, E. (2008). Coordinated regulation of AP2 uncoating from clathrin-coated vesicles by rab5 and hRME-6. J Cell Biol *183*, 499-511.

Shen, J., Tareste, D.C., Paumet, F., Rothman, J.E., and Melia, T.J. (2007). Selective activation of cognate SNAREpins by Sec1/Munc18 proteins. Cell *128*, 183-195.

Shewan, A.M., Marsh, B.J., Melvin, D.R., Martin, S., Gould, G.W., and James, D.E. (2000). The cytosolic C-terminus of the glucose transporter GLUT4 contains an acidic cluster endosomal targeting motif distal to the dileucine signal. Biochem J *350 Pt 1*, 99-107.

Sieber, J.J., Willig, K.I., Kutzner, C., Gerding-Reimers, C., Harke, B., Donnert, G., Rammner, B., Eggeling, C., Hell, S.W., Grubmuller, H., *et al.* (2007). Anatomy and dynamics of a supramolecular membrane protein cluster. Science *317*, 1072-1076.

Sinha, R., Ahmed, S., Jahn, R., and Klingauf, J. (2011). Two synaptobrevin molecules are sufficient for vesicle fusion in central nervous system synapses. Proc Natl Acad Sci U S A *108*, 14318-14323.

Slot, J.W., Geuze, H.J., Gigengack, S., James, D.E., and Lienhard, G.E. (1991a). Translocation of the glucose transporter GLUT4 in cardiac myocytes of the rat. Proc Natl Acad Sci U S A *88*, 7815-7819.

Slot, J.W., Geuze, H.J., Gigengack, S., Lienhard, G.E., and James, D.E. (1991b). Immuno-localization of the insulin regulatable glucose transporter in brown adipose tissue of the rat. J Cell Biol *113*, 123-135.

Smith, R.M., Charron, M.J., Shah, N., Lodish, H.F., and Jarett, L. (1991). Immunoelectron microscopic demonstration of insulin-stimulated translocation of glucose transporters to the plasma membrane of isolated rat adipocytes and masking of the carboxyl-terminal epitope of intracellular GLUT4. Proc Natl Acad Sci U S A *88*, 6893-6897.

Smithers, N.P., Hodgkinson, C.P., Cuttle, M., and Sale, G.J. (2008). Insulin-triggered repositioning of munc18c on syntaxin-4 in GLUT4 signalling. Biochem J *410*, 255-260.

Smyth, A.M., Duncan, R.R., and Rickman, C. (2010). Munc18-1 and syntaxin1: unraveling the interactions between the dynamic duo. Cell Mol Neurobiol *30*, 1309-1313.

Soderberg, O., Gullberg, M., Jarvius, M., Ridderstrale, K., Leuchowius, K.J., Jarvius, J., Wester, K., Hydbring, P., Bahram, F., Larsson, L.G., *et al.* (2006). Direct observation of individual endogenous protein complexes in situ by proximity ligation. Nature methods *3*, 995-1000.

Soderberg, O., Leuchowius, K.J., Gullberg, M., Jarvius, M., Weibrecht, I., Larsson, L.G., and Landegren, U. (2008). Characterizing proteins and their interactions in cells and tissues using the in situ proximity ligation assay. Methods *45*, 227-232.

Sollner, T., Bennett, M.K., Whiteheart, S.W., Scheller, R.H., and Rothman, J.E. (1993a). A protein assembly-disassembly pathway in vitro that may correspond to sequential steps of synaptic vesicle docking, activation, and fusion. Cell *75*, 409-418.

Sollner, T., Whiteheart, S.W., Brunner, M., Erdjument-Bromage, H., Geromanos, S., Tempst, P., and Rothman, J.E. (1993b). SNAP receptors implicated in vesicle targeting and fusion. Nature *362*, 318-324.

Sollner, T.H. (2003). Regulated exocytosis and SNARE function (Review). Mol Membr Biol *20*, 209-220.

Sorensen, J.B., Nagy, G., Varoqueaux, F., Nehring, R.B., Brose, N., Wilson, M.C., and Neher, E. (2003). Differential control of the releasable vesicle pools by SNAP-25 splice variants and SNAP-23. Cell *114*, 75-86.

Spurlin, B.A., Park, S.Y., Nevins, A.K., Kim, J.K., and Thurmond, D.C. (2004). Syntaxin 4 transgenic mice exhibit enhanced insulin-mediated glucose uptake in skeletal muscle. Diabetes *53*, 2223-2231.

Spurlin, B.A., Thomas, R.M., Nevins, A.K., Kim, H.J., Kim, Y.J., Noh, H.L., Shulman, G.I., Kim, J.K., and Thurmond, D.C. (2003). Insulin resistance in tetracycline-repressible Munc18c transgenic mice. Diabetes *52*, 1910-1917.

St-Denis, J.F., Cabaniols, J.P., Cushman, S.W., and Roche, P.A. (1999). SNAP-23 participates in SNARE complex assembly in rat adipose cells. Biochem J *338 (Pt 3)*, 709-715.

Stein, A., Weber, G., Wahl, M.C., and Jahn, R. (2009). Helical extension of the neuronal SNARE complex into the membrane. Nature *460*, 525-528.

Stenkula, K.G., Lizunov, V.A., Cushman, S.W., and Zimmerberg, J. (2010). Insulin controls the spatial distribution of GLUT4 on the cell surface through regulation of its postfusion dispersal. Cell Metab *12*, 250-259.

Stenmark, H. (2009). Rab GTPases as coordinators of vesicle traffic. Nat Rev Mol Cell Biol *10*, 513-525.

Stockli, J., Fazakerley, D.J., and James, D.E. (2011). GLUT4 exocytosis. J Cell Sci *124*, 4147-4159.

Sudhof, T.C. (2004). The synaptic vesicle cycle. Annual review of neuroscience *27*, 509-547.

Sudhof, T.C., and Rothman, J.E. (2009). Membrane fusion: grappling with SNARE and SM proteins. Science *323*, 474-477.

Sutton, R.B., Fasshauer, D., Jahn, R., and Brunger, A.T. (1998). Crystal structure of a SNARE complex involved in synaptic exocytosis at 2.4 A resolution. Nature *395*, 347-353.

Suzuki, K., and Kono, T. (1980). Evidence that insulin causes translocation of glucose transport activity to the plasma membrane from an intracellular storage site. Proc Natl Acad Sci U S A *77*, 2542-2545.

Tamori, Y., Kawanishi, M., Niki, T., Shinoda, H., Araki, S., Okazawa, H., and Kasuga, M. (1998). Inhibition of insulin-induced GLUT4 translocation by Munc18c through interaction with syntaxin4 in 3T3-L1 adipocytes. J Biol Chem *273*, 19740-19746.

Tellam, J.T., Macaulay, S.L., McIntosh, S., Hewish, D.R., Ward, C.W., and James, D.E. (1997). Characterization of Munc-18c and syntaxin-4 in 3T3-L1 adipocytes. Putative role in insulin-dependent movement of GLUT-4. J Biol Chem *272*, 6179-6186.

TerBush, D.R., Maurice, T., Roth, D., and Novick, P. (1996). The Exocyst is a multiprotein complex required for exocytosis in Saccharomyces cerevisiae. EMBO J *15*, 6483-6494.

TerBush, D.R., and Novick, P. (1995). Sec6, Sec8, and Sec15 are components of a multisubunit complex which localizes to small bud tips in Saccharomyces cerevisiae. J Cell Biol *130*, 299-312.

Thurmond, D.C., Ceresa, B.P., Okada, S., Elmendorf, J.S., Coker, K., and Pessin, J.E. (1998). Regulation of insulin-stimulated GLUT4 translocation by Munc18c in 3T3L1 adipocytes. J Biol Chem *273*, 33876-33883.

Thurmond, D.C., Kanzaki, M., Khan, A.H., and Pessin, J.E. (2000). Munc18c function is required for insulin-stimulated plasma membrane fusion of GLUT4 and insulin-responsive amino peptidase storage vesicles. Mol Cell Biol *20*, 379-388.

Thurmond, D.C., and Pessin, J.E. (2000). Discrimination of GLUT4 vesicle trafficking from fusion using a temperature-sensitive Munc18c mutant. EMBO J *19*, 3565-3575.

Tokumaru, H., Umayahara, K., Pellegrini, L.L., Ishizuka, T., Saisu, H., Betz, H., Augustine, G.J., and Abe, T. (2001). SNARE complex oligomerization by synaphin/complexin is essential for synaptic vesicle exocytosis. Cell *104*, 421-432.

Toonen, R.F., and Verhage, M. (2003). Vesicle trafficking: pleasure and pain from SM genes. Trends Cell Biol *13*, 177-186.

Toonen, R.F., and Verhage, M. (2007). Munc18-1 in secretion: lonely Munc joins SNARE team and takes control. Trends Neurosci *30*, 564-572.

Trimble, W.S., Cowan, D.M., and Scheller, R.H. (1988). VAMP-1: a synaptic vesicle-associated integral membrane protein. Proc Natl Acad Sci U S A *85*, 4538-4542.

Tripathi, A., Ren, Y., Jeffrey, P.D., and Hughson, F.M. (2009). Structural characterization of Tip20p and Dsl1p, subunits of the Dsl1p vesicle tethering complex. Nat Struct Mol Biol *16*, 114-123.

Ullrich, O., Stenmark, H., Alexandrov, K., Huber, L.A., Kaibuchi, K., Sasaki, T., Takai, Y., and Zerial, M. (1993). Rab GDP dissociation inhibitor as a general regulator for the membrane association of rab proteins. J Biol Chem *268*, 18143-18150.

Umahara, M., Okada, S., Yamada, E., Saito, T., Ohshima, K., Hashimoto, K., Yamada, M., Shimizu, H., Pessin, J.E., and Mori, M. (2008). Tyrosine phosphorylation of Munc18c regulates platelet-derived growth factor-stimulated

glucose transporter 4 translocation in 3T3L1 adipocytes. Endocrinology *149*, 40-49.

Ungar, D., and Hughson, F.M. (2003). SNARE protein structure and function. Annual review of cell and developmental biology *19*, 493-517.

van den Bogaart, G., Holt, M.G., Bunt, G., Riedel, D., Wouters, F.S., and Jahn, R. (2010). One SNARE complex is sufficient for membrane fusion. Nat Struct Mol Biol *17*, 358-364.

van Vliet, C., Thomas, E.C., Merino-Trigo, A., Teasdale, R.D., and Gleeson, P.A. (2003). Intracellular sorting and transport of proteins. Progress in biophysics and molecular biology *83*, 1-45.

van Weering, J.R., Toonen, R.F., and Verhage, M. (2007). The role of Rab3a in secretory vesicle docking requires association/dissociation of guanidine phosphates and Munc18-1. PLoS One *2*, e616.

Vellai, T., and Vida, G. (1999). The origin of eukaryotes: the difference between prokaryotic and eukaryotic cells. Proceedings Biological sciences / The Royal Society *266*, 1571-1577.

Verhage, M., Maia, A.S., Plomp, J.J., Brussaard, A.B., Heeroma, J.H., Vermeer, H., Toonen, R.F., Hammer, R.E., van den Berg, T.K., Missler, M., *et al.* (2000). Synaptic assembly of the brain in the absence of neurotransmitter secretion. Science *287*, 864-869.

Vigneri, R., Squatrito, S., and Sciacca, L. (2010). Insulin and its analogs: actions via insulin and IGF receptors. Acta diabetologica *47*, 271-278.

Vogel, S.S., Thaler, C., and Koushik, S.V. (2006). Fanciful FRET. Science's STKE : signal transduction knowledge environment *2006*, re2.

Volchuk, A., Sargeant, R., Sumitani, S., Liu, Z., He, L., and Klip, A. (1995). Cellubrevin is a resident protein of insulin-sensitive GLUT4 glucose transporter vesicles in 3T3-L1 adipocytes. J Biol Chem *270*, 8233-8240.

Volchuk, A., Wang, Q., Ewart, H.S., Liu, Z., He, L., Bennett, M.K., and Klip, A. (1996). Syntaxin 4 in 3T3-L1 adipocytes: regulation by insulin and participation in insulin-dependent glucose transport. Mol Biol Cell *7*, 1075-1082.

Wang, G., Witkin, J.W., Hao, G., Bankaitis, V.A., Scherer, P.E., and Baldini, G. (1997). Syndet is a novel SNAP-25 related protein expressed in many tissues. J Cell Sci *110 (Pt 4)*, 505-513.

Watanabe, T., Smith, M.M., Robinson, F.W., and Kono, T. (1984). Insulin action on glucose transport in cardiac muscle. J Biol Chem *259*, 13117-13122.

Watson, R.T., Shigematsu, S., Chiang, S.H., Mora, S., Kanzaki, M., Macara, I.G., Saltiel, A.R., and Pessin, J.E. (2001). Lipid raft microdomain compartmentalization of TC10 is required for insulin signaling and GLUT4 translocation. J Cell Biol *154*, 829-840.

Weber, T., Zemelman, B.V., McNew, J.A., Westermann, B., Gmachl, M., Parlati, F., Sollner, T.H., and Rothman, J.E. (1998). SNAREpins: minimal machinery for membrane fusion. Cell *92*, 759-772.

Weibrecht, I., Leuchowius, K.J., Clausson, C.M., Conze, T., Jarvius, M., Howell, W.M., Kamali-Moghaddam, M., and Soderberg, O. (2010). Proximity ligation assays: a recent addition to the proteomics toolbox. Expert Rev Proteomics *7*, 401-409.

Whyte, J.R., and Munro, S. (2002). Vesicle tethering complexes in membrane traffic. J Cell Sci *115*, 2627-2637.

Widberg, C.H., Bryant, N.J., Girotti, M., Rea, S., and James, D.E. (2003). Tomosyn interacts with the t-SNAREs syntaxin4 and SNAP23 and plays a role in insulin-stimulated GLUT4 translocation. J Biol Chem *278*, 35093-35101.

Wuestehube, L.J., Duden, R., Eun, A., Hamamoto, S., Korn, P., Ram, R., and Schekman, R. (1996). New mutants of Saccharomyces cerevisiae affected in the transport of proteins from the endoplasmic reticulum to the Golgi complex. Genetics *142*, 393-406.

Yamada, E., Okada, S., Saito, T., Ohshima, K., Sato, M., Tsuchiya, T., Uehara, Y., Shimizu, H., and Mori, M. (2005). Akt2 phosphorylates Synip to regulate docking and fusion of GLUT4-containing vesicles. J Cell Biol *168*, 921-928.

Yamaguchi, T., Dulubova, I., Min, S.W., Chen, X., Rizo, J., and Sudhof, T.C. (2002). Sly1 binds to Golgi and ER syntaxins via a conserved N-terminal peptide motif. Developmental cell *2*, 295-305.

Yamakawa, H., Seog, D.H., Yoda, K., Yamasaki, M., and Wakabayashi, T. (1996). Uso1 protein is a dimer with two globular heads and a long coiled-coil tail. Journal of structural biology *116*, 356-365.

Yang, B., Gonzalez, L., Jr., Prekeris, R., Steegmaier, M., Advani, R.J., and Scheller, R.H. (1999). SNARE interactions are not selective. Implications for membrane fusion specificity. J Biol Chem *274*, 5649-5653.

Yang, B., Steegmaier, M., Gonzalez, L.C., Jr., and Scheller, R.H. (2000). nSec1 binds a closed conformation of syntaxin1A. J Cell Biol *148*, 247-252.

Yang, C., Coker, K.J., Kim, J.K., Mora, S., Thurmond, D.C., Davis, A.C., Yang, B., Williamson, R.A., Shulman, G.I., and Pessin, J.E. (2001). Syntaxin 4 heterozygous knockout mice develop muscle insulin resistance. J Clin Invest *107*, 1311-1318.

Yang, J., Clark, A.E., Harrison, R., Kozka, I.J., and Holman, G.D. (1992). Trafficking of glucose transporters in 3T3-L1 cells. Inhibition of trafficking by phenylarsine oxide implicates a slow dissociation of transporters from trafficking proteins. Biochem J *281 (Pt 3)*, 809-817.

Yokoyama, S., Shirataki, H., Sakisaka, T., and Takai, Y. (1999). Three splicing variants of tomosyn and identification of their syntaxin-binding region. Biochem Biophys Res Commun *256*, 218-222.

Zerial, M., and McBride, H. (2001). Rab proteins as membrane organizers. Nat Rev Mol Cell Biol *2*, 107-117.

Zhao, P., Yang, L., Lopez, J.A., Fan, J., Burchfield, J.G., Bai, L., Hong, W., Xu, T., and James, D.E. (2009). Variations in the requirement for v-SNAREs in GLUT4 trafficking in adipocytes. J Cell Sci *122*, 3472-3480.

Zimmet, P., Alberti, K.G., and Shaw, J. (2001). Global and societal implications of the diabetes epidemic. Nature *414*, 782-787.